

***Ab initio*-Berechnung der
Wechselwirkungspotentiale von Helium, Neon
und Methan sowie theoretische Untersuchungen
zu ihren thermophysikalischen Eigenschaften
und denen von Wasserdampf**

Dissertation

zur Erlangung des akademischen Grades
doctor rerum naturalium (Dr. rer. nat.)
der Mathematisch-Naturwissenschaftlichen Fakultät
der Universität Rostock

vorgelegt von
Robert Hellmann, geb. am 12.11.1981 in Rostock
aus Rostock

Rostock, April 2009

urn:nbn:de:gbv:28-diss2009-0177-1

Gutachter der Dissertation:

Prof. Dr. Eckhard Vogel, Universität Rostock

Prof. Dr. Barbara Kirchner, Universität Leipzig

Prof. Dr. Georg Jansen, Universität Duisburg-Essen

Termin des wissenschaftlichen Kolloquiums: 16. Juni 2009

Die vorliegende Dissertation wurde im Zeitraum zwischen Oktober 2005 und April 2009 in der Abteilung Physikalische Chemie am Institut für Chemie der Universität Rostock unter der Betreuung von Herrn Prof. Dr. Eckhard Vogel angefertigt.

An dieser Stelle möchte ich meinen besonderen Dank an Herrn Prof. Dr. Eckhard Vogel für die interessante Themenstellung sowie für die umfangreiche Betreuung und Unterstützung aussprechen. Bei Herrn Dr. Eckard Bich bedanke ich mich für die Klärung vieler Fragen der Theorie und die stete Unterstützung.

Herrn Prof. Dr. Alan S. Dickinson und Herrn Dr. Velisa Vesovic danke ich für die fortwährende und fruchtbare Zusammenarbeit auf dem Gebiet der kinetischen Gastheorie. Bei Herrn Prof. Dr. Alan S. Dickinson möchte ich mich außerdem für die Betreuung während meines Aufenthaltes an der Newcastle University bedanken.

Bei Frau Prof. Dr. Barbara Kirchner und Herrn Prof. Dr. Georg Jansen möchte ich mich für die Begutachtung der Arbeit bedanken.

Den Mitarbeitern des Rechenzentrums der Universität Rostock danke ich für die Administrierung der für die Durchführung dieser Arbeit beschafften Rechentechnik.

Ich danke allen Mitarbeitern der Abteilung Physikalische Chemie für die angenehme Arbeitsatmosphäre.

Abschließend möchte ich mich bei meinen Eltern und meinen Freunden für ihre Geduld und Unterstützung bedanken.

Zusammenfassung

Thermophysikalische Eigenschaften der reinen Gase Helium, Neon, Methan und Wasserdampf wurden für niedrige Dichten über weite Temperaturbereiche berechnet. Die statistische Thermodynamik wurde dabei für die Ermittlung der Druckvirialkoeffizienten genutzt. Für die Ermittlung der Transport- und Relaxationseigenschaften wurde die kinetische Gastheorie verwendet. Diese war bisher auf lineare Moleküle beschränkt und wurde für die Berechnungen an Methan und Wasserdampf auf Moleküle beliebiger Geometrie erweitert. Die für alle Berechnungen benötigten Wechselwirkungspotentiale wurden für Helium, Neon und Methan mit quantenchemischen *ab initio*-Methoden nach dem Supermolekülansatz ermittelt und für Wasser aus dem Schrifttum entnommen. Die berechneten Werte für die thermophysikalischen Eigenschaften der vier Gase stimmen sehr gut mit den besten experimentellen Daten überein. Für sehr tiefe und sehr hohe Temperaturen sind die theoretischen Werte genauer als die experimentellen Daten.

Summary

Thermophysical properties of the pure gases helium, neon, methane and water vapor were calculated for low densities over wide temperature ranges. Statistical thermodynamics was used for the determination of the pressure virial coefficients. The kinetic theory of gases was utilized for the calculation of the transport and relaxation properties. So far kinetic theory was limited to linear molecules and has now been extended to molecules of arbitrary geometry to enable calculations on methane and water vapor. The interaction potentials, which are needed for all computations, were determined for helium, neon and methane from the supermolecular approach using quantum chemical *ab initio* methods. For water the interaction potentials were taken from the literature. The calculated values of the thermophysical properties for the four gases show very good agreement with the best experimental data. At very low and very high temperatures the theoretical values are more accurate than experimental data.

Inhaltsverzeichnis

1	Aufgabenstellung	1
2	Bisheriger Stand der Forschung	3
2.1	Wechselwirkungspotentiale für Helium, Neon, Methan und Wasser	3
2.1.1	Helium	3
2.1.2	Neon	5
2.1.3	Methan	6
2.1.4	Wasser	8
2.2	Theoretische Berechnung thermophysikalischer Eigenschaften reiner Gase .	9
2.2.1	Zweite und dritte Druckvirialkoeffizienten	9
2.2.2	Transport- und Relaxationseigenschaften	11
3	Ergebnisse und Diskussion	14
3.1	<i>Ab initio</i> -Potentialenergiekurve für das Helium-Atompaar und thermophysikalische Eigenschaften des verdünnten Heliumgases	14
3.1.1	I. Interatomares Helium-Helium-Potential	14
3.1.2	II. Thermophysikalische Standardwerte für Helium bei niedrigen Dichten	17
3.2	<i>Ab initio</i> -Potentialenergiekurve für das Neon-Atompaar und thermophysikalische Eigenschaften des verdünnten Neongases	19
3.2.1	I. Interatomares Neon-Neon-Potential und Rotations-Schwingungsspektren	19
3.2.2	II. Thermophysikalische Eigenschaften von Neon bei niedrigen Dichten	21
3.3	<i>Ab initio</i> -Wechselwirkungspotentialenergiefläche und zweite Druckvirialkoeffizienten des Methans	23
3.4	Transporteigenschaften asymmetrischer Kreiselmoleküle	26
3.5	Berechnung der Transport und Relaxationseigenschaften des Methans . . .	29
3.5.1	I. Scherviskosität, viskomagnetische Effekte und Selbstdiffusion . .	29

3.5.2	II. Wärmeleitfähigkeit, thermomagnetische Effekte, Volumenviskosität und Kernspin-Relaxation	31
3.6	Berechnung der Transport- und Relaxationseigenschaften von verdünntem Wasserdampf	34
4	Originalpublikationen	36
4.1	<i>Ab initio</i> potential energy curve for the helium atom pair and thermophysical properties of dilute helium gas	36
4.1.1	I. Helium-helium interatomic potential	36
4.1.2	II. Thermophysical standard values for low-density helium	48
4.2	<i>Ab initio</i> potential energy curve for the neon atom pair and thermophysical properties of the dilute neon gas	64
4.2.1	I. Neon-neon interatomic potential and rovibrational spectra	64
4.2.2	II. Thermophysical properties for low-density neon	73
4.3	<i>Ab initio</i> intermolecular potential energy surface and second pressure virial coefficients of methane	89
4.4	Transport properties of asymmetric-top molecules	99
4.5	Calculation of the transport and relaxation properties of methane	108
4.5.1	I. Shear viscosity, viscomagnetic effects, and self-diffusion	108
4.5.2	II. Thermal conductivity, thermomagnetic effects, volume viscosity, and nuclear-spin relaxation	122
4.6	Calculation of the transport and relaxation properties of dilute water vapor .	134
5	Zusammenfassung	146

1 Aufgabenstellung

Das Ziel der vorliegenden Arbeit bestand darin, thermophysikalische Eigenschaften der reinen Gase Helium, Neon, Methan und Wasserdampf im Bereich kleiner Dichten mit hoher bis höchster Genauigkeit zu bestimmen. Dabei sollten speziell Transport- und Relaxationseigenschaften sowie Druckvirialkoeffizienten mittels der kinetischen Gastheorie bzw. der statistischen Thermodynamik untersucht werden.

Eine Grundvoraussetzung für solche Berechnungen ist die Kenntnis der Potentialenergiekurve bzw. Potentialenergiehyperfläche der wechselwirkenden Gasteilchen, die vom Abstand der Teilchen und im Falle molekularer Gase auch von deren gegenseitiger Orientierung abhängen. Für Helium, Neon und Methan sollten die Wechselwirkungspotentiale durch eigene quantenchemische *ab initio*-Berechnungen ermittelt werden, da die zahlreichen im Schrifttum verfügbaren Potentiale bezüglich ihrer Genauigkeit als nicht ausreichend eingeschätzt wurden. Für Wasser hingegen sind ausreichend genaue Wechselwirkungspotentiale im Schrifttum verfügbar.

Für die Berechnung der Transport- und Relaxationseigenschaften von Methan und Wasserdampf sollte die Methode der klassischen Trajektorien verwendet werden. Dabei werden so genannte generalisierte Streuquerschnitte durch klassisch-mechanische Simulation der zwischenmolekularen Stoßprozesse bestimmt. Die kinetische Gastheorie kann dann verwendet werden, um aus diesen Streuquerschnitten Transport- und Relaxationseigenschaften zu berechnen. Im Hinblick darauf, dass die Methode der klassischen Trajektorien nur für Stöße zwischen linearen Molekülen entwickelt und auch nur für diese ein Softwarecode im Schrifttum verfügbar war, sollten der vorhandene Programmcode und die zugrunde liegende Theorie klassischer generalisierter Streuquerschnitte erweitert werden, um für die nichtlinearen Moleküle Methan und Wasser die generalisierten Streuquerschnitte ermitteln zu können.

Schließlich sollten für alle Gase die zweiten Druckvirialkoeffizienten, die Scherviskositäten und die Wärmeleitfähigkeiten über große Temperaturbereiche berechnet werden. Für die atomaren Gase Helium und Neon sollten zusätzlich die dritten Druckvirialkoeffizienten und die Rotations-Schwingungsspektren ermittelt werden, für Methan und Wasserdampf zusätzlich Volumenviskosität und Selbstdiffusionskoeffizienten sowie nur für Methan visko- und

thermomagnetische Effekte und Kernspinrelaxation durch Spin-Rotation. Durch Vergleich mit den besten experimentellen Daten sollten die Qualität der verwendeten Potentiale und der Methode der klassischen Trajektorien für molekulare Gase überprüft und zuverlässige Daten für Temperaturbereiche generiert werden, die experimentell nicht oder nur mit sehr großen Unsicherheiten zugänglich sind.

2 Bisheriger Stand der Forschung

2.1 Wechselwirkungspotentiale für Helium, Neon, Methan und Wasser

Die hier gegebene Übersicht beschränkt sich auf die wichtigsten neueren Publikationen, die zu Beginn der Arbeiten an dieser Dissertationsschrift (2005) verfügbar waren.

2.1.1 Helium

Das Potential zwischen zwei Heliumatomen ist das genaueste bekannte Wechselwirkungspotential für zwei stabile nichtradikalische Teilchen. Es hängt nur vom Abstand der beiden Atome ab. Bereits viele frühe Arbeiten zeigten, dass die Potentialtiefe ε/k_B ($k_B = 1,38065 \times 10^{-23} \text{JK}^{-1}$) nur etwa 11,0 K beträgt, wobei der zugehörige Teilchenabstand R_ε bei etwa $5,6 a_0$ ($1 a_0 = 0,5291772083 \times 10^{-10} \text{m}$) liegt. Vor allem der Bereich großer Helium-Helium-Abstände, in dem die Wellenfunktionen der beiden Atome nicht mehr überlappen, ist sehr genau untersucht worden. Hier wird das Wechselwirkungspotential allein durch Dispersionswechselwirkungen bestimmt. Hochgenaue Werte für die wichtigsten Dispersionskoeffizienten sind bereits 1993 von Bishop und Pipin berechnet worden [1].

1997 berechneten Korona *et al.* [2] Wechselwirkungsenergien für 12 Abstände R zwischen $3 a_0$ und $7 a_0$ mittels symmetrieadaptierter Störungstheorie (*symmetry-adapted perturbation theory*, SAPT) [3], einer Methode, die nicht auf dem normalerweise eingesetzten Supermolekülansatz beruht, sondern die einzelnen Wechselwirkungsbeiträge direkt berechnet. Eine analytische Potentialfunktion wurde an die berechneten Energien sowie weitere Werte für kleine Abstände aus dem Schrifttum angepasst. Es zeigte sich jedoch bald, dass die von Korona *et al.* ermittelte Potentialtiefe von $(11,06 \pm 0,03) \text{K}$ zu groß ist. 1999 ermittelten van de Bovenkamp und van Duijneveldt [4] durch MRCI-Berechnungen mit für die Wechselwirkungsenergie optimierten Basissätzen und zusätzlichen Basisfunktionen zwischen den beiden Heliumatomen (so genannte Bindungsfunktionen) nur eine Tiefe von $(10,99 \pm 0,02) \text{K}$. Den gleichen Wert erhielten van Mourik und Dunning [5] im gleichen Jahr durch eine Kombination von r_{12} -CCSD(T)-, CCSDT- und *full*-CI-Rechnungen. Komasa [6] bestimmte

strikte Obergrenzen für die Wechselwirkungsenergien bei zahlreichen Abständen aus variationalen Rechnungen mit exponentiell korrelierten Gaussian-Funktionen (ECG). Die ermittelte Obergrenze der Wechselwirkungsenergie im Minimum lag bei $-10,947$ K, das heißt die wahre Wechselwirkungsenergie ist vom Betrag her größer. Komasa führte die Berechnungen auch bei sehr kleinen Abständen bis hin zu $R = 0$ durch.

Aus diesen Werten bei kleinen Abständen ($R < 3 a_0$), den Werten von Korona *et al.* zwischen $3 a_0$ und $7 a_0$, den Werten für die Dispersionskoeffizienten von Bishop und Pipin und den aus Extrapolationsformeln von Thakkar [7] erhaltenen höheren Dispersionskoeffizienten konstruierten Hurly und Moldover [8] eine Potentialfunktion, die sie benutzten, um Standardwerte für die wichtigsten thermophysikalischen Eigenschaften des Heliums bei kleinen Dichten zu berechnen. Durch die Verwendung der Werte von Korona *et al.* ist dieses Potential insgesamt jedoch zu attraktiv.

Gdanitz [9] ermittelte 2001 aus r_{12} -MR-ACPF-Rechnungen eine Potentialtiefe von $(10,980 \pm 0,004)$ K durch Extrapolation zu vollständigem Basissatz. Anderson [10] führte 2001 exakte Quanten-Monte-Carlo-Rechnungen (EQMC) durch und fand eine Potentialtiefe von $(10,98 \pm 0,02)$ K. Durch Vergrößerung der Anzahl der Monte-Carlo-Punkte erhielt Anderson 2004 [11] einen verbesserten Wert für die Potentialtiefe von $(10,998 \pm 0,005)$ K. Die Ergebnisse von Anderson zeigen, dass die Fehlerabschätzung von Gdanitz deutlich zu optimistisch war. Cencek *et al.* [12] berechneten sehr genaue Wechselwirkungsenergien für die Abstände $R = 4 a_0$, $R = 5,6 a_0$ und $R = 7 a_0$. Dabei wurden verschiedene Methoden kombiniert. Die CCSD-Wechselwirkungsenergien wurden mit Gaussian-Geminal-Funktionen ermittelt, wobei man dem Limit des vollständigen Basissatzes sehr nahe kommt. Für die Abschätzung höherer Anregungsterme wurden konventionelle CCSD(T)- und *full*-CI-Rechnungen ausgeführt und die Beiträge zu vollständigem Basissatz extrapoliert. Die bei $R = 5,6 a_0$ ermittelte Potentialtiefe liegt bei $-(11,009 \pm 0,008)$ K. 2005 berichteten Cencek *et al.* [13] eine neue variationale Obergrenze für die Wechselwirkungsenergie bei $5,6 a_0$ mit $-10,9985$ K.

Obwohl damit die Wechselwirkungsenergien im Potentialminimum und bei einigen weiteren Abständen genügend genau ermittelt worden waren, benötigt man für die Anpassung einer genauen Potentialfunktion Wechselwirkungsenergien hoher Genauigkeit bei weitaus mehr Abständen. Zudem müssen auf diesem Genauigkeitslevel weitere Effekte berücksichtigt werden. Dabei handelt es sich im Wesentlichen um relativistische Effekte und Korrekturen zur Born-Oppenheimer-Näherung, die aber nur in sehr wenigen Arbeiten für das Potentialminimum berechnet wurden. So wurde die diagonale adiabatische Korrektur, auch diagonale Born-Oppenheimer-Korrektur (*diagonal Born-Oppenheimer correction*, DBOC) genannt, von Komasa *et al.* [14] für zahlreiche Abstände R berechnet. Bei $R = 5,6 a_0$ be-

trägt die Korrektur $-13,2$ mK. Später ergab eine genauere Berechnung nur für $R = 5,6a_0$ einen Wert von -9 mK (Referenz [7] bei Cencek *et al.* [13]). Die relativistische Korrektur zur Wechselwirkungsenergie wurde für $R = 5,6a_0$ von Cencek *et al.* [13] ermittelt, wobei ein Wert von $(+15,4 \pm 0,6)$ mK erhalten wurde. Dieser Wert setzt sich aus verschiedenen Beiträgen zusammen, wovon der größte die Orbit-Orbit-Korrektur ist. Diese ist Teil des Casimir-Polder-Effektes [15, 16], der das Verhalten des Potentials bei großen Abständen von C_6/R^6 in C_7/R^7 ändert. Chen und Chung [17] führten präzise Berechnungen des Casimir-Polder-Effektes für sehr viele Helium-Helium-Abstände durch. Die weiteren relativistischen Effekte sind die 1- und 2-Elektronen-Darwin-Korrekturen und die Massengeschwindigkeits-Korrektur. Cencek *et al.* [13] zeigten, dass zumindest im Potentialminimum die 2-Elektronen-Darwin-Korrektur vernachlässigbar ist. Die anderen beiden Korrekturen bilden die so genannte Cowan-Griffin-Korrektur [18], die in vielen Quantenchemie-Programmpaketen implementiert ist.

2.1.2 Neon

Das Wechselwirkungspotential zwischen zwei Neonatomen wurde weit weniger genau untersucht als das zwischen zwei Heliumatomen. Daher ist es nicht verwunderlich, dass das genaueste Paarpotential nicht aus *ab initio*-Rechnungen erhalten wurde: Aziz und Slaman [19] verwendeten experimentelle Daten für verschiedene Eigenschaften des verdünnten Neongases, die mit dem Wechselwirkungspotential berechnet werden können, um eine analytische Potentialfunktion abzuleiten. Das Potential hat eine Tiefe von $\varepsilon/k_B = 42,25$ K bei $R = 3,091 \text{ \AA}$ ($1 \text{ \AA} = 10^{-10} \text{ m}$).

1999 führten van Mourik *et al.* [20] erstmals *frozen-core*-CCSD(T)-Berechnungen mit sehr großen Basissätzen bis d-aug-cc-pV6Z für mehrere Neon-Neon-Abstände durch und erhielten dabei eine Potentialtiefe von $40,92$ K bei $3,10 \text{ \AA}$. Sie vermuteten, dass die Differenz zu den Werten von Aziz und Slaman teilweise auf die approximative Behandlung der Tripel-Terme in CCSD(T) zurückzuführen sein könnte und daher CCSDT-Rechnungen ausgeführt werden müssten, um die Genauigkeit der Berechnungen zu verbessern. Die Korrektur für Kern-Kern- und Kern-Valenz-Korrelation wurde nur im Potentialminimum mit der CCSD(T)-Methode und dem d-aug-cc-pwCV5Z-Basissatz bestimmt. Sie verringert die Potentialtiefe um etwa $0,07$ K, macht das Potential also etwas repulsiver.

Van de Bovenkamp und van Duijneveldt [21] berichteten auch 1999 über CCSD(T)-Rechnungen für mehrere Abstände unter Verwendung eines für die Wechselwirkungsenergie optimierten Basissatzes mit Bindungsfunktionen. Sie fanden eine Potentialtiefe von

40,99 K bei 3,10 Å. Ebenfalls 1999 führten Cybulski und Toczyłowski [22] CCSD(T)-Berechnungen für mehrere Abstände durch, wobei Basissätze bis aug-cc-pV5Z mit Bindungsfunktionen verwendet wurden. Cybulski und Toczyłowski zeigten, dass die Bindungsfunktionen die Konvergenz der aug-cc-pVXZ-Basissätze zum Basissatzlimit erheblich verbessern und ermittelten eine Potentialtiefe von 41,19 K bei 3,0988 Å, ohne zu vollständigem Basissatz zu extrapolieren. 2001 ergänzte Gdanitz [23] die Berechnungen von Cybulski und Toczyłowski um Korrekturen für vollständigen Basissatz, *full-CI*, relativistische Effekte sowie für Kern-Kern- und Kern-Valenz-Korrelation, die bis dahin in allen Arbeiten außer bei van Mourik *et al.* vernachlässigt worden waren. Die von Gdanitz gefundene Potentialtiefe von 41,535 K bei 3,1007 Å war immer noch kleiner als die von Aziz und Slaman [19], wobei darauf hinzuweisen ist, dass die eingesetzten Methoden zur Bestimmung der Korrekturen sehr fragwürdig sind. Gdanitz hat in seiner Arbeit keine analytische Potentialfunktion angegeben, jedoch ist eine solche 2003 auf Basis der von ihm berechneten Wechselwirkungsenergien von Venkatraj *et al.* [24] bestimmt worden. Ebenfalls 2003 passten Wüest und Merkt [25] ein Potential an die von ihnen sehr präzise gemessenen Rotations-Schwingungsspektren der ^{20}Ne - ^{20}Ne - und ^{22}Ne - ^{20}Ne -Dimere an. Nasrabad *et al.* [26] extrapolierten 2004 die Ergebnisse von Cybulski und Toczyłowski zu vollständigem Basissatz und ermittelten ebenfalls eine analytische Potentialfunktion. Dieses Potential weist eine Tiefe von 41,35 K bei 3,097 Å auf.

Schließlich konnte Lee [27] 2005 zeigen, dass CCSDT-Rechnungen nötig sind, um die Abweichungen zum Potential von Aziz und Slaman (42,25 K bei 3,097 Å) zu erklären. Er extrapolierte die Differenz der CCSDT- und CCSD(T)-Wechselwirkungsenergien bei 3,1 Å zu vollständigem Basissatz und addierte sie zur Potentialtiefe von Cybulski und Toczyłowski (41,19 K). Die so ermittelte Potentialtiefe beträgt 41,87 K.

2.1.3 Methan

Das Methan-Methan-Wechselwirkungspotential ist erstaunlicherweise nur sehr wenig genau bekannt, trotz der immensen Bedeutung von Methan in Wissenschaft und Industrie. Das liegt zum Teil daran, dass immer noch weithin die Annahme vorherrscht, dass das Methan-Methan-Potential quasi sphärisch ist, also dass das Potential in guter Näherung nur vom Abstand der wechselwirkenden Moleküle, nicht aber von deren gegenseitiger Orientierung abhängt. In molekulardynamischen Simulationen werden die Methan-Moleküle oft als Punktteilchen approximiert, die über ein Lennard-Jones-Potential wechselwirken. Die zwei Parameter des Lennard-Jones-Potentials, Potentialtiefe und Stoßdurchmesser, werden

an experimentelle Eigenschaften angepasst, wobei das resultierende Potential diese Eigenschaften nur in begrenzten Temperatur- und Dichtebereichen gut beschreibt und andere Eigenschaften, an die nicht angepasst wurde, oft unzureichend wiedergibt. Um das Potential und seine Anisotropie korrekt zu beschreiben, sind *ab initio*-Berechnungen für eine Vielzahl von Molekülabständen und gegenseitigen Orientierungen notwendig. Im Vergleich zu den Edelgasen waren für Methan aufgrund der Größe seines Dimers die hochgenauen *Coupled-Cluster*-Methoden lange Zeit nicht einsetzbar.

So schlugen Tsuzuki *et al.* [28] 1998 ein Potential vor, welches nur auf MP3-Rechnungen basiert. Sie berechneten für insgesamt 132 Konfigurationen, verteilt auf 12 verschiedene Winkelorientierungen, Punkte auf der Potentialenergiehyperfläche mit dem Supermolekülansatz, wobei sie die Counterpoise-Korrektur von Boys und Bernardi [29] nutzten und die Methan-Moleküle als starr betrachteten. Dabei verwendeten sie einen 6-311G(d,p)-Basissatz, den sie um diffuse Polarisationsfunktionen ergänzten. Es wurden weder Bindungsfunktionen berücksichtigt, noch wurde versucht, zum Basissatzlimit zu extrapolieren. Auch ist zu kritisieren, dass Tsuzuki *et al.* die Geometrie der Monomere nur auf dem MP2/6-31G(d)-Niveau optimierten. Die Autoren passten eine analytische *site-site*-Potentialfunktion an die berechneten Wechselwirkungsenergien an, wobei die Positionen der jeweils fünf Wechselwirkungszentren pro Molekül mit den Positionen der Atome zusammenfallen. Die maximale Potentialtiefe beträgt 224 K. Die zugehörige Konfiguration der Methan-Moleküle entspricht einer Anordnung, bei der sich jeweils Dreiecksflächen der Methan-Tetraeder parallel gegenüberstehen, aber gegeneinander so verdreht sind, dass die Wasserstoffatome in den Ecken dieser beiden Dreiecke „auf Lücke“ stehen.

1999 publizierten Rowley und Pakkanen [30] ein Potential, für das 146 Punkte auf der Potentialhyperfläche, verteilt auf 11 verschiedene Winkelorientierungen, ermittelt wurden. Dabei setzten sie die MP2-Methode mit dem Basissatz 6-311+G(2df,2pd) ein. Analog zu Tsuzuki *et al.* passten auch sie eine *site-site*-Potentialfunktion an ihre berechneten Wechselwirkungsenergien an. Dabei erhielten sie eine maximale Potentialtiefe von nur 168 K. Um das Potential zu verbessern, berechneten Rowley und Pakkanen fünf Punkte auf der Potentialhyperfläche auf MP4/aug-cc-pVTZ-Niveau und adjustierten die Parameter ihrer Potentialfunktion an diese fünf Wechselwirkungsenergien. Auf diese Weise erhielten sie eine deutlich größere Potentialtiefe von 237 K.

Die Potentialhyperflächen von Tsuzuki *et al.* und Rowley und Pakkanen sind für die präzise Berechnung thermophysikalischer Eigenschaften völlig unzureichend.

2.1.4 Wasser

Da Wasser vor allem in kondensierter Phase von Bedeutung ist, wurden zahlreiche Paarpotentiale entwickelt, die an Eigenschaften für die Flüssigphase angepasst wurden. Dabei handelt es sich überwiegend um *site-site*-Potentialmodelle mit Lennard-Jones-Zentren, die außerdem Partiaalladungen tragen. Solche Potentiale sind jedoch für Wasser in der Gasphase völlig ungeeignet. Das liegt daran, dass nichtadditive Mehrkörperwechselwirkungen in Wasser sehr stark ausgeprägt sind, was vor allem auf induktive Wechselwirkungen zurückzuführen ist, die generell nichtadditiv sind. Bei den für die Flüssigphase optimierten Paarpotentialen sind diese nichtadditiven Mehrkörperwechselwirkungen implizit in den Zweikörperwechselwirkungen enthalten, was eine grobe Näherung darstellt. Ein echtes Paarpotential für ein isoliertes Molekülpaar ist besser für Rechnungen in flüssiger oder fester Phase geeignet, wenn zusätzlich die nichtadditiven Mehrkörperanteile explizit berücksichtigt werden.

Für die Dampfphase sind neben Paarpotentialen, die aus der Inversion von Rotations-Schwingungsspektren erhalten wurden und relativ ungenau sind (vor allem bei kleinen Abständen), auch einige *ab initio*-Potentiale entwickelt worden. Vor allem die Gruppe um Krzysztof Szalewicz in Delaware (USA), die auch schon Beiträge zum Wechselwirkungspotential zweier Heliumatome geleistet hat, entwickelte mehrere SAPT-basierte Potentiale. Vor allem die im Jahr 2000 publizierten SAPT-5s- [31] und SAPT-5st-Potentiale [32] sind hier zu nennen. Letzteres ist aus SAPT-5s durch Adjustierung einiger Potentialparameter an Rotations-Schwingungsspektren hervorgegangen. Mit beiden Potentialen konnten die zweiten Druckvirialkoeffizienten und Rotations-Schwingungsspektren zufriedenstellend reproduziert werden.

Diese Potentiale wurden für die Berechnung von Transporteigenschaften und der Volumenviskosität als gut geeignet eingeschätzt, so dass im Rahmen der vorliegenden Arbeit kein eigenes Potential entwickelt wurde.

2.2 Theoretische Berechnung thermophysikalischer Eigenschaften reiner Gase

2.2.1 Zweite und dritte Druckvirialkoeffizienten

Einatomige Gase

Der zweite Druckvirialkoeffizient $B(T)$ eines einatomigen Gases ist klassisch-mechanisch nach der statistischen Thermodynamik gegeben durch:

$$B_{\text{cl}}(T) = -2\pi N_{\text{A}} \int_0^{\infty} \left[e^{-\beta V(R)} - 1 \right] R^2 dR. \quad (2.1)$$

$N_{\text{A}} = 6,02214179 \times 10^{23} \text{ mol}^{-1}$ ist die Avogadro-Konstante, $V(R)$ das nur vom Abstand R abhängige Wechselwirkungspotential und $\beta = \frac{1}{k_{\text{B}}T}$. Diese klassische Formel versagt bei tiefen Temperaturen und/oder sehr leichten Gasteilchen (z.B. Helium). In diesen Fällen kann die klassische Formel um Quantenkorrekturen verschiedener Ordnungen ergänzt werden [33]. Der allgemeine Ansatz lautet:

$$B(T) = B_{\text{cl}}(T) + \lambda B_{\text{qm},1}(T) + \lambda^2 B_{\text{qm},2}(T) + \lambda^3 B_{\text{qm},3}(T) + \dots \quad (2.2)$$

mit $\lambda = \frac{\hbar^2 \beta}{12m}$ und $\hbar = \frac{h}{2\pi}$. Dabei ist $h = 6,626075 \times 10^{-34} \text{ Js}$ das plancksche Wirkungsquantum und m die Atommasse. Der Ausdruck für die Quantenkorrektur erster Ordnung lautet:

$$B_{\text{qm},1}(T) = 2\pi N_{\text{A}} \int_0^{\infty} [\beta V'(R)]^2 e^{-\beta V(R)} R^2 dR \quad (2.3)$$

wobei $V'(R)$ die erste Ableitung des Potentials nach R ist. Höhere Quantenkorrekturen enthalten auch höhere Ableitungen des Potentials.

Bei nicht zu tiefen Temperaturen reicht es in der Regel aus, nur die Quantenkorrektur erster Ordnung zu berücksichtigen, um die Genauigkeit der besten experimentellen Daten zu erreichen, vorausgesetzt das Potential ist genau genug. Bei sehr tiefen Temperaturen sollten auch die höheren Quantenkorrekturen mit berücksichtigt werden. Allerdings divergiert die Reihenentwicklung entsprechend Gleichung 2.2 bei sehr niedrigen Temperaturen, so dass hier der zweite Virialkoeffizient vollständig quantenmechanisch berechnet werden muss. Für solche Berechnungen muss die Schrödingergleichung für die Streuung und für die gebundenen Zustände zweier Partikel, die über das Potential $V(R)$ wechselwirken, gelöst werden. Für die entsprechenden Beziehungen wird beispielsweise auf Referenz [34] und darin enthaltene weitere Referenzen verwiesen.

Für den dritten Virialkoeffizienten $C(T)$ ist keine exakte quantenmechanische Lösung bekannt, jedoch ist neben der klassischen Näherung auch die Quantenkorrektur erster Ordnung abgeleitet worden. Für die Berechnung von $C(T)$ wird das Potential dreier wechselwirkender Gasteilchen benötigt, welches bei Annahme von paarweiser Additivität als Summe der drei Zweikörperpotentiale approximiert werden kann. Die geringe Abweichung von der paarweisen Additivität wird durch den von Axilrod und Teller abgeleiteten Tripel-Dipol-Term [35, 36] dominiert. Die Formeln für die Berechnung von $C(T)$ einschließlich der Quantenkorrektur sind unter anderem in [37] angegeben.

Mehratomige Gase

Der Ausdruck für den zweiten Druckvirialkoeffizienten eines mehratomigen Gases ist dem für einatomige Gase sehr ähnlich. Es erfolgt lediglich noch eine Mittelung über alle Orientierungen Ω_1 und Ω_2 der beiden Moleküle:

$$B_{cl}(T) = -2\pi N_A \left\langle \int_0^\infty \left[e^{-\beta V(R, \Omega_1, \Omega_2)} - 1 \right] R^2 dR \right\rangle_{\Omega_1, \Omega_2}. \quad (2.4)$$

Die Mittelung über die Orientierungen kann durch entsprechende Integration über die Eulerwinkel, die die gegenseitige Orientierung der Moleküle beschreiben, realisiert werden. Innere Freiheitsgrade werden dabei vernachlässigt, das heißt die Moleküle werden als starr angenommen.

Die erste Quantenkorrektur ist deutlich komplizierter als bei den einatomigen Gasen. Sie enthält neben der ersten Ableitung des Potentials nach dem Molekülabstand auch die ersten Ableitungen nach den Eulerwinkeln. Die entsprechenden Formeln wurden von Pack [38] für lineare Moleküle sowie sphärische und symmetrische Kreiselmoleküle und von Wormer [39] für asymmetrische Kreisel angegeben. Höhere Quantenkorrekturen sind für nichtlineare Moleküle bisher nicht abgeleitet worden. Um trotzdem eine Verbesserung gegenüber der ersten Quantenkorrektur zu erhalten, schlugen Takahashi und Imada [40] vor, das Wechselwirkungspotential $V(R, \Omega_1, \Omega_2)$ im Exponentialterm von Gleichung 2.4 durch ein effektives Potential $V_{\text{eff}}(R, \Omega_1, \Omega_2)$ zu ersetzen, ein Ansatz der auf die Pfadintegralmethode von Feynman [41, 42] zurückgeht. Das effektive Potential setzt sich dabei additiv aus dem Potential $V(R, \Omega_1, \Omega_2)$ und einem Ausdruck zusammen, der der ersten Quantenkorrektur entspricht. Durch Entwicklung der Exponentialfunktion erhält man eine unendliche Reihe von Quantenkorrekturen, wobei der erste Term der normalen ersten Quantenkorrektur entspricht. Die weiteren Quantenkorrekturen ergeben sich dann als Potenzen der ersten Quantenkorrektur,

was eine erhebliche Näherung darstellt. Schenter [43] verglich die mit dem Verfahren von Takahashi und Imada für Wasser erhaltenen Werte mit zweiten Virialkoeffizienten, die er exakt quantenmechanisch mit der Pfadintegralmethode von Feynman berechnete. Dieser exakte Ansatz ist sehr komplex und hat bisher keine weitere Anwendung im Schrifttum gefunden. Schenter konnte zeigen, dass die Methode von Takahashi und Imada eine erhebliche Verbesserung gegenüber der alleinigen Verwendung der ersten Quantenkorrektur darstellt.

Dritte Virialkoeffizienten sind bisher nicht für mehratomige Gase berechnet worden, da die Integration über die Orientierungen dreier Teilchen den Rechenaufwand erheblich erhöht. Prinzipiell ist die klassisch-mechanische Berechnung aber möglich. Quantenkorrekturen sind jedoch noch nicht abgeleitet worden.

2.2.2 Transport- und Relaxationseigenschaften

Um die Transport- und Relaxationseigenschaften von Gasen zu bestimmen, muss die Boltzmann-Gleichung, welche die Grundgleichung der kinetischen Gastheorie darstellt, gelöst werden. Dabei handelt es sich um eine nichtlineare Integro-Differentialgleichung, die die räumliche und zeitliche Entwicklung der Einteilchen-Verteilungsfunktion beschreibt. Die ursprünglich von Boltzmann formulierte Gleichung ist nur im klassisch-mechanischen Limit für einatomige Gase ohne innere Freiheitsgrade gültig. Sie lautet für reine Gase:

$$\frac{\partial f}{\partial t} + \mathbf{c} \cdot \nabla f + \frac{1}{m} \mathbf{F} \cdot \frac{\partial f}{\partial \mathbf{c}} = \int \int d\mathbf{e}' d\mathbf{c}_1 (f' f'_1 - f f_1) \sigma_{c_r}. \quad (2.5)$$

Dabei ist f die Einteilchen-Verteilungsfunktion, t die Zeit, \mathbf{c} der Teilchengeschwindigkeitsvektor, \mathbf{F} ein eventuell vorhandener äußerer Kraftvektor, \mathbf{e} der Richtungseinheitsvektor der Relativgeschwindigkeit c_r und σ der differentielle Streuquerschnitt. Der Index 1 bezeichnet die jeweiligen Größen für ein zweites Teilchen, die gestrichenen Größen beziehen sich auf Zustände vor dem Stoß zweier Teilchen und die ungestrichenen auf die Zustände nach dem Stoß. Die entsprechende quantenmechanische Boltzmann-Gleichung ist die Uehling-Uhlenbeck-Gleichung [44]. Später ist die Boltzmann-Gleichung auch für mehratomige Gase verallgemeinert worden, wobei im klassischen Limit die Curtiss-Kagan-Maksimov-Gleichung [45, 46, 47, 48] und im quantenmechanischen Fall die Waldmann-Snyder-Gleichung [49, 50] resultiert.

Die Lösung der Boltzmann-Gleichung für den globalen Gleichgewichtsfall ist die orts- und zeitunabhängige Maxwell-Verteilung (auch Maxwell-Boltzmann-Verteilung genannt); für ein lokales Gleichgewicht ist es die orts- und zeitabhängige lokale Maxwell-Verteilung. Eine allgemeine Lösung für den Nichtgleichgewichtsfall ist bisher nicht gefunden worden.

Jedoch sind es gerade Nichtgleichgewichtszustände, welche die unterschiedlichen Transport- und Relaxationsphänomene hervorrufen. Um also einen Formalismus zur Berechnung von Transport- und Relaxationseigenschaften zu entwickeln, muss eine Näherungslösung der Boltzmann-Gleichung für den Nichtgleichgewichtsfall gefunden werden.

Chapman und Enskog [51, 52] gelang es unabhängig voneinander, eine solche Lösung für einatomige Gase zu erhalten. Dabei nahmen sie an, dass die Abweichung vom Gleichgewicht gering ist, wodurch sich die Boltzmann-Gleichung linearisieren und folglich lösen ließ. Die von Chapman und Enskog gefundenen Ausdrücke für die Transportkoeffizienten sind jedoch noch nicht für praktische Berechnungen geeignet. Deshalb wird die Lösung der Boltzmann-Gleichung durch eine endliche Anzahl orthogonaler Basisfunktionen approximiert. Mit diesen Basisfunktionen lassen sich wiederum generalisierte Streuquerschnitte definieren, die bei Kenntnis des zwischenatomaren Wechselwirkungspotentials durch Berechnung klassischer oder, im Falle der Uehling-Uhlenbeck-Gleichung, quantenmechanischer Stoßtrajektorien bestimmt werden können. Die Transporteigenschaften können dann als relativ einfache Funktionen dieser Streuquerschnitte formuliert werden, wobei verschiedene Näherungsordnungen resultieren, je nachdem wieviele Basisfunktionen bzw. Streuquerschnitte verwendet werden. Eine exakte Lösung ist nur mit einem unendlich großen Basissatz möglich. Für weitere Details sei auf die umfangreiche Literatur zu dem Thema verwiesen [53, 54, 55, 56, 57].

Für mehrlatomige Gase können die entsprechenden verallgemeinerten Boltzmann-Gleichungen analog gelöst und die Lösungen durch orthogonale Basisfunktionen approximiert werden, aus denen wiederum generalisierte Streuquerschnitte resultieren. Der Formalismus dafür ist allerdings deutlich komplexer als für einatomige Gase. Die Beziehungen zur Berechnung klassischer generalisierter Streuquerschnitte sind nur für starre lineare Moleküle von Curtiss abgeleitet [58] und schließlich von Heck und Dickinson in einen Programmcode, TRAJECT, umgesetzt worden [59]. Mit diesem Code konnten erfolgreich die Transport- und Relaxationseigenschaften der reinen Gase Stickstoff, Kohlenmonoxid und Kohlendioxid berechnet werden, siehe hierzu unter anderem [60, 61, 62] und darin enthaltene Referenzen. Die Erweiterung der Theorie von Curtiss und des TRAJECT-Codes auf nichtlineare Moleküle ist Voraussetzung für die Berechnung der Transport- und Relaxationseigenschaften von Methan und Wasserdampf.

Es ist noch anzumerken, dass die vollständig quantenmechanische Berechnung von Transport- und Relaxationseigenschaften mehratomiger Gase bis heute aufgrund des zu hohen Rechenaufwandes praktisch nicht möglich ist. Für Stöße zwischen einem Heliumatom und einem Stickstoffmolekül wurden quantenmechanische Streuquerschnitte berechnet und mit

den entsprechenden klassischen Werten verglichen [63, 64]. Es zeigte sich, dass Quanteneffekte, abgesehen von tiefen Temperaturen, klein sind und für die meisten Anwendungen vernachlässigbar sein sollten.

3 Ergebnisse und Diskussion

3.1 *Ab initio*-Potentialenergiekurve für das Helium-Atompaar und thermophysikalische Eigenschaften des verdünnten Heliumgases

3.1.1 I. Interatomares Helium-Helium-Potential

Robert Hellmann, Eckard Bich, Eckhard Vogel
Mol. Phys. **105**, 3013-3023 (2007).

Ziel dieser Arbeit war es, eine vollständige Potentialenergiekurve für zwei Heliumatome mit der höchsten derzeit möglichen Genauigkeit zu bestimmen. Wie bereits in Abschnitt 2.1.1 dargelegt, waren hochpräzise Werte für die Wechselwirkungsenergie nur für sehr wenige zwischenatomare Abstände verfügbar. Auch waren relativistische Korrekturen und Korrekturen für die Born-Oppenheimer-Näherung nicht mit hoher Genauigkeit oder wenn dann nur für sehr wenige Abstände bekannt.

Da Programmcodes zur Berechnung von Wechselwirkungsenergien mit explizit korrelierten *Coupled-Cluster*-Methoden, wie sie unter anderem von Cencek *et al.* [12] sehr erfolgreich eingesetzt wurden, noch nicht allgemein verfügbar waren, mussten konventionelle Orbital-basierte Methoden angewendet werden. Um mit den explizit korrelierten Methoden dennoch konkurrieren zu können, sind extrem große Basissätze erforderlich. Der größte für Helium verfügbare Basissatz war der von Gdanitz konstruierte aug-cc-pV7Z [65], der allerdings nicht mit den regulären aug-cc-pVXZ-Basissätzen mit $X \leq 6$ konsistent ist und daher für Basissatzextrapolationen in Kombination mit den regulären Basissätzen weniger geeignet ist.

Zunächst wurde daher ein regulärer cc-pV7Z nach den Richtlinien von Dunning [66] konstruiert. Um daraus den aug-cc-pV7Z zu erhalten, wurden Diffusfunktionen in einer gegenüber der Originalvorschrift [67] abweichenden, jedoch gegenüber der Methode von Gdanitz deutlich systematischeren Weise generiert. Mit den so gewonnenen Erfahrungen

wurde analog ein aug-cc-pV8Z-Basissatz konstruiert. Die Erweiterung der Basissätze um einen weiteren Satz von Diffusfunktionen wurde nach der Standardprozedur durchgeführt [67]. So wurden auch die d-aug-cc-pV7Z und d-aug-cc-pV8Z-Basissätze erhalten.

Zuerst wurden counterpoise-korrigierte [29], supermolekulare CCSD-Rechnungen für 21 verschiedene Abstände $2,25 a_0 \leq R \leq 8 a_0$ mit den Basissätzen d-aug-cc-pV7Z und d-aug-cc-pV8Z durchgeführt, wobei jeweils ein großer Satz von Bindungsfunktionen, bestehend aus 4 s-, 4 p-, 3 d-, 3 f- und 2 g-Funktionen, mittig zwischen den beiden Heliumatomen hinzugefügt wurde. Pro Abstand R wurden so zwei Wechselwirkungsenergien erhalten, die zum Limit des vollständigen Basissatzes extrapoliert wurden. Die dabei verwendete Extrapolationsformel enthält einen freien Parameter, der für alle R gleichgesetzt und so gewählt wurde, dass der mit Gaussian-Geminal-Funktionen berechnete CCSD-Wert von Cencek *et al.* [12] für die Wechselwirkungsenergie bei $R = 4 a_0$ exakt wiedergegeben wird.

Als nächstes wurden in analoger Weise Wechselwirkungsenergien auf CCSD- und CCSDT-Niveau für die Basissätze d-aug-cc-pVXZ ($X = 4, 5, 6$) einschließlich Bindungsfunktionen berechnet und die Differenz der erhaltenen Wechselwirkungsenergien zu vollständigem Basissatz extrapoliert. Durch die Verwendung von drei Basissätzen bei der Extrapolation ist keine Anpassung eines Parameters wie bei den CCSD-Wechselwirkungsenergien nötig. Die Differenz im Basissatzlimit wurde zu den extrapolierten CCSD-Wechselwirkungsenergien hinzuaddiert und auf diese Weise das Basissatzlimit auf CCSDT-Niveau sehr genau abgeschätzt. Anschließend wurde die Differenz der CCSDT- und *full*-CI-Wechselwirkungsenergien mit dem d-aug-cc-pV5Z-Basissatz berechnet und ebenfalls hinzuaddiert.

Die so erhaltenen 21 Wechselwirkungsenergien entsprechen damit in etwa dem Basissatzlimit in der nichtrelativistischen Born-Oppenheimer-Näherung auf *full*-CI-Niveau. Die Wechselwirkungsenergie bei $5,6 a_0$ liegt mit $-11,001$ K im erwarteten Bereich, siehe Abschnitt 2.1.1.

Des Weiteren wurden mit der CCSD(T)-Methode und dem d-aug-cc-pV6Z-Basissatz die relativistischen Korrekturen für alle Abstände mit der Cowan-Griffin-Methode [18] berechnet. Die diagonale Born-Oppenheimer-Korrektur (DBOC) wurde ebenfalls für alle Abstände für das Isotop ^4He bestimmt. Als problematisch erwies sich dabei, dass die Berechnung der DBOC zum Zeitpunkt der Entstehung dieser Arbeit nicht mit *Coupled-Cluster*-Methoden, sondern nur auf SCF- oder CI-Niveau möglich war. Idealerweise würde man die DBOC mit großen Basissätzen auf *full*-CI-Niveau berechnen, was sich jedoch mit der aktuellen Rechentechnik als undurchführbar herausstellte. Daher wurden die Berechnungen zunächst mit der CISD-Methode und dem d-aug-cc-pV5Z-Basissatz durchgeführt, wobei zur Korrektur der fehlenden Größenkonsistenz ein modifizierter Supermolekülansatz verwendet wurde.

Dabei wurde zur Berechnung der DBOC-Korrektur für einen Abstand R die Energie eines Dimers bei einem extrem großem Abstand anstatt der Energien der Einzelatome von der Energie eines Dimers mit Abstand R subtrahiert. Bei diesem Ansatz ist keine Korrektur des Basissatzsuperpositionsfehlers (BSSE) möglich. Da die Elektronenkorrelation bei CISD-Rechnungen nur ungenügend beschrieben wird, wurde die DBOC außerdem auf CISD- und CISDT-Niveau mit dem d-aug-cc-pVQZ-Basissatz berechnet und die Differenz der beiden DBOC-Energien für jeden Abstand zu den entsprechenden CISD/d-aug-cc-pV5Z-Werten hinzuaddiert. Dadurch wird eine DBOC erhalten, die in etwa CISDT-Niveau mit dem Basissatz d-aug-cc-pV5Z entspricht. Der erhaltene Wert bei $R = 5,6 a_0$ ist mit $-9,3 \text{ mK}$ in hervorragender Übereinstimmung mit dem genauesten Wert aus dem Schrifttum von -9 mK , siehe Referenz [7] bei Cencek *et al.* [13].

Die Werte für die relativistischen Korrekturen und die DBOC wurden zu den zuvor erhaltenen Werten für das *full-CI*-Basissatzlimit hinzuaddiert. An die resultierenden 21 Werte der Wechselwirkungsenergie sowie 5 Werte von Komasa [6] für Abstände $R < 2,25 a_0$ (ergänzt um die beiden letztgenannten Korrekturen) wurde eine flexible analytische Potentialfunktion angepasst, wobei der Anpassungsfehler vernachlässigbar ist. Abschließend wurde die Korrektur für den Casimir-Polder-Effekt [15, 16] in die Potentialfunktion integriert. Dazu wurden die von Chen und Chung [17] berechneten Werte verwendet.

Während der Entstehung dieser Arbeit sind im Schrifttum weitere Arbeiten zum Helium-Helium-Potential erschienen. Hurly und Mehl [68] veröffentlichten 2007 eine Potentialfunktion, die sie an eine Reihe von Wechselwirkungsenergien anpassten, die aus verschiedenen Arbeiten des Schrifttums entnommen wurden. Mit diesem Potential berechneten sie unter anderem die zweiten Druckvirialkoeffizienten, die zweiten akustischen Virialkoeffizienten sowie Viskosität und Wärmeleitfähigkeit. Ebenfalls 2007 veröffentlichten Patkowski *et al.* [69] nichtrelativistische Wechselwirkungsenergien in der Born-Oppenheimer-Näherung für 12 verschiedene Abstände zwischen $3 a_0$ und $9 a_0$, die in sehr ähnlicher Weise wie von Cencek *et al.* [12] ermittelt wurden (siehe Abschnitt 2.1.1). Dabei erhielten sie bei $R = 5,6 a_0$ eine Wechselwirkungsenergie von $-11,0037 \text{ K}$. Ebenfalls 2007 publizierten Jeziorska *et al.* [70] neue SAPT-Wechselwirkungsenergien, die mit den Werten von Patkowski *et al.* kombiniert wurden, um eine analytische Potentialfunktion anzupassen. Die SAPT-Wechselwirkungsenergie bei $R = 5,6 a_0$ beträgt $-11,000 \text{ K}$. Für die Anpassung der Potentialfunktion wurden nur SAPT-Werte mit $R \geq 7 a_0$ verwendet und ansonsten die Werte von Patkowski *et al.*. In keiner dieser Arbeiten sind relativistische Effekte oder die DBOC berücksichtigt. In einer noch neueren Arbeit aus dem Jahr 2008 von Cencek und Szalewicz [71] wurden explizit korrelierte Gaussian-Funktionen (ECG) verwendet, um den

bisher genauesten Wert für die nichtrelativistische Wechselwirkungsenergie in der Born-Oppenheimer-Näherung bei $R = 5,6a_0$ zu bestimmen. Dabei wurden eine strikte Obergrenze von $-11,00035$ K und ein Basissatzlimit von $-11,0006$ K ermittelt. Die extrem geringe Abweichung zu dem in der vorliegenden Arbeit erhaltenen Wert von $11,001$ K für die Potentialtiefe unterstreicht die hohe Qualität des an der Universität Rostock entwickelten Potentials. Leider enthält die Arbeit von Cencek und Szalewicz keinen Verweis auf die Rostocker Arbeit, obwohl Cencek und Szalewicz ihr Manuskript mehrere Monate nach deren Erscheinen einreichten.

Insgesamt ist festzustellen, dass das in Rostock generierte Wechselwirkungspotential allen bis einschließlich 2008 publizierten Potentialen überlegen ist.

3.1.2 II. Thermophysikalische Standardwerte für Helium bei niedrigen Dichten

Eckard Bich, Robert Hellmann, Eckhard Vogel
Mol. Phys. **105**, 3035-3049 (2007).

In dieser Arbeit sollte das in der vorhergehenden vorgestellte Helium-Helium-Potential genutzt werden, um extrem genaue Referenzwerte für die zweiten und dritten Druckvirialkoeffizienten, die Scherviskosität und die Wärmeleitfähigkeit der Isotope ^3He und ^4He über einen großen Temperaturbereich zu bestimmen.

Genauere Werte für die Druckvirialkoeffizienten werden unter anderem in der Helium-Gasthermometrie zur Festlegung der Temperaturskala und bei der hochpräzisen Bestimmung der Boltzmann-Konstante benötigt, siehe beispielsweise [72]. Für die Kalibrierung von Apparaturen zur Messung der Scherviskosität und der Wärmeleitfähigkeit von Gasen sind zuverlässige Referenzwerte dieser Transporteigenschaften erforderlich. Diese können zur Zeit mit keinem absoluten Messverfahren so genau ermittelt werden, wie es durch Berechnung mit der kinetischen Gastheorie bei Verwendung eines akkuraten Wechselwirkungspotentials möglich ist.

Alle in dieser Arbeit berechneten Eigenschaften wurden mit der jeweils genauesten bekannten Theorie ermittelt. Der zweite Druckvirialkoeffizient wurde im Temperaturintervall von 1 K bis $10\,000$ K exakt quantenmechanisch berechnet, wobei zu berücksichtigen war, dass ^3He ein Fermion und ^4He ein Boson ist, so dass für die beiden Isotope unterschiedliche Quantenstatistiken anzuwenden sind. Für die Berechnung des zweiten Druckvirialkoeffizienten müssen zudem alle Bindungszustände bekannt sein. Für das ^3He -Atompaar wurde

kein Bindungszustand gefunden, für das ^4He -Atompaar einer mit einer Bindungsenergie von nur 1,64 mK. Experimentell wurden Werte von 1 mK [73] und $(1,1 + 0,3 / - 0,2)$ mK [74] bestimmt. Die Analyse der Bindungszustände wurde mit dem Programm Level 7.7 von LeRoy [75] durchgeführt. Für die Berechnung des dritten Druckvirialkoeffizienten von ^4He wurde die klassische Formel einschließlich der ersten Quantenkorrektur sowie einer Korrektur für die Nichtadditivität der paarweisen Wechselwirkungen nach Axilrod und Teller [35, 36] genutzt. Da dieser Ansatz bei sehr tiefen Temperaturen versagt, wurde hier als tiefste Temperatur 20 K gewählt. Für ^3He wurden keine dritten Druckvirialkoeffizienten berechnet, da diese in der Praxis nur eine geringe Rolle spielen. Die Berechnung der Scherviskosität und der Wärmeleitfähigkeit im Limit von Nulldichte erfolgte vollständig quantenmechanisch für die fünfte Näherung der kinetischen Gastheorie. Eine solch hohe Näherung der kinetischen Theorie ist dabei eigentlich nicht notwendig, da bereits die dritte ausreichend ist, um Viskosität und Wärmeleitfähigkeit mit einer Unsicherheit von weniger als $\pm 0,01\%$ zu erhalten.

Es ist davon auszugehen, dass die Unsicherheiten der berechneten thermophysikalischen Eigenschaften durch die Unsicherheit des Wechselwirkungspotentials dominiert werden, abgesehen vom dritten Druckvirialkoeffizienten bei tieferen Temperaturen. Für die Transporteigenschaften wurde die Unsicherheit konservativ mit $\pm 0,02\%$ für Temperaturen über 15 K abgeschätzt.

Die für alle thermophysikalischen Eigenschaften erhaltenen Werte wurden mit den experimentellen Daten des Schrifttums und mit den von Hurly und Mehl [68] berechneten verglichen. Dabei zeigte sich im Allgemeinen, dass die Differenzen zwischen den mit dem Potential dieser Arbeit und den mit dem Potential von Hurly und Mehl berechneten Werten viel kleiner sind als die Streuungen der experimentellen Daten untereinander, obwohl das Potential von Hurly und Mehl deutlich ungenauer als das dieser Arbeit ist. Es sind daher durch künftige Verbesserungen des Wechselwirkungspotentials nur noch minimale Änderungen der berechneten Eigenschaften zu erwarten.

3.2 *Ab initio*-Potentialenergiekurve für das Neon-Atompaar und thermophysikalische Eigenschaften des verdünnten Neongases

3.2.1 I. Interatomares Neon-Neon-Potential und Rotations-Schwingungsspektren

Robert Hellmann, Eckard Bich, Eckhard Vogel
Mol. Phys. **106**, 133-140 (2008).

Nachdem für Helium ein hochgenaues Wechselwirkungspotential ermittelt wurde und damit Referenzwerte für verschiedene thermophysikalische Eigenschaften bestimmt wurden, sollte versucht werden, diese Berechnungen auf Neon auszudehnen. Dabei war von vornherein klar, dass die erreichbare Genauigkeit deutlich geringer sein würde als bei Helium, da Neon gegenüber Helium die fünffache Elektronenzahl aufweist, was den Aufwand für die quantenchemische *ab initio*-Berechnung der Potentialkurve um ein Vielfaches erhöht und folglich die Grenzen bezüglich der einsetzbaren Methoden und der Größe der Basissätze gegenüber Helium stark einschränkt.

Zunächst wurden für 32 Abstände R mit $1,4\text{Å} \leq R \leq 8\text{Å}$ counterpoise-korrigierte [29], supermolekulare *frozen-core*-CCSD(T)-Rechnungen mit den Basissätzen t-aug-cc-pV5Z und t-aug-cc-pV6Z durchgeführt. In beiden Fällen wurde wie schon bei Helium ein aus 4 s-, 4 p-, 3 d-, 3 f- und 2 g-Funktionen bestehender Satz von Bindungsfunktionen hinzugefügt. Eine Zweipunkt-Extrapolationsformel wurde verwendet, um die resultierenden Wechselwirkungsenergien zum Limit des vollständigen Basissatzes zu extrapolieren.

Da die Berechnungen in der *frozen-core*-Approximation durchgeführt wurden, war es erforderlich, die Effekte von Kern-Kern- und Kern-Valenz-Korrelation abzuschätzen. Dazu wurden für alle Abstände R sowohl *frozen-core*-CCSD(T)- als auch *full*-CCSD(T)-Berechnungen der Wechselwirkungsenergie mit dem d-aug-cc-pwCV5Z-Basissatz durchgeführt. Die Differenzen wurden zum Basissatzlimit der *frozen-core*-CCSD(T)-Wechselwirkungsenergien hinzuaddiert. Dadurch wird das *full*-CCSD(T)-Basissatzlimit angenähert.

Im Rahmen der *full*-CCSD(T)-Berechnungen mit dem d-aug-cc-pwCV5Z-Basissatz wurden auch die relativistischen Cowan-Griffin-Korrekturen [18] berechnet. Diese sind für Neon deutlich größer als für Helium, da der Einfluss der relativistischen Korrekturen bezüglich der elektronischen Energie eines Atoms allgemein in etwa mit der vierten Potenz der Kernladungszahl anwächst, was sich letztlich auch auf die Wechselwirkungsenergien auswirkt.

Wie bereits in Abschnitt 2.1.2 erwähnt, ist es besonders wichtig, *Coupled-Cluster*-Methoden zu nutzen, die über das CCSD(T)-Niveau hinausgehen, um eine signifikante Verbesserung gegenüber früheren *ab initio*-Potentialen zu erzielen. Nimmt man in guter Näherung an, dass relativistische Effekte und Kern-Kern- und Kern-Valenz-Korrelation die Größe dieser höheren *Coupled-Cluster*-Beiträge nicht signifikant beeinflussen, so können diese nichtrelativistisch mit der *frozen-core*-Näherung bestimmt werden. Die Differenz zwischen CCSDT- und CCSD(T)-Wechselwirkungsenergien wurde so mit einem d-aug-cc-pVQZ-Basissatz berechnet, wobei auch ein kleiner Satz von Bindungsfunktionen, bestehend aus 3 s-, 3 p- und 2 d-Funktionen sowie einer f-Funktion, verwendet wurde. Weiterhin wurde analog auch die Differenz zwischen CCSDT(Q)- und CCSDT-Wechselwirkungsenergien mit einem aug-cc-pVTZ-Basissatz und dem gleichen Satz von Bindungsfunktionen ermittelt. Beide Korrekturen wurden zu den Wechselwirkungsenergien hinzuaddiert, wobei letztere Korrektur sehr klein ist, was vermuten lässt, dass noch höhere *Coupled-Cluster*-Beiträge vernachlässigbar sein sollten.

An die 32 berechneten Wechselwirkungsenergien wurde eine analytische Potentialfunktion angepasst. Bis auf den höchsten Wert bei $R = 8 \text{ \AA}$ ist die Abweichung zwischen berechneten und gefitteten Werten kleiner als $\pm 0,1\%$. Eine Retardationskorrektur nach Casimir und Polder [15, 16] ist für zwei Neonatome bisher nicht berechnet worden. Eigene Rechnungen dazu hätten den Umfang der vorliegenden Dissertation deutlich erweitert und wurden daher nicht versucht.

Für das so erhaltene Wechselwirkungspotential sowie für die Potentiale von Wüest und Merkt [25], Cybulski und Toczyłowski [22] und Aziz und Slaman [19] wurden mit dem Programm Level 7.7 von LeRoy [75] die Rotations-Schwingungsspektren der ^{20}Ne - ^{20}Ne - und ^{22}Ne - ^{20}Ne -Dimere berechnet und mit dem experimentellen Spektrum von Wüest und Merkt verglichen. Außerdem wurden einige von Gdanitz [23] für sein Potential berechnete charakteristische Größen des Rotations-Schwingungsspektrums in den Vergleich mit einbezogen. Insgesamt zeigte sich, dass die Potentiale von Wüest und Merkt, Aziz und Slaman und der vorliegenden Arbeit die experimentellen Daten sehr gut wiedergeben, während für die Potentiale von Cybulski und Toczyłowski sowie Gdanitz deutliche Abweichungen resultieren. Da die Rotations-Schwingungsspektren sehr empfindlich bezüglich des attraktiven Teils des Potentials sind, aber relativ unempfindlich bezüglich des repulsiven Teils, müssen weitere Eigenschaften untersucht werden, um die Qualität der verschiedenen Potentiale genauer beurteilen zu können. Dies ist Schwerpunkt der folgenden Arbeit.

3.2.2 II. Thermophysikalische Eigenschaften von Neon bei niedrigen Dichten

Eckard Bich, Robert Hellmann, Eckhard Vogel

Mol. Phys. **106**, 1107-1122 (2008).

Mit dem neuen Neon-Neon-Wechselwirkungspotential sollten wie schon für Helium die zweiten und dritten Druckvirialkoeffizienten, die Scherviskosität und die Wärmeleitfähigkeit mit der jeweils besten verfügbaren Theorie berechnet werden. Das ist komplizierter als bei den Heliumisotopen, da Neon immer als Mischung der Isotope ^{20}Ne , ^{21}Ne und ^{22}Ne in der Natur vorkommt. Um die höchste mögliche Genauigkeit zu erzielen, müssen daher alle möglichen Wechselwirkungen der einzelnen Isotope untereinander untersucht werden.

Für die Berechnung des zweiten Druckvirialkoeffizienten wurde für jede der sechs möglichen Isotopenkombinationen bezüglich der Wechselwirkung zweier Teilchen ein individueller zweiter Druckvirialkoeffizient vollständig quantenmechanisch berechnet. Dabei waren aufgrund der verschiedenen Quantenstatistiken für die jeweiligen Isotopenkombinationen sehr unterschiedliche Berechnungsformeln erforderlich. In die Berechnungen gingen außerdem die bereits in der vorhergehenden Arbeit diskutierten Bindungszustände der jeweiligen Dimere ein. Aus den sechs so erhaltenen zweiten Druckvirialkoeffizienten wurde der zweite Druckvirialkoeffizient der Gesamtmischung durch entsprechende Molenbruchwichtung erhalten.

Als alternativer Ansatz zur Ermittlung des zweiten Druckvirialkoeffizienten wurde die klassisch-mechanische Beziehung einschließlich Quantenkorrekturen getestet. Für deren Berechnung wurde Neon als reines Gas mit einer mittleren Isotopenmasse angenommen. Der klassische Anteil ist massenunabhängig. Es zeigte sich, dass die Übereinstimmung mit den exakt quantenmechanischen Berechnungen umso besser wird, je mehr Quantenkorrekturen berücksichtigt wurden, wobei solche bis einschließlich dritter Ordnung notwendig waren, um auch bei den tiefsten Temperaturen sehr gute Übereinstimmung zu erhalten.

Der dritte Druckvirialkoeffizient wurde klassisch-mechanisch unter Einbeziehung der Quantenkorrektur erster Ordnung berechnet. Die Nichtadditivität der paarweisen Wechselwirkungen wurde mittels der Axilrod-Teller-Formel [35, 36] korrigiert.

Die Transporteigenschaften sollten wie schon bei Helium vollständig quantenmechanisch für die fünfte Näherung der kinetischen Gastheorie berechnet werden. Da eine solch hohe Näherung für Mischungen nicht verfügbar ist, wurde die kinetische Theorie erster Näherung für Gasmischungen verwendet. Die darin auftretenden Wechselwirkungsviskositäten bzw. -wärmeleitfähigkeiten für die sechs Isotopenkombinationen wurden dabei wie für ein

reines Gas für die fünfte Näherung berechnet. In einer zweiten Variante wurden die Transporteigenschaften zunächst quantenmechanisch für die erste Näherung der kinetischen Theorie von Gasmischungen berechnet. Anschließend wurden die Beiträge höherer Näherungen unter der Annahme berechnet, dass Neon als reines Gas mit mittlerer Isotopenmasse aufgefasst werden kann, wobei die in der Isotopenmischung am häufigsten vorkommende Quantenstatistik verwendet wurde. Beide Ansätze lieferten praktisch identische Ergebnisse.

Alle thermophysikalischen Eigenschaften wurden für den Temperaturbereich von 25 K bis 10 000 K mit den schon in der vorherigen Arbeit getesteten Potentialen berechnet. Die experimentellen Daten für die zweiten und dritten Druckvirialkoeffizienten erwiesen sich allerdings als zu ungenau, um die Qualität der verschiedenen Potentiale einem strengen Test zu unterziehen. Bei den Transporteigenschaften resultierten für das Potential von Wüest und Merkt [25] erhebliche Abweichungen von den meisten experimentellen Daten. Das liegt daran, dass Wüest und Merkt ihr Potential nur an die Rotations-Schwingungsspektren anpassten, die keine Aussage über den repulsiven Teil des Potentials erlauben. Mit den Potentialen von Cybulski und Toczyłowski [22] und Aziz und Slaman [19] wurden deutlich kleinere Abweichungen erhalten. Allerdings beschreibt das vorgestellte neue Potential als einziges die genauesten Raumtemperaturwerte der Viskosität und der Wärmeleitfähigkeit innerhalb der experimentellen Fehlerschranken. Aus dem umfassenden Vergleich mit den experimentellen Daten kann die Unsicherheit der berechneten Viskositäts- und Wärmeleitfähigkeitswerte mit etwa $\pm 0,1\%$ abgeschätzt werden.

3.3 *Ab initio*-Wechselwirkungspotentialenergiefläche und zweite Druckvirialkoeffizienten des Methans

Robert Hellmann, Eckard Bich, Eckhard Vogel

J. Chem. Phys. **128**, 214303(1-9) (2008).

In dieser Arbeit sollte das Wechselwirkungspotential zweier Methan-Moleküle als Funktion des Abstandes und der gegenseitigen Orientierung der Monomere ermittelt werden. Dazu wurden counterpoise-korrigierte Supermolekülrechnungen für 17 verschiedene Winkelkonfigurationen (Abb. 3.1) durchgeführt. Pro Winkelkonfiguration wurden jeweils 16 Schwerpunktabstände R mit $2,25 \text{ \AA} \leq R \leq 8 \text{ \AA}$ berücksichtigt, so dass insgesamt 272 Wechselwirkungsenergien auf der Potentialhyperfläche resultierten. Dabei wurde die CCSD(T)-Methode in der *frozen-core*-Näherung mit den Basissätzen aug-cc-pVTZ und aug-cc-pVQZ angewendet. Die erhaltenen Wechselwirkungsenergien wurden dann zum Limit des vollständigen Basissatzes extrapoliert. Die Monomergeometrien wurden bei allen Berechnungen als starr angenommen, wobei die CH-Bindungslängen auf den nullpunktsschwingungsgemittelten Wert von $1,099 \text{ \AA}$ festgelegt wurden. Dieser Wert ergibt sich sowohl aus experimentellen [76] als auch aus theoretischen [77, 78] Untersuchungen und ist daher als gesichert anzusehen.

An die berechneten Wechselwirkungsenergien wurde eine *site-site*-Potentialfunktion mit neun Wechselwirkungszentren pro Methan-Molekül angepasst. Dabei befindet sich ein Wechselwirkungszentrum im Massenschwerpunkt (Kohlenstoffatom), vier befinden sich auf der CH-Bindung sehr dicht am Wasserstoff und weitere vier liegen oberhalb der Dreiecksflächen der Methan-Tetraeder. Bei der Anpassung wurden Zwangsbedingungen bezüglich einiger Potentialparameter verwendet. So wurden die Partialladungen der Wechselwirkungszentren an das Oktupolmoment des freien Monomers adjustiert. Die Dispersionskoeffizienten wurden so bestimmt, dass für $R \rightarrow \infty$ die korrekten Grenzwerte, also der isotrope C_6 -Koeffizient und der isotrope Anteil $C_{8,iso}$ des C_8 -Koeffizienten, resultierten. Während letzterer mit ausreichender Genauigkeit im Schrifttum verfügbar ist, wurde ersterer durch supermolekulare Berechnungen bei sehr großen Molekülabständen im Rahmen der vorliegenden Arbeit ermittelt. Die Abweichungen zwischen berechneten und gefitteten Wechselwirkungsenergien sind meist kleiner als 2%. Größere Abweichungen treten nur bei sehr kleinen Abständen und bei den Nulldurchgängen auf. Die maximale Potentialtiefe beträgt $273,9 \text{ K}$ bei $R = 3,633 \text{ \AA}$ von Orientierung 1 in Abb. 3.1.

Mit der erhaltenen Potentialhyperfläche wurde der zweite Druckvirialkoeffizient als Funk-

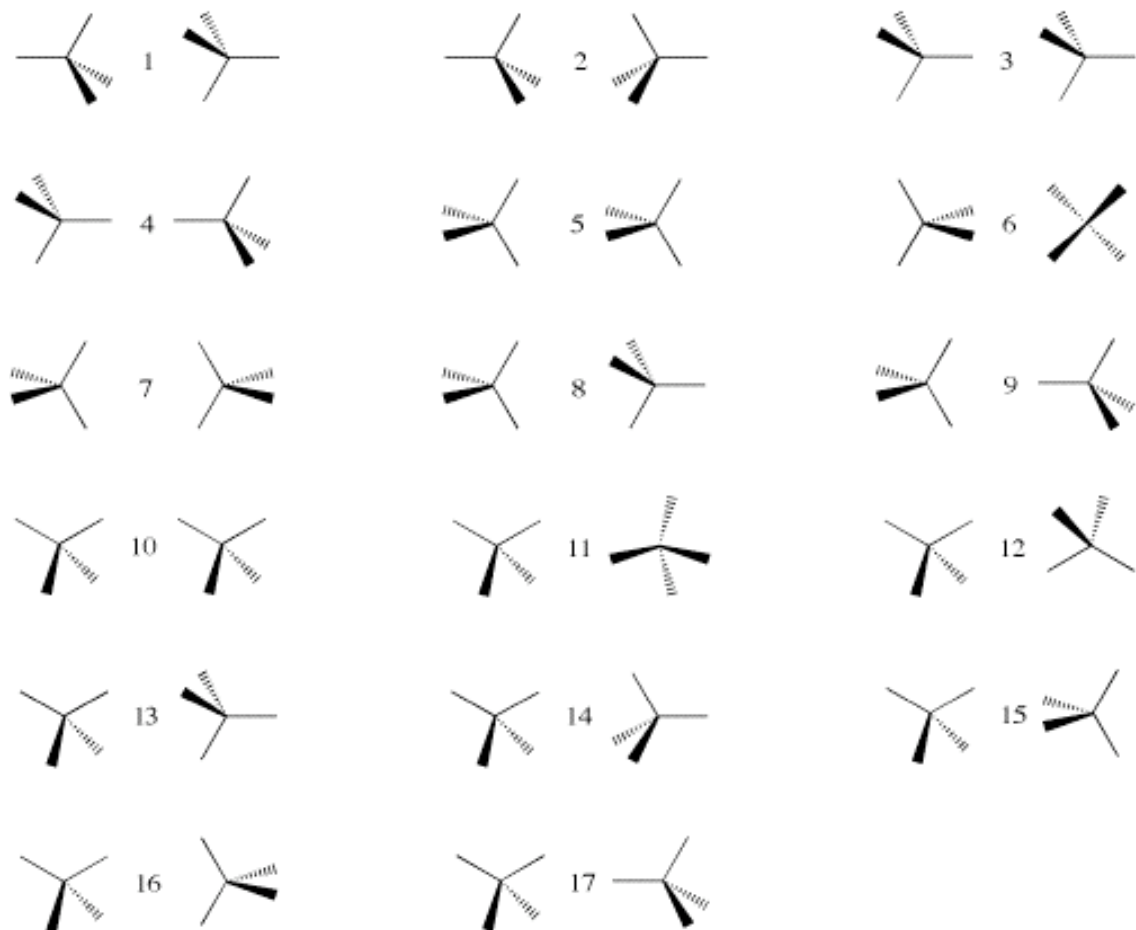


Abbildung 3.1: Gegenseitige Orientierungen der Methan-Moleküle für die Bestimmung der Potentialhyperfläche.

tion der Temperatur nach der Methode von Takahashi und Imada [40] berechnet. Dabei ergaben sich große Abweichungen zwischen experimentellen und berechneten Werten, die nur dadurch erklärt werden können, dass die Potentialhyperfläche zu repulsiv ist. *Ab initio*-Berechnungen zur Polarisierbarkeit von Methan [79, 80] zeigten, dass diese durch die Nullpunktsschwingungen deutlich vergrößert wird. Die Nullpunktsschwingungen sind allerdings nur durch die Verwendung der schwingungsgemittelten Geometrie der Methan-Moleküle in den supermolekularen *ab initio*-Berechnungen berücksichtigt. Damit lässt sich erklären, warum der direkt mit der Polarisierbarkeit zusammenhängende C_6 -Koeffizient nach der Supermolekülmethode etwa 5% kleiner ist als der sehr genaue experimentelle Wert [81], der durch die Nullpunktsschwingungen beeinflusst ist. Mit der Annahme, dass für $C_{8,iso}$ die gleiche relative Abweichung resultiert, wurde eine einfache isotrope additive Korrektur für das Wechselwirkungspotential entwickelt, die einen frei anpassbaren Parame-

ter enthält. Dieser wurde so gewählt, dass der nach der Methode von Takahashi und Imada berechnete zweite Druckvirialkoeffizient bei Raumtemperatur den genauesten experimentellen Wert, der von Kleinrahm *et al.* [82] mit einer Zwei-Senkkörper-Dichtemessanlage bestimmt wurde, exakt reproduziert. Durch diese Korrektur erhöht sich die Potentialtiefe auf 286,0 K bei 3,624 Å. Die Abweichungen zwischen den verfügbaren experimentellen Daten und den mit dem korrigierten Potential berechneten Werten liegen für den gesamten Temperaturbereich meist innerhalb der experimentellen Unsicherheiten. Die berechneten Werte können daher als Referenzdaten empfohlen werden. Vor allem bei tiefen Temperaturen, bei denen nur wenige und zudem durch große Unsicherheiten charakterisierte experimentelle Daten vorliegen, ergibt sich durch die berechneten Werte eine deutliche Verbesserung der Datenlage.

3.4 Transporteigenschaften asymmetrischer Kreisel­moleküle

Alan S. Dickinson, Robert Hellmann, Eckard Bich, Eckhard Vogel

Phys. Chem. Chem. Phys. **9**, 2836-2843 (2007).

Zur Berechnung der Transport- und Relaxationseigenschaften von Methan und Wasserdampf bei kleinen Dichten ist die kinetische Theorie molekularer Gase in klassisch-mechanischer Näherung unter Annahme starrer Moleküle die Methode der Wahl. Obwohl Curtiss die entsprechende verallgemeinerte Boltzmann-Gleichung (die Curtiss-Kagan-Maksimov-Gleichung) sowohl für lineare [45] als auch für nichtlineare Moleküle [46] formulierte, entwickelte er nur für lineare Moleküle den Formalismus zur Berechnung der generalisierten Streuquerschnitte [58], die für die Berechnung der Transport- und Relaxationseigenschaften benötigt werden. Das Ziel dieser Arbeit bestand deshalb darin, den Formalismus für die klassisch-mechanische Berechnung von generalisierten Streuquerschnitten auf nichtlineare Moleküle zu erweitern und in einen Computercode umzusetzen.

Um den Aufwand so gering wie möglich zu halten, wurden die gleichen Basisfunktionen (abgesehen von der Normierung) wie für lineare Moleküle verwendet. Dabei ist anzumerken, dass mit diesen Basisfunktionen im Fall von symmetrischen und asymmetrischen Kreisel­molekülen nie das Limit eines vollständigen Basissatzes erreicht werden kann, da sie nur die Ausrichtung des Drehimpulsvektors im Laborsystem, nicht jedoch seine Ausrichtung relativ zum Trägheitsellipsoid explizit berücksichtigen. Lediglich über die Rotationsenergie, von der die Basisfunktionen auch abhängen, erfolgt eine implizite Berücksichtigung. Durch diese Basisfunktionen kann daher für die Einteilchen-Verteilungsfunktion ein Nichtgleichgewichtszustand (eine so genannte Polarisierung) bezüglich der Ausrichtung der Drehimpulsvektoren relativ zu den Trägheitsellipsoiden nur unzureichend dargestellt werden. Es erfolgt letztlich neben der impliziten Berücksichtigung durch die Rotationsenergie eine Mittelung der Einteilchen-Verteilungsfunktion über die Ausrichtung der Drehimpulsvektoren relativ zu den Trägheitsellipsoiden. Bei linearen Molekülen tritt dieses Problem nicht auf, da das Trägheitsellipsoid in diesen Fällen eine Kreisscheibe ist, wobei der Drehimpulsvektor in der Kreisscheibe liegt, sodass das Trägheitsmoment immer konstant ist und folglich keine entsprechende Polarisierung möglich ist. Bei sphärischen Kreisel­molekülen ist das Trägheitsellipsoid eine Kugel, so dass auch hier keine entsprechende Polarisierung auftreten kann, da immer das gleiche Trägheitsmoment wirkt. Damit ist auch klar, dass für symmetrische und asymmetrische Kreisel­moleküle der Effekt der Polarisierung der Drehimpulsvektoren bezüglich der Ausrichtung relativ zu den Trägheitsellipsoiden umso größer ist, je stärker anisotrop

die Trägheitsellipsoide sind. Jedoch kann intuitiv vermutet werden, dass der generelle Einfluss dieser Art von Polarisation auf die Werte der Transport- und Relaxationseigenschaften deutlich kleiner sein sollte als der Einfluss einer Polarisation bezüglich der räumlichen Ausrichtung der Drehimpulsvektoren im Laborsystem. Erfahrungsgemäß ist jedoch der explizite (nicht gemittelte) Einfluss letzterer Polarisation auf die Werte der klassischen Transporteigenschaften Viskosität, Wärmeleitfähigkeit und Diffusion schon sehr gering (meist $< 1\%$), sodass der explizite Einfluss der Polarisation der Drehimpulsvektoren bezüglich ihrer Ausrichtung relativ zu den Trägheitsellipsoiden in den meisten Fällen vernachlässigbar klein sein sollte. Bei der Beschreibung des Einflusses eines magnetischen oder elektrischen Feldes auf die Transporteigenschaften ist dieser Einfluss wahrscheinlich nicht mehr vernachlässigbar.

Durch die Verwendung der vereinfachten Basisfunktionen verläuft die Herleitung der Formeln für die generalisierten Streuquerschnitte im Fall von asymmetrischen Kreiselmolekülen weitestgehend analog zur Herleitung für lineare Moleküle. Dabei müssen vor allem unterschiedliche Normierungsfaktoren, die unterschiedlichen klassischen Wärmekapazitäten und zusätzliche Mittelungen über die Variablen, die die Lage des Drehimpulsvektors relativ zum Trägheitsellipsoid beschreiben, berücksichtigt werden. Die Transformation der Streuquerschnitte vom Massenschwerpunktssystem zweier stoßender Moleküle in das Laborsystem verläuft exakt wie bei linearen Molekülen. Im Ergebnis der Ableitungen zeigte sich, dass aufgrund der Verwendung der gleichen Basisfunktionen die Streuquerschnitte für nichtlineare Moleküle die gleiche Grundstruktur wie die für lineare Moleküle haben. Die Formeln für die Transport- und Relaxationseigenschaften als Funktion der Streuquerschnitte entsprechen ebenfalls denen linearer Moleküle, wobei die Streuquerschnitte alle relevanten Informationen über das Wechselwirkungspotential sowie über die Geometrie der Moleküle enthalten.

Für die Umsetzung in einen Computercode sollte der für lineare Moleküle bereits vorhandene Code TRAJECT [59] als Basis dienen. Die Routinen für die Berechnung der Stoßtrajektorien, die die Grundlage für die Berechnung der Streuquerschnitte bilden, wurden neu geschrieben, so dass Stöße sowohl zwischen linearen als auch zwischen nichtlinearen Molekülen präzise durch numerische Integration der Hamilton-Gleichungen berechnet werden können. Die erforderlichen Ableitungen des zwischenmolekularen Wechselwirkungspotentials nach den so genannten *action-angle*-Variablen, die zur Beschreibung der Stoßdynamik verwendet werden, wurden analytisch formuliert, wobei der Aufwand gegenüber linearen Molekülen erheblich vergrößert ist. Die Korrektheit der analytischen Ableitungen wurde überprüft, indem numerische Ableitungen zum Vergleich berechnet wurden. Für die

Berechnung der generalisierten Streuquerschnitte asymmetrischer Kreiselmoleküle ist es erforderlich, 14-dimensionale Integrale (10-dimensionale für lineare Moleküle) über den Phasenraum der Anfangszustände zweier Moleküle vor dem Stoß zu berechnen, wobei der Integrand jeweils von der Art des zu berechnenden Streuquerschnittes sowie von den Anfangs- und Endzuständen der Trajektorie abhängt. Während die Integration über die Gesamtenergie als letztem Integrationsschritt nach einem komplexen und sehr genauen Integrationsverfahren durchgeführt wird, werden die anderen 13 Integrationen so transformiert, dass sie durch eine Monte-Carlo-Mittelung über einzelne Trajektorien ersetzt werden können.

Es bleibt anzumerken, dass sphärische und symmetrische Kreisel sowohl im Rahmen der klassischen Hamilton-Mechanik als auch der klassischen kinetischen Gastheorie als Spezialfälle des asymmetrischen Kreisels aufgefasst werden können. Im Rahmen der Erweiterung des TRAJECT-Codes wurde dieser von FORTRAN-77 in Fortran 95 umgeschrieben; dabei wurden veraltete Konstrukte wie COMMON-Blöcke, GOTO-Anweisungen usw. entfernt. Der Code soll in Zukunft für Gasmischungen erweitert und dann veröffentlicht werden.

3.5 Berechnung der Transport und Relaxationseigenschaften des Methans

3.5.1 I. Scherviskosität, viskomagnetische Effekte und Selbstdiffusion

Robert Hellmann, Eckard Bich, Eckhard Vogel, Alan S. Dickinson, Velisa Vesovic
J. Chem. Phys. **129**, 064302(1-13) (2008).

Die zuvor beschriebenen Erweiterungen der kinetischen Gastheorie sollten in dieser Arbeit auf das neue Methan-Wechselwirkungspotential angewendet werden, um die Scherviskosität, die viskomagnetischen Effekte und den Selbstdiffusionskoeffizienten von Methan im Limit von Nulldichte und im Temperaturbereich von 80 K bis 1500 K zu berechnen. Wie schon bei den Arbeiten zu Helium und Neon ermöglicht der Vergleich zwischen berechneten Werten und experimentellen Daten für die Scherviskosität eine eindeutige Aussage über die Qualität des Wechselwirkungspotentials, da diese Transporteigenschaft experimentell am besten zugänglich ist.

Die in dieser und der folgenden Arbeit benötigten generalisierten Streuquerschnitte wurden mit der neuen erweiterten Version des TRAJECT-Codes berechnet, wobei in das Wechselwirkungspotential die Korrektur für die Nullpunktsschwingungen eingeschlossen wurde. Zunächst wurden energieabhängige Streuquerschnitte für 29 verschiedene Gesamtenergien (Translation und Rotation) im Bereich von 20 K bis 40 000 K berechnet. Zu jeder Energie wurden bis zu 1 000 000 Trajektorien berechnet. Lediglich bei sehr niedrigen Energien musste die Zahl der Trajektorien erheblich reduziert werden, da der Rechenaufwand zu niedrigen Stoßenergien erheblich ansteigt. Für jede Trajektorie wurde der Anfangsabstand der Teilchen vor dem Stoß so gewählt, dass diese genügend weit voneinander entfernt sind, so dass der Einfluss des Potentials verschwindet. Dabei ist nur wichtig, dass der Abstand groß genug ist, wie groß genau spielt keine Rolle. Die hohe Anzahl der pro Energie berechneten Trajektorien sorgt dafür, dass der Phasenraum der Startbedingungen sehr dicht abgetastet wird, so dass selbst die relativ ungenaue Monte-Carlo-Methode für die Integration über den Phasenraum numerisch konvergierte Streuquerschnitte liefert. Durch präzise Integration der energieabhängigen Streuquerschnitte über die Gesamtenergie einschließlich entsprechender Wichtung wurden die temperaturabhängigen generalisierten Streuquerschnitte erhalten, die Ausgangspunkt für die Berechnung der verschiedenen Transport- und Relaxationseigenschaften sind. Die CPU-Zeit für die TRAJECT-Rechnungen betrug insgesamt etwa 11 Tage auf einem 2,5 GHz PPC970MP-Prozessorkern einer Linux-Workstation unter Verwendung

eines hochoptimierenden Compilers.

Die Scherviskosität wurde mit den aus den TRAJECT-Rechnungen erhaltenen generalisierten Streuquerschnitten für die dritte Näherung der kinetischen Theorie berechnet. Der Unterschied zwischen der dritten und der zweiten Näherung ist im betrachteten Temperaturintervall sehr klein, höchstens 0,04%, während der Unterschied zwischen erster und zweiter Näherung bei maximal etwa 0,6% liegt. Der Beitrag der Drehimpulspolarisation, der erstmals in der zweiten Näherung auftritt, ist nie größer als 0,1%.

Der Vergleich der berechneten Viskositäten mit den sehr genauen experimentellen Daten von May *et al.* [83], die 2007 am *National Institute of Standards and Technology* (NIST) bestimmt wurden und eine Unsicherheit von weniger als $\pm 0,1\%$ aufweisen, ergibt im Temperaturbereich der Messungen von 210 K bis 390 K systematische Differenzen (bezogen auf die berechneten Werte) von $-0,52\%$ bis $-0,66\%$. In diesem Zusammenhang ist darauf hinzuweisen, dass kürzlich in der eigenen Arbeitsgruppe Präzisionsmessungen mit einem Schwingscheibenviskosimeter zwischen 290 K und 680 K durchgeführt wurden, die noch nicht veröffentlicht sind. Die Messungen erbrachten Viskositätsdaten, die mit den Resultaten von May *et al.* innerhalb von $\pm 0,1\%$ übereinstimmen und zugleich über den gesamten Temperaturbereich der Temperaturfunktion der berechneten Werte folgen. Dieses macht deutlich, dass das Potential die Temperaturabhängigkeit der Viskosität korrekt beschreibt. Aufgrund der sehr guten Übereinstimmung der Temperaturfunktionen der berechneten und der gemessenen Viskositätswerte ist es möglich, die sehr zuverlässigen experimentellen Daten mit der berechneten Temperaturabhängigkeit zu kombinieren und dann über den Messbereich hinaus zu hohen und tiefen Temperaturen zu extrapolieren.

Die viskomagnetischen Effekte werden durch die Ausrichtung der Drehimpulsvektoren molekularer Gasteilchen in einem magnetischen Feld hervorgerufen, wodurch der Viskositätskoeffizient seinen isotropen skalaren Charakter verliert. Für sphärische Kreiselmoleküle wie Methan gibt es fünf verschiedene viskomagnetische Effekte. Diese können nach der kinetischen Theorie für die erste Näherung berechnet werden, wofür sieben verschiedene Streuquerschnitte benötigt werden, von denen einer der Streuquerschnitt ist, der die Viskosität in erster Näherung bestimmt. Die anderen sechs Streuquerschnitte beschreiben explizit verschiedene Arten der Drehimpulspolarisation. Sie würden im Limit eines sphärisch-symmetrischen Potentials gegen Null gehen und sind daher ein direkter Indikator für die Anisotropie der Potentialhyperfläche. Es soll noch darauf hingewiesen werden, dass keine höheren Näherungen der kinetischen Theorie für viskomagnetische Effekte abgeleitet wurden.

Die berechneten Werte für die fünf viskomagnetischen Effekte zeigen insgesamt eine gu-

te Übereinstimmung mit den verfügbaren experimentellen Daten, wobei zu berücksichtigen ist, dass die Messungen mit großen experimentellen Schwierigkeiten verbunden und die Resultate verschiedener Gruppen nicht völlig konsistent sind. Daher kann nicht mit Sicherheit gesagt werden, ob die beobachteten Abweichungen auf experimentelle Fehler oder auf Unzulänglichkeiten der Potentialhyperfläche zurückzuführen sind.

Für den Selbstdiffusionskoeffizienten ist ebenfalls nur die erste Näherung verfügbar, die durch einen einzigen Streuquerschnitt bestimmt wird. Die Unsicherheiten der experimentellen Daten und die daraus resultierenden Streuungen sind derart groß, dass der Selbstdiffusionskoeffizient keine Aussage über die Güte des Wechselwirkungspotentials ermöglicht. Selbst für die erste Näherung der kinetischen Theorie sind die berechneten Werte als deutlich genauer einzuschätzen als die experimentellen Daten.

Zusätzlich zu den Berechnungen auf Basis vollständiger klassischer Trajektorien mit dem TRAJECT-Code wurden die Streuquerschnitte, die die Viskosität und den Selbstdiffusionskoeffizienten bestimmen, auch mit Näherungsverfahren ermittelt. In der sphärischen Approximation wird die Potentialhyperfläche sphärisch gemittelt, Methan also wie ein Edelgasatom aufgefasst. Die Mason-Monchick-Approximation [84, 85] berücksichtigt zwar die vollständige anisotrope Potentialhyperfläche, vernachlässigt jedoch bei der Beschreibung der Stoßdynamik die Rotationsfreiheitsgrade. Mit beiden Approximationen resultierten sowohl für die Viskosität als auch für den Selbstdiffusionskoeffizienten Abweichungen von mehreren Prozent zu den Werten, die auf Basis vollständiger klassischer Trajektorien ermittelt wurden.

3.5.2 II. Wärmeleitfähigkeit, thermomagnetische Effekte, Volumenviskosität und Kernspin-Relaxation

Robert Hellmann, Eckard Bich, Eckhard Vogel, Alan S. Dickinson, Velisa Vesovic
J. Chem. Phys. **130**, 124309(1-11) (2009).

Diese Arbeit schließt sich thematisch direkt an die vorhergehende an und ergänzt diese um weitere Transport- und Relaxationseigenschaften von Methan im Temperaturintervall von 80 K bis 1500 K. Abgesehen von der Wärmeleitfähigkeit repräsentieren die thermomagnetischen Effekte, die Volumenviskosität und die Kernspin-Relaxation durch Spin-Rotation direkte Indikatoren für die Anisotropie des Wechselwirkungspotentials und verschwinden im Falle eines isotropen Potentials.

Bei der Berechnung der Wärmeleitfähigkeit und der thermomagnetischen Effekte müssen

die Streuquerschnitte für den Einfluss von Schwingungen korrigiert werden, da die Wärmeleitfähigkeit den Transport von Energie einschließlich Schwingungsenergie beschreibt. Auch für die korrekte Berechnung der Volumenviskosität müssen Schwingungsfreiheitsgrade berücksichtigt werden. Dazu wurden alle generalisierten Streuquerschnitte nach der in [61] beschriebenen Vorgehensweise korrigiert. Dabei wird angenommen, dass sich der Schwingungszustand eines Moleküls durch Stöße nicht verändert, was dazu führt, dass der Streuquerschnitt für den Transport von Schwingungsenergie mit dem Streuquerschnitt für die Selbstdiffusion gleichgesetzt werden kann. Außerdem wird angenommen, dass die Stoßtrajektorien zweier Moleküle nicht durch deren Schwingungszustände beeinflusst werden, eine Annahme, die generell für alle Transport- und Relaxationseigenschaften gemacht wird und deren Gültigkeit durch die guten Resultate für die Viskosität bestätigt wird. Für die Schwingungskorrektur wird unter diesen Näherungsannahmen lediglich der Schwingungsanteil an der Wärmekapazität benötigt, der aus Experimenten sehr genau bekannt ist. Die gesamte Korrektur für die Wärmeleitfähigkeit ist sehr klein und beträgt maximal 0,24%. Das liegt zum einen daran, dass der Streuquerschnitt für den Transport von Schwingungsenergie fast genauso groß wie der Selbstdiffusionsstreuquerschnitt ist, und zum anderen daran, dass die stark schwingungsbeeinflussten Streuquerschnitte, die die Kopplung zwischen dem Fluss von Translationsenergie und dem Fluss von Rotations- und Schwingungsenergie beschreiben, sehr klein sind und daher wenig Einfluss auf die Wärmeleitfähigkeit haben.

Die Wärmeleitfähigkeit wurde für die zweite Näherung der kinetischen Theorie berechnet, deren Einfluss bei maximal 0,5% liegt, wobei für Temperaturen unter 400 K der Beitrag der Drehimpulspolarisation dominierend ist. Der Beitrag der zweiten Näherung würde bei bis zu 1% liegen, wenn die Streuquerschnitte nicht für den Einfluss der Schwingungsfreiheitsgrade korrigiert wären.

Der beste verfügbare experimentelle Wert, der von Assael und Wakeham [86] mit der instationären Hitzdrahtmethode bei 308 K mit einer Unsicherheit von $\pm 0,2\%$ ermittelt wurde, weist eine Differenz von lediglich $-0,45\%$ zum berechneten Wert auf, was die hohe Qualität des Wechselwirkungspotentials unterstreicht. Die meisten anderen experimentellen Daten zeigen große Streuungen um die berechneten Werte, jedoch ist keine systematische Abweichung zu erkennen. Damit kann wie schon im Fall der Viskosität die Temperaturfunktion der berechneten Wärmeleitfähigkeitswerte zusammen mit dem experimentellen Wert von Assael und Wakeham benutzt werden, um Referenzwerte höchster Genauigkeit über einen weiten Temperaturbereich zu generieren.

Die thermomagnetischen Effekte haben die gleichen molekularen Ursachen wie die viskomagnetischen Effekte. Für sphärische Kreisel-moleküle wie Methan ergeben sich drei ver-

schiedene thermomagnetische Effekte, die für die erste Näherung der kinetischen Theorie berechnet werden können. Der Vergleich mit den experimentellen Daten zeigt eine nahezu quantitative Übereinstimmung bei der tiefsten Temperatur von nur 85 K, was durchaus bemerkenswert ist, da im Prinzip bei solch tiefen Temperaturen starke Abweichungen durch Quanteneffekte zu erwarten sind. Bei höheren Temperaturen bis 300 K unterschätzen die berechneten Werte die experimentellen Daten leicht.

Für die Volumenviskosität und die Kernspin-Relaxation ist die Übereinstimmung mit den experimentellen Daten zum Teil sehr schlecht. Bei der Volumenviskosität kann man davon ausgehen, dass die experimentellen Daten relativ ungenau sind, da die Messungen kompliziert sind und die meisten Experimentatoren nicht die Volumenviskosität, sondern Rotationsrelaxationszeiten gemessen haben, die nicht exakt in die Volumenviskosität umgerechnet werden können. Für die Kernspin-Relaxation sind jedoch die experimentellen Daten relativ genau und konsistent zwischen verschiedenen Arbeitsgruppen und Messverfahren. Die Ursache für dieses offensichtliche Versagen der Methode der klassischen Trajektorien ist noch unklar.

3.6 Berechnung der Transport- und Relaxationseigenschaften von verdünntem Wasserdampf

Robert Hellmann, Eckard Bich, Eckhard Vogel, Alan S. Dickinson, Velisa Vesovic
J. Chem. Phys. **131**, 014303(1-11) (2009).

Für Wasserdampf sollten die Scherviskosität, die Wärmeleitfähigkeit, der Selbstdiffusionskoeffizient und die Volumenviskosität bei niedrigen Dichten im Temperaturbereich von 250 K bis 2500 K mittels der kinetischen Gastheorie berechnet werden. Die Vorgehensweise ist dabei im wesentlichen analog zu der für Methan. Es wurden vier Wechselwirkungspotentiale des Schrifftums für die Berechnungen verwendet: Die SAPT-5s- und SAPT-5st-Potentiale [31, 32] aus dem Jahr 2000 basieren auf SAPT; das 2006 publizierte SDFT-5s-Potential [87] wurde mittels SAPT(DFT) [88] berechnet, einer Variante von SAPT, bei der die Dichtefunktionaltheorie (DFT) für die Beschreibung der Monomere verwendet wird; das CC-Pol-Potential aus dem Jahr 2007 [89, 90, 91] basiert auf supermolekularen CCSD(T)-Berechnungen.

Die klassischen Trajektorien wurden für 25 Gesamtenergien im Bereich zwischen 120 K und 50 000 K (200 K bis 50 000 K für CC-pol) berechnet. Die Zahl der Trajektorien betrug maximal 100 000 pro Energie (80 000 für CC-pol). Diese Einschränkungen bezüglich Trajektorienzahl und Energiebereich im Vergleich zu Methan waren notwendig, da der Rechenaufwand für die Trajektorien im Falle von Wasser um mehrere Größenordnungen erhöht ist, was auf die deutlich größere Tiefe und die stärkere Anisotropie des Wasser-Wasser-Potentials zurückzuführen ist. Die CPU-Zeit für die TRAJECT-Rechnungen lag bei jeweils etwa einem Monat für die SAPT-5s-, SAPT-5st- und SDFT-5s-Potentiale. Eine deutlich erhöhte Rechenzeit von etwa 3 Monaten resultierte für CC-pol, da diese Potentialfunktion einen polarisierbaren Term beinhaltet, für den die Ableitungen nach den *action-angle*-Variablen numerisch berechnet werden müssen.

Die Scherviskosität wurde für die zweite Näherung der kinetischen Theorie berechnet. Für CC-pol liegt der Beitrag der zweiten Näherung im Vergleich mit dem der ersten bei maximal 0,55 %, wobei der Beitrag der Drehimpulspolarisation bei maximal 0,01 % liegt. Für die anderen drei Potentiale sind die Effekte sehr ähnlich.

Der Vergleich zwischen den mit CC-pol berechneten Viskositätswerten und experimentellen Daten zeigt, bezogen auf die berechneten Werte, nahezu konstante Differenzen von +0,4% bis +0,5% für die besten experimentellen Daten, die von Teske *et al.* [92] mit einem Schwingscheibenviskosimeter in der eigenen Gruppe für Temperaturen zwischen 297 K

und 440 K gemessen wurden. Es ist sehr wahrscheinlich, dass, wie schon im Falle von Methan, die berechneten Werte auch bei deutlich höheren Temperaturen die Temperaturfunktion des Viskositätskoeffizienten sehr gut wiedergeben. Durch eine Skalierung mit dem Faktor 1,0045 für alle Temperaturen sollten berechnete Viskositäten resultieren, die den wahren Werten sehr gut entsprechen. Bei Verwendung der drei auf SAPT basierten Potentiale ergaben sich Abweichungen von $+(1 - 2)\%$ bei Raumtemperatur.

Für die Wärmeleitfähigkeit von Wasserdampf im Bereich kleiner Dichten ist die experimentelle Situation sehr schlecht, die Daten weichen untereinander um bis zu 6% ab. Die von der *International Association for the Properties of Water and Steam* (IAPWS) vorgeschlagene und empfohlene Korrelation, die routinemäßig in der Industrie verwendet wird, weist im Bereich um Raumtemperatur vergleichsweise geringe Abweichungen zu den mit dem CC-pol-Potential berechneten Werten auf. In dem für die Industrie relevanten Bereich hoher Temperaturen steigen die Abweichungen auf bis zu +5%. Die Vernachlässigung inelastischer und resonanter Stöße bezüglich der Schwingungsenergieniveaus sind von Seiten der Theorie als mögliche Fehlerquellen in Betracht zu ziehen. Die Schwingungsniveaus sind allerdings bei Wasser zu schwach angeregt, um die Abweichungen erklären zu können. Es ist wahrscheinlich, dass die experimentellen Daten bei hohen Temperaturen fehlerhaft sind. Weitere theoretische und experimentelle Untersuchungen sind notwendig, um diese Frage abschließend klären zu können.

Die berechneten Werte für den Selbstdiffusionskoeffizienten und die Volumenviskosität weisen zum Teil erhebliche Abweichungen zu den wenigen verfügbaren experimentellen Daten auf. In Anbetracht der Schwierigkeiten bei der experimentellen Bestimmung dieser Eigenschaften und den daraus resultierenden großen Unsicherheiten ist die Übereinstimmung zwischen berechneten Werten und experimentellen Daten jedoch als befriedigend anzusehen. Für Rückschlüsse auf die Qualität der Wechselwirkungspotentiale sind diese Eigenschaften ungeeignet.

4 Originalpublikationen

4.1 *Ab initio* potential energy curve for the helium atom pair and thermophysical properties of dilute helium gas

4.1.1 I. Helium-helium interatomic potential

Robert Hellmann, Eckard Bich, Eckhard Vogel

Mol. Phys. **105**, 3013-3023 (2007).

Alle quantenchemischen Berechnungen einschließlich der Konstruktion der Basissätze sowie die Anpassung des Potentials wurden selbst durchgeführt. Der eigene Anteil beträgt etwa 85%.

Ab initio potential energy curve for the helium atom pair and thermophysical properties of dilute helium gas. I. Helium–helium interatomic potential

ROBERT HELLMANN, ECKARD BICH and ECKHARD VOGEL*

Institut für Chemie, Universität Rostock, Albert-Einstein-Straße 3a,
D-18059 Rostock, Germany

(Received 8 August 2007; in final form 2 October 2007)

A helium–helium interatomic potential energy curve was determined from quantum-mechanical *ab initio* calculations. Very large atom-centred basis sets including a newly developed d-aug-cc-pV8Z basis set supplemented with bond functions and *ab initio* methods up to full CI were applied. The aug-cc-pV7Z basis set of Gdanitz (J. Chem. Phys. **113**, 5145 (2000)) was modified to be more consistent with the aug-cc-pV5Z and aug-cc-pV6Z basis sets. The diagonal Born–Oppenheimer corrections as well as corrections for relativistic effects were also calculated. A new analytical representation of the interatomic potential energy was fitted to the *ab initio* calculated values. In a following paper this potential model will be used in the framework of quantum-statistical mechanics and of the corresponding kinetic theory to calculate the most important thermophysical properties of helium governed by two-body and three-body interactions.

Keywords: Helium pair potential; *Ab initio*; Electronic structure; Quantum chemistry; Computational chemistry

1. Introduction

Hurly and Moldover [1] as well as Hurly and Mehl [2] reported that the most accurate values of the thermophysical properties of helium at low densities can be obtained in two steps. First, the *ab initio* potential energy $V(R)$ for the helium–helium interaction at discrete values of the interatomic separation R including limiting forms of $V(R)$ at large R has to be calculated. The resulting values of $V(R)$ then have to be fitted to a model potential for the interaction of helium atoms. In a second step, the thermophysical properties at low density can be derived from $V(R)$ using the kinetic theory of gases together with standard formulae from quantum-statistical mechanics.

In 2000, Hurly and Moldover argued on the basis of their analysis that the uncertainties of the calculated values for the thermophysical properties in the temperature range 1 K to 10^4 K were dominated by those of the potential. Hence, in 2007, Hurly and Mehl improved the interatomic potential model using more recent *ab initio*

$V(R)$ values of a multitude of research groups preferably calculated at $R=4.0 a_0$ and $R=5.6 a_0$ ($1a_0=1$ bohr = 0.052917721 nm). They concluded that it would be desirable to compute $V(R)$ values with comparably low uncertainties for further interatomic distances. In addition, Hurly, Moldover, and Mehl stated that the uncertainties of the calculated thermophysical property values are smaller than the corresponding uncertainties of the experimental data, even for temperatures at which high-precision measurements can comparably easily be performed. They recommended the calculated values be used as standards in different applications in metrology and to calibrate instruments in order to measure the density, dielectric virial coefficients, viscosity, thermal conductivity, speed of sound, and further properties.

In this contribution, new helium–helium interatomic potential energy values are derived from quantum-mechanical *ab initio* calculations using larger basis sets than ever before and including the diagonal Born–Oppenheimer correction and corrections for relativistic effects. The calculations were not only performed for $R=4.0 a_0$ and $R=5.6 a_0$, but also for a number of further interatomic separations according to

*Corresponding author. Email: eckhard.vogel@uni-rostock.de

the request of Hurly and Mehl. Furthermore, a new potential model for helium is constructed on the basis of these new values and some from the literature. The *ab initio* values for the potential should be accurate enough to determine the viscosity and thermal conductivity coefficients of helium up to an accuracy of four to five digits. A further aim of the investigation is to extend such calculations to neon in order to generate values of the thermophysical properties to be used for the calibration of measuring instruments.

2. Towards an accurate helium–helium interaction potential curve

The pair-potential energy between two helium atoms represents the best known interatomic potential to date. Being only a four-electron system it is possible to apply *ab initio* methods up to full CI with large basis sets. Different theoretical approaches have established that the well depth of the potential is around 11.0 K at a distance of about $5.6 a_0$. A short résumé of the development of the last ten years with regard to a highly accurate potential energy curve for the helium–helium interaction is given here in order to rank the efforts described in this report.

In 2000, Hurly and Moldover [1] summarized and evaluated the results of different *ab initio* calculations for the helium–helium interaction potential from the literature. To determine the parameters of their analytical representation of $V(R)$ they used for the region of small R ($1 a_0 < R < 2.5 a_0$) the rigorous upper bounds of variational computations of Komasa [3], for intermediate distances ($3 a_0 < R < 7 a_0$) results obtained by Korona *et al.* [4] with the symmetry-adapted perturbation theory (SAPT), and in the region of large R the asymptotic dispersion coefficients of Bishop and Pipin [5].

The well depth of 11.06 ± 0.03 K at $R = 5.6 a_0$, which resulted from the SAPT calculations of Korona *et al.* in 1997, was greater than most *ab initio* values in the literature. Similarly, their potential energies at other interatomic distances were less repulsive, for example $V(R) = 291.64 \pm 0.9$ K at $R = 4.0 a_0$. These results were incompatible with more recent high-level *ab initio* calculations. In 1999, van de Bovenkamp and van Duijneveldt [6] performed multireference configuration interaction (MRCI) calculations, employing an atom-centred basis set and a set of midbond functions, and extrapolated to the complete basis set (CBS) limit, yielding a well depth of only 10.99 ± 0.02 K and a value of $V(R) = 292.72 \pm 0.2$ K at $R = 4.0 a_0$. In the same year, van Mourik and Dunning [7] employed double augmented correlation-consistent (d-aug-cc-pVXZ) basis sets and used the coupled cluster theory with single,

double and full triple excitations (CCSDT) and the full configuration interaction method (full CI) in combination with the CCSD(T)-R12 results of Noga *et al.* [8]. They found 10.990 K for the well depth and $V(R) = 292.578$ K at $R = 4.0 a_0$. Anderson [9] obtained $V(R) = -10.98 \pm 0.02$ K in 2001 using ‘exact’ quantum Monte Carlo (EQMC) calculations and improved this in 2004 [10] to -10.998 ± 0.005 K, whereas he found $V(R) = 292.60 \pm 0.20$ K at $R = 4.0 a_0$. Using the averaged coupled-pair functional (r_{12} -MR-ACPF) method, which is close to FCI calculations, as well as a large atom-centred basis set including k functions and employing an extrapolation to the basis set limit, Gdanitz [11] found $V(R) = -10.980 \pm 0.004$ K at $R = 5.6 a_0$ and $V(R) = 292.75 \pm 0.01$ K at $R = 4.0 a_0$. Klopper [12] also discussed the extrapolated estimates of the helium–helium interaction energies and recommended $V(R) = -10.99 \pm 0.02$ K at $R = 5.6 a_0$ and $V(R) = 292.6 \pm 0.3$ K at $R = 4.0 a_0$ based on the CCSD(T) method using d-aug-cc-pV6Z and d-aug-cc-pV7Z basis sets for extrapolation to the CBS limit. Cencek *et al.* [13] performed very high-level *ab initio* calculations. First, they employed the Gaussian geminal implementation of the coupled cluster singles and doubles model. Then effects of triple and higher excitations were included using the conventional orbital approach CCSD(T) as well as FCI methods and applying very large correlation-consistent basis sets up to doubly augmented septuple-zeta supplemented with large sets of bond functions. Finally, extrapolation procedures to obtain the CBS limit led to potential values $V(R) = -11.009 \pm 0.008$ K at $R = 5.6 a_0$ and $V(R) = 292.54 \pm 0.04$ K at $R = 4.0 a_0$. Shortly after, Cencek *et al.* [14] recommended a new rigorous upper bound of -10.9985 K for the non-relativistic Born–Oppenheimer interaction energy at $5.6 a_0$. Very recently, Patkowski *et al.* [15] calculated highly accurate interaction energies in the non-relativistic Born–Oppenheimer approximation for 12 internuclear separations between $3.0 a_0$ and $9.0 a_0$ in a similar way as Cencek *et al.* [13]. They used the Gaussian geminal CCSD results from Cencek *et al.* for $R = 4.0 a_0$, $R = 5.6 a_0$, and $R = 7.0 a_0$ and performed Gaussian geminal CCD calculations for the other nine distances, whereas the singles contribution and the post-CCSD terms were obtained from conventional orbital calculations with still larger basis sets than used by Cencek *et al.* [13]. Patkowski *et al.* [15] obtained $V(R) = -11.0037 \pm 0.031$ K at $R = 5.6 a_0$ and $V(R) = 292.570 \pm 0.015$ K at $R = 4.0 a_0$. A new upper bound value of $V(R) = -11.0003$ K at $R = 5.6 a_0$ was also given (see Ref. [83] of [15]) and, additionally, a new SAPT value of $V(R) = -11.000 \pm 0.011$ K at $R = 5.6 a_0$ (see Ref. [53] of [15]).

In principle, at this level of accuracy, some further effects have to be taken into account. The diagonal adiabatic correction was calculated from explicitly correlated Gaussian functions by Komasa *et al.* [16] to be -13.2 mK at $R=5.6a_0$ for ^4He , whereas a newer computation concerning only the minimum resulted in -9 mK (see Ref. [7] of [14]). Cencek *et al.* [14] computed the lowest-order relativistic correction to the helium–helium interaction energy, again only at the minimum, and obtained $+15.4 \pm 0.6$ mK. The main contribution of this correction comes from the Casimir–Polder retardation [17, 18] which changes for asymptotic separations the C_6/R^6 behaviour of the potential to C_7/R^7 . This effect, which is also of importance for the only vibrational state of the ^4He dimer [19, 20], will be included in the representation of the helium–helium interaction potential used for the calculation of the thermophysical properties under discussion. Finally, Pachucki and Komasa [21] calculated, only at the minimum, the leading-order radiative correction according to the quantum electrodynamics to be -1.27 mK. Since this effect is very small, we did not further consider the radiative correction for the complete interaction potential.

3. Basis sets

The cc-pV7Z basis set of Gdanitz [22] consists of a contracted 14s set (Ref. [52] of [22]), of which the six most diffuse Gaussian functions are also present as primitives and of even-tempered shells of polarization functions that were generated following the guidelines of Dunning [23]. To be more consistent with the cc-pV5Z basis set (8s set with the four most diffuse functions also as primitives) and the cc-pV6Z basis set (10s set with the five most diffuse functions also as primitives) we replaced the 14s set used by Gdanitz in his cc-pV7Z basis set with a 12s set that we obtained from the Karlsruhe basis set library [24]. Furthermore, the polarization functions were re-optimized for the 12s set.

To obtain the aug-cc-pV7Z basis set, diffuse functions should be added, in principle following Woon and Dunning [25] by scaling the exponent of the most diffuse function of each angular momentum in the cc-pV7Z basis set for helium using the ratio of the exponents of the two most diffuse functions of the same angular momentum of the aug-cc-pV7Z basis set for hydrogen. However, neither a regular aug-cc-pV7Z nor a cc-pV7Z basis set for hydrogen has become available until now. In order to avoid the construction of a full aug-cc-pV7Z basis set for hydrogen we adopted a different approach. We started by taking a 12s set for hydrogen from the Karlsruhe basis set library [26] and optimized a single

diffuse s function by minimizing the ground state SCF energy of H^- resulting in the s part of an aug-cc-pV7Z basis set for hydrogen. This corresponds to the first step in the procedure suggested by Woon and Dunning. Subsequently, in a second step, all the diffuse polarization functions should be optimized at the CISD level for the ground state of H^- , a route we did not follow, because this requires the construction of the polarization functions of the cc-pV7Z basis set. Instead of this we used the finding that, in the aug-cc-pV6Z basis set, the ratio of the two most diffuse polarization function exponents of each angular momentum is very close to the ratio of the two most diffuse s function exponents except for the highest angular momentum where the spacing between the exponents increases. Consequently, we adopted the ratio of the two most diffuse s functions, which we optimized in the first step to generate the diffuse p, d, f, g and h functions of the aug-cc-pV7Z basis set for helium. The diffuse i function exponent was extrapolated as the square of the diffuse h function exponent in aug-cc-pV6Z divided by the diffuse g function exponent in aug-cc-pV5Z. Finally, the d-aug-cc-pV7Z basis set was constructed as proposed by Woon and Dunning [25] by expanding the exponents of the two most diffuse functions of each angular momentum in the aug-cc-pV7Z basis set in an even-tempered manner.

To develop a d-aug-cc-pV8Z basis set we started by constructing a new contracted 14s set by minimizing the ground state SCF energy of the helium atom. The seven most diffuse functions are also present as primitives. Shells of even-tempered polarization functions of up to k symmetry were generated following the guidelines of Dunning [23]. Diffuse functions were added in the same way as for aug-cc-pV7Z. In the first step a 14s set for hydrogen from the Karlsruhe basis set library [27] was used to optimize a single diffuse s function. In the second step the ratio of the exponent of this function and of the exponent of the most diffuse function in the 14s set was applied to generate the diffuse functions up to i symmetry. The diffuse k function exponent was then extrapolated as for aug-cc-pV7Z from the highest angular momentum diffuse functions of aug-cc-pV6Z and aug-cc-pV7Z. Table A1 shows the new d-aug-cc-pV7Z and d-aug-cc-pV8Z basis sets.

In most of our calculations of the helium interaction energy a (4s4p3d3f2g) set of bond functions centred between the two interacting helium atoms was applied. The bond function exponents are sp: 0.06, 0.18, 0.54, 1.62; df: 0.15, 0.45, 1.35; g: 0.3, 0.9. This set is abbreviated as (44332) throughout this paper. Furthermore, the standard abbreviations aVXZ for aug-cc-pVXZ and daVXZ for d-aug-cc-pVXZ are used.

4. *Ab initio* calculations

The interaction energies were calculated for 21 different He–He distances between $2.25 a_0$ and $8.0 a_0$. All calculations were performed using the supermolecular approach including a full counterpoise correction [28] as follows:

$$V(R) = \Delta E_{\text{He-He}}(R) = E_{\text{He-He}}(R) - 2E_{\text{He-Q}}(R), \quad (1)$$

where $E_{\text{He-Q}}(R)$ corresponds to the energy of a helium atom with a ghost basis set at the distance R . Cencek *et al.* [13] obtained highly accurate results of the CCSD interaction energies within the Gaussian geminal approach [29, 30] for $R=4.0 a_0$, $R=5.6 a_0$, and $R=7.0 a_0$. Therefore, we first calculated the CCSD interaction energies with the daVXZ + (44332) basis sets with $X=7, 8$ using the conventional CCSD method. Then we extrapolated the correlation part of the CCSD interaction energies $V(\text{CCSD}_{\text{corr}})$ obtained with these two basis sets to the complete basis set (CBS) limit with the formula

$$V_{\text{CCSD corr}}^{\text{daVXZ}} = V_{\text{CCSD corr}}^{\text{CBS}} + \alpha(X-1)^{-\beta}, \quad (2)$$

where the value of β was fixed to 2.13 (see below). The SCF interaction energies were not extrapolated and taken from the daV8Z + (44332) calculations. This is justified by the fact that the SCF part of the interaction energies always converges much faster than the correlation part. With this extrapolation scheme the value for β was chosen to agree precisely with the result of Cencek *et al.* for $V(\text{CCSD})$ at $R=4.0 a_0$ (304.935 K). We notice that the values at $R=5.6 a_0$ (-9.1520 K compared with -9.1509 K by Cencek *et al.*) and at $R=7.0 a_0$ (-4.1799 K vs. -4.1796 K) are also in close agreement.

The next step was to calculate the differences between CCSDT and CCSD for all distances. This contribution accounts for almost all the correlation energy not considered in CCSD. One way to compute this contribution is to split it into two parts. The CCSD(T) [31] and the CCSDT interaction energies are each calculated for the highest possible basis set. Then the differences between CCSD(T) and CCSD as well as the differences between CCSDT and CCSD(T) are extrapolated separately to the CBS limit. The second approach is to extrapolate directly the differences between CCSDT and CCSD to the CBS limit. The first approach seems to be more sensible, because CCSD(T) calculations can be performed with larger basis sets than CCSDT. Furthermore, the differences between CCSDT and CCSD(T) are much smaller and can therefore often be evaluated with sufficient accuracy

using smaller basis sets. However, we chose the second approach due to the fact that the differences between CCSDT and CCSD converge very fast to the CBS limit, whereas the two contributions in the first approach converge slower and in opposite directions. Figure 1 illustrates this for $R=5.6 a_0$. We used daVXZ + (44332) basis sets with $X=4, 5, 6$ and applied equation (2) for the extrapolation of the energy differences where α and β are fitting parameters.

The remaining differences between full CI (equivalent to CCSDTQ and CISDTQ for a pair of helium atoms) and CCSDT energies are very small. They were calculated with the daV5Z basis set without bond functions and were not extrapolated to the CBS limit.

Results for the CCSD correlation energies for $X=4$ to $X=8$ are summarized in table 1. The differences between CCSDT and CCSD for $X=4, 5, 6$ as well as the differences between full CI and CCSDT for $X=4, 5$ are given in table 2. The SCF interaction energies and the extrapolated correlation contributions are listed in table 3 together with the final potential in the non-relativistic Born–Oppenheimer approximation. The resulting interaction energy at $R=5.6 a_0$ of -11.001 K agrees very well with the result of Anderson [10] (-10.998 ± 0.005 K) and with the result of Patkowski *et al.* [15] (-11.0037 ± 0.0031 K). Still better agreement is found with the upper bound value -11.0003 K and with the SAPT value of -11.000 ± 0.011 K, both given in [15]. We estimate the uncertainties of our potential energy values to be ± 30 mK at $R=4.0 a_0$, ± 3 mK at $R=5.6 a_0$, and ± 2 mK at $R=7.0 a_0$ in the non-relativistic Born–Oppenheimer approximation. These estimates are based on the observed convergence behaviour of the individual contributions (of the differences between CCSDT and CCSD as well as between full CI and CCSDT) and are supported by the deviations of our extrapolated CCSD results from the Gaussian geminal CCSD results of Cencek *et al.* [13].

The lowest-order relativistic correction to the interaction energy was calculated by Cencek *et al.* [14] at $R=5.6 a_0$ using the Breit–Pauli approximation [32]. It consists of four terms for a pair of helium atoms: the mass–velocity term, the orbit–orbit term, and the one- and two-electron Darwin terms. Cencek *et al.* found that the orbit–orbit term, which is implicitly included in the Casimir–Polder retardation [17, 18], is the dominating effect, whereas the two-electron Darwin term is negligible. Since we account for the retardation effect in the final potential function (see the next section), we limited our computations for the relativistic corrections to the mass–velocity and one-electron Darwin terms which together form the so-called Cowan–Griffin approximation [33]. The calculations were carried out at the

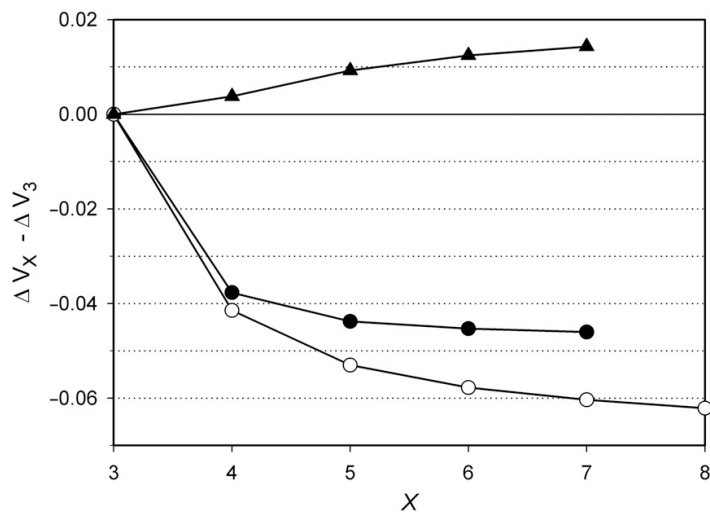


Figure 1. Convergence of the differences CCSDT-CCSD , CCSD(T)-CCSD and CCSDT-CCSD(T) at $R=5.6 a_0$ with the daVXZ+(44332) basis sets with X ranging from 3 to 8. The energy differences were shifted so that the $X=3$ value of each contribution gives zero for better comparability. (●) CCSDT-CCSD , (○) CCSD(T)-CCSD , (▲) CCSDT-CCSD(T) .

Table 1. CCSD correlation energy $V(\text{CCSD}_{\text{corr}})$ obtained with the da VXZ + (44332) basis sets. All energies are in Kelvin.

R/a_0	$V(\text{CCSD}_{\text{corr}})$				
	$X=4$	$X=5$	$X=6$	$X=7$	$X=8$
2.25	-1278.3832	-1299.3072	-1308.4305	-1313.5367	-1316.7730
2.50	-897.6723	-911.8263	-917.9003	-921.2374	-923.3969
2.75	-632.9536	-642.3037	-646.2734	-648.4541	-649.8389
3.00	-449.1651	-455.2035	-457.7645	-459.1552	-460.0542
3.25	-321.0761	-324.8855	-326.5090	-327.3779	-327.9482
3.50	-231.1453	-233.4965	-234.5045	-235.0390	-235.4191
3.75	-167.4621	-168.8840	-169.4958	-169.8210	-170.0425
4.00	-122.0022	-122.8490	-123.2109	-123.4070	-123.5306
4.25	-89.3391	-89.8378	-90.0466	-90.1627	-90.2358
4.50	-65.7544	-66.0441	-66.1620	-66.2288	-66.2717
4.75	-48.6567	-48.8222	-48.8870	-48.9243	-48.9494
5.00	-36.2165	-36.3095	-36.3439	-36.3640	-36.3788
5.25	-27.1322	-27.1829	-27.2002	-27.2105	-27.2194
5.50	-20.4714	-20.4971	-20.5051	-20.5101	-20.5154
5.60	-18.3284	-18.3475	-18.3531	-18.3567	-18.3610
5.75	-15.5636	-15.5751	-15.5783	-15.5803	-15.5834
6.00	-11.9273	-11.9311	-11.9320	-11.9324	-11.9342
6.25	-9.2164	-9.2162	-9.2161	-9.2157	-9.2167
6.50	-7.1817	-7.1794	-7.1790	-7.1783	-7.1789
7.00	-4.4717	-4.4680	-4.4677	-4.4668	-4.4671
8.00	-1.9048	-1.9022	-1.9021	-1.9015	-1.9017

Table 2. Differences between $V(\text{CCSDT})$ and $V(\text{CCSD})$ obtained with daVXZ + (44332) basis sets as well as differences between $V(\text{full CI})$ and $V(\text{CCSDT})$ obtained with daVXZ basis sets. All energies are in Kelvin.

R/a_0	$\Delta V(\text{CCSDT} - \text{CCSD})$			$\Delta V(\text{full CI} - \text{CCSDT})$	
	$X=4$	$X=5$	$X=6$	$X=4$	$X=5$
2.25	-79.1379	-79.5787	-79.7566	-0.1949	-0.2218
2.50	-62.6064	-62.9095	-63.0273	-0.1907	-0.2100
2.75	-49.1100	-49.3202	-49.3980	-0.1894	-0.2031
3.00	-38.0467	-38.1923	-38.2443	-0.1801	-0.1897
3.25	-29.0855	-29.1863	-29.2214	-0.1623	-0.1691
3.50	-21.9650	-22.0357	-22.0593	-0.1393	-0.1442
3.75	-16.4238	-16.4742	-16.4899	-0.1148	-0.1185
4.00	-12.1932	-12.2298	-12.2403	-0.0918	-0.0946
4.25	-9.0145	-9.0414	-9.0486	-0.0717	-0.0738
4.50	-6.6553	-6.6752	-6.6804	-0.0551	-0.0567
4.75	-4.9192	-4.9341	-4.9379	-0.0420	-0.0432
5.00	-3.6482	-3.6595	-3.6624	-0.0318	-0.0327
5.25	-2.7197	-2.7284	-2.7305	-0.0241	-0.0247
5.50	-2.0410	-2.0478	-2.0495	-0.0183	-0.0187
5.60	-1.8235	-1.8296	-1.8312	-0.0164	-0.0168
5.75	-1.5437	-1.5489	-1.5503	-0.0139	-0.0142
6.00	-1.1775	-1.1815	-1.1827	-0.0107	-0.0109
6.25	-0.9063	-0.9094	-0.9104	-0.0082	-0.0084
6.50	-0.7040	-0.7064	-0.7072	-0.0064	-0.0065
7.00	-0.4364	-0.4379	-0.4385	-0.0040	-0.0040
8.00	-0.1853	-0.1859	-0.1862	-0.0017	-0.0017

Table 3. SCF and extrapolated CCSD interaction energies, extrapolated triple contributions, full CI – CCSDT contributions, and the final non-relativistic potential without the DBOC. All energies are in Kelvin.

R/a_0	$V(\text{SCF})$	$V(\text{CCSD})$	$\Delta V(\text{CCSDT} - \text{CCSD})$	$\Delta V(\text{full CI} - \text{CCSDT})$	$V(\text{final, non-rel BO})$
	daV8Z + (44 332)	daV(78)Z + (44 332)	daV(456)Z + (44 332)	daV5Z	
2.25	22 313.06	20 987.96	-79.9916	-0.2218	20 907.75
2.50	12 952.24	12 023.29	-63.1718	-0.2100	11 959.91
2.75	7461.939	6808.536	-49.4856	-0.2031	6758.848
3.00	4268.348	3805.981	-38.2993	-0.1897	3767.492
3.25	2425.108	2095.693	-29.2568	-0.1691	2066.267
3.50	1369.077	1132.680	-22.0813	-0.1442	1110.454
3.75	768.3004	597.6879	-16.5031	-0.1185	581.0663
4.00	428.7828	304.9345	-12.2481	-0.0946	292.5918
4.25	238.0540	147.6302	-9.0535	-0.0738	138.5028
4.50	131.5339	65.1517	-6.6837	-0.0567	58.4113
4.75	72.3585	23.3444	-4.9403	-0.0432	18.3610
5.00	39.6448	3.2278	-3.6641	-0.0327	-0.4689
5.25	21.6407	-5.6015	-2.7319	-0.0247	-8.3580
5.50	11.7727	-8.7563	-2.0506	-0.0187	-10.8255
5.60	9.2200	-9.1520	-1.8322	-0.0168	-11.0010
5.75	6.3844	-9.2072	-1.5512	-0.0142	-10.7727
6.00	3.4523	-8.4866	-1.1836	-0.0109	-9.6811
6.25	1.8619	-7.3576	-0.9113	-0.0084	-8.2773
6.50	1.0016	-6.1790	-0.7081	-0.0065	-6.8936
7.00	0.2880	-4.1799	-0.4393	-0.0040	-4.6232
8.00	0.0233	-1.8789	-0.1868	-0.0017	-2.0675

Table 4. Relativistic Cowan–Griffin correction at the CCSD(T)/daV5Z and CCSD(T)/daV6Z levels as well as the DBOC at the CISD/daV5Z, CISD/daVQZ, and CISDT/daVQZ levels and the final estimate of the DBOC. All energies are in Kelvin.

R/a_0	Cowan–Griffin correction		Diagonal Born–Oppenheimer correction (DBOC)			Final estimate
	CCSD(T)/daV5Z	CCSD(T)/daV6Z	CISD/daV5Z	CISD/daVQZ	CISDT/daVQZ	
1.00	-22.8753	-23.1946	157.2975	157.4258	158.1839	158.0556
1.25	-19.0499	-19.0923	71.9284	71.9926	72.2730	72.2087
1.50	-13.8452	-13.8878	36.2596	36.2888	36.4554	36.4263
1.75	-9.2750	-9.2735	20.1249	20.1490	20.2810	20.2570
2.00	-5.9138	-5.8830	11.7220	11.7410	11.8473	11.8283
2.25	-3.6376	-3.6126	6.9292	6.9425	7.0253	7.0120
2.50	-2.1779	-2.1640	4.0826	4.0918	4.1540	4.1449
2.75	-1.2763	-1.2700	2.3742	2.3814	2.4269	2.4197
3.00	-0.7328	-0.7315	1.3535	1.3598	1.3923	1.3860
3.25	-0.4115	-0.4126	0.7516	0.7565	0.7794	0.7746
3.50	-0.2256	-0.2272	0.4032	0.4068	0.4229	0.4193
3.75	-0.1202	-0.1218	0.2059	0.2090	0.2203	0.2172
4.00	-0.0617	-0.0632	0.0971	0.1001	0.1081	0.1051
4.25	-0.0300	-0.0313	0.0393	0.0416	0.0472	0.0450
4.50	-0.0133	-0.0142	0.0100	0.0109	0.0150	0.0141
4.75	-0.0048	-0.0055	-0.0037	-0.0041	-0.0012	-0.0008
5.00	-0.0007	-0.0011	-0.0095	-0.0104	-0.0083	-0.0073
5.25	0.0011	0.0009	-0.0111	-0.0118	-0.0103	-0.0096
5.50	0.0017	0.0015	-0.0107	-0.0109	-0.0098	-0.0096
5.60	0.0018	0.0017	-0.0103	-0.0103	-0.0093	-0.0093
5.75	0.0018	0.0017	-0.0095	-0.0093	-0.0084	-0.0086
6.00	0.0016	0.0016	-0.0081	-0.0076	-0.0069	-0.0074
6.25	0.0014	0.0015	-0.0068	-0.0060	-0.0055	-0.0063
6.50	0.0012	0.0012	-0.0056	-0.0047	-0.0043	-0.0052
7.00	0.0008	0.0009	-0.0035	-0.0031	-0.0028	-0.0033
8.00	0.0003	0.0003	-0.0014	-0.0020	-0.0019	-0.0013

CCSD(T)/daV6Z level. The results are given along with CCSD(T)/daV5Z values in table 4.

The calculation of the diagonal Born–Oppenheimer correction (DBOC) to the interaction energies is quite difficult, because calculations are only possible for SCF and CI wavefunctions with the currently publicly available programs. The SCF level is not accurate enough to compute this correction and the CI methods are not size consistent apart from full CI. However, full CI is not applicable with the large basis sets required to obtain a converged result for the DBOC. We therefore evaluated the DBOC at the CISD/daV5Z level. In addition, the BSSE correction was not possible. To correct for the missing size consistency, we modified equation (1) and subtracted the energy of the atom pair at a very large separation ($R \geq 20 a_0$) instead of the energy of the two separate atoms. To account for the missing electron correlation in CISD we calculated the DBOC differences between CISDT and CISD with the daVQZ basis set and added

them to the CISD/daV5Z values. The calculations were performed for the ^4He isotope. The results are also given in table 4.

Our values are in excellent agreement with the calculations of the DBOC from explicitly correlated Gaussian functions by Komasa *et al.* [16] at short range, but differ at intermediate and long range. As an example, our value of -9.3 mK at $R = 5.6 a_0$ is inconsistent with the corresponding value of Komasa *et al.* of -13.2 mK . However, a more recent computation resulted in -9 mK at $R = 5.6 a_0$ (see Ref. [7] of [14]), which is in very close agreement with our value. This justifies using the DBOC values of the present paper for our new potential function.

The Mainz–Austin–Budapest version of ACES II [34] was utilized for all CCSDT calculations and for the determination of the relativistic corrections. For the full CI and DBOC computations we used PSI3 [35]. All other calculations were carried out with both program packages.

Table 5. *Ab initio* calculated and fitted He–He interaction energies without retardation for the potentials of the present paper and of Hurly and Mehl [2] as well as the retardation correction. All energies are in Kelvin.

R/a_0	This work		Hurly and Mehl		
	$V(ab\ initio)$	$V(\text{fitted})$	$V(ab\ initio)$	$V(\text{fitted})$	$\Delta V(\text{retardation})$
1.00	286 570.1 ^a	286 542.4	286 593.0	286 597.0	0.1
1.25	173 854.3 ^a	173 947.2		174 085.7	0.1
1.50	104 342.9 ^a	104 291.2	104 356.0	104 356.0	0.1
1.75	61 787.46 ^a	61 756.89		61 786.88	0.09
2.00	36 150.54 ^a	36 143.86	36 148.7	36 158.94	0.10
2.25	20 911.15	20 914.80		20 921.81	0.11
2.50	11 961.89	11 963.96	11 966.1	11 966.32	0.10
2.75	6 759.997	6 760.387		6 760.539	0.082
3.00	3 768.146	3 767.974	3 769.37	3 767.467	0.064
3.25	2 066.629	2 066.434		2 066.005	0.050
3.50	1 110.646	1 110.670	1 111.41	1 110.509	0.040
3.75	581.1617	581.1887		581.2313	0.0331
4.00	292.6337	292.6195	292.74	292.7471	0.0328
4.25	138.5165	138.5169		138.6437	0.0278
4.50	58.4111	58.4128	58.409	58.5017	0.0236
4.75	18.3547	18.3550		18.4029	0.0199
5.00	−0.4774	−0.4775	−0.513	−0.45850	0.0168
5.10		−4.5592	−4.534	−4.54770	0.0157
5.25	−8.3667	−8.3665		−8.36240	0.0142
5.50	−10.8336	−10.8333		−10.83390	0.0120
5.60	−11.0085	−11.0084	−11.003	−11.00920	0.0112
5.75	−10.7796	−10.7795		−10.77960	0.0101
6.00	−9.6869	−9.6871	−9.682	−9.68500	0.0086
6.25	−8.2821	−8.2824		−8.27820	0.0072
6.50	−6.8976	−6.8976	−6.895	−6.89240	0.0062
6.60		−6.3832	−6.347	−6.37780	0.0058
7.00	−4.6257	−4.6256	−4.624	−4.62090	0.0046
7.50		−3.0758	−3.077	−3.07270	0.0034
8.00	−2.0684	−2.0684	−2.068	−2.06680	0.0026
9.00		−0.9907	−0.991	−0.99040	0.0016
10.00		−0.5130	−0.514	−0.51300	0.0010
12.00		−0.1660	−0.166	−0.16610	0.0005
15.00		−0.0424	−0.0423	−0.04240	0.0002

^aValues by Komasa [3] including relativistic corrections and DBOCs.

5. Analytical potential function

Table 5 shows the *ab initio* data including the relativistic corrections (apart from retardation) and the DBOCs chosen for the fit of the potential function. For the short-range part of the potential from $1.0 a_0$ to $2.0 a_0$ we used the rigorous upper bound values of Komasa [3], which are still the best values for very small distances, whereas for the range between $2.25 a_0$ and $8.0 a_0$, our new *ab initio* values were taken.

A modification of the potential function given by Tang and Toennies [36] was fitted to the calculated

interaction energies:

$$\begin{aligned}
 V(R) = & A \exp \left(a_1 R + a_2 R^2 + a_{-1} R^{-1} \right. \\
 & \left. + a_{-2} R^{-2} + d_1 \sin(d_2 R + d_3) \right) \\
 & - \sum_{n=3}^8 f_{2n}(R) \frac{C_{2n}}{R^{2n}} \left[1 - \exp(-bR) \sum_{k=0}^{2n} \frac{(bR)^k}{k!} \right]. \quad (3)
 \end{aligned}$$

The coefficients A , a_1 , a_2 , a_{-1} , a_{-2} , b , d_1 , d_2 and d_3 were fitted to the values in table 5 with $f_{2n}(R)=1$ for all n , whereas the dispersion coefficients C_6 to C_{10} were taken

Table 6. Potential parameters (ϵ/k_B , R_e , and σ for the retarded potential).

A (K)	0.307092338615E+07
$a_1(a_0^{-1})$	-0.201651289932E+01
$a_{-1}(a_0)$	-0.431646276045E+00
$a_2(a_0^{-2})$	-0.459521265125E-01
$a_{-2}(a_0^2)$	0.138539045980E+00
d_1	0.167127323768E-02
$d_2(a_0^{-1})$	0.178284243205E+01
d_3	0.176635702255E+01
$b(a_0^{-1})$	0.203625105759E+01
C_6 (K a_0^6)	0.4616213781E+06
C_8 (K a_0^8)	0.4460565781E+07
C_{10} (K a_0^{10})	0.5803352873E+08
C_{12} (K a_0^{12})	0.1031677697E+10
C_{14} (K a_0^{14})	0.2415716766E+11
C_{16} (K a_0^{16})	0.7191492488E+12
ϵ/k_B (K)	10.997898
R_e (a_0)	5.608068
σ (a_0)	4.990672

from Zhang *et al.* [37] and the higher ones were extrapolated using the formulae of Thakkar [38]. We slightly modified the C_6 value of Zhang *et al.* by adding the relativistic correction δC_6 calculated by Moszynski *et al.* [39] with their bas281 basis set within the Cowan–Griffin approximation. For consistency, the higher dispersion coefficients were extrapolated with the non-relativistic value of C_6 . The potential parameters are listed in table 6.

Hurly and Mehl [2] applied the same model potential, apart from the sin function in the exponential term. It should be noted that Hurly and Mehl did not consider relativistic corrections apart from retardation so that they utilized the unmodified C_6 value of Zhang *et al.* The *ab initio* calculated values for $V(R)$ used in the fit of Hurly and Mehl are also listed in table 5. In addition, this table gives the unretarded values resulting from the fit of our *ab initio* data to equation (3) as well as the corresponding values obtained by Hurly and Mehl with the somewhat simpler equation without the sin function. The table shows that a different weighting was applied by Hurly and Mehl than in the present paper. Their *ab initio* values below $R=3.0 a_0$ are better represented by the fit, but this region of the potential is not of great importance for the calculation of the thermophysical properties at low density. On the contrary, the values above $R=3.0 a_0$, which are of greater significance for the thermophysical properties, are distinctly better described by our modified potential model.

The functions $f_{2n}(R)$ account for the relativistic retardation of the dipole–dipole term as well as of the

next higher dispersion terms for all R if $n=3-5$ [40–42]. For $n > 5$ the approximation $f_{2n}(R)=1$ was used. The $f_{2n}(R)$ values given in [42] were interpolated using Lagrange’s polynomial for five points and applied to the potential after the fit. The retardation correction (i.e. the difference between the retarded and the unretarded potentials), which is practically the same for both potential functions, is also shown in table 5.

6. Summary and conclusions

A new interaction potential for the helium atom pair has been obtained from highly accurate *ab initio* calculations at a large number of helium–helium separations. For this purpose, new basis sets were constructed and the series of correlation-consistent basis sets for helium was extended up to cc-pV8Z. Thereby, diffuse functions for cc-pV7Z and cc-pV8Z were generated using a simplification of the approach proposed by Woon and Dunning. The results of CCSD calculations with the d-aug-cc-pV7Z and d-aug-cc-pV8Z basis sets supplemented with bond functions were extrapolated to the complete basis set limit (CBS). The differences between the interaction energies at the CCSD and CCSDT levels were also extrapolated utilizing basis sets of up to d-aug-cc-pV6Z quality with bond functions. The contributions beyond CCSDT were calculated with the d-aug-cc-pV5Z basis set. The resulting interaction energies are in close agreement with other high-level *ab initio* results from the literature. Relativistic corrections to the interaction energies were estimated within the Cowan–Griffin approximation. The diagonal Born–Oppenheimer correction (DBOC) was also determined. Its value at the potential minimum agrees very well with the most accurate value from the literature.

An analytical potential function was fitted to the calculated interaction energies. At small distances, additional values from the literature supplemented with the DBOCs and the relativistic corrections of the present paper were incorporated into the fit. The large number of helium–helium distances used for the fit made it possible to use a more flexible analytic representation for the potential than was previously possible. The errors originating from the fit are practically negligible.

In the second paper of this series [43] we will use this potential function to determine the most important two-body and three-body properties of helium which are accurate enough to be used as standard values over a wide range of temperatures.

Appendix A: d-aug-cc-pV7Z and d-aug-cc-pV8Z basis sets for helium

Table A1. d-aug-cc-pV7Z and d-aug-cc-pV8Z basis sets for helium. Diffuse functions are separated by a blank line.

d-aug-cc-pV7Z									
Contracted 12s set		Correlation function exponents							
Exponent	Contr. coeff.	s	p	d	f	g	h	i	
18 090.1201	0.00001142	8.0089	21.770	17.744	13.956	10.569	7.588	4.911	
2709.1179	0.00008877	3.2991	9.466	7.757	5.962	4.277	2.780		
616.5260	0.00046646	1.4073	4.116	3.391	2.547	1.731		1.3070	
174.6204	0.00196311	0.6121	1.790	1.482	1.088		0.8701	0.3478	
56.9629	0.00706669	0.2702	0.7782	0.6481		0.5418	0.2723		
20.5602	0.02227400	0.1186	0.3384		0.3406	0.1696			
8.0089	0.06086507			0.2029	0.1066				
3.2991	0.13869491	0.03712	0.1059	0.06352					
1.4073	0.25156787	0.01162	0.03314						
0.6121	0.34077009								
0.2702	0.27715625								
0.1186	0.07272833								
d-aug-cc-pV8Z									
Contracted 14s set		Correlation function exponents							
Exponent	Contr. coeff.	s	p	d	f	g	h	i	k
69 636.5762	0.00000212	12.7483	28.215	23.624	19.487	15.405	11.787	8.605	5.654
10 421.3753	0.00001649	5.5248	13.263	11.240	9.159	7.007	5.054	3.336	
2369.7889	0.00008683	2.4714	6.235	5.348	4.304	3.187	2.167		1.681
670.7140	0.00036718	1.1247	2.931	2.544	2.023	1.450		1.078	0.4997
218.7325	0.00133582	0.5167	1.378	1.211	0.9508		0.6999	0.3483	
78.9727	0.00433716	0.2393	0.6476	0.5759		0.4684	0.2261		
30.7962	0.01277297	0.1094	0.3044		0.3071	0.1513			
12.7483	0.03409673			0.1860	0.09919				
5.5248	0.08050425	0.03534	0.09832	0.06007					
2.4714	0.16153434	0.01142	0.03176						
1.1247	0.26378403								
0.5167	0.32460548								
0.2393	0.23597951								
0.1094	0.05426079								

References

- [1] J. J. Hurly and M. R. Moldover, *J. Res. Natn. Inst. Stand. Technol.* **105**, 667 (2000).
- [2] J. J. Hurly and J. B. Mehl, *J. Res. Natn. Inst. Stand. Technol.* **112**, 75 (2007).
- [3] J. Komasa, *J. Chem. Phys.* **110**, 7909 (1999).
- [4] T. Korona, H. L. Williams, R. Bukowski, B. Jeziorski, and K. Szalewicz, *J. Chem. Phys.* **106**, 5109 (1997).
- [5] D. M. Bishop and J. Pipin, *Int. J. Quant. Chem.* **45**, 349 (1993).
- [6] J. van de Bovenkamp and F.B. van Duijneveldt, *J. Chem. Phys.* **110**, 11141 (1999).
- [7] T. van Mourik and T. H. Dunning Jr, *J. Chem. Phys.* **111**, 9248 (1999).
- [8] J. Noga, W. Klopper, and W. Kutzelnigg, in *Recent Advances in Coupled-cluster Methods*, edited by R. J. Bartlett (World Scientific, London, 1997), p. 1.
- [9] J. B. Anderson, *J. Chem. Phys.* **115**, 4546 (2001).
- [10] J. B. Anderson, *J. Chem. Phys.* **120**, 9886 (2004).
- [11] R. J. Gdanitz, *Molec. Phys.* **99**, 923 (2001).
- [12] W. Klopper, *J. Chem. Phys.* **115**, 761 (2001).
- [13] W. Cencek, M. Jeziorska, R. Bukowski, M. Jaszuński, B. Jeziorski, and K. Szalewicz, *J. Phys. Chem. A* **108**, 3211 (2004).
- [14] W. Cencek, J. Komasa, K. Pachucki, and K. Szalewicz, *Phys. Rev. Lett.* **95**, 233004 (2005).

- [15] K. Patkowski, W. Cencek, M. Jeziorska, B. Jeziorski, and K. Szalewicz, *J. Phys. Chem. A* **111**, 7611 (2007).
- [16] J. Komasa, W. Cencek, and J. Rychlewski, *Chem. Phys. Lett.* **304**, 293 (1999).
- [17] H. B. G. Casimir and D. Polder, *Phys. Rev.* **73**, 360 (1948).
- [18] W. J. Meath and J. O. Hirschfelder, *J. Chem. Phys.* **44**, 3210 (1966).
- [19] F. Luo, G. C. McBane, G. Kim, C. F. Giese, and W. R. Gentry, *J. Chem. Phys.* **98**, 3564 (1993).
- [20] W. Schöllkopf and J. P. Toennies, *Science* **266**, 1345 (1994).
- [21] K. Pachucki and J. Komasa, *J. Chem. Phys.* **124**, 064308 (2006).
- [22] R. J. Gdanitz, *J. Chem. Phys.* **113**, 5145 (2000).
- [23] T. H. Dunning Jr, *J. Chem. Phys.* **90**, 1007 (1989).
- [24] Unpublished 12s set for helium from <ftp://ftp.chemie.uni-karlsruhe.de/pub/basen/he>
- [25] D. E. Woon and T. H. Dunning Jr, *J. Chem. Phys.* **100**, 2975 (1994).
- [26] Unpublished 12s set for hydrogen from <ftp://ftp.chemie.uni-karlsruhe.de/pub/basen/h>
- [27] Unpublished 14s set for hydrogen from <ftp://ftp.chemie.uni-karlsruhe.de/pub/basen/h>
- [28] S. F. Boys and F. Bernardi, *Molec. Phys.* **19**, 553 (1970).
- [29] R. Bukowski, B. Jeziorski, and K. Szalewicz, *J. Chem. Phys.* **110**, 4165 (1999).
- [30] R. Bukowski, B. Jeziorski, and K. Szalewicz, in *Explicitly Correlated Functions in Molecular Physics and Quantum Chemistry*, edited by J. Rychlewski (Kluwer, Dordrecht, 2003), p. 185.
- [31] K. Raghavachari, G. W. Trucks, J. A. Pople, and M. Head-Gordon, *Chem. Phys. Lett.* **157**, 479 (1989).
- [32] H. A. Bethe and E. E. Salpeter, *Quantum Mechanics of One- and Two-electron Atoms* (Academic Press, New York, 1957), p. 170.
- [33] R. D. Cowan and D. C. Griffin, *J. Opt. Soc. Am.* **66**, 1010 (1976).
- [34] J.F. Stanton, J. Gauss, J.D. Watts, P.G. Szalay, R.J. Bartlett with contributions from A.A. Auer, D.B. Bernholdt, O. Christiansen, M.E. Harding, M. Heckert, O. Heun, C. Huber, D. Jonsson, J. Jusélius, W.J. Lauderdale, T. Metzroth, C. Michauk, D.P. O'Neill, D.R. Price, K. Ruud, F. Schiffmann, A. Tajti, M.E. Varner, J. Vázquez, and the integral packages: *MOLECULE* (J. Almlöf and P. R. Taylor), *PROPS* (P. R. Taylor), and *ABACUS* (T. Helgaker, H. J. Aa. Jensen, P. Jørgensen, and J. Olsen). See also J.F. Stanton, J. Gauss, J.D. Watts, W.J. Lauderdale, and R.J. Bartlett, *Int. J. Quant. Chem. Symp.* **26**, 879 (1992). Current version, see <http://www.aces2.de>
- [35] *PSI3: An Open-source Ab Initio Electronic Structure Package*, T.D. Crawford, C.D. Sherrill, E.F. Valeev, J.T. Fermann, R.A. King, M.L. Leininger, S.T. Brown, C.L. Janssen, E.T. Seidl, J.P. Kenny, and W.D. Allen, *J. Comp. Chem.* **28**, 1610 (2007).
- [36] K. T. Tang and J. P. Toennies, *J. Chem. Phys.* **80**, 3726 (1984).
- [37] J.-Y. Zhang, Z.-C. Yan, D. Vrinceanu, J. F. Babb, and H. R. Sadeghpour, *Phys. Rev. A* **74**, 14704 (2006).
- [38] A. J. Thakkar, *J. Chem. Phys.* **89**, 2092 (1988).
- [39] R. Moszynski, G. Lach, M. Jaszunski, and B. Bussery-Honvault, *Phys. Rev. A* **68**, 052706 (2003).
- [40] M. J. Jamieson, G. W. F. Drake, and A. Dalgarno, *Phys. Rev. A* **51**, 3358 (1995).
- [41] A. R. Janzen and R. A. Aziz, *J. Chem. Phys.* **107**, 914 (1997).
- [42] M.-K. Chen and K. T. Chung, *Phys. Rev. A* **53**, 1439 (1996).
- [43] E. Bich, R. Hellmann, and E. Vogel, *Molec. Phys.*, accepted.

4.1.2 II. Thermophysical standard values for low-density helium

Eckard Bich, Robert Hellmann, Eckhard Vogel

Mol. Phys. **105**, 3035-3049 (2007).

Teile der Publikation und des Gesamtkonzeptes wurden selbst erarbeitet. Der eigene Anteil beträgt etwa 20%.

Ab initio potential energy curve for the helium atom pair and thermophysical properties of the dilute helium gas. II. Thermophysical standard values for low-density helium

ECKARD BICH, ROBERT HELLMANN and ECKHARD VOGEL*

Institut für Chemie, Universität Rostock, Albert-Einstein-Straße 3a,
D-18059 Rostock, Germany

(Received 17 August 2007; in final form 11 October 2007)

A helium–helium interatomic potential energy curve determined from quantum-mechanical *ab initio* calculations and described with an analytical representation considering relativistic retardation effects (R. Hellmann, E. Bich, and E. Vogel, *Molec. Phys.* (in press)) was used in the framework of the quantum-statistical mechanics and of the corresponding kinetic theory to calculate the most important thermophysical properties of helium governed by two-body and three-body interactions. The second pressure virial coefficient as well as the viscosity and thermal conductivity coefficients, the last two in the so-called limit of zero density, were calculated for ^3He and ^4He from 1 to 10 000 K and the third pressure virial coefficient for ^4He from 20 to 10 000 K. The transport property values can be applied as standard values for the complete temperature range of the calculations characterized by an uncertainty of $\pm 0.02\%$ for temperatures above 15 K. This uncertainty is superior to the best experimental measurements at ambient temperature.

Keywords: helium pair potential; helium gas property standards; second and third pressure virial coefficients; viscosity; thermal conductivity

1. Introduction

Hurly and Moldover [1] as well as Hurly and Mehl [2] stated that standard values of the thermophysical properties of helium at low densities which can be used for different applications in metrology and for the calibration of measuring instruments are derived best from the helium–helium interatomic potential energy curve. For that purpose the interatomic potential has to be determined from quantum-mechanical *ab initio* calculations and should be described by a suitable analytical representation. Then the thermophysical properties at low density should follow from calculations using the kinetic theory of gases together with standard formulae from quantum-statistical mechanics. Furthermore, Hurly, Moldover, and Mehl established that the uncertainties of the calculated thermophysical property values, such as second pressure and dielectric virial coefficients, viscosity and thermal conductivity coefficients, speed of sound, and further properties, are smaller than the corresponding uncertainties of

the experimental data, even for temperatures at which high-precision measurements can comparably easily be performed.

In our paper I [3] a new helium–helium interatomic potential energy curve was determined for a comparably large number of interatomic separations from quantum-mechanical *ab initio* calculations using very large atom-centred basis sets, including a newly developed d-aug-cc-pV8Z basis set supplemented with bond functions, and *ab initio* methods up to Full CI. The diagonal Born–Oppenheimer corrections as well as corrections for relativistic effects were also enclosed. An improved analytical representation of the interatomic potential energy was fitted to the new *ab initio* calculated values and to some from the literature. Hurly and Mehl constructed their potential from literature values only. Some of these values are nearly as accurate as the new values from paper I, but they are only available for very few interatomic separations. Hence Hurly and Mehl had to use significantly less accurate values for most of the helium–helium distances. It should also be stressed that their analytical representation of the potential function is less flexible than the

*Corresponding author. Email: eckhard.vogel@uni-rostock.de

one used in our paper I. As a result the analytical potential of Hurlly and Mehl is characterized by comparably large fitting errors in the regions of the potential to which the thermophysical properties are most sensitive. For the potential of paper I the fitting errors are nearly negligible in these regions (see table 5 of paper I).

In this contribution the new helium–helium interatomic potential model has been used in the framework of the quantum-statistical mechanics and of the corresponding kinetic theory to calculate the most important thermophysical properties of helium governed by two-body and three-body interactions. In a second series of papers the investigation shall be extended to neon in order to generate standard values of the thermophysical properties for a second substance to be used for the calibration of measuring instruments.

2. Analytical helium–helium potential function

The *ab initio* calculated interatomic potential energy values $V(R)$ including some relativistic corrections and the diagonal Born–Oppenheimer corrections, but without retardation, which were chosen for the fit of the analytical potential function, and the fitted unretarded potential values have been listed in table 5 of paper I [3]. A modification of the potential function given by Tang and Toennies [4] was used as the potential model:

$$V(R) = A \exp(a_1 R + a_2 R^2 + a_{-1} R^{-1} + a_{-2} R^{-2}) + d_1 \sin(d_2 R + d_3) - \sum_{n=3}^8 f_{2n}(R) \frac{C_{2n}}{R^{2n}} \times \left[1 - \exp(-bR) \sum_{k=0}^{2n} \frac{(bR)^k}{k!} \right]. \quad (1)$$

Whereas the details of the fit (with $f_{2n}(R) = 1$ for all n) were communicated in paper I, the potential parameters are repeatedly given for convenience in table 1.

The retardation effects, which change for asymptotic separations the C_6/R^6 behaviour of the potential into C_7/R^7 as demonstrated by Casimir and Polder [5] and which are also of importance for the only vibrational state of ^4He [6–8], have to be included in the representation of the helium–helium interaction potential used for the calculation of the thermophysical properties under discussion. The functions $f_{2n}(R)$ take into consideration for all separations the relativistic retardation of the dipole–dipole term as well as of the next higher dispersion terms with $n = 3 - 5$ [9–11]. The approximation $f_{2n}(R) = 1$ was used for $n > 5$. The $f_{2n}(R)$ values given in [11] were interpolated using

Lagrange’s polynomial for five points and implemented for the potential after the fit. The retardation correction (i.e. the difference between the retarded and the unretarded potentials) is also listed in table 5 of paper I. The potential parameters ε/k_B , R_e , and σ for the retarded potential are given in table 1, too.

3. Quantum-mechanical calculation of thermophysical properties

Very accurate values for the thermophysical properties of helium can only be gained by a fully quantum-mechanical treatment of the elastic scattering considering the interatomic potential $V(R)$. The eigenfunction of a particle with the reduced mass $\mu = (m_1 m_2)/(m_1 + m_2)$ related to the centre of mass can be expressed as the infinite sum over partial waves, each of them corresponds to a particular state of the angular momentum of the system. The Schrödinger equation for the radial factor $\psi_l(R)$ of the l th partial wave with the angular momentum quantum number l and the wave number $k = (2\mu E)^{1/2}/\hbar$ is given as

$$\left(\frac{d^2}{dR^2} + k^2 - \frac{2\mu}{\hbar^2} V(R) - \frac{l(l+1)}{R^2} \right) \psi_l(R) = 0. \quad (2)$$

Here E is the energy of the incoming wave, \hbar is Planck’s constant h divided by 2π .

It is to be stressed that the reduced mass results from the atomic masses in the framework of the

Table 1. Potential parameters (ε/k_B , R_e , and σ for the retarded potential).

A (K)	0.307092338615E+07
$a_1(a_0^{-1})$	−0.201651289932E+01
$a_{-1}(a_0)$	−0.431646276045E+00
$a_2(a_0^{-2})$	−0.459521265125E−01
$a_{-2}(a_0^2)$	0.138539045980E+00
d_1	0.167127323768E−02
$d_2(a_0^{-1})$	0.178284243205E+01
d_3	0.176635702255E+01
$b(a_0^{-1})$	0.203625105759E+01
$C_6(K a_0^6)$	0.4616213781E+06
$C_8(K a_0^8)$	0.4460565781E+07
$C_{10}(K a_0^{10})$	0.5803352873E+08
$C_{12}(K a_0^{12})$	0.1031677697E+10
$C_{14}(K a_0^{14})$	0.2415716766E+11
$C_{16}(K a_0^{16})$	0.7191492488E+12
ε/k_B (K)	10.997898
$R_e(a_0)$	5.608068
$\sigma(a_0)$	4.990672

Born–Oppenheimer approximation following the discussion by Handy and Lee [12] as well as Kutzelnigg [13].

3.1. Evaluation of the phase shifts

To calculate the thermophysical properties of helium the relative phase shifts δ_l are needed. They correspond to the difference in the relative phase of the radial part of the outgoing wave functions $\psi_l(R)$ and $\psi_l^{(0)}(R)$. Here $\psi_l(R)$ is perturbed by the influence of the interatomic potential $V(R)$, whereas $\psi_l^{(0)}(R)$ is unperturbed, i.e. $V(R) = 0$. The phase shifts δ_l have to be evaluated as asymptotic limiting values of the relative phases of the perturbed and unperturbed waves. For that purpose nodes of the outgoing waves located at R_n of the n th zero far from the scattering centre have to be used. McConville and Hurly [14] discussed problems in the evaluation of the phase shifts in connection with two codes available in the literature [15, 16] and recommended to determine the phase shifts using the relation

$$\delta'_l(k, n) = \arctan \frac{j_l(k, R_n)}{n_l(k, R_n)}. \quad (3)$$

Here $j_l(k, R_n)$ and $n_l(k, R_n)$ are Bessel and Neumann functions for the angular momentum quantum number l and the wave number k . In the asymptotic limit the phase shift becomes independent of the node number. The numerical integration was performed from node to node and was stopped when the change of the phase shifts $|\Delta\delta'_l(k, n)|$ between two successive nodes became smaller than 10^{-9} . Because of the restricted range of the arctan function the phase shifts $\delta'_l(k)$ resulting from equation (3) have to be corrected by an integer multiple of π in order to get the true values:

$$\delta_l(k) = \delta'_l(k, n) + n_\pi\pi. \quad (4)$$

The value n_π follows from

$$n_\pi = n - \left\lfloor \frac{\theta_l + \delta'_l}{\pi} + 0.5 \right\rfloor \quad (5)$$

with

$$\begin{aligned} \theta_l \approx x - & \left(\frac{1}{2}l + \frac{1}{4} \right) \pi + \frac{\lambda - 1}{2(4x)} + \frac{(\lambda - 1)(\lambda - 25)}{6(4x)^3} \\ & + \frac{(\lambda - 1)(\lambda^2 - 114\lambda + 1073)}{5(4x)^5} \\ & + \frac{(\lambda - 1)(5\lambda^3 - 1535\lambda^2 + 54703\lambda - 375733)}{14(4x)^7} + \dots \end{aligned} \quad (6)$$

and

$$\lambda = 4l^2, \quad x = kR_n.$$

θ_l represents the phase of the partial wave $\psi_l^{(0)}(R)$ in the asymptotic limit (equation 9.2.29 in [17]) of the ideal system.

The fully quantum-mechanical calculation of the phase shifts at a multiplicity of wave numbers k for a large number of l values is very expensive with respect to the computing time. Hence it is reasonable to minimize this time by using suitable approximations, such as the JWKB method. In this semi-classical approximation the phase shifts result from

$$\begin{aligned} \delta_l(k) = & \frac{(2\mu)^{1/2}}{h} \left\{ \int_{R_1}^{R_2} \left(\frac{\hbar^2 k^2}{2\mu} - \frac{l(l+1)\hbar^2}{2\mu R^2} - V(R) \right)^{1/2} dR \right. \\ & + \int_{R_3}^{\infty} \left(\frac{\hbar^2 k^2}{2\mu} - \frac{l(l+1)\hbar^2}{2\mu R^2} - V(R) \right)^{1/2} dR \\ & \left. - \int_{R_0}^{\infty} \left(\frac{\hbar^2 k^2}{2\mu} - \frac{l(l+1)\hbar^2}{2\mu R^2} \right)^{1/2} dR \right\}. \end{aligned} \quad (7)$$

Here R_1 , R_2 and R_3 correspond to the three roots of the separation after equating the energy with the effective potential characterized by a centrifugal barrier at small and medium l values. In the case that the centrifugal barrier disappears at high l values as well as in the case that the energy is higher than the centrifugal barrier, only one root occurs and the first integral in equation (7) can be neglected. This corresponds to the usual procedure in the classical treatment of the scattering to use only the outer root. R_0 is the smallest separation in the case that there is no influence of the interatomic potential $V(R)$.

The calculation of the phase shifts $\delta_l(k)$ was performed for 585 values of the energy E in the range from zero to 250 000 K and for a number of l values increasing with rising energy. The phase shifts were determined fully quantum-mechanically using equations (3) to (6) as long as their values did not become too small. Parallel to it phase shifts according to the JWKB approximation using equation (7) were calculated, and their results were compared with those of the fully quantum-mechanical evaluation. In the case that the values of both procedures came into close agreement for certain values of the angular momentum quantum number l , the fully quantum-mechanical evaluation (QM) was replaced by the semi-classical JWKB procedure at the higher l values. The number of phase shifts which were evaluated according to both procedures and used in

the further calculations are listed for some reduced energies $E^* = E/\varepsilon$ in table 2. The large number of phase shifts has been chosen to avoid uncertainties in the results of the calculated thermophysical properties. This applies particularly to the second virial coefficient discussed next.

3.2. Calculation of the second pressure virial coefficient

The second virial coefficient is given following Boyd *et al.* [18] in two contributions: B_{direct} and B_{exch} . This separation is reasonable, because the effects due to symmetry are explicitly displayed and the role of spin is demonstrated in a simple manner. B_{direct} and B_{exch} can be represented by means of summations over only the even l values and only the odd l values:

$$B_{\text{direct}} = B_{\text{even}} + B_{\text{odd}}, \quad (8)$$

$$B_{\text{exch}} = \left(\frac{1}{2s+1} \right) \left(B_{\text{even}} - B_{\text{odd}} - \frac{N_A A^3}{16} \right) \quad (9)$$

following from the relationship:

$$B(T) = -\frac{N_A A^3}{2} \left[\sum_{n=0}^{n_{\text{max}}} \sum_l^{l_{\text{max}}(n)} (2l+1) \left(\exp(-\beta E_{nl}^-) - 1 \right) + \int_0^\infty \sum_l (2l+1) \frac{\delta_l(E)}{\pi} \exp(-\beta E) d(\beta E) \right]. \quad (10)$$

Here A is the thermal wavelength:

$$A = \left(\frac{h^2 \beta}{2\pi\mu} \right)^{1/2}, \quad \beta = \frac{1}{k_B T}.$$

The spin quantum number is $s = 1/2$ for ^3He and $s = 0$ for ^4He , hence ^3He is a fermion and ^4He is a boson. The third term in equation (9) represents the ideal-gas term which is only important at low temperatures. B_{exch} , considering spin and quantum statistics, goes rapidly to zero with increasing temperature. The first term of equation (10) corresponds to the contribution of the bound states, where E_{nl}^- is the negative eigenvalue of the n th state with the angular-momentum quantum number l which is obtained from the solution of the Schrödinger equation for the radial factor of a partial wave. It is to note that there exists no bound state for the ^3He - ^3He pair, whereas only one bound state occurs for ^4He - ^4He about 1 mK below the dissociation limit [6–8]. The bound state contribution is only of importance at very

low temperatures in the case of ^4He . The second term of equation (10) is the most important contribution at medium and higher temperatures and is related to the scattering resulting from binary collisions and to the phase shifts δ_l .

The term B_{direct} which corresponds to the complete summation over all l values in equation (10) corresponds to the Boltzmann statistics:

$$B_B = B_{\text{direct}}, \quad (11)$$

whereas for particles with spin s according to the Bose–Einstein (BE) or to the Fermi–Dirac (FD), the statistics hold as:

$$B_{\text{BE}} = B_{\text{direct}} + B_{\text{exch}}, \quad (12)$$

$$B_{\text{FD}} = B_{\text{direct}} - B_{\text{exch}}. \quad (13)$$

The sum over l and the integral in equation (10) have limits from 0 to ∞ and could lead to serious errors in the computation when truncated inadequately. Hence it was tested that the energies for which the calculations were performed and particularly the number of the phase shifts were chosen large enough (see table 2).

3.3. Calculation of the third pressure virial coefficient

To obtain the third virial coefficient the three-body interatomic interaction potential $V_3(R_{12}, R_{13}, R_{23})$ is needed. If it is assumed that apart from the pairwise additivity of the two-body interatomic potentials an extra genuine term $C_{\text{non-add}}$ for the non-additivity $\Delta V_3(R_{12}, R_{13}, R_{23})$ occurs and quantum effects as a first-order correction $C_{\text{qm},1}$ are taken into account,

Table 2. Number of calculated phase shifts for some reduced energies.

E^*	Total number	QM [equations (3)–(6)]
0	1	1
1×10^{-5}	4	4
1×10^{-2}	13	6
1×10^{-1}	34	12
1	87	24
10	454	42
100	454	70
1000	454	106
10000	618	196
24000	790	230
25000	809	0

the third virial coefficient is calculated as a sum of three contributions [19, 20]:

$$C_{\text{add}} = -6b_0^2 \int_0^\infty (\exp[-\beta V(R_{12})] - 1) R_{12}^2 \times \int_0^\infty (\exp[-\beta V(R_{13})] - 1) R_{13}^2 \times \int_{-1}^1 (\exp[-\beta V(R_{23})] - 1) dX dR_{13} dR_{12}, \quad (14)$$

$$C_{\text{non-add}} = -6b_0^2 \int_0^\infty \exp[-\beta V(R_{12})] R_{12}^2 \times \int_0^\infty \exp[-\beta V(R_{13})] R_{13}^2 \times \int_{-1}^1 \exp[-\beta V(R_{23})] (\exp[-\beta \Delta V_3(R_{12}, R_{23}, R_{13})] - 1) \times dX dR_{13} dR_{12}, \quad (15)$$

$$C_{\text{qm},1} = 18b_0^2 \frac{\hbar^2 \beta}{12mR_e^2} \int_0^\infty \exp[-\beta V(R_{12})] \left[\frac{d^2 \beta V(R_{12})}{dR_{12}^2} + \frac{2}{R_{12}} \frac{d\beta V(R_{12})}{dR_{12}} \right] R_{12}^2 \int_0^\infty (\exp[-\beta V(R_{13})] - 1) R_{13}^2 \times \int_{-1}^1 (\exp[-\beta V(R_{23})] - 1) dX dR_{13} dR_{12} \quad (16)$$

with

$$b_0 = \frac{2}{3} \pi N_A R_e^3, \quad R_{23} = (R_{12}^2 + R_{13}^2 - 2R_{12}R_{13}X)^{1/2}, \\ X = \cos \theta_1. \quad (17)$$

Here the integration has to be performed for reduced distances.

The genuine three-body potential for the interaction between three atoms 1, 2 and 3 with the angles θ_1 , θ_2 and θ_3 between the distance vectors \mathbf{R}_{12} , \mathbf{R}_{23} , and \mathbf{R}_{31} of the triplet is approximated by the triple-dipole potential term proposed by Axilrod and Teller [21, 22]:

$$\Delta V_3^{\text{AT}}(\mathbf{R}_1, \mathbf{R}_2, \mathbf{R}_3) = \frac{C_9}{R_{12}^3 R_{23}^3 R_{31}^3} (1 + 3 \cos \theta_1 \cos \theta_2 \cos \theta_3) \\ = \frac{C_9}{R_{12}^3 R_{23}^3 R_{31}^3} \left(1 + \frac{3}{8} \frac{(R_{12}^2 + R_{31}^2 - R_{23}^2)(R_{31}^2 + R_{23}^2 - R_{12}^2)(R_{23}^2 + R_{12}^2 - R_{31}^2)}{R_{12}^2 R_{23}^2 R_{31}^2} \right) \\ = \frac{C_9}{R_{12}^3 R_{23}^3 R_{31}^3} \left(1 - 3 \frac{(\mathbf{R}_{12} \cdot \mathbf{R}_{23})(\mathbf{R}_{12} \cdot \mathbf{R}_{31})(\mathbf{R}_{23} \cdot \mathbf{R}_{31})}{R_{12}^2 R_{23}^2 R_{31}^2} \right). \quad (18)$$

The non-additivity coefficient of the triple-dipole term was calculated for helium by Kumar and Meath [23] to be $C_9 = 1.472$ hartree a_0^9 (1 hartree = 3.1577465×10^5 K).

3.4. Calculation of the transport properties

The transport properties of dilute gases are formulated in different approximations of increasing order with dependence on quantum cross-sections $Q^{(m)}(E)$ and quantum collision integrals $\Omega^{(m,s)}(T)$. The numbers m and s are connected with certain approximations of the solution of the Boltzmann equation. The quantum cross-sections are given by Meeks *et al.* [24] in analogy to the second virial coefficient for particles with spin s according to the Bose–Einstein (BE) or to the Fermi–Dirac (FD) statistics as:

$$Q_{\text{BE}}^{(m)} = \left[\frac{s+1}{2s+1} \right] Q_{\text{even}}^{(m)} + \left[\frac{s}{2s+1} \right] Q_{\text{odd}}^{(m)}, \quad (19)$$

$$Q_{\text{FD}}^{(m)} = \left[\frac{s+1}{2s+1} \right] Q_{\text{odd}}^{(m)} + \left[\frac{s}{2s+1} \right] Q_{\text{even}}^{(m)}. \quad (20)$$

$Q_{\text{odd}}^{(m)}$ and $Q_{\text{even}}^{(m)}$ are again given in the following relationships as sums over the phase shifts δ_l , either over only the odd l values or over only the even l values:

$$Q^{(0)} = Q^{(1)} = Q^{(3)} = \dots = \sum_l (2l+1) \sin^2 \delta_l, \quad (21)$$

$$Q^{(2)} = \frac{3}{2} \sum_l \frac{(l+1)(l+2)}{(2l+3)} \sin^2(\delta_l - \delta_{l+2}), \quad (22)$$

$$Q^{(4)} = \frac{5}{4} \sum_l \left[\frac{2(l+1)(l+2)(2l^2+6l-3)}{(2l-1)(2l+3)(2l+7)} \sin^2(\delta_l - \delta_{l+2}) + \frac{(l+1)(l+2)(l+3)(l+4)}{(2l+3)(2l+5)(2l+7)} \sin^2(\delta_l - \delta_{l+4}) \right]. \quad (23)$$

It should be pointed out that equations (22) and (23) for even m values can be applied for the Bose–Einstein and Fermi–Dirac statistics as well as for the Boltzmann statistics, whereas for the latter one the complete sums have to be used. But the simple equation (21) for odd m values is valid only for the Bose–Einstein

and Fermi–Dirac statistics, if the summation is to be performed either over the odd or over the even l values. In the case of the Boltzmann (B) statistics more

complicated relations are to be applied for the different odd m values:

$$Q_B^{(1)} = \sum_l (l+1) \sin^2(\delta_l - \delta_{l+1}), \quad (24)$$

$$Q_B^{(3)} = \sum_l \left[\frac{3(l+1)(l^2+2l-1)}{(2l-1)(2l+5)} \sin^2(\delta_l - \delta_{l+1}) + \frac{(l+1)(l+2)(l+3)}{(2l+3)(2l+5)} \sin^2(\delta_l - \delta_{l+3}) \right]. \quad (25)$$

Analogous relationships for $m=5$ and $m=6$ were given by Meeks *et al.* [24]. A factor $4\pi/k^2$, where k is again the wave number, has been dropped in this paper in all expressions for the quantum cross-sections $Q^{(m)}$ compared with the relationships of Meeks *et al.* This factor is taken into account in the quantum collision integrals $\Omega^{(m,s)}$ defined as

$$\Omega^{(m,s)}(T) = \frac{8\pi\hbar^2}{2\mu k_B T (s+1)!} \int_0^\infty Q^{(m)}(E) \exp(-\beta E) (\beta E)^s d(\beta E).$$

The viscosity and the thermal conductivity coefficients of a monatomic gas in the limit of zero density can be expressed in the n th-order approximation as

$$[\eta]_n = \frac{5}{16} \frac{(2\pi\mu k_B T)^{1/2}}{\Omega^{(2,2)}(T)} f_\eta^{(n)}, \quad (26)$$

$$[\lambda]_n = \frac{75}{64} \frac{(2\pi\mu k_B^3 T)^{1/2}}{2\mu \Omega^{(2,2)}(T)} f_\lambda^{(n)}. \quad (27)$$

The $\Omega^{(2,2)}$ collision integral is related to the first-order approximations for the viscosity and thermal conductivity, whereas $f_\eta^{(n)}$ and $f_\lambda^{(n)}$ represent the correction factors needed in n th-order approximations of the kinetic theory. Explicit expressions up to the fifth-order approximations including computer programs were prepared by Viehland *et al.* [25] and used for the calculations in this paper.

It should be pointed out that according to our calculations the effect of the fifth-order corrections to the viscosity and to the thermal conductivity compared with the fourth-order corrections is below $\pm 0.01\%$. In this connection we refer to figure 2 of the paper by Hurly and Moldover [1] who obtained the same results for their potential in the temperature range 10–10 000 K.

4. Comparison with experimental data

4.1. Second pressure virial coefficient

The calculation of the second virial coefficient requires one to determine the possible existing bound states.

For that purpose the program Level 7.7 of LeRoy [26] was used and only one bound state was found to be $E_{00} = -1.64$ mK for ^4He . This value is to be compared with -1 mK for the first experimental proof by Luo *et al.* [6]. In 2000 Grisenti *et al.* [8] obtained $E_{00} = -(1.1 + 0.3 / -0.2)$ mK using diffraction experiments of a molecular beam of small helium clusters.

The comparison with the experimental data shown as absolute deviations $B_{\text{exp}} - B_{\text{cal}}$ is restricted to the best available data. For ^4He at low temperatures figure 1 not only demonstrates a very good agreement for the excellent data of Berry [27] resulting from constant-volume gas thermometry, but also for the dielectric constant isotherms by Gugan and Michel [28]. The B values by Kemp *et al.* [30] obtained also by constant-volume gas thermometry between 27 K and room temperature fall into line at low temperatures with the mentioned data by Berry as well as Gugan and Michel. Figure 1 also reveals a very close agreement between the B values calculated with the potential model by Hurly and Mehl [2] and those obtained from the new interatomic potential of the present paper. There exists only a very small difference at the lowest temperatures.

In figure 2 absolute deviations $B_{\text{exp}} - B_{\text{cal}}$ are presented for temperatures $T > 50$ K. The figure shows an excellent agreement between the very new data by McLinden and Lösch-Will [38], measured with

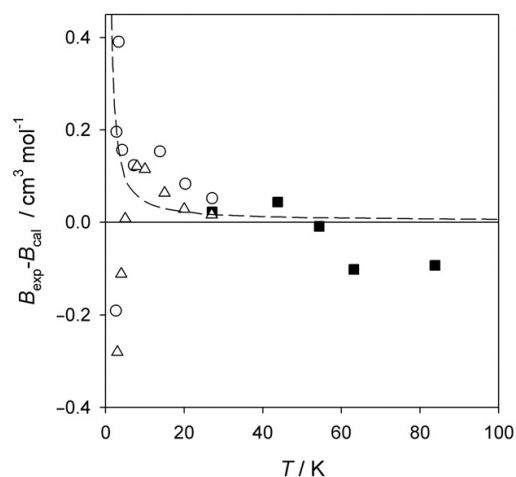


Figure 1. Deviations of experimental and calculated second pressure virial coefficients from values calculated with the new interatomic potential for ^4He at low temperatures. Experimental data: (○) Berry [27]; (△) Gugan and Michel [28], smoothed data from Aziz [29]; (■) Kemp *et al.* [30]. Calculated values: (---) Hurly and Mehl [2].

a high-precision two-sinker densimeter between 220 and 320 K, and the values calculated for the interatomic potential of this paper. This demonstrates the high quality of the experiments by McLinden and Lösch-Will, but also of the potential and of the statistical-mechanical calculation of the second virial coefficients. It is further illustrated that the data of Kemp *et al.* [30] agree at the higher temperatures with the second virial coefficients determined by Blancett *et al.* [33] and by Holste *et al.* [37]. Above room temperature the data by Schneider and co-workers [31, 32], Waxman [34], and Kell *et al.* [36] are in close agreement up to about 500 K.

Even at high temperatures above 1000 K the differences between the experimental data by Schneider and co-workers [31, 32] and the calculated values are not large. It is to be stressed that the calculated values are more reliable at such high temperatures.

The comparison in the case of ^3He is shown in figure 3. It becomes evident that the results of four measurement series of the constant-volume gas thermometry between 1.5 and 20.3 K performed by Maticotta *et al.* [40] are in close agreement with the calculated values for the interatomic helium potential. Surprisingly, the older data by Keller [39] are also reasonably consistent with the calculated values.

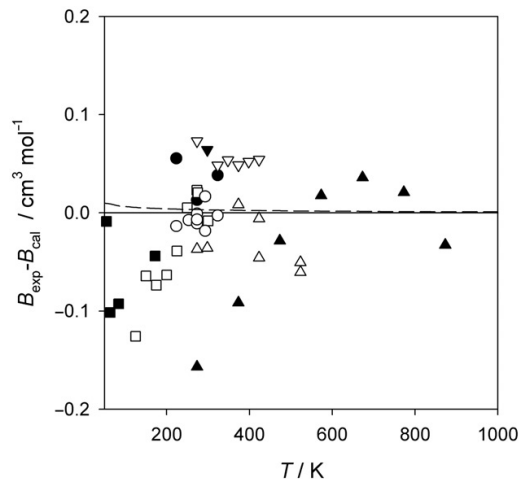


Figure 2. Deviations of experimental and calculated second pressure virial coefficients from values calculated with the new interatomic potential for ^4He at medium and higher temperatures. Experimental data: (■) Kemp *et al.* [30]; (▲) Schneider and Duffie [31] as well as Yntema and Schneider [32]; (●) Blancett *et al.* [33]; (▽) Waxman [34]; (▼) Waxman and Davis [35]; (△) Kell *et al.* [36]; (□) Holste *et al.* [37]; (○) McLinden and Lösch-Will [38]. Calculated values: (---) Hurly and Mehl [2].

4.2. Third pressure virial coefficient

It should be pointed out that experimental data for the third pressure virial coefficient are not independent of the values for the second pressure virial coefficient derived from the same experiments. Hence only third pressure virial coefficients combined with second ones, which are in reasonably close agreement with the best experimental data and with the calculated values of the present paper, are included in the comparison. Thus the experimental data determined by McLinden and Lösch-Will [38] represent a strong criterion due to their very close agreement with regard to the second pressure virial coefficient. Figure 4 shows a comparison between experimental data and the values calculated for the new interatomic potential. This figure elucidates that the excellent agreement of the experimental data of McLinden and Lösch-Will with the calculated values is only achieved, if the third virial coefficient corresponds to the complete sum of the contributions for the pairwise additivity C_{add} , for the non-additivity of the three-body interatomic interactions according to Axilrod and Teller $C_{\text{non-add}}$, and for the first-order quantum-mechanical correction $C_{\text{qm},1}$. Good agreement is also found for the experimental data by Pfefferle *et al.* [41], Hoover *et al.* [42], Blancett *et al.* [33] as well as Vogl and Hall [44]. This makes evident that the calculation procedure for the third pressure virial coefficient predicts excellent values.

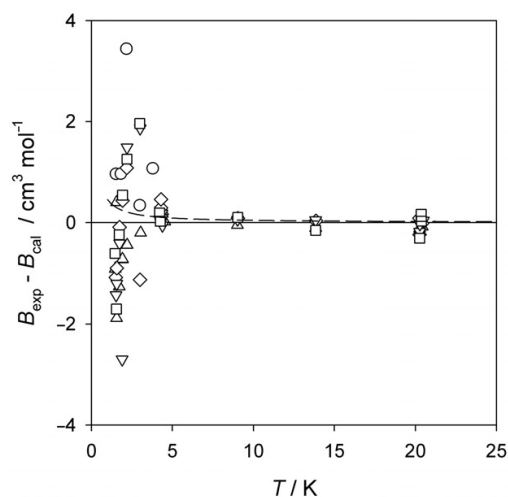


Figure 3. Deviations of experimental and calculated second pressure virial coefficients from values calculated with the new interatomic potential for ^3He . Experimental data: (○) Keller [39]; (△), (◇), (▽), (□), run 1 to 4, Maticotta *et al.* [40]. Calculated values: (---) Hurly and Mehl [2].

4.3. Viscosity

In principle, the initial density dependence of the experimental data for the transport properties should be considered in the discussion, since many measurements were performed at atmospheric pressure, whereas the theoretical results correspond to the limit of zero density. But this effect is comparably small ($<0.1\%$) for most temperatures, apart from the very low temperatures near to the normal boiling point of helium. On the other hand, the experimental uncertainty is rather high at these low temperatures so that the initial density dependence was taken into account only in one case for the thermal conductivity.

For the viscosity the situation is complicated by the fact that it is difficult to perform genuine absolute measurements of the gas viscosity with an uncertainty $<\pm 0.1\%$, even at ambient temperature. This is demonstrated in figure 5 for ^4He . The measurements by Kestin and Leidenfrost [45], approved as one of the most accurate and additionally one of the few absolute measurements on gases, can only partly be considered as absolute ones. Kestin and Leidenfrost applied the theory by Newell [54], developed for absolute measurements with an oscillating-disc viscometer, and calculated first the so-called Newell's constant from the geometric dimensions of the viscometer. Then the value of Newell's constant was changed by 0.16% in order to take into account a paddle effect of the mirror used in

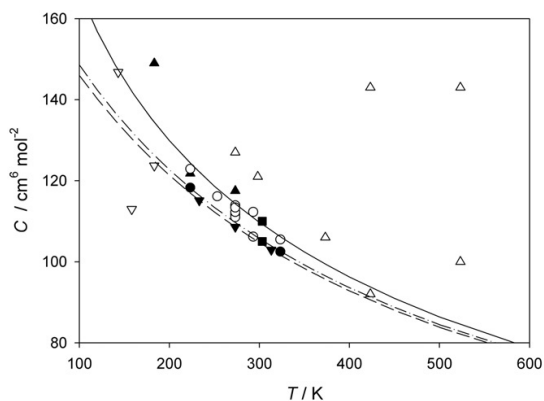


Figure 4. Comparison of experimental data and of values for the third pressure virial coefficient derived from the new interatomic potential for ^4He . Experimental data: (■) Pfefferle *et al.* [41]; (▲) Hoover *et al.* [42]; (●) Blancett *et al.* [33]; (▽) Provine and Canfield [43]; (▼) Vogl and Hall [44]; (△) Kell *et al.* [36]; (○) McLinden and Lösch-Will [38]. Calculated values: (---) classical contribution C_{add} , (- · - · - ·) classical and non-additivity contributions $C_{\text{add}} + C_{\text{non-add}}$, (—) sum of classical and non-additivity contributions and of the first-order quantum correction $C_{\text{add}} + C_{\text{non-add}} + C_{\text{qm},1}$.

the measurements. But for that purpose Kestin and Leidenfrost utilized a value for the viscosity of air at 20°C and at atmospheric pressure determined by Bearden [55] in an absolute measurement with a rotating-cylinder viscometer. Hence the genuine absolute measurement is that of Bearden. The measurements by Kestin and Nagashima [46] were analogously evaluated, but the change in Newell's constant was 0.5% . In 1972 Kestin *et al.* [47] reported a best estimate of their measurements in the foregoing years, but with a change by nearly $+0.1\%$ of the value at 298.15K in comparison with the data by Kestin and Leidenfrost as well as Kestin and Nagashima. Hence it is to expect that all measurements which are related to these best estimates for the noble gases as well as for nitrogen should be characterized by a tendency to values increased by $+0.1\%$. This holds for two measurement series of Vogel [50] with an all-quartz oscillating-disc viscometer which were performed in a relative manner with a Newell's constant determined from the best estimates by Kestin *et al.* The absolute measurements by Flynn *et al.* [48] and Gracki *et al.* [49] performed with nearly the same capillary viscometer led to values differing by $\pm 0.2\%$. Recently, Evers *et al.* [51] utilized a rotating-cylinder viscometer for absolute measurements on several gases at different temperatures and pressures. Their result for helium at 293.15K agrees with our calculations within $\pm 0.1\%$ with a tendency to higher experimental data. Very recently, Berg [52, 53] performed highly accurate absolute measurements with

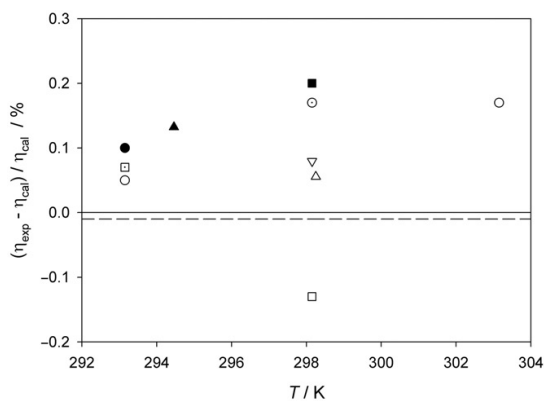


Figure 5. Deviations of experimental and calculated viscosity coefficients from values calculated with the new interatomic potential for ^4He at room temperature. Experimental data: (●) Kestin and Leidenfrost [45]; (○) Kestin and Nagashima [46]; (○) Kestin *et al.* [47]; (■) Flynn *et al.* [48]; (□) Gracki *et al.* [49]; (▲) Vogel [50], 1st series of measurements; (△) Vogel [50], 2nd series of measurements; (□) Evers *et al.* [51]; (▽) Berg [52, 53]. Calculated values: (- - -) Hurly and Mehl [2].

a capillary viscometer only at room temperature. The experimental datum by Berg at 298.15 K $\eta = (19.842 \pm 0.014) \mu\text{Pa s}$ (standard deviation: 2σ) deviates nearly +0.1% from the calculated value $\eta = 19.8262 \mu\text{Pa s}$ of this paper. On the other hand, the very recent calculations by Hurly and Mehl [2] with an improved interatomic potential for helium compared with that of Hurly and Moldover [1] led to a value of $\eta = (19.8245 \pm 0.004) \mu\text{Pa s}$ at 298.15 K. The agreement between the calculations of Hurly and Mehl and that of the present paper in which the interatomic potential was further improved shows clearly that the uncertainty of the theoretical values is about one order of magnitude lower than that of the experiments.

The situation changes further to the disadvantage of the experiment, if the measurements are carried out away from ambient temperature. In figure 6 experimental data at low temperatures down to 1.3 K and at medium temperatures up to 374 K are compared with the values calculated for the new potential energy curve. A close agreement within $\pm 0.5\%$ is only found for the absolute capillary measurements of Flynn *et al.* [48], Gracki *et al.* [49] and Kao and Kobayashi [60] as well as for the absolute measurements by Evers *et al.* [51] with their rotating-cylinder viscometer. All other measurements are relative measurements in which the value used for the calibration plays the decisive role. Johnston and Grilly [56] (oscillating-disc viscometer) as well as Clarke and Smith [61] and Gough *et al.* [62]

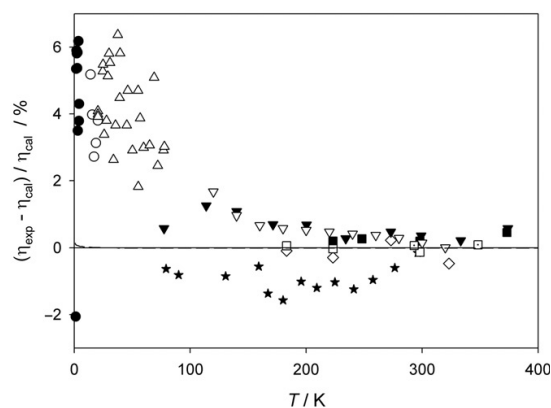


Figure 6. Deviations of experimental and calculated viscosity coefficients from values calculated with the new interatomic potential for ${}^4\text{He}$ at low and medium temperatures. Experimental data: (\star) Johnston and Grilly [56]; (\bullet) Becker *et al.* [57]; (\circ) Becker and Misenta [58]; (Δ) Coremans *et al.* [59]; (\blacksquare) Flynn *et al.* [48]; (\square) Gracki *et al.* [49]; (\diamond) Kao and Kobayashi [60]; (\blacktriangledown) Clarke and Smith [61]; (∇) Gough *et al.* [62]; (\square) Evers *et al.* [51]. Calculated values: (---) Hurly and Mehl [2].

(capillary viscometers) based their measurements on reasonable values for air and nitrogen at ambient temperature resulting in deviations within $\pm 2\%$. Conversely, Becker *et al.* [57] and Becker and Misenta [58] used an old value for ${}^4\text{He}$ at 77.3 K from Keesom [63] for calibration in their measurements with an oscillating-cylinder viscometer so that the differences amount to about +5%. Similarly, the measurements with an oscillating-disc viscometer by Coremans *et al.* [59] based on an even older value for ${}^4\text{He}$ at 20 K from Kamerlingh Onnes and Weber [64] show positive deviations up to 5%. All these results could have been much better, if they had been based on more reliable values for calibration. It should be mentioned that in the case of measurements at atmospheric pressure a consideration of the initial density dependence of the viscosity would increase the values in the limit of zero density which means the differences would become somewhat larger. In addition, figure 6 shows only at the lowest temperatures small differences to the calculated values by Hurly and Mehl [2].

Figure 7 illustrates the comparison between the best experimental viscosity data and the calculated values at higher temperatures. For that purpose the data of the two measurement series of Vogel [50] were recalibrated at room temperature with the theoretically calculated values of ${}^4\text{He}$ of this report. The temperature dependence of the experimental data agrees in an excellent manner with the calculated values at all other

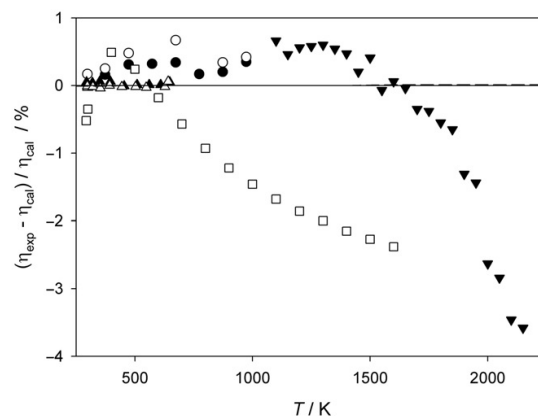


Figure 7. Deviations of experimental and calculated viscosity coefficients from values calculated with the new interatomic potential for ${}^4\text{He}$ at higher temperatures. Experimental data: (\bullet) Kestin *et al.* [47]; (\circ) Kestin *et al.* [65]; (\blacktriangledown) Guevara *et al.* [66]; (\square) Dawe and Smith [67]; (\blacktriangle) Vogel [50], 1st series of measurements recalibrated; (Δ) Vogel [50], 2nd series of measurements recalibrated. Calculated values: (---) Hurly and Mehl [2].

temperatures up to 650 K. The measurements by Vogel with his all-quartz oscillating-disc viscometer represent the best experiments in this temperature range.

Although the values of the best estimate by Kestin *et al.* [47] and the experimental data of a further paper by Kestin *et al.* [65] were not recalibrated, figure 7 reveals a systematic trend in the data by Kestin *et al.* to higher values with increasing temperature. But this tendency is well known for all the measurements by Kestin and his co-workers with the oscillating-disc viscometer developed by Di Pippo *et al.* [68]. These systematic deviations are a consequence of a temperature measurement error with thermocouples extensively discussed by Vogel *et al.* [69] and are still relatively small for helium due to the large thermal conductivity coefficient compared with those of other common gases. The relative measurements of Guevara *et al.* [66] and of Dawe and Smith [67] with capillary viscometers based on a reasonable calibration at room temperature make it obvious that they are influenced by systematic errors and that the theoretical calculation is distinctly superior to the experiment at these high temperatures.

Figure 8 displays the deviations of the experimental viscosity data by Becker *et al.* [57] and Becker and Misenta [58] from the theoretically calculated values for ^3He . These differences are not too large with respect to the uncertainty of $\pm 5\%$ estimated by those authors.

4.4. Thermal conductivity

Accurate measurements of the thermal conductivity are difficult to carry out due to different experimental problems.

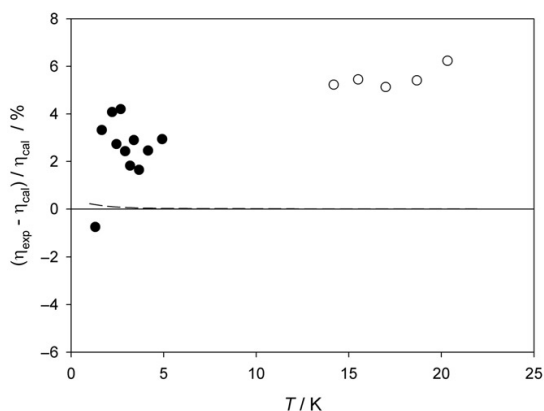


Figure 8. Deviations of experimental and calculated viscosity coefficients from values calculated with the new interatomic potential for ^3He . Experimental data: (●) Becker *et al.* [57]; (○) Becker and Misenta [58]. Calculated values: (---) Hurly and Mehl [2].

Results for ^4He near to room temperature obtained with the transient hot-wire technique, the most accurate method for determining thermal conductivity coefficients, are compared in figure 9 with the values theoretically calculated. This comparison is a further stringent test of the new potential and of the correct application of the kinetic theory including the quantum-mechanical effects. The experimental data by Kestin *et al.* [71] and Assael *et al.* [72] as well as by Johns *et al.* [74] differ from the calculated values by $< \pm 0.1\%$ and $< \pm 0.2\%$, less than the uncertainties estimated by those authors themselves ($\pm 0.3\%$). The deviation of the first experiment with this method by Haarman [70] is only somewhat larger, whereas that of Mustafa *et al.* [73] is distinctly increased.

It should be noted that the differences between the calculated values by Hurly and Mehl [2] and those of the present paper are too small to become obvious in figures 9–11.

The experimental thermal conductivity data for ^4He below ambient temperature are compared in figure 10 with the calculated values. It becomes evident that there exists an excellent agreement for the experimental data of Acton and Kellner [81] obtained between 3.3 and 20 K with a parallel-plate apparatus. It is to be stressed that we extrapolated the experimental density series of Acton and Kellner to the limit of zero density for this comparison. But the experimental data between 2.08 and 3.95 K by Kerrisk and Keller [77] resulting also from parallel-plate measurements show large positive differences. These values were not corrected, since the measurements were carried out only at one pressure of

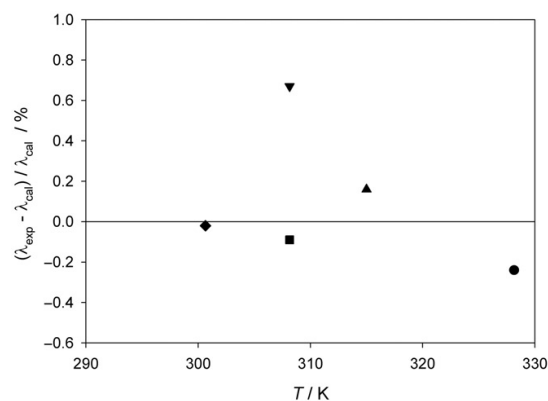


Figure 9. Deviations of experimental and calculated thermal conductivity coefficients from values calculated with the new interatomic potential for ^4He at room temperature. Experimental data: (●) Haarman [70]; (◆) Kestin *et al.* [71]; (■) Assael *et al.* [72]; (▼) Mustafa *et al.* [73]; (▲) Johns *et al.* [74]. Calculated values: (---) Hurly and Mehl [2].

about 10 torr. The effect of the density dependence is distinctly smaller than the deviations. The experimental data between 7.7 and 273 K by Popov and Zarev [82] using the concentric-cylinder method show similar positive differences to the theoretically calculated values with decreasing temperature. These data could also

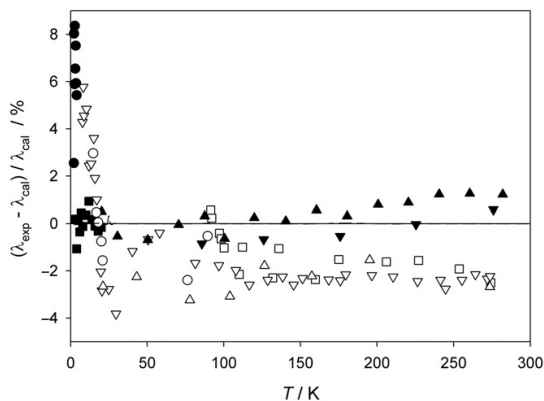


Figure 10. Deviations of experimental and calculated thermal conductivity coefficients from values calculated with the new interatomic potential for ^4He at low and medium temperatures. Experimental data: (○) Ubbink and de Haas [75]; (△) Golubev and Shpagina [76]; (●) Kerrisk and Keller [77]; (▲) Roder [78, 79]; (□) Shashkov *et al.* [80]; (■) Acton and Kellner [81]; (▽) Popov and Zarev [82]; (▼) Zarev *et al.* [83]. Calculated values: (---) Hurly and Mehl [2].

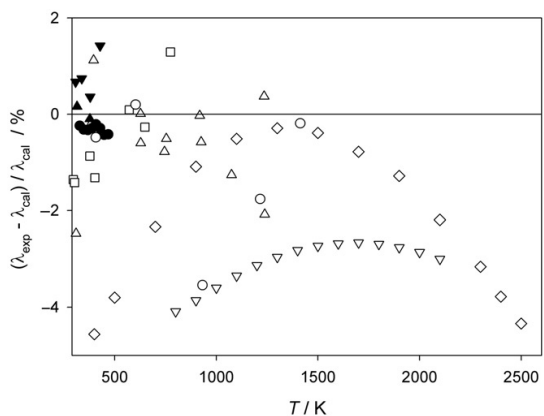


Figure 11. Deviations of experimental and calculated thermal conductivity coefficients from values calculated with the new interatomic potential for ^4He at higher temperatures. Experimental data: (△) Vargaftik and Zhimina [84]; (□) LeNeindre *et al.* [85]; (●) Haarman [70]; (▽) Faubert and Springer [86]; (○) Martchenko and Shashkov [87]; (◇) Jody *et al.* [88]; (▼) Mustafa *et al.* [73]; (▲) Johns *et al.* [74]. Calculated values: (---) Hurly and Mehl [2].

not be corrected with respect to the initial density dependence, since details about the pressure or density of the measurements are missing. The experimental data by Zarev *et al.* [83] (concentric-cylinder method) and by Roder [78, 79] (parallel-plate technique) are characterized by comparable small deviations from the calculated values.

Figure 11 illustrates the comparison above ambient temperature. The measurement of Johns *et al.* [74] at 378 K agrees again within $\pm 0.1\%$ with the calculated value. Furthermore, the results of the measurements of Haarman [70] between 328 and 468 K deviate on average by -0.4% , but show nearly the same temperature dependence as the calculated values. The differences of the measurements by Mustafa *et al.* [73] cannot be explained with respect to the much valued transient hot-wire technique. The experimental data by Vargaftik and Zhimina [84] (common hot-wire technique) and by Le Neindre *et al.* [85] (concentric-cylinder method) are characterized by not too large deviations from the calculated values, but do not allow any test of the potential and of the kinetic theory.

Figure 12 shows for ^3He the deviations of the experimental thermal conductivity data by Kerrisk and Keller [77] between 1.5 and 3.95 K and by Zarev *et al.* [83] between 79 and 276 K from the theoretical values. The differences correspond approximately to those for ^4He .

5. Conclusion

A new potential function for helium [3] was used for the quantum-mechanical calculation of the second and

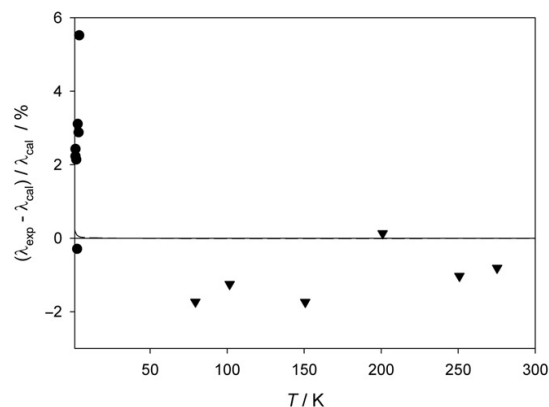


Figure 12. Deviations of experimental and calculated thermal conductivity coefficients from values calculated with the new interatomic potential for ^3He . Experimental data: (●) Kerrisk and Keller [77]; (▼) Zarev *et al.* [83]. Calculated values: (---) Hurly and Mehl [2].

third pressure virial of the viscosity and of the thermal conductivity coefficients for ^4He and ^3He in the range from 1 to 10 000 K. The extensive comparison with experimental data as well as with recent calculations by Hurly and Mehl [2] using a potential function obtained from a fit to various *ab initio* calculations from the literature makes evident that the theoretically calculated values of the thermophysical properties are characterized by uncertainties superior to any experiment. In the case of the second pressure virial coefficient the differences between the results obtained by our potential and the potential of Hurly and Mehl give an estimate of the uncertainties of this property. Values of the third pressure virial coefficient calculated classically including a non-additive contribution according to the Axilrod–Teller potential model and a quantum-mechanical correction are in excellent agreement with very recent experimental data by McLinden and Lösch-Will [38]. For both viscosity and thermal conductivity the relative differences between the results obtained from the two potentials do not exceed $\pm 0.01\%$ for temperatures above 15 K and increase to $\pm 0.13\%$ at 1 K. This shows that the transport properties are practically insensitive to small changes in the potential function. To get reliable error bars we stress that contributions from the kinetic theory beyond the fifth-order approximation are distinctly smaller than $\pm 0.01\%$ (see figure 2 of [1]). In addition, all digits

of the calculated values given by Hurly and Mehl for viscosity and thermal conductivity could be reproduced when applying their potential function and using our computer code. Hence the uncertainties in viscosity and thermal conductivity should be primarily due to the errors in the potential. Since our potential is more accurate than the one of Hurly and Mehl, we would suggest $\pm 0.02\%$ as a conservative estimate of the relative uncertainties for both properties down to 15 K. At temperatures lower than 15 K the uncertainty increases to $\pm 0.2\%$ at 1 K, but is still far below any experimental uncertainty. The theoretical values for all calculated thermophysical properties can safely be recommended as standard values for ^3He and ^4He in the temperature range from 1 K to 10 000 K apart from the third pressure virial coefficient, for which the quantum correction is certainly not applicable at temperatures below 20 K. The calculated values are listed in the Appendix.

We wish to thank Larry Viehland for providing his Fortran code.

Appendix A: Thermophysical properties of ^4He and ^3He calculated in this work

The thermophysical properties of ^4He and ^3He are given in table 3.

Table 3. Thermophysical properties of ^4He and ^3He calculated in this work.

$T(\text{K})$	^4He				^3He		
	$B(\text{cm}^3 \text{mol}^{-1})$	$C(\text{cm}^6 \text{mol}^{-2})$	$\eta(\mu\text{Pa s})$	$\lambda(\text{mWm}^{-1} \text{K}^{-1})$	$B(\text{cm}^3 \text{mol}^{-1})$	$\eta(\mu\text{Pa s})$	$\lambda(\text{mWm}^{-1} \text{K}^{-1})$
1.00	-475.93		0.32875	2.6288	-236.32	0.55936	5.7842
1.20	-370.40		0.34015	2.7166	-205.50	0.66407	6.8674
1.40	-302.50		0.35796	2.8422	-180.96	0.76250	7.8906
1.60	-255.41		0.38408	3.0296	-161.04	0.85015	8.8094
1.80	-220.88		0.41793	3.2800	-144.60	0.92505	9.6041
2.00	-194.45		0.45824	3.5852	-130.84	0.98722	10.274
2.25	-168.96		0.51567	4.0268	-116.54	1.0491	10.952
2.50	-149.15		0.57869	4.5156	-104.70	1.0969	11.485
2.75	-133.28		0.64523	5.0334	-94.764	1.1345	11.908
3.00	-120.24		0.71357	5.5656	-86.312	1.1651	12.254
3.50	-100.05		0.85058	6.6326	-72.723	1.2153	12.807
4.00	-85.089		0.98279	7.6619	-62.293	1.2603	13.281
4.50	-73.531		1.1072	8.6316	-54.042	1.3060	13.745
5.00	-64.323		1.2234	9.5375	-47.354	1.3546	14.231
6.00	-50.558		1.4333	11.179	-37.169	1.4609	15.290
7.00	-40.750		1.6203	12.645	-29.776	1.5756	16.444
8.00	-33.404		1.7913	13.987	-24.162	1.6940	17.647
9.00	-27.697		1.9509	15.239	-19.751	1.8127	18.864
10.00	-23.135		2.1018	16.423	-16.193	1.9303	20.074

(continued)

Table 3. Continued.

$T(K)$	^4He				^3He		
	$B(\text{cm}^3 \text{mol}^{-1})$	$C(\text{cm}^6 \text{mol}^{-2})$	$\eta(\mu\text{Pa s})$	$\lambda(\text{mWm}^{-1} \text{K}^{-1})$	$B(\text{cm}^3 \text{mol}^{-1})$	$\eta(\mu\text{Pa s})$	$\lambda(\text{mWm}^{-1} \text{K}^{-1})$
11.00	-19.407		2.2458	17.552	-13.262	2.0456	21.265
12.00	-16.304		2.3841	18.637	-10.807	2.1583	22.431
14.00	-11.439		2.6468	20.695	-6.9255	2.3757	24.685
16.00	-7.8037		2.8943	22.635	-3.9990	2.5830	26.837
18.00	-4.9899		3.1296	24.478	-1.7171	2.7814	28.897
20.00	-2.7515	310.0	3.3548	26.242	0.10887	2.9722	30.878
22.00	-0.93187	291.5	3.5713	27.937	1.6004	3.1561	32.788
23.00	-0.14494	284.4	3.6767	28.763	2.2474	3.2458	33.720
24.00	0.57370	278.0	3.7803	29.574	2.8394	3.3341	34.637
25.00	1.2323	272.5	3.8823	30.373	3.3827	3.4212	35.541
26.00	1.8377	267.4	3.9828	31.160	3.8829	3.5069	36.432
28.00	2.9119	258.7	4.1795	32.700	4.7723	3.6750	38.178
30.00	3.8346	251.2	4.3710	34.199	5.5378	3.8389	39.880
35.00	5.6493	236.4	4.8302	37.794	7.0478	4.2327	43.969
40.00	6.9740	225.1	5.2662	41.206	8.1528	4.6073	47.858
45.00	7.9739	216.1	5.6832	44.469	8.9878	4.9661	51.583
50.00	8.7482	208.6	6.0842	47.607	9.6342	5.3116	55.169
60.00	9.8508	196.6	6.8472	53.575	10.552	5.9697	62.000
70.00	10.578	187.1	7.5682	59.215	11.154	6.5924	68.462
80.00	11.075	179.3	8.2558	64.592	11.561	7.1868	74.630
90.00	11.425	172.6	8.9160	69.754	11.842	7.7579	80.555
100.00	11.673	166.7	9.5531	74.735	12.038	8.3092	86.275
120.00	11.977	156.8	10.770	84.250	12.267	9.3631	97.208
140.00	12.126	148.5	11.926	93.283	12.364	10.364	107.59
160.00	12.186	141.5	13.032	101.93	12.386	11.323	117.54
180.00	12.191	135.4	14.099	110.26	12.364	12.248	127.12
200.00	12.163	129.9	15.130	118.32	12.314	13.142	136.39
225.00	12.099	123.9	16.378	128.07	12.229	14.225	147.62
250.00	12.015	118.7	17.588	137.52	12.128	15.274	158.51
273.15	11.927	114.3	18.678	146.04	12.028	16.220	168.30
275.00	11.920	114.0	18.764	146.71	12.020	16.294	169.07
298.15	11.826	110.0	19.826	155.01	11.916	17.215	178.63
300.00	11.818	109.8	19.910	155.66	11.908	17.288	179.38
325.00	11.714	105.9	21.030	164.41	11.795	18.260	189.46
350.00	11.609	102.4	22.128	172.98	11.682	19.212	199.32
375.00	11.504	99.22	23.204	181.39	11.571	20.146	209.00
400.00	11.400	96.27	24.261	189.64	11.462	21.064	218.51
450.00	11.199	90.98	26.325	205.76	11.252	22.855	237.07
500.00	11.006	86.38	28.331	221.42	11.053	24.596	255.11
600.00	10.651	78.73	32.196	251.60	10.688	27.951	289.87
700.00	10.332	72.56	35.905	280.55	10.362	31.170	323.22
800.00	10.045	67.46	39.488	308.51	10.071	34.279	355.43
900.00	9.7857	63.15	42.966	335.66	9.8077	37.299	386.70
1000.00	9.5497	59.44	46.357	362.12	9.5689	40.242	417.18
1200.00	9.1348	53.36	52.922	413.35	9.1500	45.940	476.20
1400.00	8.7799	48.56	59.253	462.75	8.7924	51.436	533.10
1600.00	8.4711	44.65	65.398	510.68	8.4816	56.771	588.32
1800.00	8.1987	41.38	71.390	557.42	8.2078	61.972	642.17
2000.00	7.9556	38.60	77.253	603.15	7.9636	67.062	694.85
2500.00	7.4446	33.17	91.461	713.95	7.4506	79.395	822.50
3000.00	7.0330	29.16	105.17	820.87	7.0379	91.299	945.67
3500.00	6.6905	26.06	118.52	924.88	6.6945	102.88	1065.5

(continued)

Table 3. Continued.

$T(K)$	^4He				^3He		
	$B(\text{cm}^3 \text{mol}^{-1})$	$C(\text{cm}^6 \text{mol}^{-2})$	$\eta(\mu\text{Pa s})$	$\lambda(\text{mWm}^{-1} \text{K}^{-1})$	$B(\text{cm}^3 \text{mol}^{-1})$	$\eta(\mu\text{Pa s})$	$\lambda(\text{mWm}^{-1} \text{K}^{-1})$
4000.00	6.3988	23.58	131.56	1026.6	6.4022	114.21	1182.7
4500.00	6.1457	21.55	144.38	1126.5	6.1486	125.33	1297.7
5000.00	5.9229	19.84	157.00	1224.9	5.9254	136.29	1411.1
6000.00	5.5459	17.14	181.80	1418.1	5.5480	157.81	1633.6
7000.00	5.2363	15.08	206.12	1607.6	5.2379	178.92	1852.0
8000.00	4.9752	13.46	230.11	1794.5	4.9765	199.75	2067.2
9000.00	4.7505	12.14	253.83	1979.3	4.7519	220.34	2280.1
10000.00	4.5542	11.05	277.35	2162.5	4.5551	240.76	2491.2

References

- [1] J. J. Hurly and M. R. Moldover, *J. Res. Natl. Inst. Stand. Technol.* **105**, 667 (2000).
- [2] J. J. Hurly and J. B. Mehl, *J. Res. Natl. Inst. Stand. Technol.* **112**, 75 (2007).
- [3] R. Hellmann, E. Bich, and E. Vogel, *Molec. Phys.* (in press).
- [4] K. T. Tang and J. P. Toennies, *J. Chem. Phys.* **80**, 3726 (1984).
- [5] H. B. G. Casimir and D. Polder, *Phys. Rev.* **73**, 360 (1948).
- [6] F. Luo, G. C. McBane, G. Kim, C. F. Giese, and W. R. Gentry, *J. Chem. Phys.* **98**, 3564 (1993).
- [7] W. Schöllkopf and J. P. Toennies, *Science* **266**, 1345 (1994).
- [8] R. E. Grisenti, W. Schöllkopf, J. P. Toennies, G. C. Hegerfeldt, T. Köhler, and M. Stoll, *Phys. Rev. Lett.* **85**, 2284 (2000).
- [9] M. J. Jamieson, G. W. F. Drake, and A. Dalgarno, *Phys. Rev. A* **51**, 3358 (1995).
- [10] A. R. Janzen and R. A. Aziz, *J. Chem. Phys.* **107**, 914 (1997).
- [11] M.-K. Chen and K. T. Chung, *Phys. Rev. A* **53**, 1439 (1996).
- [12] N. C. Handy and A. M. Lee, *Chem. Phys. Lett.* **252**, 425 (1996).
- [13] W. Kutzelnigg, *Molec. Phys.* **90**, 909 (1997).
- [14] G. T. McConville and J. J. Hurly, *Metrologia* (1991) **28**, 375 (1991).
- [15] R. J. LeRoy, *Computer Program for Calculating Phase Shifts and Time Delays for Scattering on a Spherical Potential*, Chemical Physics Research Report CP-107R (University of Waterloo, Waterloo, Ontario, Canada).
- [16] J. J. Hurly, G. T. McConville, and W. L. Taylor, *Algorithms and Fortran Programs to Calculate Quantum Collision Integrals for Realistic Intermolecular Potentials*, MLM-3635 (Miamisburg, EG&GMAT, 1990).
- [17] M. Abramowitz and I. A. Stegun, *Handbook of Mathematical Functions* (Dover, New York, 1972), p. 365.
- [18] M. E. Boyd, S. Y. Larsen, and J. E. Kilpatrick, *J. Chem. Phys.* **50**, 4034 (1969).
- [19] S. Kim and D. Henderson, *Proc. Nat. Acad. Sci., Wash.* **55**, 705 (1966).
- [20] K. Lucas, *Angewandte Statistische Thermodynamik* (Springer, Berlin, 1986).
- [21] B. M. Axilrod and E. Teller, *J. Chem. Phys.* **11**, 299 (1943).
- [22] B. M. Axilrod, *J. Chem. Phys.* **19**, 719 (1951).
- [23] A. Kumar and W. J. Meath, *Molec. Phys.* **54**, 823 (1985).
- [24] F. R. Meeks, T. J. Cleland, K. E. Hutchinson, and W. L. Taylor, *J. Chem. Phys.* **100**, 3813 (1994).
- [25] L. A. Viehland, A. R. Janzen, and R. A. Aziz, *J. Chem. Phys.* **102**, 5444 (1995).
- [26] R. J. LeRoy, *LEVEL 7.7. A Computer Program for Solving the Radial Schrödinger Equation for Bound and Quasibound Levels*, Chemical Physics Research Report CP-661 (University of Waterloo, Waterloo, Ontario, Canada).
- [27] K. H. Berry, *Metrologia* **15**, 89 (1979).
- [28] D. Gagan and G. W. Michel, *Metrologia* **16**, 149 (1980).
- [29] R. A. Aziz, *Molec. Phys.* **61**, 1487 (1987).
- [30] R. C. Kemp, W. R. G. Kemp, and L. M. Besley, *Metrologia* **23**, 61 (1986/87).
- [31] W. G. Schneider and J. A. H. Duffie, *J. Chem. Phys.* **17**, 751 (1949).
- [32] J. L. Yntema and W. G. Schneider, *J. Chem. Phys.* **18**, 641 (1950).
- [33] A. L. Blancett, K. R. Hall, and F. B. Canfield, *Physica* **47**, 75 (1970).
- [34] M. Waxman as cited by L. A. Guildner, and R. E. Edsinger, *J. Res. Natl. Bur. Stand.* **80**, 703 (1976).
- [35] M. Waxman and H. Davis, *J. Res. Natl. Bur. Stand.* **83**, 415 (1978).
- [36] G. S. Kell, G. E. McLaurin, and E. Whalley, *J. Chem. Phys.* **68**, 2199 (1978).
- [37] J. C. Holste, M. Q. Watson, M. T. Bellomy, P. T. Eubank, and K. R. Hall, *AIChE J.* **26**, 954 (1980).
- [38] M. O. McLinden and C. Lössch-Will, *J. Chem. Thermodyn.* **39**, 507 (2007).
- [39] W. E. Keller, *Phys. Rev.* **98**, 1571 (1955).
- [40] F. C. Maticotta, G. T. McConville, P. P. M. Steur, and M. Durieux, *Metrologia* **24**, 61 (1987).
- [41] W. C. Pfefferle, J. A. Goff, and J. G. Miller, *J. Chem. Phys.* **23**, 509 (1955).
- [42] A. E. Hoover, F. B. Canfield, R. Kobayashi, and T. W. Leland Jr, *J. Chem. Eng. Data* **9**, 568 (1964).
- [43] J. A. Provine and F. B. Canfield, *Physica* **52**, 79 (1971).
- [44] W. F. Vogl and K. R. Hall, *Physica* **59**, 529 (1972).

- [45] J. Kestin and W. Leidenfrost, *Physica* **25**, 1033 (1959).
- [46] J. Kestin and A. Nagashima, *J. Chem. Phys.* **40**, 3648 (1964).
- [47] J. Kestin, S. T. Ro, and W. A. Wakeham, *J. Chem. Phys.* **56**, 4119 (1972).
- [48] G. P. Flynn, R. V. Hanks, N. A. Lemaire, and J. Ross, *J. Chem. Phys.* **38**, 154 (1963).
- [49] J. A. Gracki, G. P. Flynn, and J. Ross, *J. Chem. Phys.* **51**, 3856 (1969).
- [50] E. Vogel, *Ber. Bunsenges. Phys. Chem.* **88**, 997 (1984).
- [51] C. Evers, H. W. Lösch, and W. Wagner, *Int. J. Thermophys.* **23**, 1411 (2002).
- [52] R. F. Berg, *Metrologia* **42**, 11 (2005).
- [53] R. F. Berg, *Metrologia* **43**, 183 (2006).
- [54] G. F. Newell, *Z. Ang. Math. Phys.* **10**, 160 (1959).
- [55] J. A. Bearden, *Phys. Rev.* **56**, 1023 (1939).
- [56] H. L. Johnston and E. R. Grilly, *J. Phys. Chem.* **46**, 948 (1942).
- [57] E. W. Becker, R. Misenta, and F. Schmeissner, *Z. Phys.* **137**, 126 (1954).
- [58] E. W. Becker and R. Misenta, *Z. Phys.* **140**, 535 (1955).
- [59] J. M. J. Coremans, A. van Itterbeek, J. J. M. Beenakker, H. F. P. Knaap, and P. Zandbergen, *Physica* **24**, 557 (1958).
- [60] J. T. F. Kao and R. Kobayashi, *J. Chem. Phys.* **47**, 2836 (1967).
- [61] A. G. Clarke and E. B. Smith, *J. Chem. Phys.* **51**, 4156 (1969).
- [62] D. W. Gough, G. P. Matthews, and E. B. Smith, *J. Chem. Soc. Faraday Trans. I* **72**, 645 (1976).
- [63] W. H. Keesom, *Helium* (Elsevier, Amsterdam, 1942), p. 107.
- [64] H. Kamerlingh Onnes and S. Weber Vers. Kon. Acad. Wetenschappen, Amsterdam **21**, 1385 (1913).
- [65] J. Kestin, S. T. Ro, and W. A. Wakeham, *J. Chem. Phys.* **56**, 5837 (1972).
- [66] F. A. Guevara, B. B. McInteer, and W. E. Wageman, *Phys. Fluids* **12**, 2493 (1969).
- [67] R. A. Dawe and E. B. Smith, *J. Chem. Phys.* **52**, 693 (1970).
- [68] R. Di Pippo, J. Kestin, and J. H. Whitelaw, *Physica* **32**, 2064 (1966).
- [69] E. Vogel, C. Küchenmeister, E. Bich, and A. Laesecke *J. Phys. Chem. Ref. Data* **27**, 947 (1998).
- [70] J. W. Haarman, *Am. Inst. Phys. Conf. Proc.* **11**, 193 (1973).
- [71] J. Kestin, R. Paul, A. A. Clifford, and W. A. Wakeham, *Physica A* **100**, 349 (1980).
- [72] M. J. Assael, M. Dix, A. Lucas, and W. A. Wakeham, *J. Chem. Soc. Faraday Trans. I* **77**, 439 (1981).
- [73] M. Mustafa, M. Ross, R. D. Trengove, W. A. Wakeham, and M. Zalaf, *Physica A* **141**, 233 (1987).
- [74] A. I. Johns, A. C. Scott, J. T. R. Watson, D. Ferguson, and A. A. Clifford, *Phil. Trans. Roy. Soc. London* **325**, 295 (1988).
- [75] J. B. Ubbink and W. J. de Haas, *Physica* **10**, 465 (1943).
- [76] I. F. Golubev and I. B. Shpagina, *Gasovaya Promyshlennost* **11**, 40 (1966).
- [77] J. F. Kerrisk and W. E. Keller, *Phys. Rev.* **177**, 341 (1969).
- [78] H. M. Roder, *Conference Proceedings of the Thermodynamiksymposium Paper VI-3*, ed. K. Schäfer (Heidelberg, Germany, 1967).
- [79] H. M. Roder, *NBS Laboratory Note, Project No. 2750426*, 29 January (1971).
- [80] A. G. Shashkov, N. A. Nesterov, V. M. Sudnik, and V. I. Alejnikova, *Inzh. Fiz. Zh.* **30**, 671 (1976).
- [81] A. Acton and K. Kellner, *Physica B* **90**, 192 (1977).
- [82] V. N. Popov and V. V. Zarev, *Trudy Mosk. Energ. Inst.* **532**, 12 (1981).
- [83] V. V. Zarev, D. N. Nagorov, V. A. Nikonorov, and V. N. Popov, *Moskvus Sb. Trudy Mosk. Energ. Inst.* **72**, 185 (1985).
- [84] N. B. Vargaftik and N. Ch. Zhimina, *Atomnaya Energiya* **19**, 300 (1965).
- [85] B. LeNeindre, R. Tufeu, P. Bury, P. Johannin, and B. Vodar, *Proceedings of the 8th Conference on Thermal Conductivity* (1968) (Plenum, New York, 1969), p. 75.
- [86] F. M. Faubert and G. S. Springer, *J. Chem. Phys.* **58**, 4080 (1973).
- [87] E. I. Martchenko and A. G. Shashkov, *Inzh. Fiz. Zh.* **26**, 1089 (1974).
- [88] B. J. Jody, S. C. Saxena, V. P. S. Nain, and R. A. Aziz, *Chem. Phys.* **22**, 53 (1977).

4.2 *Ab initio* potential energy curve for the neon atom pair and thermophysical properties of the dilute neon gas

4.2.1 I. Neon-neon interatomic potential and rovibrational spectra

Robert Hellmann, Eckard Bich, Eckhard Vogel

Mol. Phys. **106**, 133-140 (2008).

Alle quantenchemischen Berechnungen sowie die Anpassung des Potentials wurden selbst durchgeführt. Der eigene Anteil beträgt etwa 80%.

RESEARCH ARTICLE

Ab initio potential energy curve for the neon atom pair and thermophysical properties of the dilute neon gas.

I. Neon–neon interatomic potential and rovibrational spectra

Robert Hellmann, Eckard Bich and Eckhard Vogel*

Institut für Chemie, Universität Rostock, Rostock, Germany

(Received 22 October 2007; final version received 29 November 2007)

A neon–neon interatomic potential energy curve was derived from quantum-mechanical *ab initio* calculations using basis sets of up to t-aug-cc-pV6Z quality supplemented with bond functions and *ab initio* methods up to CCSDT(Q). In addition, corrections for relativistic effects were determined. An analytical potential function was fitted to the *ab initio* values and utilised to calculate the rovibrational spectra. The quality of the interatomic potential function was tested by comparison of the calculated spectra with experimental ones and those derived from other potentials of the literature. In a following paper the new interatomic potential is applied in the framework of the quantum-statistical mechanics and of the corresponding kinetic theory to determine selected thermophysical properties of neon governed by two-body and three-body interactions.

Keywords: neon *ab initio* pair potential; neon analytical potential function; rovibrational spectra

1. Introduction

In two recent papers [1,2] we demonstrated that the pair potential between two helium atoms can be determined very accurately using standard quantum chemistry software packages and that the thermophysical two-body and three-body properties of helium gas can be calculated with uncertainties which are superior to those of experimental data. Hence, the calculated properties can be applied as standard values over the complete range of temperatures from 1 to 10,000 K.

The determination of the pair potential between two neon atoms is computationally much more demanding because of the increased number of electrons. But it could be expected that the thermophysical properties (especially transport properties) of neon, derived from a state-of-the-art pair potential, could serve as a second standard in combination with helium values for calibrating high-precision measuring instruments at low density and as starting points within the development of transport property surface correlations.

In this work, it is intended to develop an accurate *ab initio* Ne–Ne interatomic potential based on CCSD(T) calculations using larger basis sets than previously possible and including an extrapolation to the complete basis set (CBS) limit. In addition, highly accurate corrections for neglected contributions should

be included. In particular, the full T_3 operator should be taken into account by adding the differences in the interaction energies between CCSDT and CCSD(T), each determined with a smaller basis set, to the extrapolated CCSD(T) results. In an analogous manner corrections for perturbative quadruple excitations, core–core and core–valence correlations as well as scalar relativistic effects should be taken into account. Corrections for the breakdown of the Born–Oppenheimer approximation which had to be considered for the helium interaction potential are negligible for neon, because the neon isotopes are about five times heavier than ^4He . To the best of our knowledge, corrections arising from the Casimir–Polder retardation [3] have not yet been calculated for neon. The retardation effect is probably very small, but should be considered in future improvements of the potential.

The second priority objective of the present paper was to calculate rovibrational energy levels which should be used to compare with experimental data as a stringent test of the interatomic pair potential. Electronic absorption spectra of the neon dimer Ne_2 were investigated by Tanaka and Yoshino [4] in the vacuum ultraviolet (VUV) region with respect to the rotational structure and used to derive the potential

*Corresponding author. Email: eckhard.vogel@uni-rostock.de

well depth as well as the first two vibrational states and their rotational constants for the ground electronic state. Some other groups utilised the data of Tanaka and Yoshino together with high-energy beam scattering data and reliable values for different thermophysical properties of neon to determine semi-empirical potential curves for its ground electronic state from which the most recent one by Aziz and Slaman [5] is certainly the best. In 2003 Wüest and Merkt [6] performed new measurements of the transition between the $X0_g^+$ ground electronic state of Ne_2 and the second electronically excited state $I10_u^+$ using high-resolution VUV laser spectroscopy. They derived a map of the rovibrational energy level structure of the ground electronic state of the ^{20}Ne – ^{20}Ne and of the ^{20}Ne – ^{22}Ne dimers and determined a semi-empirical interaction potential for the neon dimer in its ground electronic state. The rovibrational energy levels calculated in this paper are to be compared particularly with the experimental ones by Wüest and Merkt.

2. Towards an accurate neon–neon interaction potential energy curve

The precise determination of the interatomic potentials between two rare gas atoms is not an easy task, whereas the demands grow with the increasing number of electrons of the respective atoms. The progress in the process of development towards an accurate neon–neon potential curve since 1999 is reported here in order to rank our work described in this paper.

In 1999 van Mourik *et al.* [7] derived an *ab initio* neon–neon potential comparably close to the semi-empirical potential curve of Aziz and Slaman [5]. The attractive part of the interaction potential is determined solely by dispersion due to electron correlation. To describe electron correlation accurately, large basis sets with many diffuse basis functions are needed. Hence van Mourik *et al.* [7] used for their calculations multi-augmented correlation-consistent basis sets of Dunning and co-workers up to t-aug-cc-pV5Z [8–10] and additionally a d-aug-cc-pV6Z basis set established by themselves. Suitable *ab initio* methods for determining the electron correlation within the supermolecular approach are many-body perturbation theory and coupled-cluster (CC) theory, the latter showing very fast convergence to the full configuration interaction (Full CI) limit. In particular, CCSD(T) (coupled-cluster theory with iterative singles and doubles excitations and noniterative perturbational treatment of triple excitations) [11] proved to be very successful in the calculations by van Mourik *et al.* [7] when using the counterpoise correction (CP) of Boys and Bernardi

[12] for the basis set superposition error (BSSE) and extrapolating to the complete basis set (CBS) limit. Van Mourik *et al.* performed calculations in the range from $R=0.267$ nm to $R=0.466$ nm, but reported only values for the well depth, for example, 40.92 K at $R=0.310$ nm for the CBS limit with d-aug-cc-pVXZ basis sets to be compared with 42.25 K at $R=0.3091$ nm for the potential by Aziz and Slaman [5]. In addition, van Mourik *et al.* investigated the core–core and core–valence correlation effects at the equilibrium distance and found them to be comparably small.

Van de Bovenkamp and van Duijneveldt [13] performed, also in 1999, CCSD(T) calculations with an interaction optimised basis set (IO240) including mid-bond functions (3s3p2d1f1g). They calculated the Ne–Ne interaction potential at internuclear separations between $R=0.212$ nm and $R=0.476$ nm and obtained a well depth of 40.99 K at $R=0.310$ nm. Van de Bovenkamp and van Duijneveldt estimated that the missing attraction in their own potential compared with Aziz and Slaman should be due to basis set incompleteness, to incomplete consideration of triple and higher excitations, and to relativistic effects. Cybulski and Toczyłowski [14] used CCSD(T) together with the aug-cc-pV5Z basis set and a set of mid-bond functions (3s3p2d2f1g) for their calculations of the potential energy curve in the range between $R=0.225$ nm and $R=0.500$ nm and determined a well depth of 41.19 K at $R=0.30988$ nm (the fitted potential has a well depth of 41.15 K) which is also smaller than that of the semi-empirical potential of Aziz and Slaman [5]. Van de Bovenkamp and van Duijneveldt as well as Cybulski and Toczyłowski used the counterpoise procedure for the BSSE, but did not perform any extrapolation to the CBS limit and did not consider core–core and core–valence contributions. However, they proved the importance of the use of bond functions. Here caution is needed if bond functions are used with small atom-centred basis sets, since they can lead to serious imbalance effects as was shown for the Ne–Ne potential by Grochola *et al.* [15]. Fortunately, computational advances allow one to use comparably large basis sets today for Ne–Ne so that imbalance effects can be avoided.

Gdanitz [16] applied the results of Cybulski and Toczyłowski and added basic corrections for basis set incompleteness, for Full CI, for core–core and core–valence correlation as well as for scalar relativistic effects resulting in a well depth of 41.535 K at $R=0.31007$ nm. No analytical potential function was given in this paper. A potential fit was done later by Venkatraj *et al.* [17] and used in molecular dynamics simulations of gaseous and liquid neon [17] and in Monte Carlo simulations of the vapour–liquid

equilibria [18]. Giese *et al.* [19] extended the calculations of Cybulski and Toczyłowski to a larger number of internuclear separations (100 distances) and performed separate fits for the repulsive (SCF) part of the potential and for the attractive (correlation) part, whereas the fit of Cybulski and Toczyłowski for the whole potential was left unchanged. Nasrabad *et al.* [20] extrapolated the results of Cybulski and Toczyłowski to the complete basis set limit. The resulting potential has a well depth of 41.35 K at $R=0.3097$ nm. It was used together with a non-additive three-body contribution for Monte Carlo simulations of the vapour–liquid equilibria. Lee [21] carried out CCSDT [22] calculations at $R=0.31$ nm and added the difference between CCSDT and CCSD(T) to the CCSD(T) result of 41.19 K from Cybulski and Toczyłowski to estimate the binding energy of the dimer. He found a well depth of 41.87 K which shows that missing triple contributions in CCSD(T) are the main reason for the disagreement between CCSD(T) potentials and the potential of Aziz and Slaman.

3. Quantum chemical determination and analytical representation of the Ne–Ne potential

The interaction energies were determined for 32 different Ne–Ne distances between $R=0.14$ nm and $R=0.80$ nm which is sufficient for the fit of an analytical potential function. All calculations were performed using the supermolecular approach including a full counterpoise correction [12] as follows:

$$V(R) = \Delta E_{\text{Ne–Ne}}(R) = E_{\text{Ne–Ne}}(R) - 2E_{\text{Ne–Q}}(R). \quad (1)$$

Here, $E_{\text{Ne–Q}}(R)$ corresponds to the energy of a neon atom with a ghost basis set at the distance R .

First, CCSD(T) calculations were performed within the frozen-core approximation using the t-aug-cc-pV5Z and t-aug-cc-pV6Z basis sets, each supplemented by a (4s4p3d3f2g) set of bond functions centred between the two atoms. The bond function exponents are: *sp*: 0.06, 0.18, 0.54, 1.62; *df*: 0.15, 0.45, 1.35; *g*: 0.3, 0.9. These basis sets (and in an analogous manner all further basis sets) are abbreviated as taV5Z+(44332) and taV6Z+(44332). For each separation R the correlation part of the CCSD(T) interaction energies $V_{\text{CCSD(T)corr}}$ obtained with these two basis sets was extrapolated to the CBS limit with the formula proposed by Halkier *et al.* [23]:

$$V_{\text{CCSD(T)corr}}^{\text{taVYZ}} = V_{\text{CCSD(T)corr}}^{\text{CBS}} + \alpha X^{-3}. \quad (2)$$

The SCF interaction energies were not extrapolated and taken from the taV6Z+(44332) calculations.

Corrections for missing core–core and core–valence correlation, relativistic effects as well as for higher

coupled-cluster contributions were added to the CCSD(T) interaction energies:

$$V = V_{\text{CCSD(T)}}^{\text{CBS}} + \Delta V_{\text{core}} + \Delta V_{\text{rel}} + \Delta V_{\text{T–(T)}} + \Delta V_{\text{(Q)}}. \quad (3)$$

The correction for core–core and core–valence correlation ΔV_{core} was estimated using the dawCV5Z basis set [24] by computing the differences between the interaction energies at the all-electron CCSD(T) level and at the frozen-core CCSD(T) level. The effect is relatively small at the equilibrium distance (+0.068 K at $R=0.31$ nm), but becomes rather large at small distances (–110.5 K at $R=0.14$ nm).

The correction for scalar relativistic effects ΔV_{rel} was also computed at the all-electron CCSD(T)/dawCV5Z level within the so-called Cowan–Griffin approximation [25]. The resulting correction is negative for all distances and similar in magnitude to ΔV_{core} .

Missing triple contributions in the CCSD(T) calculations were estimated using a daVQZ+(3321) basis set (exponents of the bond functions: *sp*: 0.1, 0.3, 0.9; *d*: 0.25, 0.75; *f*: 0.45) in the non-relativistic frozen-core approximation by calculating the differences between the interaction energies at the CCSDT and CCSD(T) levels of theory. The resulting correction $\Delta V_{\text{T–(T)}}$ is much larger than ΔV_{core} and ΔV_{rel} at equilibrium distance (–0.646 K at $R=0.31$ nm) and relatively unimportant at small distances (–8.57 K at $R=0.14$ nm).

The correction $\Delta V_{\text{(Q)}}$ resulting from the noniterative perturbational treatment of connected quadruple excitations was determined in a similar way as $\Delta V_{\text{T–(T)}}$. The differences between the CCSDT(Q) [26] and CCSDT interaction energies were calculated with an aVTZ+(3321) basis set (exponents of the bond functions equal to the ones used for the triples contribution correction). At large R , numerical inaccuracies turned out to be problematic. Hence, the results for distances between $R=0.38$ nm and $R=0.50$ nm had to be smoothed with a polynomial, whereas the results for distances larger than $R=0.50$ nm were extrapolated by assuming that the ratio between this correction and the total correlation interaction energy is constant. The correction $\Delta V_{\text{(Q)}}$ is very small and amounts to only –0.091 K at $R=0.31$ nm which shows that CCSDT(Q) is very close to the Full CI limit and that CCSDT is a good approximation to Full CI for the calculation of interaction energies.

All *ab initio* results are given in Tables 1 and 2. The CCSD(T) calculations were performed with PSI3 [27] and with the Mainz–Austin–Budapest version of ACES II [28] which was also used for the CCSDT

Table 1. Ne–Ne SCF and CCSD(T) interaction energies for the taV5Z + (44332) and taV6Z + (44332) basis sets and the extrapolated CCSD(T) values. All energies are in Kelvin.

R/nm	V(SCF)		V(CCSD(T))		
	taV5Z + (44332)	taV6Z + (44332)	taV5Z + (44332)	taV6Z + (44332)	extrapolated
0.14	71550.433	71548.487	69122.802	69044.386	68939.345
0.16	28504.771	28503.861	27107.732	27067.581	27013.678
0.18	11385.933	11385.622	10504.957	10486.497	10461.566
0.20	4551.060	4550.932	3966.717	3957.967	3946.125
0.22	1817.497	1817.446	1421.412	1417.452	1412.082
0.24	724.521	724.515	454.750	453.070	450.770
0.25	457.077	457.078	234.567	233.499	232.029
0.26	288.193	288.196	104.787	104.124	103.208
0.27	181.605	181.610	30.507	30.110	29.559
0.28	114.373	114.379	−10.086	−10.314	−10.634
0.29	71.991	71.997	−30.554	−30.678	−30.855
0.30	45.290	45.295	−39.279	−39.328	−39.401
0.31	28.478	28.481	−41.357	−41.362	−41.375
0.32	17.897	17.900	−39.870	−39.855	−39.840
0.33	11.241	11.245	−36.658	−36.626	−36.587
0.34	7.057	7.060	−32.765	−32.726	−32.678
0.35	4.428	4.431	−28.773	−28.737	−28.690
0.36	2.778	2.780	−25.000	−24.962	−24.913
0.37	1.741	1.743	−21.576	−21.542	−21.497
0.38	1.092	1.093	−18.555	−18.523	−18.481
0.40	0.428	0.429	−13.673	−13.651	−13.623
0.42	0.167	0.168	−10.114	−10.094	−10.068
0.44	0.065	0.066	−7.542	−7.526	−7.505
0.46	0.026	0.026	−5.684	−5.671	−5.654
0.48	0.010	0.010	−4.329	−4.323	−4.314
0.50	0.004	0.004	−3.338	−3.333	−3.325
0.52	0.002	0.002	−2.603	−2.597	−2.589
0.56	0.000	0.000	−1.629	−1.626	−1.621
0.60	0.000	0.000	−1.056	−1.055	−1.052
0.65	0.000	0.000	−0.641	−0.640	−0.639
0.70	0.000	0.000	−0.405	−0.405	−0.404
0.80	0.000	0.000	−0.178	−0.178	−0.178

computations and for the determination of the relativistic corrections. The CCSDT(Q) calculations were carried out using the general coupled-cluster code MRCC of Kállay [29].

A modification of the potential function given by Tang and Toennies [30] was fitted to the *ab initio* interaction energies:

$$V(R) = A \exp(a_1 R + a_2 R^2 + a_{-1} R^{-1} + a_{-2} R^{-2}) - \sum_{n=3}^8 \frac{C_{2n}}{R^{2n}} \left[1 - \exp(-bR) \sum_{k=0}^{2n} \frac{(bR)^k}{k!} \right]. \quad (4)$$

The coefficients A , a_1 , a_2 , a_{-1} , a_{-2} , b as well as the dispersion coefficients C_6 , C_8 , and C_{10} were fitted independently. The higher dispersion coefficients were simultaneously determined within the fit using the recursion formula [30]:

$$C_{2n} = C_{2n-6} \left(\frac{C_{2n-2}}{C_{2n-4}} \right)^3, \quad n \geq 6. \quad (5)$$

Deviations between calculated and fitted potential energies are smaller than $\pm 0.1\%$ for all distances except for $R = 0.80$ nm, where the difference is slightly larger. The fitted dispersion coefficients C_6 , C_8 , and C_{10} are in very good agreement with the *ab initio* dispersion coefficients derived by Thakkar *et al.* [31] using many-body perturbation theory. The resulting potential function has a well depth of 42.153 K at a distance of $R = 0.30895$ nm. This comes very close to the corresponding values of the potential of Aziz and Slaman [5] with a well depth of 42.25 K at a distance of $R = 0.3091$ nm. The potential parameters are listed in Table 3.

4. Vibrational and rotational energy levels

A very direct and stringent test of any potential energy curve consists in the calculation of the energy differences for the rovibrational transitions in the ground electronic state. For that purpose the program

Table 2. Corrections to the extrapolated CCSD(T) interaction energies and the final potential values. All energies are in Kelvin.

R/nm	ΔV_{core} dawCV5Z	ΔV_{rel} dawCV5Z	$\Delta V_{\text{T-(T)}}$ daVQZ+(3321)	$\Delta V_{\text{(O)}}$ aVTZ+(3321)	$V(R)$
0.14	-110.504	-197.556	-8.572	11.597	68634.310
0.16	-52.833	-77.901	-7.131	4.128	26879.940
0.18	-24.471	-29.825	-5.560	0.453	10402.164
0.20	-10.933	-11.126	-4.124	-0.964	3918.978
0.22	-4.647	-4.074	-2.975	-1.159	1399.226
0.24	-1.827	-1.487	-2.124	-0.888	444.443
0.25	-1.093	-0.906	-1.793	-0.747	227.490
0.26	-0.620	-0.561	-1.513	-0.558	99.956
0.27	-0.321	-0.356	-1.277	-0.420	27.186
0.28	-0.136	-0.234	-1.077	-0.307	-12.388
0.29	-0.026	-0.161	-0.908	-0.215	-32.165
0.30	0.036	-0.116	-0.766	-0.145	-40.392
0.31	0.068	-0.087	-0.646	-0.091	-42.130
0.32	0.082	-0.069	-0.544	-0.052	-40.423
0.33	0.086	-0.056	-0.459	-0.024	-37.040
0.34	0.082	-0.046	-0.387	-0.002	-33.032
0.35	0.076	-0.039	-0.327	0.008	-28.972
0.36	0.069	-0.033	-0.277	0.017	-25.137
0.37	0.061	-0.029	-0.234	0.021	-21.678
0.38	0.053	-0.025	-0.199	0.022	-18.629
0.40	0.040	-0.019	-0.144	0.023	-13.723
0.42	0.030	-0.014	-0.105	0.020	-10.136
0.44	0.023	-0.011	-0.078	0.017	-7.554
0.46	0.017	-0.008	-0.058	0.014	-5.690
0.48	0.013	-0.006	-0.044	0.011	-4.340
0.50	0.010	-0.005	-0.034	0.009	-3.345
0.52	0.008	-0.004	-0.026	0.007	-2.605
0.56	0.005	-0.002	-0.016	0.004	-1.631
0.60	0.003	-0.002	-0.010	0.003	-1.058
0.65	0.002	-0.001	-0.006	0.002	-0.643
0.70	0.001	-0.001	-0.004	0.001	-0.406
0.80	0.001	0.000	-0.002	0.000	-0.179

Table 3. Potential parameters.

Parameter	Unit	Value	Thakkar <i>et al.</i> [31]
A	K	$4.02915058383 \times 10^7$	
a_1	$(\text{nm})^{-1}$	$-4.28654039586 \times 10^1$	
a_2	$(\text{nm})^{-2}$	-3.33818674327	
a_{-1}	nm	$-5.34644860719 \times 10^{-2}$	
a_{-2}	$(\text{nm})^2$	$5.01774999419 \times 10^{-3}$	
b	$(\text{nm})^{-1}$	$4.92438731676 \times 10^1$	
C_6	$\text{K} (\text{nm})^6$	$4.40676750157 \times 10^{-2}$	4.54364×10^{-2}
C_8	$\text{K} (\text{nm})^8$	$1.64892507701 \times 10^{-3}$	1.75423×10^{-3}
C_{10}	$\text{K} (\text{nm})^{10}$	$7.90473640524 \times 10^{-5}$	8.34962×10^{-5}
C_{12}	$\text{K} (\text{nm})^{12}$	$4.85489170103 \times 10^{-6}$	
C_{14}	$\text{K} (\text{nm})^{14}$	$3.82012334054 \times 10^{-7}$	
C_{16}	$\text{K} (\text{nm})^{16}$	$3.85106552963 \times 10^{-8}$	
ϵ/k_B	K	42.152521	
R_ϵ	nm	0.30894556	
σ	nm	0.27612487	

Table 4. Energy differences between the rotational levels for the three vibrational states of the electronic ground state of the $^{20}\text{Ne}-^{20}\text{Ne}$ dimer and comparison between values calculated for different potential energy curves and the observed values by Wüest und Merkt [6]. Last column: energy calculated for the potential of the present paper to be compared with the dissociation energy: $-D_e = -42.153$ K.

v	J	Observed	Calculated differences for the potential energy curves by				Calculated
		Wüest, Merkt [6]	Aziz, Slaman [5]	Cybulski, Toczyłowski ¹⁴	Wüest, Merkt ⁶	present	energy present
		$\frac{E_{vJ} - E_{00}}{\text{cm}^{-1}}$	$\frac{E_{vJ} - E_{00}}{\text{cm}^{-1}}$	$\frac{E_{vJ} - E_{00}}{\text{cm}^{-1}}$	$\frac{E_{vJ} - E_{00}}{\text{cm}^{-1}}$	$\frac{E_{vJ} - E_{00}}{\text{cm}^{-1}}$	$\frac{E_{vJ}}{\text{K}}$
0	0	0.0	0.0	0.0	0.0	0.0	-24.0941
0	2	0.937(10)	0.9333	0.9266	0.9300	0.9338	-22.7506
0	4	3.088(10)	3.0984	3.0757	3.0875	3.1001	-19.6338
0	6	6.426(18)	6.4630	6.4145	6.4406	6.4666	-14.7901
0	8	10.947(19)	10.9691	10.8833	10.9319	10.9753	-8.3031
0	10	16.464(26)	16.5159	16.3769	16.4608	16.5247	-0.3187
0	12		22.8836	22.6512	22.8044	22.8877	8.8362
0	14		29.8065				
1	0	13.76(14)	13.8443	13.4551	13.7746	13.7928	-4.2494
1	2	14.36(14)	14.4514	14.0478	14.3756	14.3944	-3.3838
1	4	15.73(14)	15.8174	15.3762	15.7275	15.7455	-1.4398
1	6		17.7436	17.2201	17.6321	17.6352	1.2791
2	0		16.9199	16.2551	16.8146	16.7333	-0.0187

LEVEL 7.7 by Le Roy [32] was used. The results for the $^{20}\text{Ne}-^{20}\text{Ne}$ and the $^{20}\text{Ne}-^{22}\text{Ne}$ dimers calculated for the potential energy curves of Aziz and Slaman [5], of Cybulski and Toczyłowski [14], of Wüest and Merkt [6] as well as of the present paper are listed in Tables 4 and 5. In general, three vibrational states were found for both dimers, whereas the energy of each ground vibrational state $v=0$ is only at about 60% of the dissociation energy ($-D_e = -42.153$ K) characterizing the weakly bound nature of the potential. The energies for the rotationally excited states differ from that of the $J=0$ states by the addition of the centrifugal potential. Only the bound states with negative energies E_{vJ} are accessible with the experimental arrangement by Wüest and Merkt [6], whereas the lifetimes for the quasibound levels with positive energies are too short.

As shown in Table 4, Wüest and Merkt [6] observed actually nine of the ten bound rovibrational levels of the $^{20}\text{Ne}-^{20}\text{Ne}$ dimer. The energy differences calculated for the potential of Wüest and Merkt agree of course with the observed values of these authors within the uncertainties of the spectra (numbers in brackets in the third column of the table), since the potential energy curve was derived on the basis of these observed data. The deviations between the energy differences calculated with the new potential of this paper and the observed values for $v=0$ increase with increasing J and exceed the experimental uncertainties for higher J . Conversely, the deviations between the

values for the new potential and the observed data for $v=1$ are in reasonable agreement because of the ten times higher experimental uncertainties. The same findings result from a comparison of the values calculated for the semi-empirical potential by Aziz and Slaman [5] and of the observed data by Wüest and Merkt [6]. In addition, the values calculated for the potentials of Aziz and Slaman and of the present paper agree with each other better than with the observed data for $v=0$. Finally, the values determined from the potential by Cybulski and Toczyłowski [14] show comparably large deviations from the experimentally observed data.

Table 5 illustrates that the spectra of the $^{20}\text{Ne}-^{22}\text{Ne}$ dimer are of poorer quality and characterised by larger experimental uncertainties. Hence, only five of altogether 18 bound rovibrational levels were found by Wüest and Merkt [6]. Furthermore, the values calculated for all four considered potentials agree within the experimental uncertainties with the observed data.

In Table 6, the dissociation energy D_e , the equilibrium internuclear distance R_e , the vibrational-ground-state dissociation energy D_{00} , and the vibrational interval $\Delta G_{1/2}$ of the $^{20}\text{Ne}-^{20}\text{Ne}$ dimer in the ground electronic state are compared for the considered potential energy curves including that of Gdanitz [16]. The table makes evident that the semi-empirical potential by Aziz and Slaman fitted primarily to different experimental data, the potential by Wüest and Merkt [6] adjusted to their rovibrational spectra,

Table 5. Energy differences between the rotational levels for the three vibrational states of the electronic ground state of the $^{20}\text{Ne}-^{22}\text{Ne}$ dimer and comparison between values calculated for different potential energy curves and the observed values by Wüest und Merkt [6]. Last column: energy calculated for the potential of the present paper to be compared with the dissociation energy: $-D_c = -42.153$ K.

v	J	Observed	Calculated differences for the potential energy curves by				Calculated
		Wüest, Merkt [6]	Aziz, Slaman [5]	Cybulski, Toczyłowski ¹⁴	Wüest, Merkt ⁶	present	energy present
		$\frac{E_{vJ} - E_{00}}{\text{cm}^{-1}}$	$\frac{E_{vJ} - E_{00}}{\text{cm}^{-1}}$	$\frac{E_{vJ} - E_{00}}{\text{cm}^{-1}}$	$\frac{E_{vJ} - E_{00}}{\text{cm}^{-1}}$	$\frac{E_{vJ} - E_{00}}{\text{cm}^{-1}}$	$\frac{E_{vJ}}{\text{K}}$
0	0	0.0	0.0000	0.0000	0.0000	0.0000	-24.4466
0	1		0.2983	0.2962	0.2973	0.2985	-24.0172
0	2	0.896(51)	0.8940	0.8876	0.8908	0.8945	-23.1597
0	3	1.791(76)	1.7851	1.7722	1.7788	1.7861	-21.8769
0	4	2.92(11)	2.9686	2.9471	2.9583	2.9703	-20.1731
0	5	4.35(19)	4.4404	4.4079	4.4251	4.4430	-18.0542
0	6		6.1949	6.1491	6.1738	6.1986	-15.5282
0	7		8.2251	8.1633	8.1974	8.2301	-12.6054
0	8		10.5217	10.4411	10.4867	10.5282	-9.2989
0	9		13.0728	12.9699	13.0297	13.0809	-5.6261
0	10		15.8622	15.7325	15.8103	15.8718	-1.6107
0	11		18.8662	18.7033	18.8046	18.8765	2.7125
0	12		22.0429	21.8327	21.9698	22.0511	7.2800
0	13		25.3217	25.0583	25.2351	25.3268	11.9929
0	14		28.7526	28.4745	28.6602	28.7706	16.9479
1	0		13.8240	13.4465	13.7604	13.7803	-4.6198
1	1		14.0228	13.6409	13.9573	13.9775	-4.3362
1	2		14.4170	14.0261	14.3476	14.3684	-3.7738
1	3		14.9996	14.5945	14.9243	14.9455	-2.9433
1	4		15.7581	15.3327	15.6751	15.6961	-1.8634
1	5		16.6715	16.2170	16.5787	16.5978	-0.5661
1	6		17.6953	17.1917	17.5908	17.6003	0.8762
1	7		18.7871	18.1871	18.6701	18.6865	2.4390
2	0		17.1421	16.4813	17.0373	16.9606	-0.0441
2	1		17.1860	17.0825			

Table 6. Dissociation energy D_c , equilibrium internuclear distance R_e , vibrational-ground-state dissociation energy D_{00} , and vibrational interval $\Delta G_{1/2}$ of the $^{20}\text{Ne}-^{20}\text{Ne}$ dimer in the ground electronic state for different potential energy curves.

D_c K	R_e nm	D_{00} K	$\Delta G_{1/2}$ K	Reference
42.25	0.3091	24.07	19.91	[5]
41.155	0.30988	23.399	19.37	[6]
41.535 ± 0.29	0.31007 ± 0.0002	23.605 ± 0.29	19.592 ± 0.14	[16]
42.30 ± 0.17	0.3094 ± 0.0001	24.22	19.82 ± 0.17	[6]
42.153	0.30895	24.094	19.845	Present

and the potential of this paper derived from quantum-mechanical *ab initio* calculations are in close agreement.

5. Summary and conclusions

The interaction energies for the neon atom pair were calculated for a large number of interatomic separations. Basis sets of up to t-aug-cc-pV6Z quality with bond functions at the CCSD(T) level were utilised. In addition, highly accurate corrections for higher-

order coupled-cluster excitations up to CCSDT(Q) as well as corrections for core-core and core-valence correlations and for scalar relativistic effects were determined. It could be shown that, when going from CCSD(T) to CCSDT, the well depth increases considerably, whereas a further enhancement to CCSDT(Q) has only a marginal effect.

An analytical potential function was fitted to the *ab initio* values and used to derive the rovibrational spectra of the $^{20}\text{Ne}-^{20}\text{Ne}$ and $^{20}\text{Ne}-^{22}\text{Ne}$ dimers in the

ground electronic state. These values were compared with highly accurate experimental data of Wüest and Merkt [6] and with values calculated for other potential energy curves from the literature. The comparison makes evident that the potentials of Aziz and Slaman [5], of Wüest and Merkt [6], and of the present paper are in close agreement. One should keep in mind that the rovibrational spectra are essentially governed by the attractive part of the potential around its minimum. Hence, a comprehensive comparison with experimental data for the transport properties, which are strongly influenced by the repulsive part of the potential, represents a further stringent test and will become the focus of the second paper of this series [33].

References

- [1] R. Hellmann, E. Bich, and E. Vogel, *Mol. Phys.* **105**, 3013 (2007).
- [2] E. Bich, R. Hellmann, and E. Vogel, *Mol. Phys.* **105**, 3035 (2007).
- [3] H.B.G. Casimir and D. Polder, *Phys. Rev.* **73**, 360 (1948).
- [4] Y. Tanaka and K. Yoshino, *J. Chem. Phys.* **57**, 2964 (1972).
- [5] R.A. Aziz and M.J. Slaman, *Chem. Phys.* **130**, 187 (1989).
- [6] A. Wüest and F. Merkt, *J. Chem. Phys.* **118**, 8807 (2003).
- [7] T. van Mourik, A.K. Wilson, and T.H. Dunning Jr, *Mol. Phys.* **96**, 529 (1999).
- [8] T.H. Dunning Jr, *J. Chem. Phys.* **90**, 1007 (1989).
- [9] R.A. Kendall, T.H. Dunning Jr, and R.J. Harrison, *J. Chem. Phys.* **96**, 6796 (1992).
- [10] D.E. Woon and T.H. Dunning Jr, *J. Chem. Phys.* **100**, 2975 (1994).
- [11] K. Raghavachari, G.W. Trucks, and J.A. Pople, *Chem. Phys. Lett.* **157**, 479 (1989).
- [12] S.F. Boys and F. Bernardi, *Mol. Phys.* **19**, 553 (1970).
- [13] J. van de Bovenkamp and F.B. van Duijneveldt, *Chem. Phys. Lett.* **309**, 287 (1999).
- [14] S.M. Cybulski and R.R. Toczyłowski, *J. Chem. Phys.* **111**, 10520 (1999).
- [15] G. Grochola, T. Petersen, and S.P. Russo, *Mol. Phys.* **100**, 3867 (2002).
- [16] R.J. Gdanitz, *Chem. Phys. Lett.* **348**, 67 (2001).
- [17] M. Venkatraj, M.G. Müller, and H. Huber, *Collect. Czech. Chem. Commun.* **68**, 627 (2003).
- [18] M. Venkatraj, C. Bratschi, and H. Huber, *Fluid Phase Equilib.* **218**, 285 (2004).
- [19] T.J. Giese, V.M. Audette, and D.M. York, *J. Chem. Phys.* **119**, 2618 (2003).
- [20] A.E. Nasrabad, R. Laghaei, and U.K. Deiters, *J. Chem. Phys.* **121**, 6423 (2004).
- [21] J.S. Lee, *Theor. Chem. Acc.* **113**, 87 (2005).
- [22] J. Noga and R.J. Bartlett, *J. Chem. Phys.* **86**, 7041 (1987); **89**, 3401(E) (1988).
- [23] A. Halkier, T. Helgaker, and P. Jørgensen, *Chem. Phys. Lett.* **286**, 243 (1998).
- [24] K.A. Peterson and T.H. Dunning Jr, *J. Chem. Phys.* **117**, 10548 (2002).
- [25] R.D. Cowan and D.C. Griffin, *J. Opt. Soc. Am.* **66**, 1010 (1976).
- [26] M. Kállay and J. Gauss, *J. Chem. Phys.* **123**, 214105 (2005).
- [27] PSI3: an open-source *ab initio* electronic structure package, T.D. Crawford, C.D. Sherrill, and E.F. Valeev, *J. Comp. Chem.* **28**, 1610 (2007).
- [28] J.F. Stanton, J. Gauss, J.D. Watts, P.G. Szalay, and R.J. Bartlett, with contributions from A.A. Auer, D.B. Bernholdt, O. Christiansen, M.E. Harding, M. Heckert, O. Heun, C. Huber, D. Jonsson, J. Jusélius, W.J. Lauderdale, T. Metzroth, C. Michauk, D.R. Price, K. Ruud, F. Schiffmann, A. Tajti, M.E. Varner, J. Vázquez, and the integral packages: MOLECULE (J. Almlöf and P.R. Taylor), PROPS (P.R. Taylor), and ABACUS (T. Helgaker, H.J.Aa. Jensen, P. Jørgensen, and J. Olsen). See also J.F. Stanton, J. Gauss and J.D. Watts, *Int. J. Quantum Chem. Symp.* **26**, 879 (1992). Current version see <http://www.aces2.de>
- [29] MRCC, a string-based general coupled cluster program suite written by M. Kállay. See also M. Kállay and P.R. Surján, *J. Chem. Phys.* **115**, 2945 (2001); <http://www.mrcc.hu>
- [30] K.T. Tang and J.P. Toennies, *J. Chem. Phys.* **80**, 3726 (1984).
- [31] A.J. Thakkar, H. Hettema, and P.E.S. Wormer, *J. Chem. Phys.* **97**, 3252 (1992).
- [32] R.J. Le Roy, *Level 7.7: a computer program for solving the radial Schrödinger equation for bound and quasi-bound levels*, University of Waterloo, Chemical Physics Research Report No. CP-661 (Waterloo, Ontario, Canada, 2005).
- [33] E. Bich, R. Hellmann, and E. Vogel, submitted.

4.2.2 II. Thermophysical properties for low-density neon

Eckard Bich, Robert Hellmann, Eckhard Vogel

Mol. Phys. **106**, 1107-1122 (2008).

Teile der Publikation und des Gesamtkonzeptes wurden selbst erarbeitet. Der eigene Anteil beträgt etwa 20%.

RESEARCH ARTICLE

***Ab initio* potential energy curve for the neon atom pair and thermophysical properties for the dilute neon gas.**
II. Thermophysical properties for low-density neon

Eckard Bich, Robert Hellmann and Eckhard Vogel*

Institut für Chemie, Universität Rostock, Rostock, Germany

(Received 5 December 2007; final version received 5 February 2008)

A neon–neon interatomic potential energy curve determined from quantum-mechanical *ab initio* calculations and described with an analytical representation (R. Hellmann, E. Bich, and E. Vogel, *Molec. Phys.* **106**, 133 (2008)) was used in the framework of the quantum-statistical mechanics and of the corresponding kinetic theory to calculate the most important thermophysical properties of neon governed by two-body and three-body interactions. The second and third pressure virial coefficients as well as the viscosity and thermal conductivity coefficients, the last two in the so-called limit of zero density, were calculated for natural Ne from 25 to 10,000 K. Comparison of the calculated viscosity and thermal conductivity with the most accurate experimental data at ambient temperature shows that these values are accurate enough to be applied as standard values for the complete temperature range of the calculations characterized by an uncertainty of about $\pm 0.1\%$ except at the lowest temperatures.

Keywords: neon pair potential; neon gas property standards; second and third pressure virial coefficients; viscosity; thermal conductivity

1. Introduction

Recently we calculated standard values for some thermophysical two-body and three-body properties of helium over the temperature range from 1 to 10,000 K with uncertainties that are superior to experimental data [1]. Prerequisite for it was the determination of a state-of-the-art pair potential between two helium atoms [2]. In order to establish a second standard for the calibration of high-precision measuring instruments at low density, we developed very recently a new interatomic pair potential for neon from high-level supermolecular *ab initio* calculations for a large number of internuclear separations R (paper I [3]). The *ab initio* calculated interatomic potential energy values $V(R)$, including core–core and core–valence correlation and relativistic corrections as well as coupled-cluster contributions up to CCSDT(Q), were listed in Table 2 of paper I. They were used for the fit of an analytical potential function, which represents a modification of the potential function given by Tang and Toennies [4]:

$$V(R) = A \exp(a_1 R + a_2 R^2 + a_{-1} R^{-1} + a_{-2} R^{-2}) - \sum_{n=3}^8 \frac{C_{2n}}{R^{2n}} \left[1 - \exp(-bR) \sum_{k=0}^{2n} \frac{(bR)^k}{k!} \right]. \quad (1)$$

Whereas the details of the fit were communicated in paper I, the potential parameters are repeated here for convenience in Table 1.

A comparison in paper I with experimental rovibrational spectra [5] showed that the new potential function is superior to the *ab initio* potential by Cybulski and Toczyłowski [6]. This potential was given as an analytical function derived from *ab initio* values calculated for a large range of internuclear distances. Furthermore, the comparison made evident that our new potential is at least as good as the best semi-empirical potential by Aziz and Slaman [7] and also compares well with the potential of Wüest and Merkt [5] fitted directly to the rovibrational spectra under discussion. It is noteworthy that the rovibrational spectra are sensitive to the shape of the potential well. Hence it could be possible that the potential of Wüest and Merkt is not so effective with respect to other regions of the potential. Conversely, the transport properties are particularly sensitive to the repulsive part of the potential. Thus the potential of Aziz and Slaman could be expected to perform well in nearly all regions of the potential, since it was determined in a fit to high-energy beam data and to viscosity coefficients, considering calculated values of the C_6 , C_8 and C_{10} dispersion coefficients.

*Corresponding author. Email: eckhard.vogel@uni-rostock.de

Table 1. Potential parameters.

A	K	0.402915058383E+08
a_1	(nm) ⁻¹	-0.428654039586E+02
a_2	(nm) ⁻²	-0.333818674327E+01
a_{-1}	nm	-0.534644860719E-01
a_{-2}	(nm) ²	0.501774999419E-02
b	(nm) ⁻¹	0.492438731676E+02
C_6	K(nm) ⁶	0.440676750157E-01
C_8	K(nm) ⁸	0.164892507701E-02
C_{10}	K(nm) ¹⁰	0.790473640524E-04
C_{12}	K(nm) ¹²	0.485489170103E-05
C_{14}	K(nm) ¹⁴	0.382012334054E-06
C_{16}	K(nm) ¹⁶	0.385106552963E-07
ε/k_B	K	42.152521
R_ε	nm	0.30894556
σ	nm	0.27612487

In this paper, we report standard values of the second and third pressure virial coefficients as well as of the viscosity and thermal conductivity coefficients in the limit of zero density for neon in its natural isotopic composition. Even though the quality of the new neon *ab initio* potential of paper I [3] is somewhat inferior compared with our recent *ab initio* potential for helium [2], the calculated thermophysical properties are expected to be as accurate as the best experimental measurements at room temperature and more accurate than available experimental data far above and far below room temperature. In order to assess as accurately as possible the quality of the potentials considered in this paper, some of the experimental viscosity data from the literature were recalibrated with reference values derived from the new interatomic potential for helium [1,2].

2. Quantum-mechanical calculation of thermophysical properties

2.1. Evaluation of the phase shifts

A quantum-mechanical treatment of the elastic scattering is needed to obtain very accurate values for the thermophysical properties of neon. For this purpose the relative phase shifts $\delta_l(k)$ have to be evaluated as asymptotic limiting values of the relative phases of the perturbed and unperturbed radial factor wave functions $\psi_l(R)$ and $\psi_l^{(0)}(R)$ (the latter with $V(R)=0$). Each of them corresponds to a particular state of the angular momentum of the system characterized by the quantum number l . To obtain the relative phase shifts $\delta_l(k)$, the Schrödinger equation is to be solved by numerical integration for many values of the wave number $k=(2\mu E)^{1/2}/\hbar$, where E is the energy of the

incoming wave and $\mu=(m_1m_2)/(m_1+m_2)$ is the reduced mass.

In principle, neon can be considered as a mixture of the three isotopes ^{20}Ne , ^{21}Ne , and ^{22}Ne with the relative atomic masses 19.9924356, 20.9938428, and 21.9913831, with the nuclear spins s of 0, 3/2, and 0, and with the natural abundances 90.48 atom%, 0.27 atom%, and 9.27 atom%. Hence there are six different interacting systems in naturally occurring neon with varying reduced masses and different statistics: ^{20}Ne - ^{20}Ne and ^{22}Ne - ^{22}Ne (both Bose-Einstein statistics), ^{21}Ne - ^{21}Ne (Fermi-Dirac statistics), ^{20}Ne - ^{21}Ne , ^{20}Ne - ^{22}Ne , and ^{21}Ne - ^{22}Ne (all Boltzmann statistics). As a consequence, the relative phase shifts have to be calculated for these six binary systems at a multiplicity of wave numbers k or of energies E for a substantial number of l values which requires plenty of computing time. In order to save time the semi-classical JWKB method was used as approximation. Problems and the procedure of the fully quantum-mechanical calculation as well as the JWKB method for the determination of the relative phase shifts were discussed in some detail in our paper on helium [1].

To avoid uncertainties in the results of the calculated thermophysical properties, a very large number of phase shifts $\delta_l(k)$ was determined for 500 values of the energy E from zero to about 135,000 K and for an increasing number of l values related to the energy. The calculations of the phase shifts were first performed fully quantum-mechanically and for comparison parallel to it according to the JWKB approximation. If the values resulting from both procedures became practically identical for certain values of the angular momentum quantum number l , the fully quantum-mechanical evaluation (QM) was finished and substituted by the semi-classical JWKB procedure at the higher l values. Table 2 gives an overview about the number of phase shifts determined for some reduced energies $E^*=E/\varepsilon$.

2.2. Calculation of the second and third pressure virial coefficients

In this paper two alternative ways were used to calculate the second virial coefficient of naturally occurring neon as a function of temperature T . In the first variant $B(T)$ is determined like that of a mixture composed of the three neon isotopes:

$$B_{\text{mix}}(T) = \sum_{i=1}^3 \sum_{j=1}^3 x_i x_j B_{ij}(T), \quad (2)$$

Table 2. Number of calculated phase shifts of neon for some reduced energies.

E^*	Total number	Full QM calculation
0	11	11
1×10^{-4}	14	12
1×10^{-3}	14	12
1×10^{-2}	29	23
5×10^{-2}	62	34
1×10^{-1}	87	41
5×10^{-1}	177	58
1	244	67
3	511	84
5	1152	93
10	1152	108
100	1152	131
3,200	1351	131

whereas the second virial coefficients B_{ij} are evaluated fully quantum-mechanically for the different statistics using two contributions B_{direct} and B_{exch} [8]. In the Boltzmann statistics (B) the second virial coefficient is given as

$$B_{\text{B}} = B_{\text{direct}}, \quad (3)$$

whereas for particles with spin quantum number s according to the Bose–Einstein (BE) or to the Fermi–Dirac (FD) statistics holds as:

$$B_{\text{BE}} = B_{\text{direct}} + B_{\text{exch}}, \quad (4)$$

$$B_{\text{FD}} = B_{\text{direct}} - B_{\text{exch}}. \quad (5)$$

B_{direct} and B_{exch} result from summations over the angular momentum quantum number l , either over only the even l values or over only the odd l values:

$$B_{\text{direct}} = B_{\text{even}} + B_{\text{odd}}, \quad (6)$$

$$B_{\text{exch}} = \left(\frac{1}{2s+1} \right) \left(B_{\text{even}} - B_{\text{odd}} - \frac{N_{\text{A}} A^3}{16} \right). \quad (7)$$

The spin quantum numbers s and the statistics have already been given in Section 2.1 for the six interacting systems composed of the three neon isotopes. The summations over l are represented by:

$$B(T) = -\frac{N_{\text{A}} A^3}{2} \left[\sum_{n=0}^{n_{\text{max}}} \sum_l^{l_{\text{max}}(n)} (2l+1) (\exp(-\beta E_{nl}^-) - 1) + \int_0^{\infty} \sum_l^{\infty} (2l+1) \frac{\delta_l(E)}{\pi} \exp(-\beta E) d(\beta E) \right]. \quad (8)$$

Here Λ is the thermal wavelength:

$$\Lambda = \left(\frac{h^2 \beta}{2\pi\mu} \right)^{1/2}, \quad \beta = \frac{1}{k_{\text{B}} T}, \quad (9)$$

whereas h is Planck's constant and N_{A} is Avogadro's number. The first term of Equation (8) corresponds to the contribution of the bound states, where E_{nl}^- is the negative eigenvalue of the n th vibrational state with the angular-momentum quantum number l which is obtained from the solution of the Schrödinger equation for the radial factor wave functions $\psi_l(R)$. Some bound states corresponding to the rotational levels for the three vibrational states of the ground electronic state of the ^{20}Ne – ^{20}Ne and ^{20}Ne – ^{22}Ne dimers were listed for the neon–neon interatomic potential under discussion in Tables 4 and 5 of our paper I [3]. The bound states contribution is particularly of importance at low temperatures. The second term of Equation (8) is the essential contribution at medium and higher temperatures and is related to the scattering resulting from binary collisions and to the phase shifts $\delta_l(E)$. Due to the fact that the sum over l and the integral in Equation (8) have limits from 0 to ∞ , serious errors in the computation may occur when truncated inadequately. Therefore, it was verified that the energies for which the evaluation was performed and particularly the number of the phase shifts were chosen large enough.

In the second variant naturally occurring neon is considered as a pure gas consisting of atoms with the average relative atomic mass 20.1797. Then the second virial coefficient $B(T)$ is derived as the sum of a classical contribution as well as of first-order, second-order, and third-order quantum corrections [9]:

$$B(T) = B_{\text{cl}}(T) + \lambda B_{\text{qm},1}(T) + \lambda^2 B_{\text{qm},2}(T) + \lambda^3 B_{\text{qm},3}(T) + \dots \quad (10)$$

with $\lambda = \hbar^2 \beta / 12m$ and $\hbar = h/2\pi$. The individual summands are given as:

$$B_{\text{cl}}(T) = -2\pi N_{\text{A}} \int_0^{\infty} [\exp(-\beta V(R)) - 1] R^2 dR, \quad (11)$$

$$B_{\text{qm},1}(T) = 2\pi N_{\text{A}} \int_0^{\infty} [\beta V'(R)]^2 \exp[-\beta V(R)] R^2 dR, \quad (12)$$

$$B_{\text{qm},2}(T) = -2\pi N_A \int_0^\infty \left\{ \frac{6}{5} [\beta V''(R)]^2 + \frac{12}{5R^2} [\beta V'(R)]^2 + \frac{4}{3R} [\beta V''(R)]^3 - \frac{1}{6} [\beta V'(R)]^4 \right\} \times \exp[-\beta V(R)] R^2 dR, \quad (13)$$

$$B_{\text{qm},3}(T) = 2\pi N_A \int_0^\infty \left\{ \frac{36}{35} [\beta V'''(R)]^2 + \frac{216}{35R^2} [\beta V''(R)]^2 + \frac{24}{21} [\beta V''(R)]^3 + \frac{24}{5R} [\beta V''(R)] [\beta V'(R)]^2 + \frac{288}{315R^3} [\beta V''(R)]^3 - \frac{6}{5} [\beta V'(R)]^2 [\beta V''(R)]^2 - \frac{2}{15R^2} [\beta V'(R)]^4 - \frac{2}{5R} [\beta V'(R)]^5 + \frac{1}{30} [\beta V'(R)]^6 \right\} \times \exp[-\beta V(R)] R^2 dR. \quad (14)$$

For the evaluation of the third pressure virial coefficient $C(T)$, naturally occurring neon is again assumed to be a pure gas composed of atoms with the same mass. Furthermore, $C(T)$ is calculated as a sum of three contributions [10,11], one term for the pairwise additivity of the two-body interatomic potentials C_{add} , an extra genuine term $C_{\text{non-add}}$ for the non-additivity $\Delta V_3(R_{12}, R_{13}, R_{23})$ of the three-body interatomic interaction potential $V_3(R_{12}, R_{13}, R_{23})$, and a first-order correction term for the quantum effects $C_{\text{qm},1}$:

$$C(T) = C_{\text{add}}(T) + C_{\text{non-add}}(T) + \lambda C_{\text{qm},1}(T) + \dots \quad (15)$$

The formulas for the three contributions have already been given in our paper on helium [1] so that it is not necessary to repeat the details. Here the only difference consists in that $\lambda = \hbar^2 \beta / 12m$ is separated in the first-order correction term of the quantum effects $C_{\text{qm},1}$. The non-additivity contribution $\Delta V_3(R_{12}, R_{13}, R_{23})$ to the three-body potential is again approximated by the Axilrod-Teller triple-dipole potential term [12,13], in which the non-additivity coefficient of the triple-dipole term calculated for neon by Kumar and Meath [14], $C_9 = 1.228 \times 10^{-5} \text{ K}(\text{nm})^9$, is used.

2.3. Calculation of the transport properties

Different alternative ways were used to determine the transport properties of naturally occurring neon as a function of temperature T . In the first variant $\eta(T)$ and $\lambda(T)$ are evaluated quantum-mechanically and approximately like that of a dilute-gas mixture in the limit of zero density composed of the three

neon isotopes. In the first-order approximation of the kinetic theory the viscosity is formulated as:

$$[\eta_{\text{mix}}]_1 = \frac{\begin{vmatrix} H_{11} & H_{12} & H_{13} & x_1 \\ H_{21} & H_{22} & H_{23} & x_2 \\ H_{31} & H_{32} & H_{33} & x_3 \\ x_1 & x_2 & x_3 & 0 \end{vmatrix}}{\begin{vmatrix} H_{11} & H_{12} & H_{13} \\ H_{21} & H_{22} & H_{23} \\ H_{31} & H_{32} & H_{33} \end{vmatrix}}, \quad (16)$$

$$H_{ij} = 2x_i m_i \sum_{k=1}^3 \frac{x_k m_k}{[\eta_{ik}]_1 (m_i + m_k)^2} \times \left[\frac{5}{3A_{ik}} (\delta_{ij} - \delta_{jk}) + \frac{m_k}{m_i} \delta_{ij} + \delta_{jk} \right], \quad (17)$$

$$[\eta_{ij}]_1 = \frac{5}{16} \frac{(2\pi \mu_{ij} k_B T)^{1/2}}{\Omega_{ij}^{(2,2)}(T)}, \quad (18)$$

$$A_{ik} = \frac{\Omega_{ik}^{(2,2)}(T)}{\Omega_{ik}^{(1,1)}(T)}, \quad \mu_{ij} = \frac{m_i m_j}{m_i + m_j}. \quad (19)$$

The symbol $[\eta_{ij}]_1$ represents the first-order approximation of the viscosity characterizing the interaction between a binary pair $i-j$. Here all different $[\eta_{ij}]_1$ are given in terms of collision integrals $\Omega_{ij}^{(2,2)}(T)$ which have to be evaluated quantum-mechanically (see below). δ_{ij} is the Kronecker symbol, A_{ik} corresponds to the ratio of two collision integrals, whereas μ_{ij} is the reduced mass of the interacting pair.

In analogy to Equation (16) an equation in which the elements H_{ij} are replaced by elements L_{ij} is applied for the thermal conductivity of a dilute gas mixture in its first-order approximation. The elements L_{ij} are expressed as:

$$L_{ij} = x_i m_i \sum_{k=1}^3 \frac{x_k m_k}{[\lambda_{ik}]_1 (m_i + m_k)^2} \times \left\{ \frac{5}{8A_{ik}^*} \left[\left(6 \frac{m_i}{m_k} + 5 \frac{m_k}{m_i} \right) \delta_{ij} - 11 \delta_{jk} \right] - \frac{3B_{ik}}{2A_{ik}} \left(\frac{m_k}{m_i} \delta_{ij} - \delta_{jk} \right) + 2(\delta_{ij} + \delta_{jk}) \right\}, \quad (20)$$

$$[\lambda_{ij}]_1 = \frac{75}{64} \frac{(2\pi \mu_{ij} k_B^3 T)^{1/2}}{2\mu_{ij} \Omega_{ij}^{(2,2)}(T)}, \quad (21)$$

$$B_{ik} = \frac{5\Omega_{ik}^{(1,2)}(T) - 4\Omega_{ik}^{(1,3)}(T)}{\Omega_{ik}^{(1,1)}(T)}. \quad (22)$$

Here $[\lambda_{ij}]_1$ is the first-order approximation of the thermal conductivity related to the interaction between a binary pair $i-j$ and again given in terms of the $\Omega_{ij}^{(2,2)}(T)$ collision integrals. B_{ik} represents a relation between different collision integrals.

In principle, exact calculations require higher-order approximations of the kinetic theory. Therefore, we used fifth-order approximations in the case of the transport properties of helium [1], but the calculations for ^3He and ^4He concerned a pure gas each. Unfortunately, approximations of such a high order are not available for mixtures so that we were forced to choose any other reasonable way for the higher-order calculations of the transport properties of naturally occurring neon and tested thus two possibilities. On the one hand, the individual viscosity and thermal conductivity coefficients η_{ij} and λ_{ij} for the binary pairs with like and unlike interactions are calculated up to the fifth-order approximation according to:

$$[\eta_{ij}]_5 = \frac{5}{16} \frac{(2\pi\mu_{ij}k_B T)^{1/2}}{\Omega_{ij}^{(2,2)}(T)} f_{\eta,ij}^{(5)}, \quad (23)$$

$$[\lambda_{ij}]_5 = \frac{75}{64} \frac{(2\pi\mu_{ij}k_B^3 T)^{1/2}}{2\mu_{ij}\Omega_{ij}^{(2,2)}(T)} f_{\lambda,ij}^{(5)}. \quad (24)$$

Here $f_{\eta,ij}^{(5)}$ and $f_{\lambda,ij}^{(5)}$ represent the correction factors for the fifth-order approximations of the kinetic theory. The resulting values for $[\eta_{ij}]_5$ and $[\lambda_{ij}]_5$ are then used in the first-order approximation for the mixture viscosity represented by Equation (16) as well as in the corresponding relation for the thermal conductivity. On the other hand, the values of the first-order approximations $[\eta_{\text{mix}}]_1$ [Equation (16)] and $[\lambda_{\text{mix}}]_1$ are corrected for the fifth-order approximations by means of correction factors $f_{\eta}^{(5)}$ and $f_{\lambda}^{(5)}$. These are derived using collision integrals which are also determined quantum-mechanically for a pure neon gas consisting of atoms with the average relative atomic mass 20.1797 and following the Bose–Einstein statistics for ^{20}Ne – ^{20}Ne . For the calculations of $f_{\eta,ij}^{(5)}$ and $f_{\lambda,ij}^{(5)}$ as well as $f_{\eta}^{(5)}$ and $f_{\lambda}^{(5)}$ we used explicit expressions and computer programs provided by Viehland *et al.* [15]. According to our calculations the effect of the fifth-order corrections to the viscosity and to the thermal conductivity compared with the fourth-order corrections is below $\pm 0.01\%$.

Expressions for the quantum cross sections $Q^{(m)}(E)$ and for the quantum collision integrals $\Omega^{(m,s)}(T)$ needed in the different approximations of the solution of the Boltzmann equation were derived by Meeks *et al.* [16]. They were again collected in our paper for helium [1] for particles with spin s according to the

Bose–Einstein (BE) or to the Fermi–Dirac (FD) statistics as well as for the Boltzmann statistics. The formulas for the different $Q^{(m)}$ are related to sums over the phase shifts δ_l , either over only the odd l values or over only the even l values, but also over complete sums (Boltzmann statistics). The quantum collision integrals $\Omega^{(m,s)}(T)$ result from the quantum cross sections $Q^{(m)}(E)$ according to:

$$\Omega^{(m,s)}(T) = \frac{4\pi\hbar^2}{2\mu k_B T(s+1)!} \times \int_0^\infty Q^{(m)}(E) \exp(-\beta E)(\beta E)^s d(\beta E). \quad (25)$$

In a second variant the viscosity of neon was determined classically for the first-order and the fifth-order approximations in order to examine whether a quantum-mechanical calculation is actually needed to achieve highly accurate values for the transport properties of neon in the zero-density limit. For this purpose the usual formulations for monatomics [17] were used, whereas neon was again considered to be a pure gas with the average relative atomic mass already given.

3. Comparison with experimental data and values for other interatomic potentials

3.1. Second and third pressure virial coefficients

The quantum-mechanical calculation of the second pressure virial coefficient requires the determination of the existing bound states. For this purpose the Level 7.7 program of LeRoy [18] was used. As already mentioned in Section 2.2, the bound states of the ^{20}Ne – ^{20}Ne and ^{20}Ne – ^{22}Ne dimers were listed in our paper I [3] in which they were compared with the experimental rovibrational spectra by Wüest and Merkt [5].

In Figure 1 the values calculated fully quantum-mechanically for the interatomic potential of the present paper are opposed to those resulting from quantum corrections of increasing order added to the classical contribution. The figure illustrates that the classical contribution alone is completely insufficient to describe adequately the second pressure virial coefficient. The agreement between both ways of calculation improves, with the quantum corrections included, what becomes obvious particularly at low temperatures. To obtain close agreement even at the lowest temperatures, the third-order quantum correction is needed.

There exists only a limited number of experimental data for second and third pressure virial coefficients of neon in the literature compared with those of common

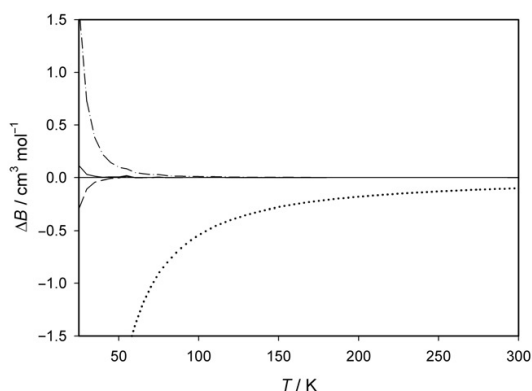


Figure 1. Differences $\Delta B = B_{\text{qm,full}} - [B_{\text{cl}} + \sum \lambda^i B_{\text{qm},i}]$ between the fully quantum-mechanically calculated values and the values resulting from the sum of a classical contribution and of different orders of quantum corrections to the second pressure virial coefficient for the new interatomic potential for Ne. Differences related to: classical contribution B_{cl} ; - - - - - sum of classical contribution and of first-order quantum correction $B_{\text{cl}} + \lambda B_{\text{qm},1}$; - - - - - sum of classical contribution as well as of first-order and second-order quantum corrections $B_{\text{cl}} + \lambda B_{\text{qm},1} + \lambda^2 B_{\text{qm},2}$; ——— sum of classical contribution as well as of first-order, second-order, and third-order quantum corrections $B_{\text{cl}} + \lambda B_{\text{qm},1} + \lambda^2 B_{\text{qm},2} + \lambda^3 B_{\text{qm},3}$.

gases like argon and nitrogen as well as with those of helium. Furthermore, one should point out that experimental data for the third pressure virial coefficient are not independent of the values for the second pressure virial coefficient derived from the same experiments. Hence third pressure virial coefficients combined with second ones are included in the comparison. Second and third pressure virial coefficients were determined by Holborn and Otto [19], Nicholson and Schneider [20], Michels *et al.* [21], and Gibbons [22] from isothermal measurements of volume (and density, respectively) and pressure. Vogl and Hall [23] used a Burnett apparatus to derive isothermal compression factors and to obtain finally second and third pressure virial coefficients. Unfortunately, in none of these papers an error propagation analysis or uncertainties of the second and third pressure virial coefficients adequately deduced from the experiments were reported.

The experimental B data are compared with the values calculated fully quantum-mechanically for the neon–neon interatomic potential of the present paper in Figure 2, in which the absolute deviations $B_{\text{exp}} - B_{\text{cal(pres)}}$ are displayed. The figure demonstrates a very good agreement for the excellent data by Michels *et al.* [21] at medium temperatures. A good

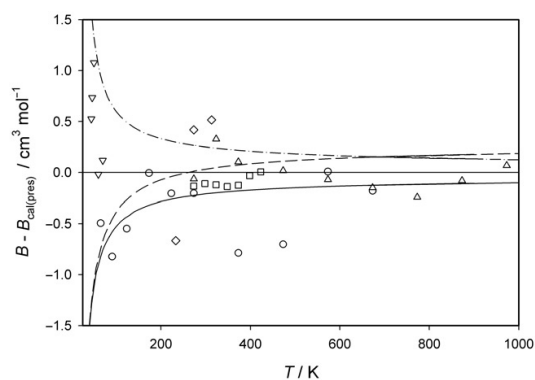


Figure 2. Differences $(B - B_{\text{cal(pres)}})$ of experimental (B_{exp}) and calculated ($B_{\text{cal(lit)}}$) second pressure virial coefficients from values ($B_{\text{cal(pres)}}$) calculated with the new interatomic potential for Ne. Experimental data: \circ Holborn and Otto [19]; \triangle Nicholson and Schneider [20]; \square Michels *et al.* [21]; ∇ Gibbons [22]; \diamond Vogl and Hall [23]. Calculated values: ——— potential by Aziz and Slaman [7]; - - - - - potential by Cybulski and Toczyłowski [6]; - - - - - potential by Wüest and Merkt [5].

agreement is also found for the data by Nicholson and Schneider [20] up to high temperatures of 1000 K. Conversely, the very old data of Holborn and Otto [19] as well as the more recent but also already 35 years old data of Vogl and Hall [23] are characterized by comparably larger differences to the theoretically calculated values. The data of Gibbons [22] determined at low temperatures show partly large deviations, but agree partly very well. In Figure 2 our calculated values are additionally compared with the values calculated for the interatomic potentials by Aziz and Slaman [7], Cybulski and Toczyłowski [6], and Wüest and Merkt [5]. The differences $B_{\text{cal(lit)}} - B_{\text{cal(pres)}}$ derived for the different interatomic potentials increase to low temperatures, where the values derived from the potentials by Aziz and Slaman [7] and Wüest and Merkt [5] are too small and the values resulting from the potential by Cybulski and Toczyłowski [6] are too large. At medium and higher temperatures the B_{cal} values for all four potentials do not differ much so that the second pressure virial coefficient is not suitable for distinguishing between the different interatomic potentials.

In Figure 3 a comparison between experimental data of the third pressure virial coefficient of neon and values calculated for the new interatomic potential is shown. The figure elucidates that good agreement of the experimental data by Michels *et al.* [21] and by Nicholson and Schneider [20] at medium temperatures and of the data by Gibbons [22] at low temperatures

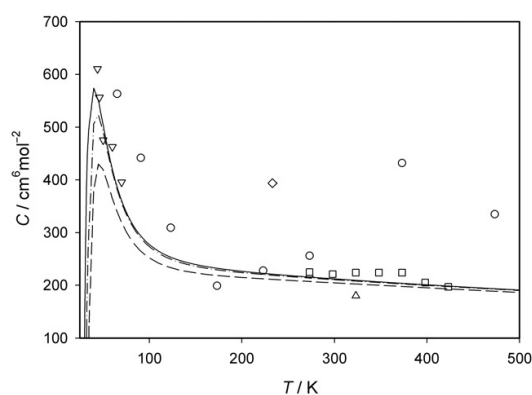


Figure 3. Comparison of experimental data and of calculated values for the third pressure virial coefficient C derived from the new interatomic potential for Ne. Experimental data: \circ Holborn and Otto [19]; \triangle Nicholson and Schneider [20]; \square Michels *et al.* [21]; ∇ Gibbons [22]; \diamond Vogl and Hall [23]. Calculated values: - - - classical contribution C_{add} , - · - · - classical and non-additivity contributions $C_{\text{add}} + C_{\text{non-add}}$, — sum of classical and non-additivity contributions and of the first-order quantum correction $C_{\text{add}} + C_{\text{non-add}} + \lambda C_{\text{qm},1}$.

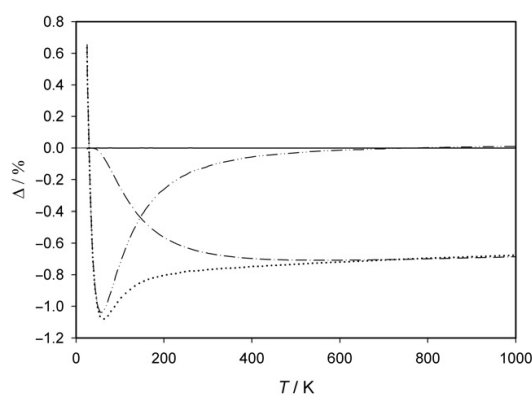


Figure 4. Relative deviations $\Delta = (\eta - \eta_{\text{qm},5}) / \eta_{\text{qm},5}$ between viscosity values calculated for different approximation procedures and viscosity values resulting from quantum-mechanical calculations up to the fifth-order approximation for the individual $[\eta_{ij}]_{\text{qm},5}$ within the first-order formulation of $[\eta_{\text{mix}}]_1$ for the new interatomic potential for Ne. Differences related to: ····· first-order classical calculation $[\eta]_{\text{cl},1}$; - · - · - fifth-order classical calculation $[\eta]_{\text{cl},5}$; — first-order quantum-mechanical calculation $[\eta_{\text{mix}}]_{\text{qm},1}$; - - - first-order quantum-mechanical calculation $[\eta_{\text{mix}}]_{\text{qm},5}$.

with the calculated values is only achieved in the case of the complete sum of the contributions for the pairwise additivity C_{add} , for the non-additivity of the three-body interatomic interactions according to Axilrod and Teller $C_{\text{non-add}}$, and for the first-order quantum-mechanical correction $\lambda C_{\text{qm},1}$. The experimental data by Holborn and Otto [19] as well as Vogl and Hall [23] possess again larger differences to the calculated values. The comparison makes evident that the calculation procedure for the third pressure virial coefficient predicts very good values.

It is to be stressed that the calculated values for the second and the third pressure virial coefficients are more reliable than the experimental data at low and high temperatures.

3.2. Viscosity

First, the results of the different alternative ways of the calculation of the transport properties of naturally occurring neon are compared. In this context it is sufficient to consider only the viscosity, since the effects are the same for the thermal conductivity. Figure 4 illustrates the relative differences between viscosity values derived for the different approximation procedures and the viscosity values obtained from the quantum-mechanical calculation up to the fifth-order

approximation for the individual $[\eta_{ij}]_{\text{qm},5}$ within the first-order formulation of $[\eta_{\text{mix}}]_1$ (see Section 2.3). The figure makes evident that the first-order approximation of the classical calculation leads to values which are nearly 1% too small in the complete temperature range except at the lowest temperatures. The agreement improves when the fifth-order approximation of the classical evaluation is applied. But even for this high-order approximation it becomes obvious that the classical evaluation is not appropriate with regard to highly accurate values. Thus the deviations from the results for the quantum-mechanical calculation of the same fifth-order approximation amount to -0.1% at room temperature increasing up to -1.1% at about 60 K. On the other hand, the first-order approximation of the quantum-mechanical calculation for a dilute-gas mixture composed of the three neon isotopes according to $[\eta_{\text{mix}}]_{\text{qm},1}$ is not adequate, too. The differences are approximately -0.7% at most temperatures and decrease to zero at the lowest temperatures. Further it is to note that there are only differences of $< \pm 0.0004\%$ (not visible in Figure 4) between the results for the two ways to correct the first-order approximation $[\eta_{\text{mix}}]_{\text{qm},1}$ to an appropriate fifth-order approximation of the quantum-mechanical determination. In the following the comparisons with experimental data are performed with values resulting

for the fifth-order approximation of the individual $[\eta_{ij}]_{\text{qm},5}$ and $[\lambda_{ij}]_{\text{qm},5}$ within the first-order formulations of $[\eta_{\text{mix}}]_1$ and $[\lambda_{\text{mix}}]_1$.

With regard to the transport properties it should be considered that most measurements at low densities were performed at atmospheric pressure, whereas the theoretical calculations are valid for the limit of zero density. Hence the initial density dependence of the experimental data would have to be taken into account. However apart from the very low temperatures near to the normal boiling point of neon, the effect of the initial density dependence on the transport properties concerning the change in density from that at atmospheric pressure to zero density is comparably small ($<0.1\%$) for all other temperatures. Furthermore, the experimental uncertainty is distinctly increased at low temperatures.

In our paper concerning the thermophysical standard values for low-density helium [1] we argued that it is difficult to perform genuine absolute measurements of the gas viscosity with an uncertainty $<\pm 0.1\%$, even at room temperature. The same complex of problems is illustrated in Figure 5 in which the best experimental data for neon near to ambient temperature are characterized by error bars for the uncertainties, given by the authors themselves, and are compared with the viscosity values calculated quantum-mechanically. For helium we demonstrated

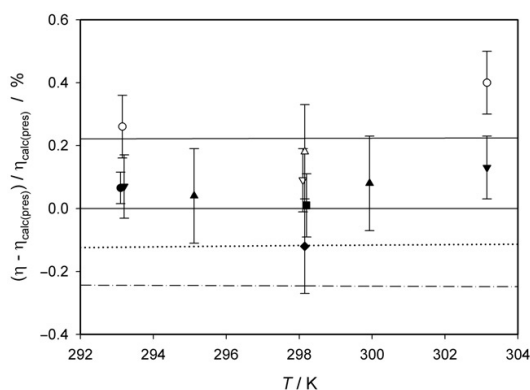


Figure 5. Relative deviations of experimental and calculated viscosity coefficients from values $\eta_{\text{cal(pres)}}$ calculated quantum-mechanically with the new interatomic potential for Ne near to room temperature. Experimental data with uncertainties characterized by error bars: ● Kestin and Leidenfrost [24]; ○ Kestin and Nagashima [25]; ▼ DiPippo *et al.* [26]; ▽ Kestin *et al.* [27], best estimate; ■ Flynn *et al.* [28]; △ Vogel [29], fitted value; ▲ Vogel [29], experimental data corrected according to new helium standard; ◆ Evers *et al.* [30]. Calculated values: ······ fifth-order classical calculation $[\eta]_{\text{cl},5}$; ——— potential by Aziz and Slaman [7]; - - - - potential by Cybulski and Toczyłowski [6].

that the measurements with an oscillating-disc viscometer by Kestin and Leidenfrost [24], approved as one of the most accurate and additionally one of the few absolute measurements on gases, can only partly be considered as absolute ones, since they were finally adjusted to a value for the viscosity of air at 293.15 K and at atmospheric pressure determined by Bearden [31] in an absolute measurement with a rotating-cylinder viscometer. Thus the viscosity value of Kestin and Leidenfrost for neon at 20°C (uncertainty: $\pm 0.05\%$) shown in Figure 5 corresponds as well to a relative measurement, whereas the genuine absolute measurement is that of Bearden in air. Measurements by Kestin and Nagashima [25], performed in a nearly analogous procedure, led to values which are 0.15–0.3% higher than those of Kestin and Leidenfrost [24], but also by the same percentage higher than further data obtained in relative measurements of the same research group by DiPippo *et al.* [26] as well as a best estimate reported by Kestin *et al.* [27] in 1972 as a result of their measurements in foregoing years. This shows that there were sometimes surprisingly large differences in the results of the measurements of this group. Nevertheless, the results of the most reliable measurements by Kestin and co-workers at ambient temperature are characterized by a tendency to values increased by +0.1% compared to the calculated values of the present paper. The same findings concerning the measurements by Kestin and co-workers were observed in the case of the values derived from our interatomic helium potential. As a consequence, the measurements on helium by Vogel [29] (uncertainty: $\pm 0.15\%$ at room temperature) performed with an all-quartz oscillating-disc viscometer in a relative manner using a viscometer constant derived from the best estimate by Kestin *et al.* should be affected by the same impact. Therefore, the viscometer of Vogel was recalibrated with the new helium standard for a rehandled evaluation of the measurements on helium [1] and on neon, too. The influence of the recalibration on the results of Vogel for neon is additionally demonstrated in Figure 5. A value at 298.15 K resulting from the fitting function given by Vogel [29] deviates from the value calculated for the interatomic neon potential of the present paper by +0.18%. Conversely, the direct experimental data of the measurement series by Vogel at room temperature show only differences of +0.04% and +0.08% after the recalibration.

Furthermore, the absolute measurements by Flynn *et al.* [28] performed with a capillary viscometer led to a datum at 293.15 K differing only by +0.01% from the theoretically calculated value (uncertainties: $\pm 0.1\%$). Recently, Evers *et al.* [30] utilized a

rotating-cylinder viscometer for absolute measurements (uncertainty: $\pm 0.15\%$) on several gases at different temperatures and pressures. Their result for neon at 298.15 K deviates from our calculated value by -0.12% . In conclusion, the comparison makes evident that the best experimental data at room temperature are characterized by an uncertainty of $\pm(0.1$ to $0.15)\%$ and that they agree within this limit with the values calculated for the interatomic neon potential of the present paper.

The situation deteriorates to the disadvantage of the experiment, if the measurements were not performed at ambient temperature. In Figure 6, experimental data at low and medium temperatures between 20 and 373 K are compared with the calculated values. Error bars for one or two (in the case that the uncertainty changes with temperature) values of each data set are additionally plotted. The figure demonstrates that excellent agreement within $\pm 0.1\%$ exists only for the absolute measurement by Evers *et al.* [30] at 348 K and that the results of the absolute measurements by Flynn *et al.* [28] are adequately consistent within $\pm 0.3\%$. The other data were determined by relative measurements, which are not only affected by the usual measurement errors, but also by the values used for the calibration. Johnston and Grilly [32] and Rietveld *et al.* [34] (both using oscillating-disc

viscometers) as well as Clarke and Smith [35] (capillary viscometer) based their measurements on reasonable values for air, helium, and nitrogen at ambient temperature and achieved results with deviations up to -2% , $+4\%$, and $+1\%$. These data are not suitable to judge the appropriateness of any interatomic neon potential. On the other hand, the measurements by Coremans *et al.* [33] carried out with an oscillating-disc viscometer, which was calibrated using a very old viscosity value for ^4He at 20 K reported by Kamerlingh Onnes and Weber [36], yielded values characterized by positive deviations up to 6% from the quantum-mechanically calculated values. These results were improved for the purposes of this paper by a recalibration with a value for ^4He at 20 K taken from our new helium standard [1]. Figure 6 makes obvious that the corrected data advanced after this correction partly in close agreement.

Figure 7 illustrates the analogous comparison at higher temperatures. The figure reveals a surprisingly large scattering of about $\pm 0.3\%$ in the data from different papers by Kestin and his research group [27,37,38] (the same order of magnitude as the uncertainty) and additionally a systematic trend to higher values with increasing temperature combined with again decreasing values at the

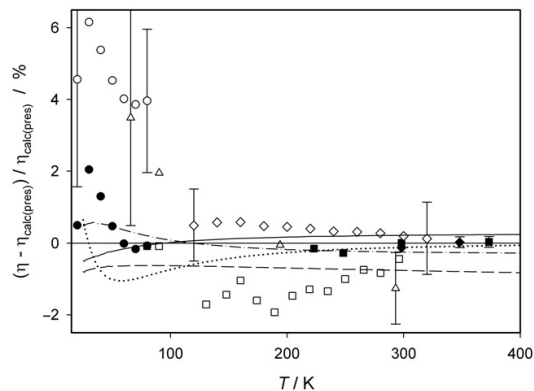


Figure 6. Relative deviations of experimental and calculated viscosity coefficients from values $\eta_{\text{cal(pres)}}$ calculated with the new interatomic potential for Ne at low and medium temperatures. Experimental data with uncertainties characterized by error bars: \square Johnston and Grilly [32]; \circ Coremans *et al.* [33]; \bullet Coremans *et al.* [33], corrected according to new helium standard; \triangle Rietveld *et al.* [34]; \blacksquare Flynn *et al.* [28]; \diamond Clarke and Smith [35]; \blacklozenge Evers *et al.* [30]. Calculated values: \cdots fifth-order classical calculation $[\eta]_{\text{cl},5}$; — potential by Aziz and Slaman [7]; $\text{-}\cdot\cdot\cdot\text{-}$ potential by Cybulski and Toczyłowski [6]; $\text{-}\text{-}\text{-}\text{-}$ potential by Wüest and Merkt [5].

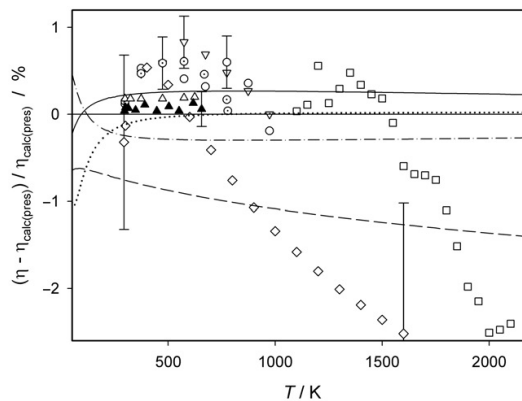


Figure 7. Deviations of experimental and calculated viscosity coefficients from values $\eta_{\text{cal(pres)}}$ calculated with the new interatomic potential for Ne at higher temperatures. Experimental data with uncertainties characterized by error bars: ∇ Kestin *et al.* [27], best estimate; \circ Helleman *et al.* [37]; \diamond Kestin *et al.* [38]; \square Dawe and Smith [39]; \square Guevara and Stensland [40]; \triangle Vogel [29], fitted values; \blacktriangle Vogel [29], experimental data corrected according to new helium standard. Calculated values: \cdots fifth-order classical calculation $[\eta]_{\text{cl},5}$; — potential by Aziz and Slaman [7]; $\text{-}\cdot\cdot\cdot\text{-}$ potential by Cybulski and Toczyłowski [6]; $\text{-}\text{-}\text{-}\text{-}$ potential by Wüest and Merkt [5].

highest temperatures. In this connection it is to be noted that all measurements by Kestin and his co-workers with the oscillating-disc viscometer by Di Pippo *et al.* [41] are affected by a temperature measurement error with thermocouples explained by Vogel *et al.* [42]. Figure 7 also makes evident that the data by Vogel [29], originally fitted to his experiments which were based on a calibration with the best estimate value at room temperature by Kestin *et al.* [27], deviate by about +0.2% from the quantum-mechanically calculated values of this paper. After a recalibration of the measurement series on neon by means of the new helium standard [1] at room temperature, the corrected experimental data do only deviate by less than +0.1% on average from the theoretical values for the new neon potential in the complete temperature range of the measurements. This demonstrates that the measurements by Vogel with his all-quartz oscillating-disc viscometer represent the best experiments in this temperature range. The comparison concerning the experimental data by Dawe and Smith [39] and by Guevara and Stensland [40], which result from relative measurements with capillary viscometers based on a reasonable calibration at room temperature, shows that these data should be influenced by systematic errors. Lastly it is concluded that the theoretical determination of viscosity values is to be preferred to experiments at these high temperatures.

Figures 5, 6, and 7 include once again a comparison with the values derived classically using the fifth-order approximation. The results of the classical calculation deviate by about -0.1% from those of the quantum-mechanical computation at ambient and higher temperatures. At lower temperatures the deviations are distinctly increased. Figure 5 elucidates further that at room temperature the results of the quantum-mechanical calculations for the potentials by Aziz and Slaman [7] and by Cybulski and Toczyłowski [6] (both $>\pm 0.2\%$) and particularly by Wüest and Merkt [5] (-0.7%, not observable in the figure) do not match the best experimental data as well as the calculated values for the potential of the present paper within $\pm 0.1\%$. Figures 6 and 7 demonstrate that the best experimental data allow one to distinguish between the different potentials proposed for neon. The values resulting from the potentials by Aziz and Slaman [7] and by Cybulski and Toczyłowski [6] and particularly by Wüest and Merkt [5] are characterized by differences from the transport data that are distinctly larger than the experimental uncertainties. Here one should point to the differences for the values determined with the potential proposed by Wüest and Merkt [5]. They arise with increasing temperature due to the fact that the rovibrational spectra used by Wüest and Merkt are

sensitive to the shape of the potential well, but not to the repulsive part of the potential to which the transport properties are particularly sensitive.

3.3. Thermal conductivity

The uncertainty of measurements of the thermal conductivity is inferior to that of viscosity measurements due to different experimental difficulties, whereas the most accurate data can be obtained with the transient hot-wire technique, but essentially restricted to ambient temperature. This is demonstrated in Figure 8, in which experimental data for neon at low and medium temperatures are compared with the values calculated quantum-mechanically. Here the experimental data are again, when available, characterized by error bars according to the uncertainties given by the experimenters themselves. The data by Kestin *et al.* [44] and Assael *et al.* [45], each gained with the transient hot-wire technique at room temperature, deviate from the calculated values by $<-0.1\%$ and $<+0.2\%$. These differences are lower than the experimental uncertainties ($\pm 0.3\%$ and $\pm 0.2\%$). Although the data by Haarman [43] are characterized by larger deviations (-0.3% to -0.4%), the temperature function of these transient hot-wire data between 328 and

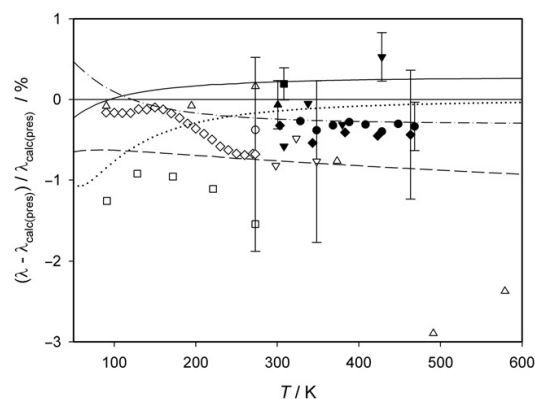


Figure 8. Deviations of experimental and calculated thermal conductivity coefficients from values $\lambda_{\text{cal(pres)}}$ calculated with the new interatomic potential for Ne at low and medium temperatures. Experimental data with uncertainties characterized by error bars: ● Haarman [43]; ▲ Kestin *et al.* [44]; ■ Assael *et al.* [45]; ▼ Millat *et al.* [46]; ◆ Hemminger [47]; ○ Weber [48]; △ Kannuliuk and Carman [49]; □ Keyes [50]; ▽ Sengers *et al.* [51]; ◇ Nesterov and Sudnik [52], smoothed values. Calculated values: fifth-order classical calculation [7]_{cl,5}; — potential by Aziz and Slaman [7]; - - - potential by Cybulski and Toczyłowski [6]; - · - potential by Wüest and Merkt [5].

468 K corresponds closely to that of the calculated values. Conversely, the temperature function of the data by Millat *et al.* [46] shows an awkward behaviour so that these data are not useful with regard to the assessment of the values calculated for the different interatomic potentials of neon. But Figure 8 makes also evident that the deviations of the experimental data of Hemminger [47], derived from measurements with a guarded parallel-plate apparatus and carefully corrected for impurities caused by desorbed air, are within -0.35% and -0.6% ; this means their temperature function and that of the calculated values are pretty much consistent from room temperature up to 470 K.

Experimental data determined with the common steady-state hot-wire technique often affected by convection are checked against the quantum-mechanically calculated values in Figure 8, too. Differences of only $<\pm 0.4\%$ are found for the very old experimental datum by Weber [48] at 273 K and also for a value by Kannuliik and Carman [49] at the same temperature. But for the complete temperature range of the measurements of Kannuliik and Carman between 90 and 580 K the deviations increase up to -3% . On the other hand, the smoothed experimental values by Nesterov and Sudnik [52] between 90 K and ambient temperature created with the same technique are characterized by comparably small differences between -0.1% and -0.7% , with the best agreement at low temperatures. Further it becomes evident from this figure that the experimental data by Keyes [50] determined with the concentric-cylinder method (differences between -1% and -1.5%) and those of Sengers *et al.* [51] obtained with a parallel-plate apparatus (differences between -0.5% and -0.85%) are not suitable for a reasonable comparison with the theoretical values.

Figure 9 illustrates the comparison at higher temperatures. Neither the experimental data by Tufeu *et al.* [54] (concentric-cylinder method) nor the experimental values by Saxena and Saxena [53] (common hot-wire technique) enable one to verify the performance of the different potentials under discussion due to the differences exceeding -1% . Conversely, there occur surprisingly only very small deviations of -0.45% to $+0.05\%$ for the experimental data by Springer and Wingeier [55] between 1000 and 1500 K using the concentric-cylinder method. In principle, this would support the new interatomic potential of this work. In addition, the values recommended by Ziebland [56] on the basis of different experimental data show deviations larger than $+1\%$ according to their estimated uncertainties. It is to note that thermal conductivity values at very high temperatures between

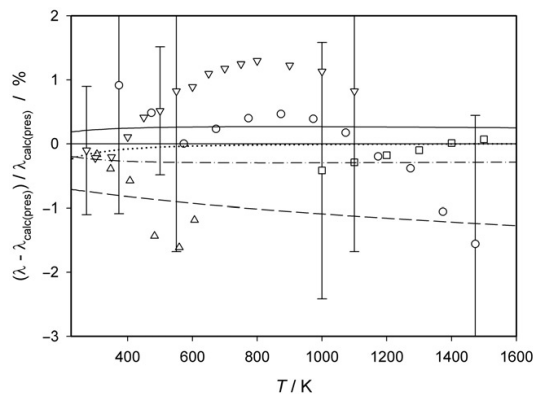


Figure 9. Deviations of experimental and calculated thermal conductivity coefficients from values $\lambda_{\text{cal(pres)}}$ calculated with the new interatomic potential for Ne at higher temperatures. Experimental data with uncertainties characterized by error bars: \circ Saxena and Saxena [53], smoothed values; \triangle Tufeu *et al.* [54]; \square Springer and Wingeier [55]; ∇ Ziebland [56], recommended values. Calculated values: \cdots fifth-order classical calculation $[\eta]_{\text{cl},5}$; — potential by Aziz and Slaman [7]; $-\cdot-\cdot-$ potential by Cybulski and Toczyłowski [6]; $-\cdot-\cdot-$ potential by Wüest and Merkt [5].

1500 K and at most 6000 K were derived from shock-tube measurements by Collins and Menard [57] and by Mařtovský [58]. Their data not shown in Figure 9 have deviations of -5.5% up to -11.5% and -2.5% up to -6.8% . At such high temperatures calculated values are to be preferred in any case.

Both figures make evident that the interatomic potential by Wüest and Merkt [5] is not qualified to describe adequately the best experimental thermal conductivity data. On the other hand, there exist only a few experimental data to distinguish between the appropriateness of the other potentials. But if the best experimental transient hot-wire-data at room temperature are selected for the comparison, then there exists a stringent test of the new potential and of the correct application of the kinetic theory including the quantum-mechanical effects.

4. Summary and conclusions

A new interatomic potential for neon derived from quantum-mechanical *ab initio* computations [3] was utilized to calculate the second and third pressure virial, the viscosity, and the thermal conductivity coefficients for dilute neon gas in its natural isotopic composition in the temperature range from 25 to 10,000 K. For the second virial coefficient and for the

transport properties fully quantum-mechanical calculations were performed with neon treated as an isotopic mixture, whereas for the third virial coefficient a classical mechanical evaluation with a quantum correction using the average mass of the isotopic mixture was applied. The comparison with available experimental data makes evident that the calculated thermophysical properties are as accurate as the best experimental data at room temperature and more accurate at temperatures above and below room temperature. The deviations between the results from the different potentials for all calculated properties increase at the lowest temperatures.

The viscosity values around ambient temperature derived theoretically with the interatomic potential of this paper are characterized by deviations smaller than $\pm 0.1\%$ compared to the best experimental data, whereas the results obtained from the potential energy curves by Cybulski and Toczyłowski, by Aziz and Slaman [7], and by Wüest and Merkt [5] show larger deviations. We estimate summarily the uncertainties of the calculated transport properties resulting from our new potential to be about $\pm 0.1\%$ except at the lowest temperatures. It is to be stressed that this uncertainty is much below the experimental uncertainties at low as well as at high temperatures. All calculated data (see Table 3 in Appendix 1) can be applied as standards values for the complete temperature range.

References

- [1] E. Bich, R. Hellmann, and E. Vogel, *Molec. Phys.* **105**, 3035 (2007).
- [2] R. Hellmann, E. Bich, and E. Vogel, *Molec. Phys.* **105**, 3013 (2007).
- [3] R. Hellmann, E. Bich, and E. Vogel, *Molec. Phys.* **106**, 133 (2008).
- [4] K.T. Tang and J.P. Toennies, *J. Chem. Phys.* **80**, 3726 (1984).
- [5] A. Wüest and F. Merkt, *J. Chem. Phys.* **118**, 8807 (2003).
- [6] S.M. Cybulski and R.R. Toczyłowski, *J. Chem. Phys.* **111**, 10520 (1999).
- [7] R.A. Aziz and M.J. Slaman, *Chem. Phys.* **130**, 187 (1989).
- [8] M.E. Boyd, S.Y. Larsen, and J.E. Kilpatrick, *J. Chem. Phys.* **50**, 4034 (1969).
- [9] E.A. Mason and T.H. Spurling, *The Virial Equation of State* (Pergamon, Oxford, 1969).
- [10] S. Kim and D. Henderson, *Proc. Nat. Acad. Sci. Wash.* **55**, 705 (1966).
- [11] K. Lucas, *Angewandte Statistische Thermodynamik* (Springer, Berlin, 1986).
- [12] B.M. Axilrod and E. Teller, *J. Chem. Phys.* **11**, 299 (1943).
- [13] B.M. Axilrod, *J. Chem. Phys.* **19**, 719 (1951).
- [14] A. Kumar and W.J. Meath, *Molec. Phys.* **54**, 823 (1985).
- [15] L.A. Viehland, A.R. Janzen, and R.A. Aziz, *J. Chem. Phys.* **102**, 5444 (1995).
- [16] F.R. Meeks, T.J. Cleland, K.E. Hutchinson, *et al.*, *J. Chem. Phys.* **100**, 3813 (1994).
- [17] G.C. Maitland, M. Rigby, E.B. Smith, *et al.*, *Intermolecular Forces. Their Origin and Determination* (Clarendon Press, Oxford, 1987).
- [18] R.J. LeRoy, *LEVEL 7.7. A Computer Program for Solving the Radial Schrodinger Equation for Bound and Quasibound Levels*, University of Waterloo, Chemical Physics Research Report CP-661 (Waterloo, Ontario, Canada, 2005).
- [19] L. Holborn and J. Otto, *Z. Phys.* **33**, 1 (1925), **38**, 359 (1926).
- [20] G.A. Nicholson and W.G. Schneider, *Can. J. Chem.* **33**, 589 (1955).
- [21] A. Michels, T. Wassenaar, and P. Louwerse, *Physica* **26**, 539 (1960).
- [22] R.M. Gibbons, *Cryogenics* **9**, 251 (1969).
- [23] W.F. Vogl and K.R. Hall, *Physica* **59**, 529 (1972).
- [24] J. Kestin and W. Leidenfrost, *Physica* **25**, 1033 (1959).
- [25] J. Kestin and A. Nagashima, *J. Chem. Phys.* **40**, 3648 (1964).
- [26] R. DiPippo, J. Kestin, and K. Oguchi, *J. Chem. Phys.* **46**, 4758 (1967).
- [27] J. Kestin, S.T. Ro, and W.A. Wakeham, *J. Chem. Phys.* **56**, 4119 (1972).
- [28] G.P. Flynn, R.V. Hanks, N.A. Lemaire, *et al.*, *J. Chem. Phys.* **38**, 154 (1963).
- [29] E. Vogel, *Ber. Bunsenges. Phys. Chem.* **88**, 997 (1984).
- [30] C. Evers, H.W. Lösch, and W. Wagner, *Int. J. Thermophys.* **23**, 1411 (2002).
- [31] J.A. Bearden, *Phys. Rev.* **56**, 1023 (1939).
- [32] H.L. Johnston and E.R. Grilly, *J. Phys. Chem.* **46**, 948 (1942).
- [33] J.M.J. Coremans, A. van Itterbeek, J.J.M. Beenakker, *et al.*, *Physica* **24**, 557 (1958).
- [34] A.O. Rietveld, A. van Itterbeek, and C.A. Velds, *Physica* **25**, 205 (1959).
- [35] A.G. Clarke and E.B. Smith, *J. Chem. Phys.* **51**, 4156 (1969).
- [36] H. Kamerlingh Onnes and S. Weber, *Vers. Kon. Acad. Wetenschappen Amsterdam* **21**, 1385 (1913).
- [37] J.M. Helleman, J. Kestin, and S.T. Ro, *Physica* **71**, 1 (1974).
- [38] J. Kestin, H.E. Khalifa, and W.A. Wakeham, *Physica A* **90**, 215 (1978).
- [39] R.A. Dawe and E.B. Smith, *J. Chem. Phys.* **52**, 693 (1970).
- [40] F.A. Guevara and G. Stensland, *Phys. Fluids* **14**, 746 (1971).
- [41] R. DiPippo, J. Kestin, and J.H. Whitelaw, *Physica* **32**, 2064 (1966).

- [42] E. Vogel, C. Küchenmeister, E. Bich, *et al.*, J. Phys. Chem. Ref. Data **27**, 947 (1998).
- [43] J.W. Haarman, Am. Inst. Phys. Conf. Proc. **11**, 193 (1973).
- [44] J. Kestin, R. Paul, A.A. Clifford, *et al.*, Physica A **100**, 349 (1980).
- [45] M.J. Assael, M. Dix, A. Lucas, *et al.*, J. Chem. Soc. Faraday Trans. I **77**, 439 (1981).
- [46] J. Millat, M. Ross, W.A. Wakeham, *et al.*, Physica A **148**, 124 (1988).
- [47] W. Hemminger, Int. J. Thermophys **8**, 317 (1987).
- [48] S. Weber, Ann. Phys. **82**, 479 (1927).
- [49] W.G. Kannuliuk and E.H. Carman, Proc. Phys. Soc. London B **65**, 701 (1952).
- [50] F.G. Keyes, Trans. ASME **76**, 809 (1954).
- [51] J.V. Sengers, W.T. Bolk, and C.J. Stigter, Physica **30**, 1018 (1964).
- [52] N.A. Nesterov and V.M. Sudnik, Inzh.-fiz. Zh. **30**, 863 (1976).
- [53] V.K. Saxena and S.C. Saxena, J. Chem. Phys. **48**, 5662 (1968).
- [54] R. Tufeu, B. LeNeindre, and P. Bury, C. R. Acad. Sci. Paris, B **271**, 589 (1970).
- [55] G.S. Springer and E.W. Wingeier, J. Chem. Phys. **59**, 2747 (1973).
- [56] H. Ziebland, Pure Appl. Chem. **53**, 1863 (1981).
- [57] D.J. Collins and W.A. Menard, Trans. ASME **88**, 52 (1966).
- [58] J. Mařtovský, *Report Z-1026/87* (ČSAV, Ústav Termomechaniky, Prague, 1987).

Appendix 1. Thermophysical properties of neon calculated in this work

The thermophysical properties of naturally occurring neon are given in Table 3.

Table 3. Thermophysical properties of neon for the interatomic potential of this work.

T (K)	B (cm ³ mol ⁻¹)	C (cm ⁶ mol ⁻²)	η (μ Pas)	λ (mW m ⁻¹ K ⁻¹)
25.00	-128.50	-1716	3.9213	6.0597
26.00	-119.87	-1130	4.0790	6.3033
27.00	-112.02	-689.5	4.2353	6.5446
28.00	-105.04	-358.4	4.3927	6.7878
30.00	-92.972	78.89	4.7097	7.2775
32.00	-82.953	325.4	5.0270	7.7676
34.00	-74.517	461.5	5.3447	8.2585
36.00	-67.316	532.2	5.6617	8.7482
38.00	-61.085	564.7	5.9784	9.2377
40.00	-55.657	574.0	6.2915	9.7214
42.00	-50.888	569.7	6.6035	10.204
44.00	-46.666	557.7	6.9132	10.682
46.00	-42.905	541.5	7.2191	11.155
48.00	-39.526	523.4	7.5245	11.627
50.00	-36.486	504.6	7.8257	12.093
55.00	-30.063	459.3	8.5658	13.237
60.00	-24.892	419.9	9.2862	14.352
65.00	-20.676	387.2	9.9868	15.436
70.00	-17.169	360.6	10.668	16.491
75.00	-14.213	339.9	11.331	17.518
80.00	-11.676	321.5	11.976	18.518
85.00	-9.4909	307.0	12.605	19.493
90.00	-7.5869	295.2	13.217	20.443
95.00	-5.9132	285.4	13.815	21.370
100.00	-4.4329	277.3	14.399	22.277
110.00	-1.9365	264.7	15.528	24.030
120.00	0.0895	255.6	16.612	25.713
130.00	1.7559	248.8	17.654	27.333
140.00	3.1490	243.5	18.660	28.896
150.00	4.3280	239.4	19.634	30.410
160.00	5.3365	236.0	20.579	31.879
170.00	6.2068	233.1	21.498	33.307

(continued)

Table 3. Continued.

T (K)	B (cm ³ mol ⁻¹)	C (cm ⁶ mol ⁻²)	η (μ Pas)	λ (mW m ⁻¹ K ⁻¹)
180.00	6.9638	230.6	22.394	34.699
190.00	7.6271	228.6	23.268	36.058
200.00	8.2116	226.5	24.122	37.385
210.00	8.7298	224.7	24.958	38.685
220.00	9.1906	223.1	25.778	39.959
230.00	9.6037	221.5	26.583	41.210
240.00	9.9744	220.0	27.372	42.436
250.00	10.308	218.6	28.149	43.643
260.00	10.610	217.3	28.912	44.829
270.00	10.884	215.9	29.665	45.999
273.15	10.964	215.5	29.900	46.364
280.00	11.133	214.6	30.408	47.153
290.00	11.360	213.9	31.139	48.289
298.15	11.530	212.9	31.728	49.203
300.00	11.567	212.2	31.860	49.410
320.00	11.930	209.8	33.277	51.610
340.00	12.237	207.4	34.660	53.758
360.00	12.497	205.2	36.014	55.859
380.00	12.719	203.0	37.339	57.917
400.00	12.909	200.8	38.640	59.937
420.00	13.072	198.8	39.918	61.921
440.00	13.212	196.7	41.174	63.871
460.00	13.333	194.8	42.411	65.789
480.00	13.437	192.8	43.628	67.679
500.00	13.527	190.9	44.829	69.542
550.00	13.700	186.4	47.761	74.091
600.00	13.819	182.1	50.604	78.502
650.00	13.896	178.0	53.370	82.793
700.00	13.943	174.2	56.068	86.977
750.00	13.968	170.6	58.703	91.065
800.00	13.975	167.2	61.284	95.067
850.00	13.968	163.9	63.814	98.990
900.00	13.952	160.8	66.298	102.84
950.00	13.927	157.9	68.739	106.63
1000.00	13.895	155.1	71.141	110.35
1100.00	13.819	149.9	75.838	117.63
1200.00	13.730	145.1	80.408	124.72
1300.00	13.634	140.7	84.866	131.63
1400.00	13.534	136.7	89.223	138.38
1500.00	13.432	132.9	93.489	144.99
1600.00	13.329	129.5	97.674	151.48
1700.00	13.226	126.2	101.78	157.85
1800.00	13.125	123.2	105.83	164.11
1900.00	13.025	120.3	109.80	170.28
2000.00	12.926	117.6	113.72	176.35
2100.00	12.830	115.1	117.59	182.34
2200.00	12.736	112.7	121.40	188.25
2300.00	12.644	110.4	125.17	194.08
2400.00	12.554	108.2	128.89	199.85
2500.00	12.467	106.2	132.57	205.55
2600.00	12.381	104.2	136.21	211.19
2700.00	12.298	102.4	139.81	216.76
2800.00	12.216	100.6	143.38	222.29
2900.00	12.137	98.92	146.91	227.76
3000.00	12.059	97.29	150.41	233.18
3100.00	11.984	95.73	153.87	238.55
3200.00	11.910	94.24	157.31	243.88
3300.00	11.838	92.80	160.72	249.16

(continued)

Table 3. Continued.

T (K)	B (cm ³ mol ⁻¹)	C (cm ⁶ mol ⁻²)	η (μ Pas)	λ (mW m ⁻¹ K ⁻¹)
3400.00	11.767	91.41	164.11	254.40
3500.00	11.698	90.08	167.46	259.60
3600.00	11.631	88.80	170.79	264.76
3700.00	11.565	87.56	174.10	269.88
3800.00	11.501	86.36	177.39	274.97
3900.00	11.438	85.21	180.65	280.02
4000.00	11.376	84.09	183.89	285.04
4100.00	11.316	83.01	187.11	290.03
4200.00	11.257	81.96	190.31	294.99
4300.00	11.199	80.95	193.49	299.91
4400.00	11.142	79.96	196.65	304.81
4500.00	11.087	79.01	199.80	309.68
4600.00	11.032	78.09	202.92	314.52
4700.00	10.979	77.19	206.03	319.33
4800.00	10.926	76.31	209.12	324.12
4900.00	10.875	75.46	212.20	328.88
5000.00	10.825	74.64	215.26	333.62
6000.00	10.366	67.45	245.09	379.81
7000.00	9.9770	61.77	273.72	424.15
8000.00	9.6396	57.14	301.40	467.00
9000.00	9.3429	53.30	328.28	508.61
10000.00	9.0788	50.05	354.48	549.16

4.3 *Ab initio* intermolecular potential energy surface and second pressure virial coefficients of methane

Robert Hellmann, Eckard Bich, Eckhard Vogel

J. Chem. Phys. **128**, 214303(1-9) (2008).

Alle quantenchemischen Berechnungen sowie die Anpassung des Potentials und die Berechnung der zweiten Druckvirialkoeffizienten wurden selbst durchgeführt. Der eigene Anteil beträgt etwa 80%.

Reprinted with permission from Robert Hellmann, Eckard Bich, Eckhard Vogel, J. Chem. Phys. 128, 21, 214303, 2008. Copyright 2008, American Institute of Physics.

Ab initio intermolecular potential energy surface and second pressure virial coefficients of methaneRobert Hellmann, Eckard Bich, and Eckhard Vogel^{a)}*Institut für Chemie, Universität Rostock, Albert-Einstein-Straße 3a, D-18059 Rostock, Germany*

(Received 7 April 2008; accepted 29 April 2008; published online 3 June 2008)

A six-dimensional potential energy hypersurface (PES) for two interacting rigid methane molecules was determined from high-level quantum-mechanical *ab initio* computations. A total of 272 points for 17 different angular orientations on the PES were calculated utilizing the counterpoise-corrected supermolecular approach at the CCSD(T) level of theory with basis sets of aug-cc-pVTZ and aug-cc-pVQZ qualities. The calculated interaction energies were extrapolated to the complete basis set limit. An analytical site-site potential function with nine sites per methane molecule was fitted to the interaction energies. In addition, a semiempirical correction to the analytical potential function was introduced to take into account the effects of zero-point vibrations. This correction includes adjustments of the dispersion coefficients and of a single-parameter within the fit to the measured values of the second virial coefficient $B(T)$ at room temperature. Quantitative agreement was then obtained with the measured B values over the whole temperature range of the measurements. The calculated B values should definitely be more reliable at very low temperatures ($T < 150$ K) than values extrapolated using the currently recommended equation of state. © 2008 American Institute of Physics. [DOI: 10.1063/1.2932103]

I. INTRODUCTION

Precise knowledge of the interaction potential between molecules is needed to calculate the thermophysical properties in the gas, liquid, or solid phases. In the case of a dilute pure gas, these properties can be determined from a molecule-molecule pair potential. Once the interaction potential is available, it is straightforward to compute the second pressure virial coefficient utilizing statistical mechanics. In addition, the transport and relaxation properties of dilute molecular gases are accessible by means of the kinetic theory of gases, which was recently extended to nonlinear molecules.¹ However, for dense gases, also liquid, and solid phases, nonadditive terms must be included in addition.

The interaction potential of the methane molecule pair was the subject of numerous studies over the past decades. In molecular simulations, the potential was very often approximated by a spherically symmetric Lennard-Jones type function in which the two adjustable parameters were fitted to experimental data. Furthermore, several *ab initio* calculations were performed, mostly concerned with the well depth at the global minimum or the distance dependence of the potential for that angular orientation providing the global minimum. To the best of our knowledge only two groups of researchers carried out *ab initio* studies in the last ten years in which multiple angular orientations were considered so that a complete anisotropic potential hypersurface could be derived.

In 1998, Tsuzuki *et al.*² calculated a total of 132 points on the potential energy hypersurface (PES) for 12 angular orientations at the MP3 level of theory. They used a

6-311G** basis set with additional diffuse polarization functions. A site-site potential energy function, with sites located at the carbon and hydrogen atoms, was then fitted to the calculated interaction energies. The resulting analytical potential function features a maximum well depth of 224 K. In 1999, Rowley and Pakkanen³ calculated 146 energy points for 11 angular configurations at the MP2/6-311+G(2df,2pd) level. They also derived a site-site potential function, with sites on the carbon and hydrogen atoms, characterized by a maximum well depth of only 168 K. In addition, Rowley and Pakkanen presented an improved potential function which was deduced by refitting to five selected points on the PES determined at the MP4 level with the aug-cc-pVTZ (Refs. 4 and 5) basis set. This procedure led to an increased well depth of 237 K. However, in 2006 Tsuzuki *et al.*⁶ showed that the global minimum should actually be still deeper. They applied the very accurate CCSD(T) method,⁷ employing basis sets up to cc-pVQZ,⁴ and obtained global well depths of 252 and 263 K, depending on different procedures in extrapolating the interaction energies to the complete basis set (CBS) limit.

In order to obtain a more accurate methane-methane potential energy surface, a number of issues have to be taken into account. Thus, more reliable CBS estimates can be achieved by considering diffuse basis functions which generally improve the basis set convergence for weakly bound systems. Further, the influence of zero-point vibrations on the interaction potential should be incorporated. This effect is expected to be quite large, since the polarizability of methane is significantly higher when vibration is taken into consideration,^{8,9} resulting in stronger attraction and therefore in a deeper well depth.

In the present paper, a new interaction potential energy

^{a)}Electronic mail: eckhard.vogel@uni-rostock.de.

surface for methane has been determined using highly accurate coupled-cluster calculations with larger basis sets, performed for more angular orientations and more center of mass separations than in the previous studies. In addition, a more flexible analytical site-site potential model has been employed to minimize fitting errors. A semiempirical correction for zero-point vibrational effects has been included in the final analytical representation. The second pressure virial coefficient has been utilized to test the quality of the new potential.

In forthcoming papers, we will report on transport and relaxation property values of dilute methane gas computed with the new PES over a wide range of temperature. Accurate experimental values of transport properties at room temperature can be used as a further test of the validity of the potential energy surface. In addition, such calculations are of importance because viscosity and thermal conductivity are difficult to experimentally determine at very low and very high temperatures. Hence, we expect the theoretically computed values to be more accurate than the experimental data at extreme temperatures.

II. QUANTUM CHEMICAL DETERMINATION AND ANALYTICAL REPRESENTATION OF THE CH₄-CH₄ POTENTIAL

Altogether 17 angular orientations with 16 center of mass separations, each between 2.5 and 8.0 Å, were chosen for the computations, resulting in a total of 272 interaction energies. These orientations are illustrated in Fig. 1. Due to the high symmetry of the methane molecule, this number of angular orientations should be adequate for the intended fit of a highly flexible analytical potential function to the calculated interaction energies.

The bond angles of CH₄ were established to give a regular tetrahedron. The length of the C-H bonds was fixed according to the experimental zero-point vibrationally averaged value of 1.099 Å.¹⁰ This value is consistent with high-level *ab initio* computations of the bond length. An equilibrium bond length of 1.0859 Å was determined at the CCSD(T) level by Stanton¹¹ who employed large basis sets and performed an extrapolation to the CBS limit. Lee *et al.*¹² found that the increase in the bond length due to zero-point vibrations is 0.0131 Å at the CCSD(T)/cc-pVQZ level. The sum of both values yields again 1.099 Å.

Each interaction energy was calculated using the supermolecular approach including a full counterpoise correction¹³ at the frozen-core CCSD(T) level with the aug-cc-pVTZ and aug-cc-pVQZ basis sets.⁵ The correlation part of the CCSD(T) interaction energies, $V_{\text{CCSD(T)corr}}$, obtained with these two basis sets was extrapolated to the CBS limit with the formula proposed by Halkier *et al.*,¹⁴

$$V_{\text{CCSD(T)corr}}^{\text{XZ}} = V_{\text{CCSD(T)corr}}^{\text{CBS}} + \alpha X^{-3}. \quad (1)$$

The self-consistent-field interaction energies were not extrapolated and were taken from the aug-cc-pVQZ calculations.

An analytical site-site potential function was fitted to the extrapolated interaction energies. The positions of the sites

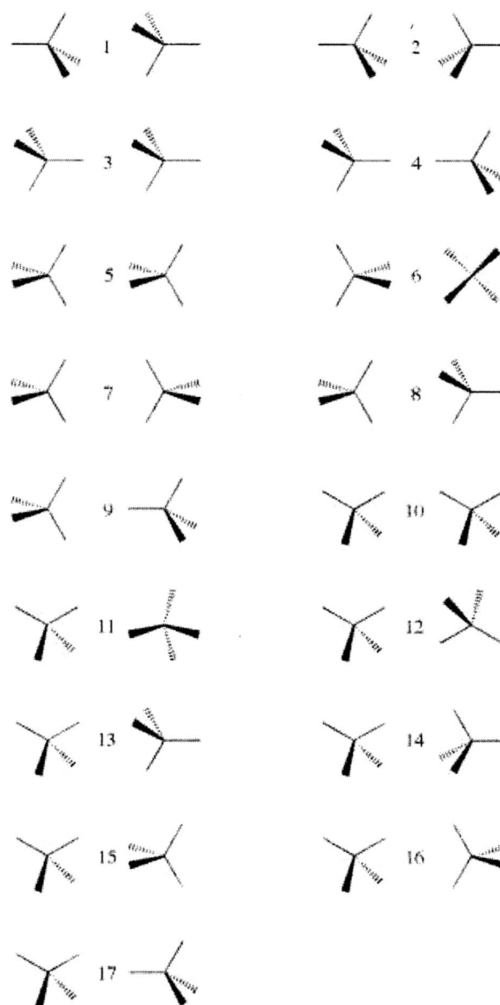


FIG. 1. Angular orientations of the methane molecules.

within the methane molecule are as follows: The CH₄ molecule is located at the center of a Cartesian coordinate system. One site denoted “C” corresponds to the carbon atom. Four sites denoted “H” are generated by scaling the Cartesian coordinates of the hydrogen atoms by 0.88, and four sites denoted “E” are obtained by scaling the Cartesian coordinates of the hydrogen atoms by -0.66. This procedure leads to a total of nine sites per molecule and enables an accurate fit of the *ab initio* values. The total potential is given as a function of the center of mass distance R and of three Eulerian angles for each of the molecules A and B,

$$V(R, \vartheta_A, \vartheta_B, \psi_A, \psi_B, \varphi_A - \varphi_B) = \sum_{i=1}^9 \sum_{j=1}^9 V_{ij}[R_{ij}(R, \vartheta_A, \vartheta_B, \psi_A, \psi_B, \varphi_A - \varphi_B)] \quad (2)$$

with

TABLE I. Comparison of the *ab initio* calculated values with the fitted ones for three angular orientations of the uncorrected CH₄-CH₄ potential.

<i>R</i> (Å)	Orientation 1		Orientation 4		Orientation 7	
	<i>Ab initio</i> (K)	Fit (K)	<i>Ab initio</i> (K)	Fit (K)	<i>Ab initio</i> (K)	Fit (K)
2.50	7843.67	8155.60	241671.0	110921.0	24103.2	23773.1
2.75	2727.14	2777.63	69568.3	52120.1	10053.8	9950.3
3.00	678.222	676.192	26117.1	23585.0	3894.51	3859.28
3.25	-52.924	-58.840	10597.0	10231.9	1303.41	1295.01
3.50	-255.262	-257.529	4251.28	4199.35	283.565	284.407
3.75	-266.072	-265.580	1582.87	1576.32	-72.226	-69.808
4.00	-220.489	-218.941	490.780	490.181	-164.163	-162.625
4.25	-167.941	-166.389	73.446	72.894	-161.761	-161.270
4.50	-123.586	-122.429	-64.519	-65.862	-132.724	-132.806
4.75	-89.924	-89.205	-94.086	-95.981	-101.597	-101.843
5.00	-65.510	-65.108	-86.512	-88.474	-75.666	-75.886
5.50	-35.669	-35.580	-53.260	-54.510	-41.474	-41.552
6.00	-20.375	-20.332	-29.862	-30.441	-23.441	-23.467
6.50	-12.218	-12.152	-17.006	-17.278	-13.886	-13.910
7.00	-7.645	-7.570	-10.134	-10.273	-8.578	-8.638
8.00	-3.323	-3.276	-4.114	-4.169	-3.667	-3.725

$$V_{ij}(R_{ij}) = A_{ij} \exp(-\alpha_{ij}R_{ij}) - f_6(R_{ij}, b_{ij}) \frac{C_{6ij}}{R_{ij}^6} - f_8(R_{ij}, b_{ij}) \left(\frac{C_{8ij}}{R_{ij}^8} + \frac{q_i q_j}{R_{ij}} \right), \quad (3)$$

where R_{ij} is the distance between site i in molecule A and site j in molecule B. The damping functions f_6 and f_8 were introduced by Tang and Toennies,¹⁵

$$f_n(R_{ij}, b_{ij}) = 1 - \exp(-b_{ij}R_{ij}) \sum_{k=0}^n \frac{(b_{ij}R_{ij})^k}{k!}. \quad (4)$$

The charges q_i on the sites E were set to be zero, and the C and H charges were fitted to the octupole moment of the methane monomer calculated at the all-electron CCSD(T)/aug-cc-pV5Z level ($\Omega_{xyz}=2.7231$ a.u. in the standard orientation), with the sum of all charges being zero.

Fitting constraints concerning the dispersion coefficients were also applied. At large center of mass distances R the site-site potential model gives isotropic dispersion interactions. This isotropy is consistent with the real long-range behavior of two uncharged tetrahedral molecules, where the interaction term with the slowest decay is the isotropic C_6R^{-6} term.¹⁶ Within the site-site potential model, the coefficient itself is given as $C_6 = \sum_{i=1}^9 \sum_{j=1}^9 C_{6ij}$ and was fixed to the value derived from supermolecular CCSD(T)/aug-cc-pVTZ calculations at asymptotic separations. These calculations were performed for distances between 20 and 30 Å for the angular orientation 7 in Fig. 1. The values of $V(R)R^6$ were calculated for each separation and then extrapolated to $R \rightarrow \infty$ resulting in $C_6^{\text{sm}} = 853\,300 \text{ K Å}^6$. This value is nearly independent of the basis set size and changes by less than 0.1% from aug-cc-pVDZ to aug-cc-pVTZ. A further constraint in the fitting process was that the isotropic part of the C_8 coefficient

resulting from the site-site potential model as $C_{8,\text{iso}} = \sum_{i=1}^9 \sum_{j=1}^9 C_{8ij}$ should be equal to the value calculated by Fowler *et al.*¹⁶ to be $C_{8,\text{iso}} = 8\,137\,743 \text{ K Å}^8$.

The relative fitting errors are smaller than 2% for most calculated points on the PES. Significantly larger errors occur only at distances, where the potential goes through zero and in the highly repulsive region. The resulting analytical potential function has a maximum well depth of 273.9 K at $R = 3.633 \text{ Å}$ for angular orientation 1 in Fig. 1. Table I shows the fitted potential curves and the respective *ab initio* data for three angular orientations.

To derive a correction for zero-point vibrational effects, the C_6 coefficient resulting from the supermolecular calculations $C_6^{\text{sm}} = 853\,300 \text{ K Å}^6$ was compared with the value inferred from spectral data by Thomas and Meath¹⁷ as $C_6^{\text{exp}} = 898\,647 \text{ K Å}^6$, which includes zero-point vibrational effects. The difference between these two values is denoted as $\Delta C_6 = C_6^{\text{exp}} - C_6^{\text{sm}}$. Assuming that the relative effect of the zero-point vibrations would be similar for the isotropic part of C_8 , an estimation of $\Delta C_{8,\text{iso}}$ follows from

$$\Delta C_{8,\text{iso}} = C_{8,\text{iso}} \frac{\Delta C_6}{C_6^{\text{sm}}}. \quad (5)$$

The corrected potential is then given as the sum of the uncorrected potential and an isotropic correction term,

$$V_{\text{corr}}(R, \vartheta_A, \vartheta_B, \psi_A, \psi_B, \varphi_A - \varphi_B) = V_{\text{uncorr}}(R, \vartheta_A, \vartheta_B, \psi_A, \psi_B, \varphi_A - \varphi_B) + \Delta V_{\text{corr}}(R) \quad (6)$$

with

$$\Delta V_{\text{corr}}(R) = -f_6(R, b_{\text{corr}}) \frac{\Delta C_6}{R^6} - f_8(R, b_{\text{corr}}) \frac{\Delta C_{8,\text{iso}}}{R^8}. \quad (7)$$

Here, the parameter b_{corr} is still adjustable and was chosen so that the second pressure virial coefficient at room temperature computed with the corrected potential agrees well with

TABLE II. Potential parameters. The number in parenthesis is the power of 10.

	A (K)	α (\AA^{-1})	b (\AA^{-1})	C_6 (K \AA^6)	C_8 (K \AA^8)
C-C	0.262 373 610(7)	0.168 784 21(1)	0.168 275 675(1)	0.112 317 356(7)	-0.120 939 119(9)
C-H	0.265 413 949(7)	0.288 272 19(1)	0.288 261 054(1)	-0.139 633 537(7)	0.385 078 060(8)
H-H	0.241 399 203(6)	0.359 175 61(1)	0.384 703 188(1)	0.294 147 230(6)	-0.264 781 786(7)
C-E	-0.271 732 286(6)	0.164 907 47(1)	0.155 011 960(1)	0.127 844 394(7)	0.174 762 764(7)
H-E	-0.749 715 218(5)	0.205 930 86(1)	0.266 424 603(1)	0.169 329 268(6)	-0.810 401 688(7)
E-E	0.123 654 939(6)	0.214 516 41(1)	0.304 993 944(1)	-0.590 727 146(6)	0.679 543 866(7)
ΔC_6	0.45347(5) K \AA^6				
$\Delta C_{8,\text{iso}}$	0.432463(6) K \AA^8				
b_{corr}	0.177(1) \AA^{-1}				
q_{H}	0.94753(2) (K \AA) ^{1/2}				
q_{C}	-0.379012(3) (K \AA) ^{1/2}				

the most accurate experimental data (see Sec. IV). The correction increases the maximum well depth to 286.0 K at 3.624 \AA associated with orientation 1. The parameters of the corrected intermolecular potential hypersurface are given in Table II, whereas V_{corr} is shown in Fig. 2 as a function of the center of mass separation R for eight of the chosen angular orientations. The minimum well depth of only 99.8 K at 4.776 \AA is represented by orientation 4 in Fig. 2, which distinctly illustrates the anisotropy of the potential, but also the “hard-sphere” size of the interaction.

All *ab initio* calculations were performed with the Mainz–Austin–Budapest version of ACES II (Ref. 18) and with GAUSSIAN 03.¹⁹

III. QUANTUM-MECHANICAL CALCULATION OF THE SECOND PRESSURE VIRIAL COEFFICIENT

The second pressure virial coefficients $B(T)$ can be very accurately measured, particularly around room temperature. Hence, such data provide a valuable test for the intermolecular pair potential of the molecules when compared with values computed using statistical mechanics. Such calculations cannot be performed reliably classically when the temperatures are low and when atoms or molecules with small

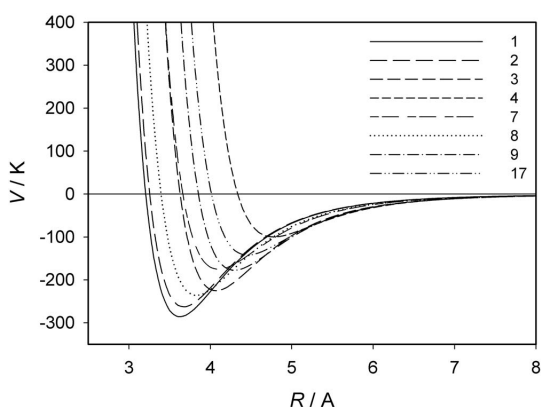


FIG. 2. The corrected intermolecular potential V as a function of the mass separation R for eight angular orientations (numbering according to Fig. 1).

masses or small moments of inertia are considered. At very low temperatures and for light spherically symmetric atoms a fully quantum mechanical treatment of the elastic scattering using phase shifts and including quantum statistical effects is needed, whereas the treatment of nonspherical systems requires the solution of the coupled-channel scattering problem.^{20,21}

In this paper, two alternative ways were used to calculate the second virial coefficient of methane as a function of temperature T . In the first variant it is assumed that a sufficiently accurate calculation of the second virial coefficients should be possible by adding quantum corrections, significant in the Boltzmann limit, to the classical contribution. Pack²¹ derived an expression for the first quantum correction to the second virial coefficient, valid for the interaction of like and unlike rigid-rotor molecules, such as diatomics, spherical tops, and symmetric tops, but excluding asymmetric tops. Using angular momentum theory, Wormer²² recently developed a formalism, correct at the level of the first-order quantum correction, for the second virial coefficient of a gas consisting of identical interacting rigid-rotor molecules of any symmetry, including asymmetric tops. Based on these papers, explicit formulae for the first quantum corrections are given here for the computation of the second virial coefficient of rigid asymmetric top molecules. Then, they are applied to methane treated as rigid spherical tops under the assumption that vibrations are negligibly excited.

The second virial coefficient $B(T)$ is related to the one-particle and two-particle partition functions Q_1 and Q_2 according to²³

$$B(T) = -\frac{N_A V}{2} \left[\frac{2Q_2(T) - Q_1^2(T)}{Q_1^2(T)} \right]. \quad (8)$$

Here, N_A is Avogadro's number and V is the volume. The classical contribution to $B(T)$ for a gas consisting of interacting asymmetric top molecules A and B is given as

$$B_{\text{cl}}(T) = -\frac{N_A}{128V\pi^4} \int \dots \int [e^{-\beta V(\mathbf{R}_A, \Omega_A; \mathbf{R}_B, \Omega_B)} - 1] \times d\mathbf{R}_A d\Omega_A d\mathbf{R}_B d\Omega_B, \quad (9)$$

where

$$\beta = 1/(k_B T), \quad d\mathbf{R}_i = R_i^2 dR_i \sin \theta d\theta d\phi, \quad (10)$$

$$d\Omega_i = \sin \vartheta_i d\vartheta_i d\varphi_i d\psi_i. \quad (11)$$

$V(\mathbf{R}_A, \Omega_A; \mathbf{R}_B, \Omega_B)$ is the intermolecular pair potential and k_B is Boltzmann's constant. \mathbf{R}_i locates the center of mass of molecule i in a space-fixed coordinate system, whereas Ω_i are the rotational coordinates. θ and ϕ are the polar angles, whereas φ_i , ϑ_i , and ψ_i are the Eulerian angles.

After transformation to the center of mass of the molecule pair and to relative coordinates

$$\mathbf{R} = \mathbf{R}_B - \mathbf{R}_A, \quad (12)$$

$$V(\mathbf{R}_A, \Omega_A; \mathbf{R}_B, \Omega_B) = V(\mathbf{R}, \Omega_A, \Omega_B), \quad (13)$$

the classical contribution is

$$B_{cl}(T) = -\frac{N_A}{128\pi^4} \int \cdots \int [e^{-\beta V(\mathbf{R}, \Omega_A, \Omega_B)} - 1] \times d\mathbf{R} d\Omega_A d\Omega_B. \quad (14)$$

The computation of $B_{cl}(T)$ can be performed under the assumption that molecule A is fixed in the space-fixed coordinate system and that the integration over the Eulerian angles of molecule A leads to

$$B_{cl}(T) = -\frac{N_A}{16\pi^2} \int_0^{2\pi} \int_0^{2\pi} \int_0^\pi \int_0^{2\pi} \int_0^\pi \int_0^\infty \times [e^{-\beta V(R, \theta, \phi, \vartheta_B, \psi_B, \varphi_B)} - 1] \times R^2 dR \sin \theta d\theta d\phi \sin \vartheta_B d\vartheta_B d\psi_B d\varphi_B. \quad (15)$$

Here, molecule B moves around molecule A (integration over R , θ , and ϕ) and rotates about its axes (integration over ϑ_B , ψ_B , and φ_B).

After transforming again to center of mass-relative coordinates and using the fact that the derivatives of the intermolecular pair potential $V(\mathbf{R}, \Omega_A, \Omega_B)$ vanish with respect to the center of mass coordinates, the first-order quantum correction to the second virial coefficient can be formulated as

$$B_{qm}^{(1)}(T) = -\frac{N_A}{128\pi^4} \int \cdots \int e^{-\beta V} \frac{\beta^2}{12} \hat{H}^0 V d\mathbf{R} d\Omega_A d\Omega_B, \quad (16)$$

$$\hat{H}^0 = \hat{H}_{tr, \mu} + \hat{H}_{rot, A} + \hat{H}_{rot, B}. \quad (17)$$

\hat{H}^0 is the translation-rotation Hamiltonian operator in which the translational part $\hat{H}_{tr, \mu}$ is that for the hypothetical particle with the reduced mass μ of the pair of molecules and is given as

$$\hat{H}_{tr, \mu} = -\frac{\hbar^2}{2\mu} \nabla_{tr, \mu} \nabla_{tr, \mu}. \quad (18)$$

The rotational part of the Hamiltonian operator $\hat{H}_{rot, i}$ of a molecule i can be written as

$$\hat{H}_{rot, i} = -\frac{\hbar^2}{2} \nabla_{rot, i} \nabla_{rot, i}. \quad (19)$$

The computation of $B_{qm}^{(1)}(T)$ is again carried out under the assumption that molecule A is fixed in the space-fixed coordinate system and that the integration over the Eulerian angles of molecule A can be performed analytically,

$$B_{qm}^{(1)}(T) = -\frac{N_A \beta^2}{16\pi^2 12} \int \cdots \int e^{-\beta V} \times (\hat{H}_{tr, \mu} + \hat{H}_{rot, A} + \hat{H}_{rot, B}) V d\mathbf{R} d\Omega_B. \quad (20)$$

It is convenient to take into account that upon integration by parts generally for any coordinates \mathbf{x}_1 and \mathbf{x}_2

$$\int e^{-\beta V} \nabla_i \nabla_j \beta V d\mathbf{x}_1 d\mathbf{x}_2 = \int e^{-\beta V} (\nabla_i \beta V)^2 d\mathbf{x}_1 d\mathbf{x}_2. \quad (21)$$

The translational part of the first-order quantum correction to the second virial coefficient related to identical molecules with the molecular mass m and the reduced mass $\mu = m/2$ is

$$B_{tr}^{(1)}(T) = \frac{N_A \hbar^2 \beta}{16\pi^2 24\mu} \int_0^{2\pi} \int_0^{2\pi} \int_0^\pi \int_0^{2\pi} \int_0^\pi \int_0^\infty \times e^{-\beta V} [\nabla_{tr, \mu} \beta V]^2 R^2 \times dR \sin \theta d\theta d\phi \sin \vartheta_B d\vartheta_B d\psi_B d\varphi_B, \quad (22)$$

with

$$(\nabla_{tr, \mu} \beta V)^2 = \left(\frac{\partial \beta V}{\partial R} \right)^2 + \frac{1}{R^2} \left(\frac{\partial \beta V}{\partial \theta} \right)^2 + \frac{1}{R^2 \sin^2 \theta} \left(\frac{\partial \beta V}{\partial \phi} \right)^2. \quad (23)$$

The rotational part of the first-order quantum correction to the second virial coefficient for two identical asymmetric top molecules with $\hat{H}_{rot, A} = \hat{H}_{rot, B}$ can be formulated as

$$B_{rot}^{(1)}(T) = \frac{N_A \hbar^2 \beta}{16\pi^2 12} \int \cdots \int e^{-\beta V} [\nabla_{rot, B} \beta V]^2 d\mathbf{R} d\Omega_B, \quad (24)$$

$$= \frac{N_A \hbar^2 \beta}{16\pi^2 12} \int_0^{2\pi} \int_0^{2\pi} \int_0^\pi \int_0^{2\pi} \int_0^\pi \int_0^\infty \times e^{-\beta V} \left(\frac{J_{x, B}^2}{I_{x, B}} + \frac{J_{y, B}^2}{I_{y, B}} + \frac{J_{z, B}^2}{I_{z, B}} \right) \times R^2 dR \sin \theta d\theta d\phi \sin \vartheta_B d\vartheta_B d\psi_B d\varphi_B. \quad (25)$$

$$J_{x, B} = \sin \psi_B \left(\frac{\partial \beta V}{\partial \vartheta_B} \right) - \frac{\cos \psi_B}{\sin \vartheta_B} \left(\frac{\partial \beta V}{\partial \varphi_B} \right) + \frac{\cos \psi_B \cos \vartheta_B}{\sin \vartheta_B} \left(\frac{\partial \beta V}{\partial \psi_B} \right), \quad (26)$$

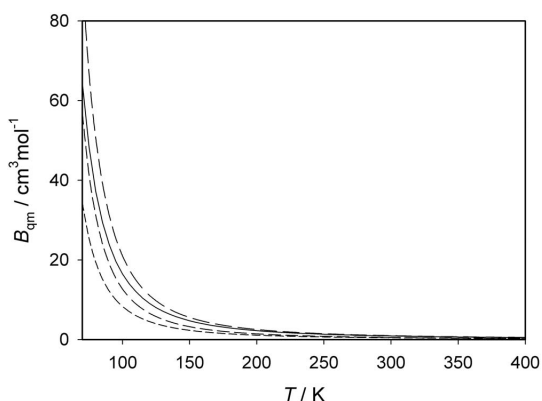


FIG. 4. Quantum corrections B_{qm} calculated for the new corrected intermolecular potential energy surface for CH_4 as a function of temperature: - - - translational part of the first-order quantum correction $B_{tr}^{(1)}$, - · - · rotational part of the first-order quantum correction for spherical-top molecules $B_{rot,sph\text{top}}^{(1)}$, — — — sum of the translational and rotational parts of the first-order quantum correction for spherical-top molecules $B_{tr}^{(1)} + B_{rot,sph\text{top}}^{(1)}$, and - - - quantum correction according to the approximated path-integration method calculated as difference $B_{qm} = B_{\text{path}} - B_{cl}$.

$B_{tr}^{(1)} + B_{rot,sph\text{top}}^{(1)}$. This is in agreement with the experience that the second-order quantum correction for monatomic gases is negative.³¹

The comparison with experimental second virial coefficients, shown as deviations ($B_{\text{exp}} - B_{\text{cal}}$) in Fig. 5, is restricted to the best available data. The comparison of experimental second virial coefficients with the values calculated theoret-

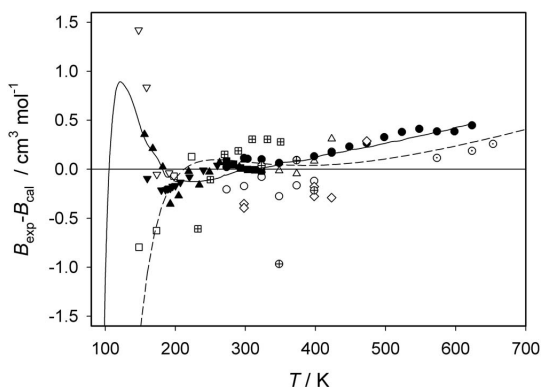


FIG. 5. Deviations of experimental and experimentally based second pressure virial coefficients from values calculated with the new corrected intermolecular potential energy surface using the path-integration method for CH_4 in a large temperature range. Experimental data: ● Douslin and Harrison (Ref. 32), ▲ Roe (Ref. 33), ■ Kleinrahn *et al.* (Ref. 30), ▼ Händel *et al.* (Ref. 34), ○ Michels and Nederbragt (Ref. 35), reevaluated by Pompe and Spurling (Ref. 36), △ Schamp, Jr. *et al.* (Ref. 37), □ Brewer (Ref. 38) (one additional value with $\Delta B = -2.64 \text{ cm}^3 \text{ mol}^{-1}$ at 123 K), ▽ Pope *et al.* (Ref. 39) (two additional values with $\Delta B = +6.14$ and $+1.96 \text{ cm}^3 \text{ mol}^{-1}$ at 127 and 137 K), ◇ Katayama *et al.* (Ref. 40), Ohgaki *et al.* (Refs. 41 and 42), ⊕ Mallu and Viswanath (Ref. 43), ⊙ Abdulgatov *et al.* (Ref. 44), and ⊞ Esper *et al.* (Ref. 45). Experimentally based data: — values from the equation of state by Wagner and de Reuck (Ref. 29) and - - - values calculated by means of an isotropic potential (fitted to experimental data) by Zarkova *et al.* (Ref. 46).

cally depends on density measurements. These must be determined from pressure and volume measurements using an EOS which employs higher virial coefficients. These coefficients are in turn dependent on the second virial coefficient of interest. In our comparison only second virial coefficients are considered so that we rely on the assessment by Wagner and de Reuck.²⁹ However, unlike Wagner and de Reuck, who assigned some second pressure virial coefficients determined from speed of sound measurements via acoustic second virial coefficients^{47,48} to their group 1 data, we did not consider them as proper primary data of highest accuracy. Hence only the data by Esper *et al.*,⁴⁵ derived from acoustic second virial coefficients, were included in the comparison, but not classified as group 1 data.

The remaining group 1 data are characterized in Fig. 5 by filled symbols and are discussed first. After adjusting the parameter b_{corr} at room temperature, the values calculated for the new intermolecular potential of methane are in excellent agreement within $\pm 0.08 \text{ cm}^3 \text{ mol}^{-1}$ in the full temperature range from 273 to 323 K with the experimental data by Kleinrahn *et al.*,³⁰ determined with an absolute uncertainty of $\pm 0.15 \text{ cm}^3 \text{ mol}^{-1}$ using the two-sinker method based on the buoyancy principle. The figure makes evident that the calculated values are also consistent in the complete temperature range of 160–260 K with the results of experiments, performed by Händel *et al.*³⁴ applying the two-sinker method with an absolute uncertainty of $\pm 0.3 \text{ cm}^3 \text{ mol}^{-1}$. The analogous statement is valid for the Burnett-method measurements carried out and evaluated by Roe³³ to gain second pressure virial coefficients. The calculated values perfectly agree again within the claimed uncertainty of $\pm 0.6 \text{ cm}^3 \text{ mol}^{-1}$ at 156 K to $\pm 0.1 \text{ cm}^3 \text{ mol}^{-1}$ at 291 K. Whereas these low-temperature data show random scatter around the calculated values, the high-temperature data by Douslin *et al.*³² between 273 and 623 K with an uncertainty of $\pm 0.2 \text{ cm}^3 \text{ mol}^{-1}$, derived from isochoric compressibility measurements, systematically differ by up to $+0.5 \text{ cm}^3 \text{ mol}^{-1}$ from the calculated values.

These calculations cast some doubt on the reliability of the second virial coefficients obtained by Wagner and de Reuck²⁹ from their optimization process for the equation of state of methane. Since the data by Händel *et al.*³⁴ were not used in generating the EOS, they systematically deviate by up to $-0.4 \text{ cm}^3 \text{ mol}^{-1}$ from the equation according to figure 1.17 of Ref. 29. On the contrary, the data of Douslin *et al.*³² show virtually no differences to the EOS, because they were used to determine the equation. This also becomes obvious from our Fig. 5, in which the second virial coefficients corresponding to the EOS of methane are presented as a solid curve. The differences of our calculated values from this curve at higher temperatures could possibly originate from a deficient consideration of the vibrational modes of motion. On the other hand, the measurements by Douslin *et al.* could possibly be influenced by small systematic errors.

The other experimental second virial coefficients included in the comparison in Fig. 5 partly deviate in a systematic manner from the curve connected with the EOS, but also from the basic line corresponding to the values theoretically calculated for the new intermolecular potential. This is

TABLE III. Second pressure virial coefficients of methane for the new intermolecular potential.

T (K)	B_{path} ($\text{cm}^3 \text{mol}^{-1}$)	B_{cl} ($\text{cm}^3 \text{mol}^{-1}$)	T (K)	B_{path} ($\text{cm}^3 \text{mol}^{-1}$)	B_{cl} ($\text{cm}^3 \text{mol}^{-1}$)	T (K)	B_{path} ($\text{cm}^3 \text{mol}^{-1}$)	B_{cl} ($\text{cm}^3 \text{mol}^{-1}$)
70.00	-847.10	-911.46	220.00	-86.22	-88.02	470.00	-4.81	-5.19
75.00	-720.69	-768.93	230.00	-78.59	-80.21	480.00	-3.56	-3.92
80.00	-623.43	-660.69	240.00	-71.75	-73.22	490.00	-2.37	-2.72
85.00	-546.64	-576.15	250.00	-65.59	-66.94	500.00	-1.23	-1.57
90.00	-484.69	-508.56	260.00	-60.02	-61.25	510.00	-0.15	0.48
95.00	-433.79	-453.45	270.00	-54.95	-56.09	520.00	0.88	0.57
100.00	-391.31	-407.76	273.15	-53.45	-54.56	530.00	1.87	1.56
105.00	-355.37	-369.32	280.00	-50.33	-51.38	540.00	2.82	2.52
110.00	-324.61	-336.59	290.00	-46.09	-47.07	550.00	3.72	3.43
115.00	-298.02	-308.40	293.15	-44.83	-45.79	560.00	4.59	4.31
120.00	-274.81	-283.90	298.15	-42.90	-43.82	570.00	5.42	5.15
125.00	-254.39	-262.42	300.00	-42.20	-43.11	580.00	6.22	5.95
130.00	-236.31	-243.44	310.00	-38.61	-39.46	590.00	6.98	6.73
135.00	-220.18	-226.57	320.00	-35.29	-36.08	600.00	7.72	7.47
140.00	-205.71	-211.46	330.00	-32.21	-32.96	610.00	8.42	8.18
145.00	-192.67	-197.88	340.00	-29.34	-30.05	620.00	9.10	8.87
150.00	-180.85	-185.59	350.00	-26.67	-27.34	650.00	11.00	10.78
155.00	-170.10	-174.43	360.00	-24.18	-24.81	700.00	13.73	13.53
160.00	-160.27	-164.25	370.00	-21.85	-22.45	750.00	16.03	15.86
165.00	-151.26	-154.93	380.00	-19.66	-20.23	800.00	17.99	17.83
170.00	-142.97	-146.36	390.00	-17.61	-18.15	850.00	19.67	19.53
175.00	-135.32	-138.46	400.00	-15.67	-16.19	900.00	21.13	21.00
180.00	-128.24	-131.16	410.00	-13.85	-14.34	950.00	22.40	22.28
185.00	-121.66	-124.39	420.00	-12.13	-12.60	1000.00	23.51	23.41
190.00	-115.54	-118.09	430.00	-10.50	-10.95	1100.00	25.37	25.27
195.00	-109.83	-112.23	440.00	-8.97	-9.40	1200.00	26.83	26.75
200.00	-104.49	-106.74	450.00	-7.51	-7.92
210.00	-94.79	-96.80	460.00	-6.12	-6.52

particularly evident for the low-temperature data by Brewer³⁸ and Pope *et al.*,³⁹ each characterized by deviations distinctly larger than the claimed uncertainties of $\pm 1.3 \text{ cm}^3 \text{ mol}^{-1}$ at 123 K to $\pm 0.4 \text{ cm}^3 \text{ mol}^{-1}$ at 223 K for the data by Brewer and of $\pm 0.7 \text{ cm}^3 \text{ mol}^{-1}$ at 126 K to $\pm 0.2 \text{ cm}^3 \text{ mol}^{-1}$ at 191 K for the data by Pope *et al.* These measurements are not suitable to judge the quality of the new intermolecular potential surface of methane.

Figure 5 also shows a comparison with values recommended as reference data by Zarkova *et al.*⁴⁶ In the case of methane the basis for these values is an isotropic three-parameter Lennard-Jones- $(n-6)$ potential obtained from a multiproperty fit to experimental data for the second pressure and acoustic virial coefficients as well as for viscosity and self-diffusion at low density. It is to point out that the increasing deviations of the values by Zarkova *et al.* from our values toward lower temperature are due to the inclusion of low-temperature B data of Byrne *et al.*⁴⁹ into their fit. However, these data were assessed by Wagner and de Reuck only as group 3 data and hence not considered for the EOS. Further these data are characterized by increasing differences to our calculated values with the maximum of $-10.2 \text{ cm}^3 \text{ mol}^{-1}$ at 111 K.

Ultimately, we are convinced that the calculations of this paper are more reliable than the EOS for low temperatures down to 70 K, for which no experimental second virial coefficients of high accuracy were available below 150 K. If

we assume that vibrational excitations have only a negligible impact on the second virial coefficient we expect further that the computations for higher temperatures are also reliable. Values for the second pressure virial coefficient of methane recommended on the basis of the intermolecular potential of this work are given in Table III for the temperature range of 70–1200 K.

V. SUMMARY AND CONCLUSIONS

A new intermolecular potential energy surface for two rigid methane molecules was determined from quantum-mechanical *ab initio* calculations. Altogether 272 interaction energies on the PES were determined at the CCSD(T) level of theory. Utilizing large basis sets up to aug-cc-pVQZ, the interaction energies were extrapolated to the CBS limit. A highly accurate site-site potential function was fitted to the calculated interaction energies, and in addition a physically reasonable correction for zero-point vibrational effects was established by a single-parameter fit to the most accurate experimental value of the second pressure virial coefficient at room temperature. The resulting potential shows a high anisotropy. It is characterized by a significantly greater well depth, 286 K, than previous interaction potentials.

The quality of the new potential was tested by computing the second pressure virial coefficient. For this purpose, explicit formulae were derived to calculate quantum correc-

tions to the classical second virial coefficient in terms of Euler angle coordinates for rigid asymmetric tops, which includes methane as the special case of a spherical top. The agreement with the most accurate experimental data is very good over a wide range of temperatures. A main contribution of this paper consists in providing accurate values down to very low temperatures where experimental data of high quality are unavailable. In a series of forthcoming papers, the new potential will be employed for the calculation of transport and relaxation properties of dilute methane gas over a wide range of temperatures.

ACKNOWLEDGMENTS

The authors would like to acknowledge inspiring discussions with A. S. Dickinson (Newcastle University) and V. Vesovic (Imperial College London). This work was supported by the Deutsche Forschungsgemeinschaft (German Research Foundation) under Contract No. VO 499/14-1.

- ¹A. S. Dickinson, R. Hellmann, E. Bich, and E. Vogel, *Phys. Chem. Chem. Phys.* **9**, 2836 (2007).
- ²S. Tsuzuki, T. Uchimaru, and K. Tanabe, *Chem. Phys. Lett.* **287**, 202 (1998).
- ³R. L. Rowley and T. Pakkanen, *J. Chem. Phys.* **110**, 3368 (1999).
- ⁴T. H. Dunning, Jr., *J. Chem. Phys.* **90**, 1007 (1989).
- ⁵D. E. Woon and T. H. Dunning, Jr., *J. Chem. Phys.* **100**, 2975 (1994).
- ⁶S. Tsuzuki, K. Honda, T. Uchimaru, and M. Mikami, *J. Chem. Phys.* **124**, 114304 (2006).
- ⁷K. Raghavachari, G. W. Trucks, J. A. Pople, and M. Head-Gordon, *Chem. Phys. Lett.* **157**, 479 (1989).
- ⁸A. J. Russell and M. A. Spackman, *Mol. Phys.* **84**, 1239 (1995).
- ⁹D. M. Bishop, F. L. Gu, and S. M. Cybulski, *J. Chem. Phys.* **109**, 8407 (1998).
- ¹⁰M. Nakata and K. Kuchitsu, *J. Chem. Soc. Jpn.*, 1446 (1986).
- ¹¹J. F. Stanton, *Mol. Phys.* **97**, 841 (1999).
- ¹²T. J. Lee, J. M. L. Martin, and P. R. Taylor, *J. Chem. Phys.* **102**, 254 (1995).
- ¹³S. F. Boys and F. Bernardi, *Mol. Phys.* **19**, 553 (1970).
- ¹⁴A. Halkier, T. Helgaker, P. Jørgensen, W. Klopper, H. Koch, J. Olsen, and A. K. Wilson, *Chem. Phys. Lett.* **286**, 243 (1998).
- ¹⁵K. T. Tang and J. P. Toennies, *J. Chem. Phys.* **80**, 3726 (1984).
- ¹⁶P. W. Fowler, P. Lazzeretti, and R. Zanasi, *Mol. Phys.* **68**, 853 (1989).
- ¹⁷G. F. Thomas and W. J. Meath, *Mol. Phys.* **34**, 113 (1977).
- ¹⁸J. F. Stanton, J. Gauss, J. D. Watts, P. G. Szalay, and R. J. Bartlett, with contributions from A. A. Auer, D. B. Bernholdt, O. Christiansen, M. E. Harding, M. Heckert, O. Heun, C. Huber, D. Jonsson, J. Jusélius, W. J. Lauderdale, T. Metzroth, C. Michauk, D. R. Price, K. Ruud, F. Schiffmann, A. Tajti, M. E. Varner, J. Vázquez, and the following integral packages: MOLECULE (J. Almlöf and P. R. Taylor), PROPS (P. R. Taylor), and ABACUS (T. Helgaker, H. J. Aa. Jensen, P. Jørgensen, and J. Olsen). See also J. F. Stanton, J. Gauss, J. D. Watts, W. J. Lauderdale, and R. J. Bartlett, *Int. J. Quantum Chem., Symp.* **26**, 879 (1992). For current version, see <http://www.aces2.de>
- ¹⁹M. J. Frisch, G. W. Trucks, H. B. Schlegel *et al.*, GAUSSIAN 03, Revision D.01, Gaussian, Inc., Wallingford, CT, 2004.
- ²⁰L. Monchick, *Chem. Phys. Lett.* **24**, 91 (1974).
- ²¹R. T. Pack, *J. Chem. Phys.* **78**, 7217 (1983).
- ²²P. E. S. Wormer, *J. Chem. Phys.* **122**, 184301 (2005).
- ²³D. A. McQuarrie, *Statistical Mechanics* (Harper and Row, New York, 1976).
- ²⁴C. G. Gray and K. E. Gubbins, *Theory of Molecular Fluids, Volume I: Fundamentals* (Clarendon, Oxford, 1984).
- ²⁵G. K. Schenter, *J. Chem. Phys.* **117**, 6573 (2002).
- ²⁶R. P. Feynman and A. R. Hibbs, *Quantum Mechanics and Path Integrals* (McGraw-Hill, New York, 1965).
- ²⁷H. Kleinert, *Path Integrals in Quantum Mechanics Statistics and Polymer Physics* (World Scientific, New Jersey, 1995).
- ²⁸M. Takahashi and M. Imada, *J. Phys. Soc. Jpn.* **53**, 3765 (1984).
- ²⁹W. Wagner and K. M. de Reuck, *Methane. International Thermodynamic Tables of the Fluid State-13*, International Union of Pure and Applied Chemistry (Blackwell, Oxford, 1996).
- ³⁰R. Kleinrahm, W. Duschek, W. Wagner, and M. Jaeschke, *J. Chem. Thermodyn.* **20**, 621 (1988).
- ³¹E. Bich, R. Hellmann, and E. Vogel, "Ab initio potential energy curve for the neon atom pair and thermophysical properties for the dilute neon gas. II. Thermophysical properties for low-density neon." *Mol. Phys.* (in press).
- ³²D. R. Douslin, R. H. Harrison, R. T. Moore, and J. P. McCullough, *J. Chem. Eng. Data* **9**, 358 (1964).
- ³³D. R. Roe, *Thermodynamic Properties of Gases and Gas Mixtures at Low Temperatures and High Pressures*, Ph.D. Thesis, University of London, 1972.
- ³⁴G. Händel, R. Kleinrahm, and W. Wagner, *J. Chem. Thermodyn.* **24**, 685 (1992).
- ³⁵A. Michels and G. W. Nederbragt, *Physica (Amsterdam)* **3**, 569 (1936).
- ³⁶A. Pompe and T. H. Spurling, "Virial Coefficients for Gaseous Hydrocarbons," CSIRO Australia Div. Appl. Organic Chem. Tech. Paper No. 1, (1974).
- ³⁷H. W. Schamp, Jr., E. A. Mason, A. C. B. Richardson, and A. Altman, *Phys. Fluids* **1**, 329 (1958).
- ³⁸J. Brewer, "Determination of Mixed Virial Coefficients," U.S. Clearinghouse Fed. Sci. Tech. Information No. AD 663448, 1967.
- ³⁹G. A. Pope, P. S. Chappellear, and R. Kobayashi, *J. Chem. Phys.* **59**, 423 (1973).
- ⁴⁰T. Katayama, K. Ohgaki, and H. Ohmori, *J. Chem. Eng. Jpn.* **13**, 257 (1980).
- ⁴¹K. Ohgaki, Y. Nakamura, H. Ariyasu, and T. Katayama, *J. Chem. Eng. Jpn.* **15**, 85 (1982).
- ⁴²K. Ohgaki, N. Sakai, Y. Kano, and T. Katayama, *J. Chem. Eng. Jpn.* **17**, 545 (1984).
- ⁴³B. V. Mallu and D. S. Viswanath, *J. Chem. Thermodyn.* **22**, 997 (1990).
- ⁴⁴I. M. Abdulagatov, A. R. Bazaev, and A. E. Ramazanova, *J. Chem. Thermodyn.* **25**, 249 (1993).
- ⁴⁵G. Esper, W. Lemming, W. Beckermann, and F. Kohler, *Fluid Phase Equilib.* **105**, 173 (1995).
- ⁴⁶L. Zarkova, U. Hohm, and M. Damyanova, *J. Phys. Chem. Ref. Data* **35**, 1331 (2006).
- ⁴⁷W. Lemming, *Fortschr.-Ber. VDI, Reihe 6* **19**, Nr. 32 (1989) (in German).
- ⁴⁸W. Beckermann, *Fortschr.-Ber. VDI, Reihe 6* **19**, Nr. 67 (1993) (in German).
- ⁴⁹M. A. Byrne, M. R. Jones, and L. A. K. Staveley, *Trans. Faraday Soc.* **64**, 1747 (1968).

4.4 Transport properties of asymmetric-top molecules

Alan S. Dickinson, Robert Hellmann, Eckard Bich, Eckhard Vogel

Phys. Chem. Chem. Phys. **9**, 2836-2843 (2007).

<http://www.rsc.org/ej/CP/2007/b618549e.pdf>

Der theoretische Formalismus wurde gemeinsam mit Prof. A. S. Dickinson abgeleitet. Die Erweiterung des Programmcodes TRAJECT [59] wurde im Wesentlichen selbst durchgeführt. Der eigene Anteil beträgt etwa 45%.

Reproduced by permission of the PCCP Owner Societies.

Transport properties of asymmetric-top molecules

A. S. Dickinson,^{*a} R. Hellmann,^b E. Bich^b and E. Vogel^b

Received 19th December 2006, Accepted 9th March 2007

First published as an Advance Article on the web 13th April 2007

DOI: 10.1039/b618549e

Kinetic theory of gases is extended from linear molecules to asymmetric tops. The integration over the velocity of the centre of mass is carried out explicitly and the results are expressed in a form suitable for classical evaluation. These results can also be employed for spherical and symmetric tops.

1. Introduction

Dilute-gas transport properties, such as the shear viscosity and the thermal conductivity, are of great interest, particularly as absolute values can be measured in favourable cases with an uncertainty less than $\pm(0.1-0.2)\%$ and $\pm(0.3-0.5)\%$, respectively.¹ The kinetic theory of dilute gases allows the calculation of these and other transport and relaxation properties from a set of effective cross sections, known as Omega integrals for atomic gases. These cross sections can be determined from a given intermolecular potential energy hypersurface and the quality of the surface can be tested by comparison with measurements of the transport properties calculated employing it. Typically, the best measurements are made at room temperature but, depending on the molecule of interest, results may be available over a wide range of temperatures, albeit with varying accuracy. Kinetic theory can also be used to predict the transport properties at temperatures outside the working range of most instruments, especially at high temperatures.

The kinetic theory of dilute monatomic gases has been very successfully applied to calculate reference values for the transport properties of helium to be used for the calibration of measuring instruments. Prerequisites for such a calibration are that the kinetic theory for monatomic gases requires only minimal approximations to be implemented practically, and that a highly precise interatomic potential has been determined.²

For linear molecules Curtiss³ has provided the necessary kinetic theory in a form amenable to numerical evaluation. Using this, calculations have been performed for nitrogen,^{4,5} carbon monoxide,^{6,7} and carbon dioxide.⁸⁻¹⁰ These calculations were based on a classical description of the two-molecule scattering process with rigid monomers and resulted in the successful evaluation of a number of transport properties and of magnetic-field effects on these properties, as well as of relaxation properties. All three molecules are relatively rigid due to their double or triple bonds and have sufficiently large masses and moments of inertia that a classical description with rigid molecules is justified for most of the transport and

relaxation properties. However, in order to describe adequately the thermal conductivity and thermo-magnetic effects, vibrational modes of motion have had to be taken into account by a physically reasonable correction.^{9,11} Since the thermomagnetic, viscomagnetic and relaxation properties vanish for a spherically symmetric potential, these properties are direct indicators of the anisotropy of the potential surfaces.

Extending kinetic theory to rigid molecules of arbitrary structure, asymmetric tops, and implementing it in a computer code using a similar classical rigid-molecule scattering description, is the next evolutionary step in this development. The present paper is concerned with deriving the necessary expressions. This development will allow the calculation, for the first time, of the transport and relaxation properties of molecules such as dilute gas-phase water, using different intermolecular potential hypersurfaces reported in the literature, *e.g.* ref. 12 and 13. Furthermore, since symmetric tops and spherical tops can be considered as special cases of asymmetric tops, this development will allow transport and relaxation properties of important molecules such as benzene, methane and sulfur hexafluoride to be calculated. However, molecules such as ethane and ammonia, which are not completely rigid, may still present additional problems, due to internal rotation for the former and “umbrella” inversion for the latter.

2. Theory

2.1 Boltzmann equation

Dilute gas transport theory is based on solving the linearised Boltzmann equation for the relevant perturbation.¹⁴ The classical Boltzmann equation for linear molecules was derived by Curtiss¹⁵ and later extended by him to non-reacting molecules of arbitrary structure.¹⁶ However, while he provided a detailed description of the calculation of effective cross sections for linear molecules,³ no such description is available for asymmetric tops.

For the classical coordinates for the asymmetric top of interest here we employ J , K , M , q_J , q_K , q_M , where J is the magnitude of the angular momentum vector, \mathbf{J} , of the top, K and M are its projections on the body-fixed and space-fixed z axes, respectively, and q_J , q_K and q_M are the corresponding conjugate angle variables. A useful figure illustrating these angles can be found in ref. 17 or in ref. 18. (Note that these coordinates for an asymmetric top are identical to those for a

^a School of Natural Sciences, Newcastle University, Newcastle upon Tyne, UK NE1 7RU. E-mail: A.S.Dickinson@ncl.ac.uk

^b Institut für Chemie, Universität Rostock, D-18059 Rostock, Germany

symmetric top.) For free motion of the top J , M and q_M are constant. For the special case of a symmetric top, K is also constant and q_J and q_K increase linearly with time, while for a spherical top q_K is also constant.

We assume that for an asymmetric-top molecule the distribution function, f_a , depends on K and q_K only implicitly through the internal energy of the top, given by^{19,20}

$$E_a(J, K, q_K) = J^2 \left(\frac{\cos^2 q_K}{2I_x^a} + \frac{\sin^2 q_K}{2I_y^a} \right) + K^2 \left(\frac{1}{2I_z^a} - \frac{\cos^2 q_K}{2I_x^a} - \frac{\sin^2 q_K}{2I_y^a} \right), \quad (2.1)$$

where I_x^a , I_y^a and I_z^a are the principal moments of inertia ($I_z^a \geq I_y^a \geq I_x^a$). Here we are following Liu *et al.*¹⁷ and Yang *et al.*¹⁸ in using the “y-convention” of Goldstein *et al.*²¹ for the definition of the conventional Euler angles used to define the orientation of the top. This choice leads to the interchange of $\sin q_K$ and $\cos q_K$ in the expression of Augustin and Miller¹⁹ for the energy of the top, our eqn (2.1). For a symmetric top we take $I_x^a = I_y^a$, regardless of the relative size of I_z^a .

Ideally, as well as this implicit dependence on K and q_K , an explicit dependence would also be introduced. This would complicate the development significantly, requiring two additional indices in the basis functions used to represent the distribution function. In turn, four additional indices would be required for the effective cross sections. Hence inclusion of this K and q_K dependence is deferred until there is clear experimental evidence that inclusion is required and we solve for the distribution function averaged over K and q_K . Such averaging is equivalent to taking the lowest term in a more general expansion of f_a which allows for the explicit dependence on K and q_K . However, the K dependence might be relevant for studying electric-field effects on transport properties, since, in general, the energy of an asymmetric top in an electric field depends on the value of K .

As for a linear molecule, we assume also that f_a is independent of q_J and of \mathbf{R} , the position of the molecule centre of mass.

The Boltzmann equation for the distribution function for an asymmetric top, species a , in collision with an asymmetric top, species b , is¹⁶

$$\begin{aligned} & \left(\frac{\partial}{\partial t} + \frac{1}{m_a} \mathbf{P}^a \cdot \nabla_a \right) f_a(\mathbf{P}_a, E_a, \cos \theta_{M_a}, q_{M_a}) \\ &= \frac{1}{8\pi^2} \int (f_a' f_b' - f_a f_b) g b \, d\phi_b \, d\mathbf{P}_b \, J_b^2 \, dJ_b \, d(\cos \theta_{K_b}) \\ & \times \, dq_{J_b} \, dq_{K_b} \, dq_{M_b} \, dq_{J_a} \, d(\cos \theta_{K_a}) \, dq_{K_a}, \end{aligned} \quad (2.2)$$

where m_a and \mathbf{P}_a are the molecular mass and momentum of species a , respectively and generally subscripts a and b denote properties of species a and b , respectively. Here \mathbf{g} and \mathbf{b} are the relative velocity and impact-parameter vectors, respectively, ϕ_b is the azimuthal angle of \mathbf{b} about \mathbf{g} , $\cos \theta_{M_a} = M_a/J_a$ and the right-hand side has been averaged over the variables q_J , K_a and q_{K_a} , extending the averaging over q_{J_a} used by Curtiss¹⁵ for the linear-molecule case. For convenience, the average over K_a

is replaced by an average over θ_{K_a} , the angle between J_a and the body-fixed z axis, and similarly for the integral over K_b . We assume no ambiguity results from the use of b to denote both the impact parameter and a species label.

The zero-order equilibrium solution for the distribution function is

$$f_a^{(0)}[P_a, E_a(J_a, K_a, q_{K_a}), T] = \frac{n_a}{(2\pi m_a k_B T)^{3/2} Z_a} \times \exp\left(-\frac{P_a^2}{2m_a k_B T} - \frac{E_a}{k_B T}\right), \quad (2.3)$$

where T is the temperature, n_a is the number of molecules of species a , $Z_a = (2\pi k_B T)^{3/2} (I_x^a I_y^a I_z^a)^{1/2}$ is proportional to the classical internal state partition function and k_B is Boltzmann's constant.

The normalization is

$$\int f_a^{(0)}[P_a, E_a(J, K, q_K), T] \, d\mathbf{P}_a \, dJ \, dM \, dq_M \, \frac{dK}{2} \, \frac{dq_K}{2\pi} = n_a. \quad (2.4)$$

To verify the normalization we note that

$$\begin{aligned} & \int_0^\infty dJ \int_{-J}^J dM \int_{-J}^J \frac{dK}{2} \int_0^{2\pi} \frac{dq_K}{2\pi} g[E_a(J, K, q_K)] \\ &= \frac{1}{\pi} \int_0^{2\pi} dq_K \int_0^\infty J \, dJ \int_0^J dK g(E_a) \\ &= \frac{1}{\pi} \int_0^{2\pi} dq_K \int_0^\infty dK \int_K^\infty J \, dJ g(E_a) \\ &= \frac{1}{\pi} \int_0^{2\pi} dq_K \int_0^\infty dK \int_{K^2/2I_x^a}^\infty \left(\frac{I_x^a I_y^a}{I_x^a \sin^2 q_K + I_y^a \cos^2 q_K} \right) g(E_a) \, dE_a \\ &= \frac{I_x^a I_y^a}{\pi} \int_0^{2\pi} \frac{dq_K}{I_x^a \sin^2 q_K + I_y^a \cos^2 q_K} \int_0^\infty g(E_a) \, dE_a \int_0^{\sqrt{2I_x^a E_a}} dK \\ &= \frac{8I_x^a I_y^a}{\pi} \int_0^{\pi/2} \frac{dq_K}{(I_x^a + I_y^a) + (I_y^a - I_x^a) \cos 2q_K} \int_0^\infty g(E_a) \, dE_a \sqrt{2I_x^a E_a} \\ &= 2(2I_x^a I_y^a)^{1/2} \int_0^\infty \sqrt{E_a} g(E_a) \, dE_a, \end{aligned} \quad (2.5)$$

where $g(E)$ is an arbitrary function of E .

2.2 Basis functions

The solution of the linearized Boltzmann equation is expressed in terms of suitable basis functions. We make minor modifications to the basis functions introduced for linear molecules in Curtiss.³ We have introduced a phase change, multiplying by a factor of $(i)^{p+q}$, $i = \sqrt{-1}$, to ensure all effective cross sections are real.⁴ This choice gives the same phase convention as that employed by McCourt *et al.*¹⁴ The second change involved alteration of one of the indices of the Associated Laguerre polynomial used for the internal energy arising from asymmetric tops requiring three generalized coordinates while the

linear molecules used previously required two.

$$\begin{aligned} \mathcal{B}_{km}^{pqst}(\mathbf{W}, \varepsilon, \hat{\mathbf{J}}) = & (-1)^{k-m} (i)^{p+q} 2\pi^{3/2} (2k+1)^{1/2} \\ & \times W^p \bar{L}_s^{p+1/2} (W^2) e^{q/2} \bar{L}_t^{q+1/2} (\varepsilon) \\ & \times \sum_{\mu\nu} \binom{p \quad q \quad k}{\mu \quad \nu \quad -m} Y_\mu^p(\hat{\mathbf{W}}) Y_\nu^q(\hat{\mathbf{J}}). \end{aligned} \quad (2.6)$$

The dimensionless linear momentum, \mathbf{W}_a , and rotational energy, ε_a , are given by

$$\mathbf{W}_a = \frac{\mathbf{P}_a}{(2m_a k_B T)^{1/2}}, \quad \varepsilon_a = \frac{E_a}{k_B T}, \quad (2.7)$$

where E_a is given by eqn (2.1). Here $\bar{L}_n^m(x)$ is the normalised Associated Laguerre polynomial satisfying³

$$\int_0^\infty x^\alpha \exp(-x) \bar{L}_n^\alpha(x) \bar{L}_{n'}^\alpha(x) dx = \delta_{nn'}, \quad (2.8)$$

$\begin{pmatrix} \cdot & \cdot & \cdot \\ \cdot & \cdot & \cdot \\ \cdot & \cdot & \cdot \end{pmatrix}$ denotes a 3- j symbol and $Y_l^m(\hat{\mathbf{R}})$ denotes a spherical harmonic. Since we are following Curtiss,³ eqn (2.6) uses the conventions of Hirschfelder *et al.*²² for spherical harmonics.

The $\mathcal{B}_{km}^{pqst}(\mathbf{W}, \varepsilon, \hat{\mathbf{J}})$ form an orthonormal set with weight function $f_a^{(0)}$:

$$\begin{aligned} & \frac{1}{n_a} \int f_a^{(0)} [P, E(J, K, q_K), T] \mathcal{B}_{km}^{p'q's't'}(\mathbf{W}, \varepsilon, \hat{\mathbf{J}})^* \\ & \times \mathcal{B}_{km}^{pqst}(\mathbf{W}, \varepsilon, \hat{\mathbf{J}}) d\mathbf{P} dJ d\hat{\mathbf{J}} \frac{dK}{2} \frac{dq_K}{2\pi} = \delta(pqstkm|p'q's't'k'm'), \end{aligned} \quad (2.9)$$

where Z^* denotes the complex conjugate of Z and $\delta(i_1 i_2 \dots i_3 i_4 \dots)$ is a shorthand for $\delta_{i_1, i_3} \delta_{i_2, i_4} \dots$. Because $\hat{\mathbf{J}}$ is independent of K and q_K , (see Child,²⁰ p. 87) or the figure in Liu *et al.*¹⁷ or in Yang *et al.*¹⁸) the integration over $\hat{\mathbf{J}}$ proceeds as for linear molecules. Also the integration over J, K, M and q_K proceeds as in eqn (2.5).

2.3 Effective cross sections

2.3.1 Laboratory frame cross sections. Using these basis functions from eqn (2.6) we then define, following Curtiss,³ temperature-dependent effective cross sections in the laboratory reference frame, as

$$\begin{aligned} \sigma' \begin{pmatrix} p & q & s & t \\ p' & q' & s' & t' \end{pmatrix}^{(k)} (T) = & -[64\pi^4 n_a n_b \bar{g}]^{-1} \\ & \times \frac{1}{2k+1} \sum_{m=-k}^k \int f_a^{(0)} f_b^{(0)} \mathcal{B}_{km}^{p'q's't'}(\mathbf{W}_a, \varepsilon_a, \hat{\mathbf{J}}_a)^* \\ & \times [\mathcal{B}_{km}^{pqst}(\mathbf{W}'_a, \varepsilon'_a, \hat{\mathbf{J}}'_a) - \mathcal{B}_{km}^{pqst}(\mathbf{W}_a, \varepsilon_a, \hat{\mathbf{J}}_a)] g b db d\phi_b \\ & \times J_a^2 J_b^2 dJ_a dJ_b dR_a^{(0)} dR_b^{(0)} d\mathbf{P}_a d\mathbf{P}_b d\hat{\mathbf{r}}_{K_a} d\hat{\mathbf{r}}_{K_b}, \end{aligned} \quad (2.10)$$

and

$$\begin{aligned} \sigma'' \begin{pmatrix} p & q & s & t \\ p' & q' & s' & t' \end{pmatrix}^{(k)} (T) = & -[64\pi^4 n_a n_b \bar{g}]^{-1} \\ & \times \frac{1}{2k+1} \sum_{m=-k}^k \int f_a^{(0)} f_b^{(0)} \mathcal{B}_{km}^{p'q's't'}(\mathbf{W}_b, \varepsilon_b, \hat{\mathbf{J}}_b)^* \\ & \times [\mathcal{B}_{km}^{pqst}(\mathbf{W}'_a, \varepsilon'_a, \hat{\mathbf{J}}'_a) - \mathcal{B}_{km}^{pqst}(\mathbf{W}_a, \varepsilon_a, \hat{\mathbf{J}}_a)] g b db d\phi_b \\ & \times J_a^2 J_b^2 dJ_a dJ_b dR_a^{(0)} dR_b^{(0)} d\mathbf{P}_a d\mathbf{P}_b d\hat{\mathbf{r}}_{K_a} d\hat{\mathbf{r}}_{K_b}, \end{aligned} \quad (2.11)$$

where \bar{g} denotes the mean relative speed and

$$dR_\alpha^{(0)} = d\hat{\mathbf{J}}_\alpha dq_{J_\alpha}, \quad d\hat{\mathbf{r}}_{K_\alpha} = d(\cos \theta_{K_\alpha}) dq_{K_\alpha}, \quad \alpha \equiv a, b. \quad (2.12)$$

The overall normalization of these expressions for the cross sections is chosen so that if all the terms in \mathcal{B} are replaced by

$$P(b) = 1, \quad 0 \leq b \leq b_0, \quad P(b) = 0 \text{ elsewhere,}$$

then $\sigma' = \sigma'' = \pi b_0^2$. Equivalently, the cross section can be defined, analogously to quantal effective cross sections, in terms of the classical cross section differential in solid angle and in final rotor action variables.

We recall that Curtiss³ uses primes for *pre-collision* values and, in Curtiss and Tonsager,²³ regards initial values as functions of final values. The classical trajectory (CT) linear-molecule code²⁴ reverses this convention. As in that paper, we shall use primes to denote post-collision values and regard final dynamical variables as functions of their pre-collision values. Note that, because of the absence of a preferred direction in space, each term in the sum in eqns (2.10) and (2.11) is independent of m .

We have used the notation

$$\sigma' \begin{pmatrix} p & q & s & t \\ p' & q' & s' & t' \end{pmatrix}^{(k)} (T)$$

and

$$\sigma'' \begin{pmatrix} p & q & s & t \\ p' & q' & s' & t' \end{pmatrix}^{(k)} (T)$$

to keep as close to Curtiss³ as possible and to keep the notation as compact as possible. In terms of the notation used by McCourt *et al.* (see ref.14, section 2.3.2 and 5.2).

$$\begin{aligned} \sigma' \begin{pmatrix} p & q & s & t \\ p' & q' & s' & t' \end{pmatrix}^{(k)} (T) & \equiv \mathfrak{S} \begin{pmatrix} p & q & s & t & | & a \\ p' & q' & s' & t' & | & a \end{pmatrix}_{ab}, \\ \sigma'' \begin{pmatrix} p & q & s & t \\ p' & q' & s' & t' \end{pmatrix}^{(k)} (T) & \equiv \mathfrak{S} \begin{pmatrix} p & q & s & t & | & a \\ p' & q' & s' & t' & | & b \end{pmatrix}_{ab}. \end{aligned}$$

Thus, following McCourt *et al.*,¹⁴ (see section 2.3.2) σ' accounts for the production of $\mathcal{B}_{km}^{pqst}(\mathbf{W}, \varepsilon, \hat{\mathbf{J}})$ in species a from $\mathcal{B}_{km}^{p'q's't'}(\mathbf{W}, \varepsilon, \hat{\mathbf{J}})$ in species a by collisions between species a and b , while σ'' accounts for the production of $\mathcal{B}_{km}^{pqst}(\mathbf{W}, \varepsilon, \hat{\mathbf{J}})$ in species a from $\mathcal{B}_{km}^{p'q's't'}(\mathbf{W}, \varepsilon, \hat{\mathbf{J}})$ in species b by collisions

between the two species. This distinction between the primed and double-primed quantities is maintained throughout the paper.

For a full discussion of a gas mixture one would need a σ' cross section for the production of $\mathcal{B}_{km}^{pqst}(\mathbf{W}, \mathbf{e}, \hat{\mathbf{J}})$ in species b from $\mathcal{B}_{km}^{p'q's't'}(\mathbf{W}', \mathbf{e}', \hat{\mathbf{J}}')$ in species a by collisions between species a and b . The derivation of this will mirror that for the species a case discussed here.

Substituting in eqns (2.10) and (2.11) for the equilibrium distribution functions from eqn (2.3) we obtain

$$\begin{aligned} \sigma' \begin{pmatrix} p & q & s & t \\ p' & q' & s' & t' \end{pmatrix}^{(k)}(T) &= -[2^9 \pi^7 (k_B T)^3 (m_a m_b)^{3/2} Z_a Z_b \bar{g}]^{-1} \\ &\times \frac{1}{2k+1} \sum_{m=-k}^k \int \exp[-(W_a^2 + W_b^2 + \varepsilon_a + \varepsilon_b)] \\ &\times \mathcal{B}_{km}^{p'q's't'}(\mathbf{W}_a, \mathbf{e}_a, \hat{\mathbf{J}}_a)^* [\mathcal{B}_{km}^{pqst}(\mathbf{W}'_a, \mathbf{e}'_a, \hat{\mathbf{J}}'_a) - \mathcal{B}_{km}^{pqst}(\mathbf{W}_a, \mathbf{e}_a, \hat{\mathbf{J}}_a)] \\ &\times gb db d\phi_b J_a^2 J_b^2 dJ_a dJ_b dR_a^{(0)} dR_b^{(0)} d\mathbf{P}_a d\mathbf{P}_b d\hat{\mathbf{r}}_{K_a} d\hat{\mathbf{r}}_{K_b}, \end{aligned} \quad (2.13)$$

and with a similar expression for $\sigma'' \begin{pmatrix} p & q & s & t \\ p' & q' & s' & t' \end{pmatrix}^{(k)}(T)$.

Again following Curtiss,³ since the dynamics of the collision are independent of the velocity of the centre of mass, we transform from \mathbf{P}_a and \mathbf{P}_b to the relative velocity, \mathbf{g} , and the centre-of-mass velocity, \mathbf{G} , yielding:

$$\begin{aligned} \sigma'' \begin{pmatrix} p & q & s & t \\ p' & q' & s' & t' \end{pmatrix}^{(k)}(T) &= -[2^9 \pi^7 (k_B T)^3 Z_a Z_b \bar{g}]^{-1} \frac{(m_a m_b)^{3/2}}{2k+1} \\ &\times \sum_{m=-k}^k \int \exp\left[-\left(\frac{MG^2}{2k_B T} + \frac{\mu g^2}{2k_B T} + \varepsilon_a + \varepsilon_b\right)\right] \\ &\times \mathcal{B}_{km}^{p'q's't'}(\mathbf{W}_a, \mathbf{e}_a, \hat{\mathbf{J}}_a)^* [\mathcal{B}_{km}^{pqst}(\mathbf{W}'_a, \mathbf{e}'_a, \hat{\mathbf{J}}'_a) - \mathcal{B}_{km}^{pqst}(\mathbf{W}_a, \mathbf{e}_a, \hat{\mathbf{J}}_a)] \\ &\times gb db d\phi_b J_a^2 J_b^2 dJ_a dJ_b dR_a^{(0)} dR_b^{(0)} d\mathbf{G} d\mathbf{g} d\hat{\mathbf{r}}_{K_a} d\hat{\mathbf{r}}_{K_b}, \end{aligned} \quad (2.14)$$

where $M = m_a + m_b$, μ denotes the reduced mass and a similar expression exists for

$$\sigma'' \begin{pmatrix} p & q & s & t \\ p' & q' & s' & t' \end{pmatrix}^{(k)}(T).$$

2.3.2 Integration over the centre of mass velocity. Now, following Curtiss,³ eqn (22), we transform the translational part of the integrand to centre-of-mass and relative coordinates. Fortunately, this proceeds exactly as for linear molecules since the internal structure of the molecules is not

involved. For asymmetric-top molecules we have

$$\begin{aligned} &\left(\frac{M}{2k_B T}\right)^{3/2} \frac{1}{2k+1} \sum_{m=-k}^k \iiint d\mathbf{G} \exp\left[-\frac{MG^2}{2k_B T}\right] \\ &\times \mathcal{B}_{km}^{p'q's't'}(\mathbf{W}_a, \mathbf{e}_a, \hat{\mathbf{J}}_a)^* [\mathcal{B}_{km}^{pqst}(\mathbf{W}'_a, \mathbf{e}'_a, \hat{\mathbf{J}}'_a) - \mathcal{B}_{km}^{pqst}(\mathbf{W}_a, \mathbf{e}_a, \hat{\mathbf{J}}_a)] \\ &= \left(\frac{4\pi^3}{2^3 \pi^{5/2}}\right) (-1)^{k+p'} (-i)^{q+q'} \frac{\pi^2}{2} \\ &\times (2q+1)^{1/2} e_a^{(q+q')/2} \sum_{\kappa} (-1)^{\kappa} (2\kappa+1) \begin{Bmatrix} q & q' & \kappa \\ p' & p & k \end{Bmatrix} \\ &\times \sum_{nl'l'} i^{l-l'} (2l+1)^{1/2} I_{ln'l':psp's'}^{(\kappa)}(y_a, y_b) \gamma^{l'} \bar{L}_n^{l'+1/2}(\gamma^2) \bar{L}_l^{q'+1/2}(\varepsilon_a) \\ &\times [(\gamma')^l \bar{L}_n^{l+1/2}(\gamma'^2) \bar{L}_l^{q+1/2}(\varepsilon'_a) X'(lq|l'q')_{\kappa} \\ &- \gamma^l \bar{L}_n^{l+1/2}(\gamma^2) \bar{L}_l^{q+1/2}(\varepsilon_a) X'(lq|l'q')_{\kappa}^{(0)}], \end{aligned} \quad (2.15)$$

where

$$\begin{Bmatrix} \cdot & \cdot & \cdot \\ \cdot & \cdot & \cdot \end{Bmatrix}$$

denotes a 6- j symbol, $I_{ln'l':psp's'}^{(\kappa)}(y_a, y_b)$ denotes the Talmi coefficient used by Curtiss,³ eqn (27), $y_a^2 = m_a/M$, $\alpha \equiv a, b, X'$ is as defined by Curtiss,³ eqn (28), and where in $X'(lq|l'q')_{\kappa}^{(0)}$ all primed dynamical variables are replaced by their unprimed equivalents. (Note that the indices $nl'l'$ of $I^{(\kappa)}$ have been transposed in Curtiss's eqns (30), (36–37) and (40–41).²⁵) In eqn (2.15) the first term in parentheses on the right-hand side is the additional factor arising from the change in the numerical factors in the basis functions between linear molecules and asymmetric-top molecules. Similarly

$$\begin{aligned} &\left(\frac{M}{2k_B T}\right)^{3/2} \frac{1}{2k+1} \sum_{m=-k}^k \iiint d\mathbf{G} \exp\left[-\frac{MG^2}{2k_B T}\right] \\ &\times \mathcal{B}_{km}^{p'q's't'}(\mathbf{W}_b, \mathbf{e}_b, \hat{\mathbf{J}}_b)^* [\mathcal{B}_{km}^{p'q's't'}(\mathbf{W}_a, \mathbf{e}_a, \hat{\mathbf{J}}_a) - \mathcal{B}_{km}^{p'q's't'}(\mathbf{W}'_a, \mathbf{e}'_a, \hat{\mathbf{J}}'_a)] \\ &= (-1)^{k+p'} (-i)^{q+q'} \times \frac{\pi^{5/2}}{4} (2q+1)^{1/2} e_a^{q/2} e_b^{q'/2} \sum_{\kappa} (-1)^{\kappa} (2\kappa+1) \\ &\times \begin{Bmatrix} q & q' & \kappa \\ p' & p & k \end{Bmatrix} \sum_{nl'l'} i^{l+l'} \left(\frac{y_a}{y_b}\right)^{(4n'+2l'-2s'-p')} \\ &\times (2l+1)^{1/2} I_{ln'l':psp's'}^{(\kappa)}(y_a, y_b) \gamma^{l'} \bar{L}_n^{l'+1/2}(\gamma^2) \bar{L}_l^{q'+1/2}(\varepsilon_b) \\ &\times [(\gamma')^l \bar{L}_n^{l+1/2}(\gamma'^2) \bar{L}_l^{q+1/2}(\varepsilon'_a) X''(lq|l'q')_{\kappa} \\ &- \gamma^l \bar{L}_n^{l+1/2}(\gamma^2) \bar{L}_l^{q+1/2}(\varepsilon_a) X''(lq|l'q')_{\kappa}^{(0)}], \end{aligned} \quad (2.16)$$

and X'' is defined by Curtiss,³ eqn (29), and where in $X''(lq|l'q')_{\kappa}^{(0)}$ all primed dynamical variables are replaced by their unprimed equivalents and where the scaled relative velocity

$$\boldsymbol{\gamma} = \left(\frac{\mu}{2k_B T}\right)^{1/2} \mathbf{g}, \quad (2.17)$$

has been introduced. Changing from integration over J_a and J_b to ε_a and ε_b , respectively, and employing eqn (30) from Curtiss,³ for asymmetric-top molecules we have, where the change of variables proceeds as in eqn (2.5),

$$\begin{aligned} \sigma' \left(\begin{array}{cccc} p & q & s & t \\ p' & q' & s' & t' \end{array} \right)^{(k)} (T) &= -[2^{11}\pi^7]^{-1} (-1)^{k+p'} (-i)^{q+q'} \\ &\times \int \exp[-\gamma^2 - \varepsilon_a - \varepsilon_b] \gamma^3 (\varepsilon_a \varepsilon_b)^{1/2} (2q+1)^{1/2} \varepsilon_a^{q+q'/2} \\ &\times \sum_{\kappa} (-1)^{\kappa} (2\kappa+1) \left\{ \begin{array}{ccc} q & q' & \kappa \\ p' & p & k \end{array} \right\} \sum_{nl'l'} i^{l-l'} (2l+1)^{1/2} \\ &\times I_{nl'l',psp's'}^{(\kappa)}(y_a, y_b) \gamma^{l'} \bar{L}_{n'}^{l'+1/2}(\gamma^2) \bar{L}_{l'}^{q'+1/2}(\varepsilon_a) \\ &\times \left[\begin{array}{l} (\gamma')^l \bar{L}_n^{l+1/2}(\gamma'^2) \bar{L}_l^{q+1/2}(\varepsilon'_a) X'(lq|l'q')_{\kappa} \\ -\gamma'^l \bar{L}_n^{l+1/2}(\gamma'^2) \bar{L}_l^{q+1/2}(\varepsilon_a) X'(lq|l'q')_{\kappa}^{(0)} \end{array} \right] h(q\kappa_a; I_x^a, I_y^a) \\ &\times h(q\kappa_b; I_x^b, I_y^b) b db d\phi_b d\gamma d\hat{g} d\varepsilon_a d\varepsilon_b dR_a^{(0)} dR_b^{(0)} d\hat{r}_{K_a} d\hat{r}_{K_b}, \end{aligned} \quad (2.18)$$

where

$$\begin{aligned} h(q; I_x, I_y) &= \frac{\sqrt{I_x I_y}}{I_x \sin^2 q + I_y \cos^2 q}, \quad K_x = \sqrt{2\varepsilon_a k_B T I_x^2} \cos \bar{\theta}_{K_x}, \\ d\hat{r}_{K_a} &= d(\cos \bar{\theta}_{K_x}) dq_{K_x}, \quad \alpha \equiv a, b. \end{aligned} \quad (2.19)$$

Here $d\hat{r}_{K_x}$ has been redefined from eqn (2.12) and no longer has the geometric interpretation introduced there. Note that for spherical and symmetric tops $h = 1$ and that for asymmetric tops $\bar{h} = \frac{2}{\pi} \int_0^{\pi/2} h dq = 1$.

Alternatively, if the geometric interpretation in eqn (2.12) is to be retained, the factor $(\varepsilon_a \varepsilon_b)^{1/2} h(q_{K_x}) h(q_{K_b})$ has to be replaced by

$$\frac{J_a J_b}{2k_B T \sqrt{I_x^a I_x^b}} \tilde{h}(\hat{r}_{K_a}; I_x^a, I_y^a, I_z^a) \tilde{h}(\hat{r}_{K_b}; I_x^b, I_y^b, I_z^b), \quad (2.20)$$

where

$$\tilde{h}(\hat{r}_K; I_x, I_y, I_z) = \frac{I_z \sqrt{I_x I_y}}{I_z (I_x \sin^2 q_K + I_y \cos^2 q_K) \sin^2 \theta_K + I_x I_y \cos^2 \theta_K}. \quad (2.21)$$

For a spherical top $\tilde{h} = 1$ and for a symmetric top \tilde{h} is independent of q_K .

Similarly

$$\begin{aligned} \sigma'' \left(\begin{array}{cccc} p & q & s & t \\ p' & q' & s' & t' \end{array} \right)^{(k)} (T) &= -[2^{11}\pi^7]^{-1} (-1)^{k+p'} (-i)^{q+q'} \\ &\times \int \exp[-\gamma^2 - \varepsilon_a - \varepsilon_b] \gamma^3 (\varepsilon_a \varepsilon_b)^{1/2} (2q+1)^{1/2} \varepsilon_a^{q/2} \varepsilon_b^{q'/2} \\ &\times \sum_{\kappa} (-1)^{\kappa} (2\kappa+1) \left\{ \begin{array}{ccc} q & q' & \kappa \\ p' & p & k \end{array} \right\} \sum_{nl'l'} i^{l+l'} \left(\frac{y_a}{y_b} \right)^{(4n'+2l'-2s'-p')} \\ &\times (2l+1)^{1/2} I_{nl'l',psp's'}^{(\kappa)}(y_a, y_b) \gamma^{l'} \bar{L}_n^{l'+1/2}(\gamma^2) \bar{L}_{l'}^{q'+1/2}(\varepsilon_b) \\ &\times [(\gamma')^l \bar{L}_n^{l+1/2}(\gamma'^2) \bar{L}_l^{q+1/2}(\varepsilon'_a) X''(lq|l'q')_{\kappa} \\ &- \gamma'^l \bar{L}_n^{l+1/2}(\gamma'^2) \bar{L}_l^{q+1/2}(\varepsilon_a) X''(lq|l'q')_{\kappa}^{(0)}] \\ &\times h(q\kappa_a; I_x^a, I_y^a) h(q\kappa_b; I_x^b, I_y^b) b db d\phi_b d\gamma d\hat{g} \\ &\times d\varepsilon_a d\varepsilon_b dR_a^{(0)} dR_b^{(0)} d\hat{r}_{K_a} d\hat{r}_{K_b}. \end{aligned} \quad (2.22)$$

Since only *relative* orientations are important we are free to choose our space-fixed axes with Oz along \mathbf{g} and Ox along \mathbf{b} . Then the integrand is independent of ϕ_b and \hat{g} so performing the integral over these variables yields a factor of $8\pi^2$.

2.3.3 Centre of mass cross sections. Following Curtiss,³ for asymmetric-top molecules we define angle averages of the integrands:

$$\begin{aligned} R' \left(\begin{array}{cccc} l & q & n & t \\ l' & q' & n' & t' \end{array} \right)_{\kappa} &= \frac{\varepsilon_a^{q/2}}{2^{10}\pi^6} \int (\gamma')^l \bar{L}_n^{l+1/2}(\gamma'^2) \\ &\times \bar{L}_{l'}^{q'+1/2}(\varepsilon'_a) X'(lq|l'q')_{\kappa} h(q\kappa_a; I_x^a, I_y^a) h(q\kappa_b; I_x^b, I_y^b) \\ &\times dR_a^{(0)} dR_b^{(0)} d\hat{r}_{K_a} d\hat{r}_{K_b}. \end{aligned} \quad (2.23)$$

Similarly, following Curtiss,³ eqn (32), we define

$$R'' \left(\begin{array}{cccc} l & q & n & t \\ l' & q' & n' & t' \end{array} \right)_{\kappa}$$

as in eqn (2.23) but with $X'(lq|l'q')_{\kappa}$ replaced by $X''(lq|l'q')_{\kappa}$.

We now define an energy-dependent cross section in the centre-of-mass frame:

$$\begin{aligned} Q' \left(\begin{array}{cccc} l & q & n & t \\ l' & q' & n' & t' \end{array} \right)_{\kappa} (\varepsilon_a, \varepsilon_b, \gamma) &= 2\pi \int_0^{\infty} b db \\ &\times \left[\delta_{l,l'} \delta_{q,q'} \delta_{\kappa,0} \gamma^l \bar{L}_n^{l+1/2}(\gamma^2) \varepsilon_a^{q/2} \bar{L}_{l'}^{q'+1/2}(\varepsilon_a) - R' \left(\begin{array}{cccc} l & q & n & t \\ l' & q' & n' & t' \end{array} \right)_{\kappa} \right]. \end{aligned} \quad (2.24)$$

In the analogous cross section,

$$Q'' \left(\begin{array}{cccc} l & q & n & t \\ l' & q' & n' & t' \end{array} \right)_{\kappa} (\varepsilon_a, \varepsilon_b, \gamma),$$

in the first term inside the square brackets there is an additional factor of $\delta_{q,0}$ and the second term is replaced by

$$R'' \begin{pmatrix} l & q & n & t \\ l' & q' & n' & t' \end{pmatrix}_\kappa.$$

Next, we introduce the thermally averaged centre-of-mass cross sections:

$$\begin{aligned} \sigma' \begin{pmatrix} l & q & n & t \\ l' & q' & n' & t' \end{pmatrix}_\kappa (T) &= i^{q-q'+l-l'} \int \exp[-\gamma^2 - \varepsilon_a - \varepsilon_b] \\ &\times (\varepsilon_a \varepsilon_b)^{1/2} \gamma^{l'} \bar{L}_{n'}^{l'+1/2}(\gamma^2) \bar{L}_{t'}^{q'+1/2}(\varepsilon_a) (\varepsilon_a)^{q'/2} \\ &\times \mathcal{Q}' \begin{pmatrix} l & q & n & t \\ l' & q' & n' & t' \end{pmatrix}_\kappa (\varepsilon_a, \varepsilon_b, \gamma) \gamma^2 d(\gamma^2) d\varepsilon_a d\varepsilon_b, \end{aligned} \quad (2.25)$$

and

$$\begin{aligned} \sigma'' \begin{pmatrix} l & q & n & t \\ l' & q' & n' & t' \end{pmatrix}_\kappa (T) &= i^{q-q'+l-l'} \int \exp[-\gamma^2 - \varepsilon_a - \varepsilon_b] \\ &\times (\varepsilon_a \varepsilon_b)^{1/2} \gamma^{l'} \bar{L}_{n'}^{l'+1/2}(\gamma^2) \bar{L}_{t'}^{q'+1/2}(\varepsilon_b) (\varepsilon_b)^{q'/2} \\ &\times \mathcal{Q}'' \begin{pmatrix} l & q & n & t \\ l' & q' & n' & t' \end{pmatrix}_\kappa (\varepsilon_a, \varepsilon_b, \gamma) \gamma^2 d(\gamma^2) d\varepsilon_a d\varepsilon_b. \end{aligned} \quad (2.26)$$

The introduction of the leading factor in i on the right-hand side ensures that σ' and σ'' are always real because $X'(lq|l'q')_\kappa$ is real or imaginary as $(q - q' + l - l')$ is even or odd, respectively.

Finally we can relate the lab and centre-of-mass temperature-dependent cross sections. We have, from eqns (2.18) and (2.25),

$$\begin{aligned} \sigma' \begin{pmatrix} p & q & s & t \\ p' & q' & s' & t' \end{pmatrix}^{(k)} (T) &= (-1)^{k+q+p'} (2q+1)^{1/2} \\ &\times \sum_\kappa (-1)^\kappa (2\kappa+1) \begin{Bmatrix} q & q' & \kappa \\ p' & p & k \end{Bmatrix} \\ &\times \sum_{nl'n'} (2l+1)^{1/2} I_{ln'l'n':psp's'}^{(k)}(y_a, y_b) \sigma' \begin{pmatrix} l & q & n & t \\ l' & q' & n' & t' \end{pmatrix}_\kappa (T), \end{aligned} \quad (2.27)$$

with, for

$$\sigma'' \begin{pmatrix} p & q & s & t \\ p' & q' & s' & t' \end{pmatrix}^{(k)} (T),$$

an additional factor of $(-1)^l (y_a/y_b)^{(4n'+2l-2s'-p')}$ inside the second summation and

$$\sigma' \begin{pmatrix} l & q & n & t \\ l' & q' & n' & t' \end{pmatrix}_\kappa (T)$$

replaced by

$$\sigma'' \begin{pmatrix} l & q & n & t \\ l' & q' & n' & t' \end{pmatrix}_\kappa (T).$$

Hence we now have the necessary relations to determine the effective cross sections employed in kinetic theory from the detailed dynamical treatment of the collisions. Practical details concerning the implementation are discussed in the Appendix.

2.4 Semiclassical aspects

While this description is entirely classical, we note here some connections with semiclassical aspects for symmetric and asymmetric tops. For the symmetric top K is a good quantum number. Hence the methods used by Liu and Dickinson²⁶ can be employed to establish the connection between classical effective cross sections and quantal cross sections approximated using the classical S-matrix theory.^{27,28}

For asymmetric tops, however, K is not a constant of the motion and transitions are described in the classical S-matrix theory by Augustin and Miller¹⁹ in terms of the angular-momentum-like variable η where, in our notation,

$$\begin{aligned} \eta^2 &= (1+\kappa)K^2 - (1-\kappa)(J^2 - K^2) \cos^2 q_K, \\ \kappa &= \frac{2I_x I_z - I_y(I_x + I_z)}{I_y(I_z - I_x)}. \end{aligned} \quad (2.28)$$

Here κ denotes the usual asymmetry parameter for asymmetric tops, rather than the tensor rank index introduced in eqn (2.15). Thus for a semiclassical description¹⁹ the natural variables are $J, M, \eta, q_J, q_M, q_\eta$ and transition amplitudes are calculated assuming a uniform distribution in q_η , the angle variable conjugate to η . Effective cross sections involve sums over the quantized values of η and, in a semiclassical approximation, these sums are converted to integrals over η . Since the transformation between the canonical pairs (η, q_η) and (K, q_K) has Jacobian one, the resulting expressions can equally be evaluated in the K, q_K representation, as employed in our fully classical description.

A further issue concerns quantal effects in the energies of the asymmetric top. The quantization of the η variable involves motion in a symmetric double-well potential, qualitatively similar to that giving the inversion splitting in ammonia. Colwell *et al.*²⁹ have shown that a uniform semiclassical approximation, including allowance for tunnelling, gives much improved results over the standard WKB approximation ignoring tunnelling. As tunnelling leads to a splitting of otherwise degenerate levels and, for low tunnelling frequencies this splitting is approximately symmetric about the degenerate level, the overall effect can be expected to be quite small when a thermal average is required. Clearly this effect can be expected to be strongest for hydrides.

3. Summary and conclusions

Previously, only for linear molecules³ was the necessary kinetic theory available for the calculation of transport and relaxation properties. Here we have extended this work to the most general rigid molecular structure, the asymmetric top. For the effective cross sections required by this theory we have performed the integration over the velocity of the centre of mass and brought the cross sections to a form suitable for classical trajectory calculation. The solution for asymmetric

tops necessarily includes the results for spherical and symmetric tops as special cases.

Calculations are in progress for methane and for water and will be reported separately.³⁰

While the theory developed here has been focussed on pure gases, much of the development can readily be extended to mixtures. In particular, the integration over the centre of mass velocity has been performed for an arbitrary mass ratio of the colliding partners (see section 2.3.2).

Appendix

3.1 Practical implementation

To follow as closely as possible the method used in the current linear-molecule code²⁴ we transform the centre of mass thermal average, eqn (2.25), to obtain just one temperature-dependent integral over the (conserved) total energy, translational and rotational. The procedure is outlined for σ' : a similar procedure may readily be adopted for σ'' . The integral appearing in eqn (2.25) is of the form

$$\mathcal{F} = \int_0^\infty \int_0^\infty \int_0^\infty \exp[-\gamma^2 - \varepsilon_a - \varepsilon_b] \gamma^2 (\varepsilon_a \varepsilon_b)^{1/2} d(\gamma^2) d\varepsilon_a d\varepsilon_b \mathcal{F}. \quad (3.29)$$

Introducing new variables

$$\mathcal{E} = E/k_B T = \gamma^2 + \varepsilon_a + \varepsilon_b, \quad x = \gamma^2/\mathcal{E} = \mu g^2/2E, \quad (3.30)$$

$$y = \varepsilon_a/[(1-x)\mathcal{E}] = E_a/[(1-x)E],$$

where E is the total energy, eqn (3.29) becomes

$$\begin{aligned} \mathcal{F} &= \int_0^\infty \mathcal{E}^4 \exp(-\mathcal{E}) d\mathcal{E} \int_0^1 x(1-x)^2 dx \\ &\times \int_0^1 \sqrt{y(1-y)} dy \mathcal{F}. \end{aligned} \quad (3.31)$$

With a view to obtaining a more uniform integrand for the Monte Carlo numerical integration we make further transformations

$$\begin{aligned} u &= 6x^2 - 8x^3 + 3x^4, \quad v = \frac{2}{\pi} \left(\alpha - \frac{1}{4} \sin 4\alpha \right), \\ y &= \sin^2 \alpha, \quad \text{or } v = \frac{2}{\pi} \left[\arcsin \sqrt{y} - (1-2y)\sqrt{y(1-y)} \right], \end{aligned} \quad (3.32)$$

yielding

$$\mathcal{F} = \frac{\pi}{96} \int_0^\infty \mathcal{E}^4 \exp(-\mathcal{E}) d\mathcal{E} \int_0^1 du \int_0^1 dv \mathcal{F}. \quad (3.33)$$

While we now have to solve eqn (3.32) numerically for $x(u)$ and $y(v)$ this is a trivial overhead. Introducing the transformed variables into eqn (2.25), the thermally averaged centre-of-mass cross section can be written

$$\begin{aligned} \sigma' \left(\begin{matrix} l & q & n & t \\ l' & q' & n' & t' \end{matrix} \right)_\kappa (T) &= i^{q-q'+l-l'} \\ &\times \frac{\pi}{96} \int_0^\infty \mathcal{E}^4 \exp(-\mathcal{E}) d\mathcal{E} \int_0^1 du \int_0^1 dv \mathcal{F}, \end{aligned} \quad (3.34)$$

where

$$\begin{aligned} \mathcal{F} &= \gamma^{l'} \bar{L}_n^{l'+1/2}(\gamma^2) \bar{L}_t^{q'+1/2}(\varepsilon_a) (\varepsilon_a)^{q'/2} \\ &\times \mathcal{Q}' \left(\begin{matrix} l & q & n & t \\ l' & q' & n' & t' \end{matrix} \right)_\kappa (\varepsilon_a, \varepsilon_b, \gamma). \end{aligned} \quad (3.35)$$

While we have written this thermal average in a form with just one explicitly temperature-dependent integral, that over \mathcal{E} , there remains an implicit temperature dependence through the variables γ , ε_a and ε_b , particularly where they appear in the associated Laguerre polynomials. Following Curtiss and Tonsager,²³ we circumvent this problem by expanding the polynomials and dealing with simple powers of γ^2 , ε_a and ε_b , where we can use $\gamma^2 = x\mathcal{E}$, etc. from eqn (3.30) and thus separate the \mathcal{E} dependence. We write

$$\begin{aligned} \bar{L}_n^{l'+1/2}(x) &= \sum_{i=0}^n L(n, l, i) (-x)^i; \\ L(n, l, i) &= \frac{\sqrt{\Gamma(n+1)\Gamma(n+l+3/2)}}{\Gamma(n-i+1)\Gamma(l+i+3/2)\Gamma(i+1)}. \end{aligned} \quad (3.36)$$

To facilitate this transformation we introduce, following eqn (2.23),

$$\begin{aligned} R' \left(\begin{matrix} l & q & n & t \\ l' & q' & n' & t' \end{matrix} \right)_\kappa^{(0)} &= \frac{\varepsilon_a^{q/2}}{2^{10}\pi^6} \int (\gamma)^l \bar{L}_n^{l'+1/2}(\gamma^2) \\ &\times \bar{L}_t^{q'+1/2}(\varepsilon_a) X'(lq|l'q')_\kappa^{(0)} \\ &\times h(q\kappa_a; I_x^a, I_y^a) h(q\kappa_b; I_x^b, I_y^b) dR_a^{(0)} dR_b^{(0)} d\hat{r}_{\kappa_a} d\hat{r}_{\kappa_b}, \\ &= (\gamma)^l \bar{L}_n^{l'+1/2}(\gamma^2) \varepsilon_a^{q/2} \bar{L}_t^{q'+1/2}(\varepsilon_a) \delta_{l,l'} \delta_{q,q'} \delta_{\kappa,0}. \end{aligned} \quad (3.37)$$

Now we can rewrite eqn (2.24)

$$\begin{aligned} \mathcal{Q}' \left(\begin{matrix} l & q & n & t \\ l' & q' & n' & t' \end{matrix} \right)_\kappa (\varepsilon_a, \gamma) &= 2\pi \int_0^\infty b db \\ &\times \left[\delta_{l,l'} \delta_{q,q'} \delta_{\kappa,0} R' \left(\begin{matrix} l & q & n & t \\ l' & q' & n' & t' \end{matrix} \right)_\kappa^{(0)} - R' \left(\begin{matrix} l & q & n & t \\ l' & q' & n' & t' \end{matrix} \right)_\kappa \right]. \end{aligned} \quad (3.38)$$

Substituting in the thermally-averaged cross section we can rewrite eqn (2.25)

$$\begin{aligned} \sigma' \left(\begin{matrix} l & q & n & t \\ l' & q' & n' & t' \end{matrix} \right)_\kappa (T) &= \sum_{i_1=0}^n \sum_{i_2=0}^l \sum_{i_3=0}^{n'} \sum_{i_4=0}^{t'} \sigma' \left(\begin{matrix} l & q & n & t & i_1 & i_2 \\ l' & q' & n' & t' & i_3 & i_4 \end{matrix} \right)_\kappa (T), \end{aligned} \quad (3.39)$$

where

$$\begin{aligned}
& \bar{\sigma}' \left(\begin{matrix} l & q & n & t & i_1 & i_2 \\ l' & q' & n' & t' & i_3 & i_4 \end{matrix} \right)_\kappa (T) = i^{q-q'+l-l'} \\
& \times \int \exp[-\gamma^2 - \varepsilon_a - \varepsilon_b] \gamma^2 (\varepsilon_a \varepsilon_b)^{1/2} \\
& \times 2\pi \int_0^\infty b db d(\gamma^2) d\varepsilon_a d\varepsilon_b \\
& \times e^{i_1+i_2+i_3+i_4+(l+l'+q+q')/2} (-1)^{i_1+i_2+i_3+i_4} \\
& \times L(n, l, i_1) L(t, q, i_2) L(n', l', i_3) L(t', q', i_4) \\
& \times \left\langle x^{i_1+i_3+(l+l')/2} [y(1-x)]^{i_2+i_4+(q+q')/2} \right. \\
& \times \left. \left\{ X'(lq|l'q')_\kappa^{(0)} - \left(\frac{x'}{x} \right)^{i_1+l/2} \left[\frac{y'(1-x')}{y(1-x)} \right]^{i_2} X'(lq|l'q')_\kappa \right\} \right\rangle \\
& \equiv \int_0^\infty \mathcal{E}^{4+i_1+i_2+i_3+i_4+(l+l'+q+q')/2} \exp(-\mathcal{E}) d\mathcal{E} \\
& \times \bar{Q}' \left(\begin{matrix} l & q & n & t & i_1 & i_2 \\ l' & q' & n' & t' & i_3 & i_4 \end{matrix} \right)_\kappa (E).
\end{aligned} \tag{3.40}$$

Here

$$\langle \mathcal{G} \rangle = \int \mathcal{G} h(q_{K_a}; I_1^a, I_2^a) h(q_{K_b}; I_1^b, I_2^b) dR_a^{(0)} dR_b^{(0)} d\hat{r}_{K_a} d\hat{r}_{K_b}, \tag{3.41}$$

denotes the orientation average, x' and y' are the final values of x and y , respectively, and

$$\begin{aligned}
& \bar{Q}' \left(\begin{matrix} l & q & n & t & i_1 & i_2 \\ l' & q' & n' & t' & i_3 & i_4 \end{matrix} \right)_\kappa (E) \\
& = \frac{\pi}{96} i^{l-l'+q-q'} \int_0^1 du \int_0^1 dv 2\pi \int_0^\infty b db (-1)^{i_1+i_2+i_3+i_4} \\
& \times L(n, l, i_1) L(t, q, i_2) L(n', l', i_3) L(t', q', i_4) \\
& \times \left\langle x^{i_1+i_3+(l+l')/2} [y(1-x)]^{i_2+i_4+(q+q')/2} \right. \\
& \times \left. \left\{ X'(lq|l'q')_\kappa^{(0)} - \left(\frac{x'}{x} \right)^{i_1+l/2} \left[\frac{y'(1-x')}{y(1-x)} \right]^{i_2} X'(lq|l'q')_\kappa \right\} \right\rangle.
\end{aligned} \tag{3.42}$$

The slight asymmetry in the coefficient of $X'(lq|l'q')_\kappa$ in this equation arises because X' depends on $(e'_a/\varepsilon_a)^{q/2}$, as well as on orientations. This orientation average, eqn (3.41), involves integrands of the form

$$\mathcal{F} = \int_0^{2\pi} h(q; I_x, I_y) g(q) dq, \tag{3.43}$$

where $g(q)$ is an arbitrary function. This can be rewritten in a form more suited to Monte Carlo integration:

$$\mathcal{F} = \int_0^{2\pi} g[\bar{q}(\bar{q})] d\bar{q}, \tag{3.44}$$

where $\tan \bar{q} = \lambda \tan q$, $\lambda = \sqrt{I_x/I_y}$, $0 \leq \bar{q} \leq \pi/2$,

and similar transformations for the rest of the \bar{q} range.

The cross section \bar{Q}' is evaluated using Monte Carlo integration in thirteen dimensions at a suitably chosen range of

total energy values, appropriate to the temperature range of interest. As in the linear-molecule code,²⁴ when evaluating this cross section each trajectory is combined with its time-reversed form. For some diagonal cross sections ($lqnt = l'q'n't'$) this ensures that the integrand is positive definite. Each cross section, $\bar{Q}'(E)$, is then fitted to a form involving Chebyshev polynomials in $\ln(E)$, which allows for inexpensive evaluation of the final thermal average in eqn (3.40) at arbitrary temperatures. Finally, the lab cross section can be determined using eqn (2.27).

Acknowledgements

This work was financially supported by the German Science Foundation (Deutsche Forschungsgemeinschaft), grant VO 499/14-1.

References

- 1 W. A. Wakeham, A. Nagashima and J. V. Sengers, in *Measurement of the Transport Properties of Fluids*, ed. W. A. Wakeham, A. Nagashima and J. V. Sengers, Blackwell, Oxford, 1991, ch. 13, pp. 439–451.
- 2 J. J. Hurly and M. R. Moldover, *J. Res. Natl. Inst. Stand. Technol.*, 2000, **105**, 667–688.
- 3 C. F. Curtiss, *J. Chem. Phys.*, 1981, **75**, 1341–1346.
- 4 E. L. Heck and A. S. Dickinson, *Mol. Phys.*, 1994, **81**, 1325–1352.
- 5 E. L. Heck, A. S. Dickinson and V. Vesovic, *Mol. Phys.*, 1994, **83**, 907–932.
- 6 E. L. Heck and A. S. Dickinson, *Physica A*, 1995, **217**, 107–123.
- 7 E. L. Heck and A. S. Dickinson, *Physica A*, 1995, **218**, 305–318.
- 8 S. Bock, E. Bich, E. Vogel, A. S. Dickinson and V. Vesovic, *J. Chem. Phys.*, 2002, **117**, 2151–2160.
- 9 S. Bock, E. Bich, E. Vogel, A. S. Dickinson and V. Vesovic, *J. Chem. Phys.*, 2004, **120**, 7987–7997.
- 10 S. Bock, E. Bich, E. Vogel, A. S. Dickinson and V. Vesovic, *J. Chem. Phys.*, 2004, **121**, 4117–4122.
- 11 E. Bich, S. Bock and E. Vogel, *Physica A*, 2002, **311**, 59–79.
- 12 G. C. Groenenboom, P. E. S. Wormer, A. van der Avoird, E. M. Mas, R. Bukowski and K. Szalewicz, *J. Chem. Phys.*, 2000, **113**, 6702–6715.
- 13 R. Bukowski, K. Szalewicz, G. C. Groenenboom and A. van der Avoird, *J. Chem. Phys.*, 2006, **125**, 044301.
- 14 F. R. W. McCourt, J. J. M. Beenakker, W. E. Köhler and I. Kučšer, *Nonequilibrium Phenomena in Polyatomic Gases*, Oxford Science Publications, Oxford, 1990, vol. 1.
- 15 C. F. Curtiss, *J. Chem. Phys.*, 1981, **75**, 376–378.
- 16 C. F. Curtiss, *J. Chem. Phys.*, 1992, **97**, 1416–1419.
- 17 W.-K. Liu, Q. Zhang, S. L. Lin, X. Z. Yu and Y. C. Zhang, *Chin. J. Phys.*, 1994, **32**, 269–287.
- 18 B. Yang, S. Lin and S. Ding, *Int. J. Quantum Chem.*, 1997, **65**, 89–96.
- 19 S. D. Augustin and W. H. Miller, *J. Chem. Phys.*, 1974, **61**, 3155–3163.
- 20 M. S. Child, *Semiclassical Mechanics with Molecular Applications*, Clarendon Press, Oxford, 1991.
- 21 H. Goldstein, C. Poole and J. Saffko, *Classical Mechanics*, Addison Wesley, San Francisco, 3rd edn, 2002.
- 22 J. O. Hirschfelder, C. F. Curtiss and R. B. Bird, *Molecular Theory of Gases and Liquids*, Wiley, New York, 1964.
- 23 C. F. Curtiss and M. W. Tonsager, *J. Chem. Phys.*, 1985, **82**, 3795–3801.
- 24 E. L. Heck and A. S. Dickinson, *Comput. Phys. Commun.*, 1996, **95**, 190–220.
- 25 C. F. Curtiss, private communication, 1992.
- 26 W.-K. Liu and A. S. Dickinson, *Mol. Phys.*, 1990, **70**, 253–264.
- 27 R. A. Marcus, *J. Chem. Phys.*, 1972, **57**, 4903.
- 28 W. H. Miller, *Adv. Chem. Phys.*, 1974, **25**, 69.
- 29 S. M. Colwell, N. C. Handy and W. H. Miller, *J. Chem. Phys.*, 1978, **68**, 745–749.
- 30 R. Hellmann, E. Bich, E. Vogel and A. S. Dickinson, 2007, in preparation.

4.5 Calculation of the transport and relaxation properties of methane

4.5.1 I. Shear viscosity, viscomagnetic effects, and self-diffusion

Robert Hellmann, Eckard Bich, Eckhard Vogel, Alan S. Dickinson, Velisa Vesovic
J. Chem. Phys. **129**, 064302(1-13) (2008).

Alle generalisierten Streuquerschnitte und die Transporteigenschaften wurden selbst berechnet. Der eigene Anteil beträgt etwa 40%.

Reprinted with permission from Robert Hellmann, Eckard Bich, Eckhard Vogel, Alan S. Dickinson, Velisa Vesovic, J. Chem. Phys. 129, 6, 064302, 2008. Copyright 2008, American Institute of Physics.

Calculation of the transport and relaxation properties of methane. I. Shear viscosity, viscomagnetic effects, and self-diffusion

Robert Hellmann,¹ Eckard Bich,¹ Eckhard Vogel,¹ Alan S. Dickinson,^{2,a)} and Velisa Vesovic³

¹*Institut für Chemie, Universität Rostock, D-18059 Rostock, Germany*

²*School of Natural Sciences (Physics), Newcastle University, Newcastle upon Tyne NE1 7RU, United Kingdom*

³*Department of Earth Science and Engineering, Imperial College London, London SW7 2AZ, United Kingdom*

(Received 16 June 2008; accepted 24 June 2008; published online 11 August 2008)

Transport properties of pure methane gas have been calculated in the rigid-rotor approximation using the recently proposed intermolecular potential energy hypersurface [R. Hellmann *et al.*, *J. Chem. Phys.* **128**, 214303 (2008)] and the classical-trajectory method. Results are reported in the dilute-gas limit for shear viscosity, viscomagnetic coefficients, and self-diffusion in the temperature range of 80–1500 K. Compared with the best measurements, the calculated viscosity values are about 0.5% too high at room temperature, although the temperature dependence of the calculated values is in very good agreement with experiment between 210 and 390 K. For the shear viscosity, the calculations indicate that the corrections in the second-order approximation and those due to the angular-momentum polarization are small, less than 0.7%, in the temperature range considered. The very good agreement of the calculated values with the experimental viscosity data suggests that the rigid-rotor approximation should be very reasonable for the three properties considered. In general, the agreement for the other measured properties is within the experimental error. © 2008 American Institute of Physics. [DOI: 10.1063/1.2958279]

I. INTRODUCTION

The transport properties of gases are a direct consequence of molecular motion and the resulting exchange of angular momentum and energy between colliding molecules. For dilute systems, where only binary interactions are significant, transport properties can be related by means of formal kinetic theory¹ to generalized cross sections. These cross sections are determined by the dynamics of the binary collisions in the gas and can, in turn, be related to the intermolecular potential energy hypersurface that describes a particular molecular interaction.

It is now possible to calculate accurately the generalized cross sections, and hence the transport and relaxation properties, of simple molecular gases directly from the intermolecular potential, both for atom-diatom systems² and molecule-molecule systems.^{3–9} The accuracy of such calculations is generally commensurate with the best available experimental data and their usefulness self-evident. These calculations provide a stringent test of the accuracy of the potential surface^{2–9} and improve our insight into the dominant microscopic processes determining macroscopic transport and relaxation properties. Furthermore, at low and high temperatures where experimental data are of lower accuracy or nonexistent, the calculations can and do provide a better way of estimating transport properties.

In principle, one should perform calculations of transport and relaxation properties from the intermolecular potential

by employing a quantum-mechanical formalism. This is at present not computationally feasible for molecule-molecule systems, except possibly for pure hydrogen at low temperatures, and instead a classical description is used. The method of choice is a classical-trajectory calculation which is nowadays computationally fast and, more importantly, accurate, at the temperatures of interest to this work. The accuracy has been attested by a detailed comparison with the quantum calculations for the He–N₂ system,^{10,11} and the recent success in reproducing highly accurate viscosity measurements near room temperature in carbon dioxide⁷ is very encouraging.

The work presented in this paper is a continuation of our previous study^{7–9} and aims to improve our knowledge of the transport and relaxation properties of methane. Methane is relevant in a particularly wide variety of both scientific and engineering contexts: it is a feedstock for artificial diamond production; it is a significant greenhouse gas whose effects must be included in climate modeling; it is of importance in planetary studies as it occurs in Titan's atmosphere; being the main constituent of natural gas, it is a critical part of the current and future energy mix; methane is stored in permafrost hydrates, a plausible future energy source. Although transport property data for methane are available, see Sec. IV below, they cluster and are of acceptable accuracy only around room temperature.

In the present paper, we report on calculations of the shear viscosity, viscomagnetic effects, and the self-diffusion coefficient of methane in the temperature range of 80–1500 K. The relevant generalized cross sections have

^{a)}Electronic mail: a.s.dickinson@ncl.ac.uk.

been evaluated by means of the classical-trajectory calculations directly from the available intermolecular potential surface for the methane-methane interaction. For linear molecules, the working expressions for the generalized cross sections in terms of properties of individual trajectories were derived by Curtiss.¹² The extension to asymmetric tops (and hence spherical tops such as methane) has been provided.¹³

For these calculations, we have employed a recent *ab initio* potential¹⁴ that has been adjusted to and validated against accurate experimental second pressure virial coefficient data. The calculations were performed on the assumption that both methane molecules behave as rigid rotors. This assumption was dictated by the nature of the available intermolecular potential, which was developed using the zero-point vibrationally averaged configuration.

For the transport properties of interest, here it has been shown that, at least for carbon dioxide,⁷ the effects of the neglect of vibrational motion are small. For methane, the lowest vibrational frequency (1306 cm⁻¹) is much higher than that in carbon dioxide (667.3 cm⁻¹). Inelastic collisions resulting in exchange of vibrational energy are rare, and it is not expected that the vibrational state of the molecule would significantly influence the transport of momentum and mass in a fluid. Nevertheless, the approximate procedure for the inclusion of the effects of the vibrational degrees of freedom, described in our previous work,⁶⁻⁹ has been implemented to correct, where necessary, the generalized cross sections.

The availability of these classical-trajectory results allows for the first assessment of the accuracy of approximations for the collisions of spherical-top molecules. In particular, the widely used Mason–Monchick^{15,16} approximation (MMA), with quantal analog the infinite-order sudden¹⁷ approximation, is investigated along with the use of simply the spherical component of the molecule-molecule potential surface.

II. THEORY

A. Field-free properties

The shear viscosity η and self-diffusion coefficient D of a polyatomic gas at zero density and in the absence of external fields can be expressed as^{1,18}

$$\eta = \frac{k_B T}{\langle v \rangle_0} \frac{f_\eta^{(n)}}{\mathfrak{S}(2000)}, \quad (1)$$

$$D = \frac{k_B T}{nm \langle v \rangle_0} \frac{f_D^{(n)}}{\mathfrak{S}'(1000)}, \quad (2)$$

where $\langle v \rangle_0 = 4(k_B T / \pi m)^{1/2}$ is the average relative thermal speed, n is the number density, m is the molecular mass, T is the temperature, and k_B is Boltzmann's constant.

The customary notation¹ $\bar{\mathfrak{S}}_{p'q's't'}^{(p,q,s,t)}(\kappa)$ is employed in labeling the generalized cross sections, which include details of the dynamics of the binary encounters in the pure gas, with appropriate statistical averaging over the internal states

and translational energy. Thus, the indices p, p' and q, q' denote tensorial ranks in the reduced relative velocity \mathbf{W} and in the rotational angular momentum \mathbf{j} , respectively. *Barred* cross sections, as calculated here,^{19,20} are defined using the tensor rank κ given by $\kappa = \mathbf{p} + \mathbf{q} = \mathbf{p}' + \mathbf{q}'$. An alternative coupling, $\kappa = \mathbf{p} + \mathbf{p}' = \mathbf{q} + \mathbf{q}'$, yields what are often described^{1,21} as *unbarred* cross sections. As differences from the unbarred cross sections arise only when both p and q or both p' and q' are nonzero, we do not indicate the bar unless the barred and unbarred cross sections differ. Relations between the barred and unbarred cross sections can be obtained in Refs. 1 and 21. For notational convenience, when $p'q's't' = pqst$ just one row is retained. If the value of κ is unique, it is omitted. Diagonal and off-diagonal cross sections are referred to as transport [those $\mathfrak{S}(pqst)$ with $p \neq 0$] or relaxation [those $\mathfrak{S}(pqst)$ with $p=0$] and production or coupling cross sections, respectively. The quantities $\mathfrak{S}(2000)$ and $\mathfrak{S}'(1000)$ are the generalized viscosity and self-diffusion cross sections, respectively (see Ref. 7 for a discussion of the primed diffusion cross section in a pure gas).

The quantities $f_\eta^{(n)}$ and $f_D^{(n)}$ are n th-order correction factors and account for the effects of higher basis-function terms in the perturbation-series expansion of the solution of the Boltzmann equation.¹ In this work, we consider the second- and third-order approximations for viscosity only since for polyatomics no higher-order expressions for diffusion have been developed, although an estimate is available, based on the correction for spherical systems (see Sec. IV D 1). All the available analyses of calculations for monatomic^{22,23} and polyatomic³⁻⁹ species indicate that contributions of higher-order approximations for shear viscosity are, at most, $\pm(1-2)\%$.

For polyatomic molecules, the tensorial basis functions describing both velocity coupling^{1,24} and angular-momentum coupling^{1,25,26} should be included in the higher-order expansion. Traditionally,¹ these polarizations were treated separately, giving rise to separate expressions for the higher-order correction factors. Here, however, following Ref. 4, we have used a single expansion describing both couplings. In the second-order expansion for viscosity, one needs to include, apart from the first-order basis function Φ^{2000} , also basis functions Φ^{2010} and Φ^{2001} , corresponding to velocity coupling⁷ (note that contrary to Ref. 27, the basis function Φ^{2011} has not been considered here) and the basis function Φ^{0200} , allowing for angular-momentum coupling.²⁵

The higher-order viscosity correction factor is given, in general, as

$$f_\eta^{(n)} = \mathfrak{S}(2000) \frac{S_{11}^{(n)}}{S^{(n)}}, \quad (3)$$

with $S^{(n)}$ as the determinant of cross sections generated by the chosen basis and $S_{11}^{(n)}$ its minor. For $S^{(2)}$, we have

$$S^{(2)} = \begin{vmatrix} \mathfrak{S}(2000) & \mathfrak{S}\left(\begin{smallmatrix} 2000 \\ 2010 \end{smallmatrix}\right) & \mathfrak{S}\left(\begin{smallmatrix} 2000 \\ 2001 \end{smallmatrix}\right) & \mathfrak{S}\left(\begin{smallmatrix} 2000 \\ 0200 \end{smallmatrix}\right) \\ \mathfrak{S}\left(\begin{smallmatrix} 2010 \\ 2000 \end{smallmatrix}\right) & \mathfrak{S}(2010) & \mathfrak{S}\left(\begin{smallmatrix} 2010 \\ 2001 \end{smallmatrix}\right) & \mathfrak{S}\left(\begin{smallmatrix} 2010 \\ 0200 \end{smallmatrix}\right) \\ \mathfrak{S}\left(\begin{smallmatrix} 2001 \\ 2000 \end{smallmatrix}\right) & \mathfrak{S}\left(\begin{smallmatrix} 2001 \\ 2010 \end{smallmatrix}\right) & \mathfrak{S}(2001) & \mathfrak{S}\left(\begin{smallmatrix} 2001 \\ 0200 \end{smallmatrix}\right) \\ \mathfrak{S}\left(\begin{smallmatrix} 0200 \\ 2000 \end{smallmatrix}\right) & \mathfrak{S}\left(\begin{smallmatrix} 0200 \\ 2010 \end{smallmatrix}\right) & \mathfrak{S}\left(\begin{smallmatrix} 0200 \\ 2001 \end{smallmatrix}\right) & \mathfrak{S}(0200) \end{vmatrix}. \quad (4)$$

To calculate the second-order viscosity correction factor $f_{\eta}^{(2)}$ [Eq. (3)], we need knowledge of three transport cross sections, one relaxation cross section, and six production cross sections. In order to assess the relative importance of the velocity and the angular-momentum coupling, we introduce $f_{\eta}^{(2')}$, where only the two velocity couplings are included⁷ and $S^{(2')}$ is a 3×3 determinant.

To include the velocity coupling up to third order, with third-order correction $f_{\eta}^{(3)}$, one needs to add three further basis functions, namely, Φ^{2020} , Φ^{2011} , and Φ^{2002} , which result in a 7×7 determinant $S^{(3)}$ similar in structure to $S^{(2)}$.

It is also of interest to examine the relation between the diffusion coefficient and the viscosity as a function of temperature. It is customary in kinetic theory to do this by defining the dimensionless parameter A^* as^{22,24}

$$A^* = \frac{5 \mathfrak{S}(2000)}{6 \mathfrak{S}'(1000)}. \quad (5)$$

The studies carried out so far on monatomic²² and polyatomic species^{7,28} indicate that the value of this parameter is nearly independent of the potential surface and only weakly dependent on the reduced temperature. These properties have led traditionally to the use of the value of A^* to infer the values of binary diffusion coefficients from measurements of the viscosity of mixtures.²²

B. Field effects

The viscosity and diffusion coefficients of polyatomic molecules are influenced by the presence of magnetic and electrical fields. Although the effect of an external field is small,¹ it has been measured for a variety of molecules²⁹ and it provides a sensitive probe of the anisotropy of the potential. For methane, the effect of a magnetic field on the viscosity,^{30–35} but not on diffusion, has been measured. In the presence of a magnetic field, the coupling between velocity and angular momentum is partially destroyed and the resulting changes in the viscosity are observed both parallel (longitudinal effects) and normal (transverse effects) to the direction of the field.^{1,34}

Since methane is a spherical-top molecule, only the polarizations present for linear molecules, $\overline{\mathbf{jj}}$, $\overline{\mathbf{WWj}}$, and $\overline{\mathbf{WWjj}}$, need be considered.¹ The theoretical expressions in terms of relevant generalized cross sections have been derived for each polarization, but to the best of our knowledge, only in the spherical approximation (see Chap. 5.2.2 of Ref. 1). All the experimental evidence points to the dominance of

the $\overline{\mathbf{jj}}$ contribution and all the analyses of the experimental data, to extract the appropriate generalized cross sections, have been performed on this basis. We are now in a position to assess the validity of this assumption by calculating the contributions from the other two polarizations and hence can test the validity of the experimental analyses based solely on the $\overline{\mathbf{jj}}$ contribution.

In the presence of a magnetic field, the changes in the viscosity coefficient, which is now a tensorial quantity, can be described in terms of five, nonzero, independent ratios:¹ three, $\Delta \eta_i^+ / \eta$, $i=0,1,2$, describing the longitudinal effects, and two, η_i^- / η , $i=1,2$, describing the transverse effects. For conciseness, here we give an expression for one longitudinal viscomagnetic ratio only,

$$\frac{\Delta \eta_1^+}{\eta} = -\psi_{02} f(\xi_{02}) + \frac{5\psi_{21}}{4} f(\xi_{21}) - \frac{\psi_{22}}{24} [7f(\xi_{22}) + 6f(2\xi_{22})], \quad (6)$$

where $f(x) = x^2 / (1 + x^2)$, and we refer the reader to p. 322 of Ref. 1 for the similar expressions for the other four ratios. The dimensionless field parameter ξ_{pq} is given by

$$\xi_{pq} = \frac{g_{\text{rot}} \mu_N k_B T}{\hbar \langle v \rangle_0} \frac{1}{\mathfrak{S}(pq00)_0} \frac{B}{P}. \quad (7)$$

Here, g_{rot} is the rotational g -factor, μ_N is the nuclear magneton, B is the magnetic flux density, and P is the pressure. The unbarred cross section $\mathfrak{S}(pq00)_0$ can be calculated as the weighted average of the related barred cross sections [see Eqs. (5.2–11) of Ref. 1].

The quantity ψ_{pq} in Eq. (6), which governs the magnitude of the contribution from each polarization, is given by

$$\psi_{pq} = \frac{\mathfrak{S}\left(\begin{smallmatrix} pq00 \\ 2000 \end{smallmatrix}\right)^2}{\mathfrak{S}(2000)\mathfrak{S}(pq00)_0}. \quad (8)$$

Knowledge of the values of the three pairs, (ξ_{02}, ψ_{02}) , (ξ_{21}, ψ_{21}) , and (ξ_{22}, ψ_{22}) , which characterize the $\overline{\mathbf{jj}}$, $\overline{\mathbf{WWj}}$, and $\overline{\mathbf{WWjj}}$ polarizations, respectively, is sufficient to describe all five viscomagnetic ratios.

When the $\overline{\mathbf{jj}}$ polarization is dominant, as has been assumed in previous analyses of the experimental data,^{32–35} only three cross sections, $\mathfrak{S}(2000)$, $\mathfrak{S}(0200)$, and $\mathfrak{S}\left(\begin{smallmatrix} 0200 \\ 2000 \end{smallmatrix}\right)$, govern the viscomagnetic effect. Then independent knowledge of the viscosity cross section, $\mathfrak{S}(2000)$, allows, after some judicious manipulation of the experimental viscomagnetic data, for the estimation of the other two: namely, $\mathfrak{S}(0200)$ and $|\mathfrak{S}\left(\begin{smallmatrix} 0200 \\ 2000 \end{smallmatrix}\right)|$.

III. CLASSICAL TRAJECTORY CALCULATIONS

The classical-trajectory calculations were performed using an extension of the TRAJECT software code for linear molecules.¹⁹ The linear-molecule program was utilized for the calculations performed for pure nitrogen,^{3,6,36} carbon monoxide,^{4–6,28} and carbon dioxide.^{7–9,37} This code has been modified²⁰ to allow for the additional variables and averaging needed for asymmetric tops. The methane molecule was

represented as a rigid spherical top forming a regular tetrahedron with bond lengths of 0.1099 nm. For a given total energy, translational plus rotational, classical trajectories describing the collision of two molecules were obtained by integrating Hamilton's equations from pre- to postcollisional values. The initial values of the momenta for the relative motion and for the rotation of the two molecules, as well as the angles defining their relative orientation, were obtained using a pseudorandom number generator. The total-energy-dependent generalized cross sections can be represented as 13-dimensional integrals, which were evaluated by means of a Monte Carlo procedure.

The classical trajectories were determined at 29 values of the total energy, divided into three ranges. In each range the energy values were chosen as the pivot points for Chebyshev interpolation in order to facilitate calculations of the cross sections at a number of temperatures.^{20,38} The highest energy used was 40 000 K, which is more than sufficient for the temperature range considered in this work. At each energy up to 1 000 000 classical trajectories were evaluated. The number of trajectories had to be reduced toward lower energies, those of the order of the well depth and smaller, because the low-energy trajectories require much longer computing times. For example, at 20 K, the lowest energy considered, only 20 000 trajectories were calculated. The precision of the calculations was assessed by estimating the convergence of the final temperature-dependent generalized cross sections as a function of the number of trajectories used. Furthermore, the symmetry of production cross sections under time reversal,

$$\mathfrak{S}\left(\begin{matrix} p & q & s & t \\ p' & q' & s' & t' \end{matrix}\right) = (-1)^{q+q'} \mathfrak{S}\left(\begin{matrix} p' & q' & s' & t' \\ p & q & s & t \end{matrix}\right),$$

allows the comparison between two cross sections calculated by two independent expressions. This was used as a further indicator of precision.

The classical trajectories have been evaluated using a recently developed six-dimensional *ab initio* intermolecular potential energy hypersurface.¹⁴ To reduce the computational effort generating the surface, the CH₄ molecule was represented as a rigid spherical top. The form of the potential function is fully described in the original publication¹⁴ and only the main characteristics will be summarized here.

Seventeen different angular orientations of the two methane molecules were considered with sixteen different center-of-mass separations for each orientation, resulting in 272 grid points. All calculations were performed within the counterpoise-corrected supermolecule approach at the CCSD(T) level of theory using the aug-cc-pVTZ and aug-cc-pVQZ basis sets. The resulting energies were extrapolated to the complete basis-set limit and an analytical site-site potential function, with nine sites per CH₄ molecule, was then fitted to the extrapolated interaction energies. (A spherical-harmonic expansion is not essential for a classical calculation.) A semiempirical correction for zero-point vibrational effects was also developed and incorporated into the final potential. This correction used only one adjustable parameter, chosen so that the calculated second pressure virial coefficient agreed with the best experimental value at room

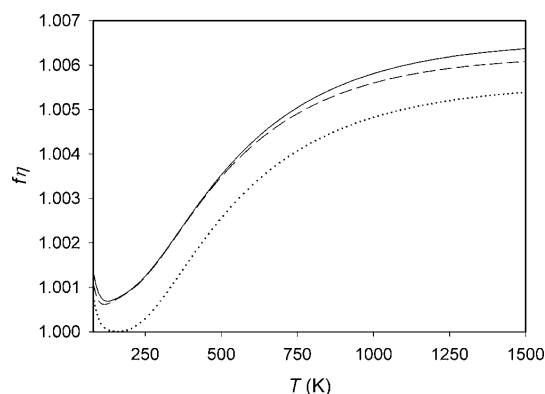


FIG. 1. Comparison of the values of the two second-order corrections: $f_{\eta}^{(2)}$ (---); $f_{\eta}^{(2')}$ (.....); and of the third-order correction $f_{\eta}^{(3)}$ (—), for the shear-viscosity coefficient.

temperature. The resulting potential exhibits a maximum in the well depth of 286 K, occurring at a separation of 0.362 nm, see the discussion in Ref. 14. The spherically averaged potential has a well depth of 170 K at a separation of 0.420 nm. This new potential is the current state-of-the-art representation of methane-methane, attested by the excellent agreement with the available experimental second virial data over the temperature range of 160–620 K.¹⁴

IV. RESULTS

The calculations of the generalized cross sections were performed on a modern Linux workstation and took about 11 days of CPU time. The evaluation of the classical trajectories was the most time-consuming part in the computations.

All the calculated transport and relaxation cross sections are characterized by the customary monotonic decrease with temperature, while some of the production cross sections exhibit a maximum at low temperature. The values of the transport and relaxation cross sections are, on average, an order of magnitude larger than those of the production cross sections. Based on the convergence tests, the precision of most of the calculated transport and relaxation cross sections is estimated to be better than $\pm 0.1\%$, while the precision of most of the production cross sections is estimated to be better than $\pm 1.0\%$ at all except the very lowest temperatures.

Tables of all the generalized cross sections, and the shear viscosity and self-diffusion coefficients calculated in this work, have been deposited with the Electronic Physics Auxiliary Publication Service.³⁹

A. Shear viscosity

1. Higher-order contributions

Before the comparison with experiment, we consider first the magnitude and temperature dependence of the higher-order contributions to the shear viscosity. Figure 1 illustrates the temperature dependence of the second- and third-order viscosity correction factors $f_{\eta}^{(2)}$, $f_{\eta}^{(2')}$, and $f_{\eta}^{(3)}$ (see Sec. II A).

Above temperatures of about 140 K, the magnitude of the higher-order correction factors increases with temperature, as shown in Fig. 1, reaching a saturation value at about 1400 K. The overall impact is small, however, and even at the highest temperature of the viscosity measurements⁴⁰ on methane (1050 K), the correction factor $f_{\eta}^{(3)}$ will contribute only 0.6% to viscosity. The contribution of the third order itself to the overall correction factor is very small, at most 0.04% in viscosity. The second-order correction factor shows a similar temperature dependence. Its magnitude is similar to that observed for nitrogen³⁶ and carbon monoxide,⁴ but smaller than that found for carbon dioxide.⁷

By comparing the values of $f_{\eta}^{(2)}$ and $f_{\eta}^{(2')}$ (see Sec. II A) it can be seen that the angular-momentum coupling is responsible for at most 0.1% of the increase in the methane viscosity, this contribution being nearly independent of temperature. This angular-momentum coupling contribution is much smaller for methane than for any of the other three gases studied, consistent with the production cross section $|\mathcal{G}_{0200}^{(2000)}|$ being smaller for methane.

To account for the vibrational degrees of freedom, we have also corrected, using the methodology described in Ref. 8, the cross sections $\mathcal{G}_{20s't'}^{(20s't')}$ with $t+t' \neq 0$ that enter the higher-order correction factors. The overall impact is small, at most 0.01% in viscosity at the highest temperature studied.

2. Comparison with experiment

A critical evaluation of viscosity measurements on methane, based on the data available in 2000, was carried out⁴¹ and used as the basis of a correlation in the limit of zero density, derived from experiments at low density. To derive values in the limit of zero density, either isothermal values as a function of density were extrapolated to this limit or individual values at low density were corrected to it using the Rainwater–Friend theory for the initial density dependence of the viscosity.^{42–44} Near to room temperature the correlation was largely based on the experimental data by Schley *et al.*⁴⁵ available at the time, but published in 2004. These data, determined using a vibrating-wire viscometer in a relative manner for isotherms between 260 and 360 K (at 20 K intervals) up to maximum pressures of 29 MPa, are characterized by uncertainties of $\pm 0.2\%$ at low densities.

Since the development of this correlation, two groups have published new experimental data. Evers *et al.*⁴⁶ used a rotating-cylinder viscometer for absolute measurements between 233 and 523 K, up to pressures of 30 MPa, with uncertainties of the results at low densities estimated by the authors to be $\pm 0.15\%$. For the comparison with theory, their low-density values were corrected to zero density, allowing for the initial density dependence of the viscosity.

The most recent measurements were carried out by May *et al.*⁴⁷ with single-capillary and two-capillary viscometers between 211 and 392 K at low densities in a manner that allowed direct extrapolation to the zero-density limit. They based their results for methane on zero-density viscosity values for helium in the same temperature range obtained from *ab initio* calculations using quantum mechanics and

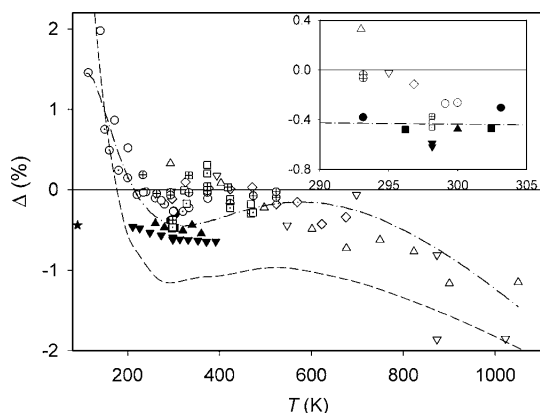


FIG. 2. Deviations of experimental zero-density viscosity coefficients from values theoretically calculated for CH_4 . Deviations are defined as $\Delta = (\eta_{\text{exp}} - \eta_{\text{cal}}) / \eta_{\text{cal}}$. Experimental data: (●) Kestin and Yata (Ref. 53), (○) Clarke and Smith (Ref. 54), (△) Dawe *et al.* (Ref. 40), (■) Kestin *et al.* (Ref. 55), (□) Hellemans *et al.* (Ref. 56), (▽) Maitland and Smith (Ref. 57), (★) Slyusar *et al.* (Ref. 58), (◇) Timrot *et al.* (Ref. 59), (○) Gough *et al.* (Ref. 60), (□) Kestin *et al.* (Ref. 61), (⊞) Abe *et al.* (Ref. 62), (⊕) Evers *et al.* (Ref. 46), (▲) Schley *et al.* (Ref. 45), (▼) May *et al.* (Ref. 47). Experimentally based data: (---), values for the zero-density correlation of methane by Vogel *et al.* (Ref. 41); (----), values calculated by means of an isotropic potential (fitted to experimental data) by Zarkova *et al.* (Ref. 63).

statistical mechanics,⁴⁸ particularly on a reference value for helium at 298 K at zero density $[\eta_{0,298.15}^{\text{He}} = (19.833 \pm 0.016) \mu\text{Pa s}]$,⁴⁹ derived from the best measurement (19.842 $\mu\text{Pa s}$),^{50,51} and the best *ab initio* calculations (19.8245 $\mu\text{Pa s}$) known at that time.⁴⁸ Note that the viscosity values for helium used by May and co-workers^{47,49} are in excellent agreement with analogous results calculated very recently by our group from *ab initio* calculations and the corresponding kinetic theory (19.8262 $\mu\text{Pa s}$ at 298.15 K).⁵² This independent calculation lends support to the uncertainty of $\pm 0.1\%$ claimed by May *et al.*⁴⁷ for their experimental data in the complete temperature range.

The comparison between the results of the best available measurements^{40,45–47,53–62} and the values calculated using the new intermolecular potential surface of methane is illustrated in Fig. 2. The results at ambient temperature, additionally shown in the inset of the figure, provide an accurate and a distinct experimental data set.

The figure demonstrates that the experimental data of May *et al.*,⁴⁷ measured in the temperature range of 210–390 K, deviate from the calculated values by $-(0.52 \text{ to } 0.66)\%$. This indicates that either the rigid-rotor assumption needs to be relaxed or the intermolecular potential needs some minor improvement. Nevertheless, it reveals also that the potential reproduces appropriately the temperature dependence of the viscosity in this temperature range. Over a more limited temperature range, 260–360 K, the temperature dependence of the viscosity data of Schley *et al.*⁴⁵ is consistent with that of the experiments by May *et al.*,⁴⁷ although the values of Schley *et al.*⁴⁵ are higher by about 0.1%. This difference arises because Schley *et al.*⁴⁵ used an

old reference value for the viscosity of argon⁶⁴ for the calibration of their vibrating-wire viscometer at room temperature.

Experimental data reported by Kestin and co-workers^{53,55,56,61,62} differ at ambient temperature from the values of May *et al.*⁴⁷ by about +(0.1 to 0.2)%. However, at temperatures between 320 and 380 K the experimental data of Kestin and co-workers,^{56,61,62} estimated uncertainty less than $\pm 0.3\%$, deviate from the experiments of May *et al.*⁴⁷ by up to +0.9%. Although the values at higher temperatures agree better with the calculated values for the potential surface of methane, they are definitely incorrect. The differences from the reliable data of May *et al.*⁴⁷ and Schley *et al.*⁴⁵ are due to a temperature measurement error in the experiments of Kestin and co-workers with their high-temperature oscillating-disk viscometer.⁶⁵ This error was extensively discussed by Vogel *et al.*⁴⁴ and was confirmed by comparison of standard viscosity values for helium⁵² and neon,⁶⁶ obtained from *ab initio* calculations and using the appropriate kinetic theory, with viscosity data of these gases measured by Kestin and co-workers using the same viscometer.

Figure 2 illustrates also that the experimental values of Evers *et al.*⁴⁶ are too high by about 0.5%–0.6% compared to the experimental data of May *et al.*,⁴⁷ Schley *et al.*,⁴⁵ Kestin and Yata,⁵³ and Kestin *et al.*⁵⁵ Although the results of the measurements on helium and neon reported by Evers *et al.*⁴⁶ in the same paper are in excellent agreement with the reliable data of other investigators (see Refs. 52 and 66), for methane this is not the case. Hence, their agreement with the calculated values is most likely fortuitous.

The experimental values of Smith and co-workers,^{40,54,57,60} obtained from relative measurements with capillary viscometers, reveal a characteristic behavior when compared with the calculated values at low and at high temperatures. The differences for the data by Clarke and Smith,⁵⁴ as well as by Gough *et al.*,⁶⁰ increase by about +(1.0 to 1.5)% with decreasing temperature down to 150 K. On the contrary, the data of Dawe *et al.*,⁴⁰ as well as of Maitland and Smith,⁵⁷ are too high by 1% at room temperature and too low by about 1% at 1000 K. Similar differences were found for the viscosity data of this group in the case of helium and neon (see again Refs. 52 and 66). The lower accuracy of these data makes them unsuitable for the validation of the *ab initio* potential energy surface.

The viscosity correlation in the limit of zero density proposed by Vogel *et al.*⁴¹ (shown in Fig. 2) displays increasing deviations from the calculated values both at low and high temperatures, consistent with the behavior of the experimental data which were used to generate the correlation. As has already been discussed, these data are of lower accuracy than the calculated values.

We believe that the present calculations provide the best estimate of the viscosity of methane at temperatures lower than 200 K. At temperatures up to 400 K, the calculated values are characterized by nearly the same temperature dependence as the experimental data of May *et al.*⁴⁷ Hence, we expect that the calculated values exhibit the proper temperature dependence also for temperatures above 400 K, unlike

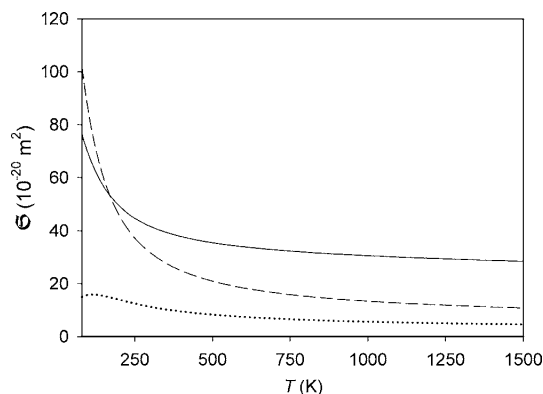


FIG. 3. Comparison of the values of the generalized cross sections $\Xi(2000)$ (—); $\Xi(0200)$ (---), and $10 \times \Xi_{2000}^{(0200)}$ (.....).

most of the experimental data. Based on the comparison with the available data, especially around room temperature, we estimate the uncertainty of the computed values to be of the order of $\pm 1\%$ at 80 and 1500 K.

Finally, Fig. 2 also shows a comparison with values recommended as reference data by Zarkova *et al.*⁶³ These values were calculated via an isotropic three-parameter Lennard-Jones ($n=6$) potential obtained from a multiproperty fit to experimental data for the second pressure and acoustic virial coefficients, as well as for viscosity and self-diffusion at low density. They agree neither with the calculated values nor with the experimental data and hence cannot be considered as standard viscosity values for methane.

B. Viscomagnetic effects

1. Relevant cross sections

In order to compare with the experimental data we have calculated the values of the relevant viscomagnetic coefficients in two ways. First, we employed the full expressions [see, for example, Eq. (6)] that include the contributions of all three polarizations, and second we made use only of the terms corresponding to the dominant $\mathbf{j}\mathbf{j}$ polarization.

Figure 3 illustrates the temperature dependence of the three cross sections that govern the viscomagnetic effect, assuming that the $\mathbf{j}\mathbf{j}$ polarization is dominant. All three cross sections decrease with increasing temperature, most markedly at low temperatures. At temperatures below about 175 K, the $\Xi(0200)$ cross section, which describes the relaxation/decay of the angular-momentum polarization, is larger than the viscosity cross section $\Xi(2000)$, while at high temperatures the reverse is true. Hence, a relaxation of angular momentum is more favorable than exchange of linear momentum at lower temperatures. The production cross section is about one to two orders of magnitude smaller than the cross sections $\Xi(0200)$ and $\Xi(2000)$, indicating that collisions are ineffective in coupling the angular-momentum polarization to that in velocity.

The cross sections that govern the $\overline{\mathbf{W}\mathbf{W}\mathbf{j}}$ and $\overline{\mathbf{W}\mathbf{W}\mathbf{j}\mathbf{j}}$ polarizations show similar qualitative features to those seen in Fig. 3. Since the relaxation cross sections $\Xi(pq00)_0$ for all

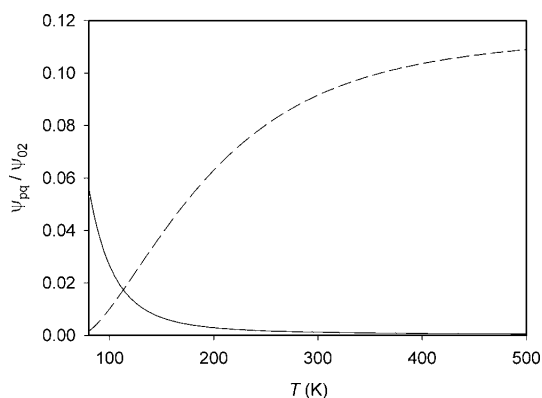


FIG. 4. Ratios of the viscomagnetic parameters ψ_{pq}/ψ_{02} for $pq=21$ (----) and $pq=22$ (—) as a function of temperature.

three polarizations are comparable, the contribution of each polarization to the viscomagnetic effect is driven primarily by the magnitude of $\mathfrak{S}_{2000}^{(pq00)}$. Figure 4 illustrates the temperature dependence of the ratios ψ_{pq}/ψ_{02} , $pq=21, 22$. As these ratios are small over most of the range studied, we can conclude that the $\mathbf{j}\mathbf{j}$ polarization is indeed dominant. However, at low temperature some influence of the $\mathbf{W}\mathbf{W}\mathbf{j}\mathbf{j}$ polarization will be present, while at high temperature, dominated by contributions from the repulsive part of the potential surface, there will be a small contribution of the $\mathbf{W}\mathbf{W}\mathbf{j}$ polarization to the viscomagnetic coefficients. Because of cancellations between the different contributions to the observables [see Eq. (6)], some viscomagnetic coefficients are more sensitive to the secondary polarizations than the relatively small values of these ratios would suggest.

2. Comparison with experiment

Six independent measurements of viscomagnetic effects in methane,^{30–35} carried out in two different laboratories, have been performed using capillary viscometers operating in a null mode. Korving and co-workers^{30,31} were the first to report that methane gas exhibits a viscomagnetic effect. They carried out the measurements of the sum of two longitudinal coefficients, $-(\Delta\eta_1^+ + \Delta\eta_2^+)/2\eta$, at room temperature at values of the magnetic flux density over pressure (B/P) of up to 0.004 T/Pa ($\equiv 5.4$ kOe/torr). We have not used these data in our analysis as they are in good agreement with the later work³⁵ that reports the experimental data for the same combination of the longitudinal coefficients over a larger range of (B/P) values.

Hulsman *et al.*³² carried out measurements on the transverse coefficients at room temperature at (B/P) values up to 0.005 T/Pa ($\equiv 7$ kOe/torr). Korving³³ measured, also at room temperature but with a stronger magnet, two longitudinal coefficients, $-\Delta\eta_1^+/\eta$ and $-(\Delta\eta_2^+ - \Delta\eta_1^+)/\eta$, at (B/P) values of as high as 0.024 T/Pa ($\equiv 32$ kOe/torr). Subsequently, Hulsman *et al.*³⁴ performed a further set of measurements to evaluate the longitudinal coefficients at room temperature in the (B/P) range up to 0.007 T/Pa ($\equiv 9.6$ kOe/torr). They used an experimental arrangement with an electromagnet

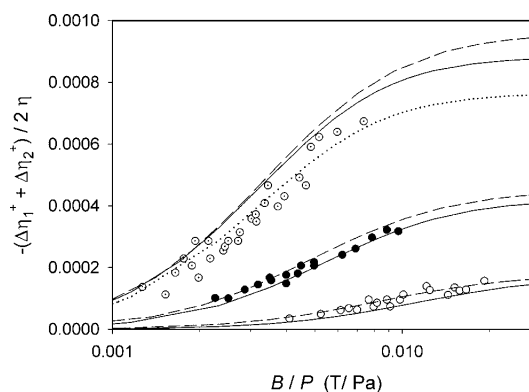


FIG. 5. Comparison of the measurements of Burgmans *et al.* (Ref. 35) of the viscomagnetic effect $-(\Delta\eta_1^+ + \Delta\eta_2^+)/2\eta$ with the present calculations. Experimental values: (○), 154 K; (●), 224 K; (○), 293 K. To distinguish between the curves for the different temperatures they are vertically shifted by dividing them by 4, 2, and 1, respectively. Calculations: (----), $\mathbf{j}\mathbf{j}$ polarization only; (—), full calculation; (⋯⋯⋯), full calculation with the value of the $\mathfrak{S}_{2000}^{(0200)}$ cross section reduced by 6%.

that could be rotated to realize different orientations between the magnetic field and the flow. Measurements at three different orientations allowed them to evaluate $-\Delta\eta_0^+/\eta$, $-\Delta\eta_1^+/\eta$, and $-(\Delta\eta_2^+ + \Delta\eta_0^+)/2\eta$. Finally, Burgmans *et al.*³⁵ measured the sum of two longitudinal coefficients, $-(\Delta\eta_1^+ + \Delta\eta_2^+)/2\eta$, at three temperatures, 154, 224, and 293 K, for (B/P) values of up to 0.02 T/Pa ($\equiv 25$ kOe/torr).

Of these six experiments, only that of Hulsman *et al.*³⁴ measured the value of $-\Delta\eta_0^+/\eta$. This ratio is the one ratio vanishing for a $\mathbf{j}\mathbf{j}$ polarization¹ and hence is expected to be much smaller than the other four ratios.

By examining the variation of the viscosity coefficients as a function of (B/P), the four more recent studies concluded that $\mathbf{j}\mathbf{j}$ polarization was dominant and used this as the basis of their analyses. They extracted the relevant cross sections $\mathfrak{S}(0200)$ and $|\mathfrak{S}_{2000}^{(0200)}|$ by fitting the theoretical expressions, such as Eq. (6), to the (B/P) dependence of their observations, treating the values of these two cross sections as adjustable parameters. For this purpose, Burgmans *et al.*³⁵ used the experimental data over the whole measured (B/P) domain, while Hulsman and co-workers^{32,34} and Korving³³ preferred a fit that gave more weight to the measurements at lower values of (B/P).

Figures 5–8 show the comparison between the calculated values of the viscomagnetic coefficients and the available experimental data (read from the published figures). No uncertainty estimate is given by the authors for the experimental data, although it is stated³⁴ that relative viscosity changes of 2×10^{-6} could be detected.

We start by comparing the calculated values to the data of Korving³³ and Burgmans *et al.*,³⁵ both sets of workers having measured the longitudinal viscomagnetic coefficients. The agreement with the data of Burgmans *et al.*³⁵ (Fig. 5) is, in general, good, although the calculated values overestimate the data at room temperature, particularly at the lower (B/P) values. This is in contrast to the comparison with the experi-

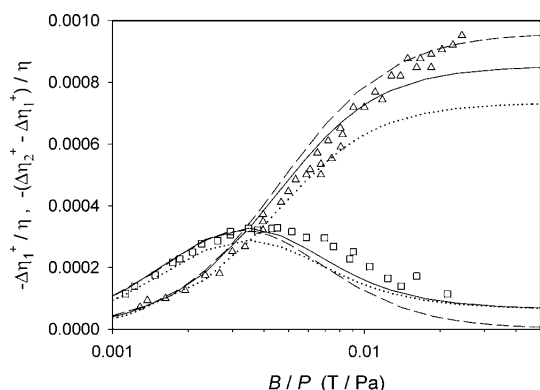


FIG. 6. Comparison of the measurements of Korving (Ref. 33) at 293 K of the viscomagnetic effect with the present calculations: (Δ), $-\Delta\eta_1^+/\eta$ and (\square), $-(\Delta\eta_2^+ - \Delta\eta_1^+)/\eta$. Calculations: (----), $\bar{j}\bar{j}$ polarization only; (—), full calculation; and (·····), full calculation with the value of the $\mathcal{E}_{2000}^{(0200)}$ cross section reduced by 6%.

mental data of Korving³³ at room temperature for different combinations of longitudinal coefficients, as shown in Fig. 6. In the (B/P) range corresponding to the observations of Burgmans *et al.*³⁵ only a slight overestimate is observed, while at high (B/P) values, a slight underestimate occurs. The calculations predict well both the (B/P) dependence and the magnitude of the measured coefficients.

Figure 7 illustrates the comparison between the calculated values and the experimental data of Hulsman *et al.*³⁴ Excellent agreement is observed for the $-\Delta\eta_0^+/\eta$ ratio, which is very encouraging as for this ratio the normally dominant $\bar{j}\bar{j}$ polarization does not contribute and only the $\overline{W}\overline{W}\bar{j}$ and $\overline{W}\overline{W}\bar{j}\bar{j}$ polarizations contribute; the former, $\overline{W}\overline{W}\bar{j}$, being the more important. The agreement with experimental data pertaining to the $-\Delta\eta_1^+/\eta$ ratio is also very good, with a slight overestimate at high (B/P) values. However, the computed values overestimate the combination $-(\Delta\eta_2^+ + \Delta\eta_0^+)/\eta$. This may not be surprising since the values of the combination

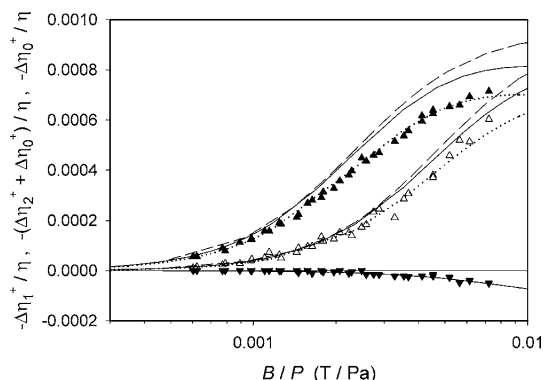


FIG. 7. Comparison of the measurements of Hulsman *et al.* (Ref. 34) at 293 K of the viscomagnetic effect with the present calculations: (Δ), $-\Delta\eta_1^+/\eta$; (\blacktriangle), $-(\Delta\eta_2^+ + \Delta\eta_0^+)/\eta$; and (\blacktriangledown), $-\Delta\eta_0^+/\eta$. Calculations: (----), $\bar{j}\bar{j}$ polarization only; (—), full calculation; and (·····), full calculation with the value of the $\mathcal{E}_{2000}^{(0200)}$ cross section reduced by 6%.

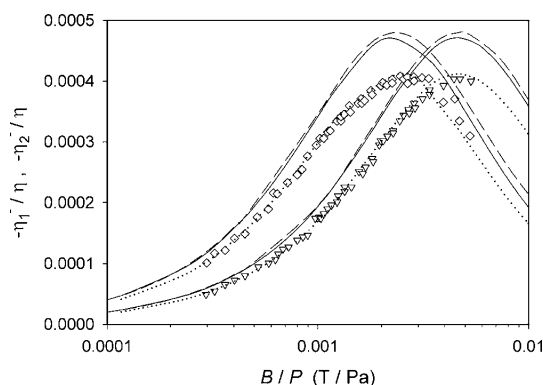


FIG. 8. Comparison of the measurements of Hulsman *et al.* (Ref. 32) at 293 K of the viscomagnetic effect with the present calculations: (∇), $-\eta_1^-/\eta$ and (\diamond), $-\eta_2^-/\eta$. Calculations: (----), $\bar{j}\bar{j}$ polarization only; (—), full calculation; and (·····), full calculation with the value of the $\mathcal{E}_{2000}^{(0200)}$ cross section reduced by 6%.

$-(\Delta\eta_1^+ + \Delta\eta_2^+)/2\eta$ derived from the experimental data of Hulsman *et al.*³⁴ are consistent with the room temperature data of Burgmans *et al.*³⁵ Hence, the overestimate observed in Figs. 5 and 7 is primarily due to the overestimate of the $-\Delta\eta_2^+/\eta$ ratio.

The significance of the overestimation of the room-temperature data of Burgmans *et al.*³⁵ is better seen when comparing the calculations with the data of Hulsman *et al.*³² (see Fig. 8), pertaining to the two transverse coefficients. We predict well the (B/P) dependence of the curves and the position of both maxima, but not the magnitude of the peaks. Hence, the overestimation of both the experimental data of Burgmans *et al.*³⁵ and of Hulsman *et al.*³² at 293 K can be attributed to the magnitude of the calculated production cross section $\mathcal{E}_{2000}^{(0200)}$ being too large.

In fact, if we reduce the calculated value of this cross section by 6%, the agreement with the experimental data from both experiments^{32,35} would be essentially perfect, as illustrated in Figs. 5, 7, and 8. However, the agreement with the data of Korving³³ would become worse, especially for the $-(\Delta\eta_2^+ - \Delta\eta_1^+)/\eta$ ratio, as illustrated in Fig. 6. It is not clear which data set is the more accurate, but at present it appears unlikely that the error in the anisotropy of the proposed methane potential is such that the production cross section at room temperature would be in error by 6%. However, the evidence of additional anisotropy-sensitive properties needs to be assessed before any firm conclusions can be drawn. Also, it should be borne in mind that the accuracy of neither the lowest-order kinetic theory nor of the spherical approximation used for analyzing these experiments has ever been assessed.

The calculations of the viscomagnetic coefficients based on the truncated expressions that include only the $\bar{j}\bar{j}$ polarization are generally in good agreement with the full calculations. Within the experimental temperature and (B/P) range studied, the secondary polarization is at most at the 5% level, hence supporting the experimentally based observation that the $\bar{j}\bar{j}$ polarization is dominant. The only exception is the combination of two longitudinal coefficients measured by

Korving³³ and Hulsman *et al.*³⁴ Figure 6 illustrates that at high (B/P) values the \overline{WWj} polarization becomes significant, especially when the difference of two viscomagnetic coefficients is measured. In this case, at the highest (B/P) value measured (0.024 T/Pa), the \overline{WWj} polarization contributes about 12%.

The excellent agreement between the calculated and the measured values for these coefficients, together with excellent agreement with the results of Hulsman *et al.*³⁴ for the $-\Delta\eta_0^*/\eta$ ratio, gives further support to the accuracy of the potential surface. In the latter case, a combination of five cross sections was required to predict the viscomagnetic effect, although a fortuitous cancellation of errors cannot be discounted.

Hulsman and co-workers,^{32,34} Korving,³³ and Burgmans *et al.*³⁵ have all made use of their data, with the assumption of only \overline{jj} polarization, to evaluate the $\mathfrak{S}(0200)$ cross section at 293 K. The values obtained range^{32–35} from 30 to 33.0 \AA^2 , with error bars³⁵ of $\pm 2.5 \text{\AA}^2$. Our calculated value is 32.3 \AA^2 , in excellent agreement with the experimental values. At 224 K, our calculated value of 41.2 \AA^2 is again in excellent agreement with the experimental value³⁵ of $40 \pm 3 \text{\AA}^2$. At the lowest temperature (154 K), the calculated value of 58.3 \AA^2 is outside the error limits of the value obtained from the experiments,³⁵ $67 \pm 5 \text{\AA}^2$. However, the comparison is misleading. In order to extract the value of $\mathfrak{S}(0200)$ from the experimental data, $\mathfrak{S}(0200)$ was treated as one of the two adjustable parameters. The (B/P) range of the experimental data, all far from the peak, is such that it does not allow for a unique determination of the two cross sections, rather a number of different combinations will give reasonably good fits, as our calculated values attest (see Fig. 5). So, in this case the comparison at the cross-section level is not appropriate.

Burgmans *et al.*³⁵ quoted the values of the production cross sections $|\mathfrak{S}_{2000}^{(0200)}|$, with uncertainties of about 6%. At both 293 and 224 K, the calculated values are just outside their uncertainties, while at 154 K, as already discussed, it is not sensible to make such a comparison.

C. Self-diffusion

There have been measurements^{67,68} of the diffusion of isotopomers of methane (excluding those involving deuterium or tritium) that have been used to infer the self-diffusion coefficient of methane. We recall that for a spherical potential the classical diffusion cross section, for a specified potential, is independent of the reduced mass of the interacting particles. Hence, differences between the various isotopomers can arise only due to the anisotropic part of the potential surface. Since the substitution of ^{13}C for ^{12}C does not change the moment of inertia of CH_4 , the calculation of $\mathfrak{S}'(1000)$ should be particularly insensitive to this substitution.

Using mass spectrometry, Winn and Ney⁶⁷ measured the diffusion of $^{13}\text{CH}_4$ in $^{12}\text{CH}_4$ at room temperature with an estimated uncertainty of $\pm 2.7\%$. Later, using the same technique, Winn⁶⁸ made measurements over the temperature range of 90–353 K, with an uncertainty estimated at $\pm 2\%$ at

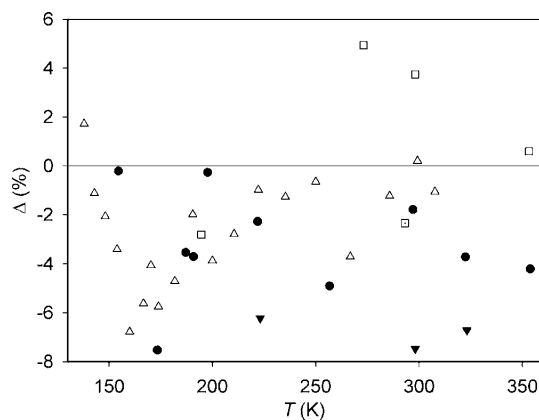


FIG. 9. Deviations of experimental self-diffusion coefficients from values theoretically calculated for CH_4 . Deviations are defined as $\Delta = [(nmD_{\text{exp},0})/(nmD_{\text{cat},0}) - 1]$. Experimental data: (\square) Winn and Ney (Ref. 67), (\square) Winn (Ref. 68), (\bullet) Dawson *et al.* (Ref. 70), (\triangle) Oosting and Trappeniers (Ref. 71), and (\blacktriangledown) Harris (Ref. 72).

and above room temperature, but up to $\pm 8\%$ at the lowest temperature. Both sets of results that were reported included a correction⁶⁹ for the effect of the mass difference between $^{13}\text{CH}_4$ and $^{12}\text{CH}_4$ on $\langle v \rangle_0$ [see Eq. (2)].

In addition to these measurements using isotopically labeled molecules, there are also results available for self-diffusion in $^{12}\text{CH}_4$ from NMR spin-echo experiments.^{70–72} We are unaware of any kinetic-theory analysis beyond first order for this type of measurement. The NMR measurements of Dawson *et al.*⁷⁰ span from 155 to 354 K and their own estimate of the total uncertainty is $\pm 6\%$, while the measurements of Oosting and Trappeniers⁷¹ cover the range from 138 to 308 K with uncertainty estimated⁷³ as $\pm 2\%$. As neither of these NMR experiments explicitly extrapolated their density-dependent results to the limit of zero density, we have made the extrapolation.

Harris⁷² performed measurements at 223.15, 298.15, and 323.15 K. We have refitted the density dependence of these measurements and hence extrapolated to the zero-density limit. Harris⁷² notes that when account is taken of the differences in calibration and of mutual uncertainties, the three sets of NMR measurements^{70–72} are consistent.

Theory and experiment are compared in Fig. 9. The room-temperature measurement of Winn and Ney⁶⁷ is consistent with the calculated values. The measurement of Winn⁶⁸ at 90 K, estimated uncertainty $\pm 8\%$, has been omitted from Fig. 9 as the deviation was very large, about 25%. Winn⁶⁸ commented that, due to the low density required, some difficulties were encountered in making measurements at this temperature. For helium-nitrogen mixtures, rotor constant of 2 cm^{-1} and only even changes in j allowed, the difference between classical and quantal results at 100 K was only 0.7%.¹⁰ Hence, while quantal effects in methane, rotor constant of 5.25 cm^{-1} , are becoming more significant at 90 K, these effects are unlikely to explain the 25% deviation. The data of Winn⁶⁸ at higher temperature, 195–353 K, are

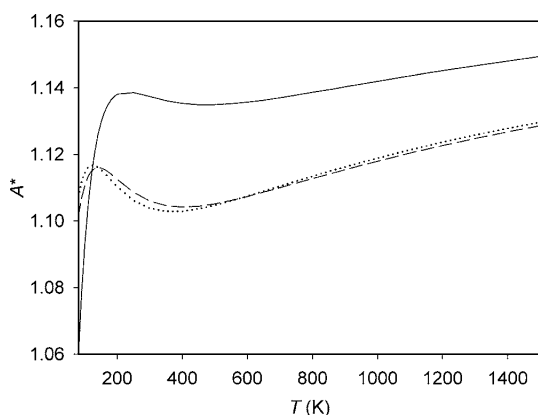


FIG. 10. Comparison of calculated values for the dimensionless parameter A^* [see Eq. (5)] as a function of temperature: (—), classical trajectories (CT); (---), Mason-Monchick approximation (MMA); and (·····), spherical-potential approximation (SPA).

broadly in agreement with the calculated values, but the deviations are up to twice his estimated uncertainty.

Apart from the measurement at 173 K, the measurements of Dawson *et al.*⁷⁰ are consistent with theory. For the data of Oosting and Trappeniers,⁷¹ the differences are generally rather larger than the authors' uncertainties, although the agreement at temperatures higher than 223 K is reasonable, with deviations just outside the quoted uncertainties. The most recent observations, those of Harris,⁷² lie about 7% below our calculated values.

Comparisons with measurements of self-diffusion in CD_4 and other isotopomers will be considered in a separate publication.

Figure 10 illustrates the temperature dependence of the calculated value of the A^* parameter, as defined by Eq. (5). The value of A^* initially increases rapidly with temperature, reaching a value of 1.14 at about 250 K. The subsequent change with increasing temperature is slow and A^* reaches a value of 1.15 at 1500 K.

It is interesting to note that there is no evidence of the leveling off with increasing reduced temperature observed for the other molecular gases studied.^{4,7,36} However, the magnitude of A^* for methane and its temperature variation are in line with what has been observed for nitrogen,²⁸ carbon monoxide,²⁸ and carbon dioxide.⁷

D. Approximate methods

Until the advent of fast classical-trajectory calculations, it was not possible to compute transport properties without approximating either the dynamics of the collision or the intermolecular potential surface. The two most common approximations were (i) use of Mason-Monchick/infinite-order-sudden-type methods and (ii) use of only the spherical component of the intermolecular potential. It is of interest to examine the reliability of these approximations for estimating the viscosity and self-diffusion coefficients of a spherical top such as methane.

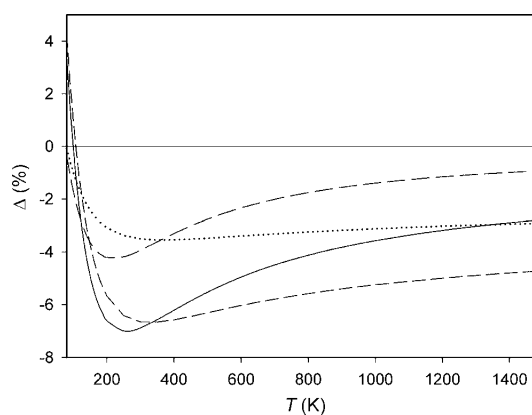


FIG. 11. Deviations of the values of generalized cross sections calculated using the Mason-Monchick approximation (MMA) and the spherical-potential approximation (SPA) from values obtained with classical trajectories (CT). Deviations defined as $\Delta = (\mathcal{G}_{\text{CT}} - \mathcal{G}_{\text{approx}}) / \mathcal{G}_{\text{CT}}$. (—), MMA $\mathcal{G}'(1000)$, (---), MMA $\mathcal{G}(2000)$, (·····), SPA $\mathcal{G}'(1000)$, and (--- · ---), SPA $\mathcal{G}(2000)$.

1. Mason-Monchick approximation

The MMA (Refs. 15 and 16) with quantal analog the infinite-order sudden approximation (IOSA),¹⁷ has a long history and has been tested most recently for the calculation of the viscosity of carbon dioxide.³⁷ The MMA/IOSA approximates the dynamics of the binary collision by making two physically reasonable assumptions:^{15-17,74,75} (i) the amount of rotational energy exchanged between the molecules is, on average, much smaller than the relative kinetic energy of the pair; and (ii) the relative orientation of the molecules can be treated as fixed during the part of the collision that is dominant in determining transport properties. Invoking both these assumptions, one can express the viscosity and self-diffusion generalized cross sections as averages over all possible orientations of the corresponding monoatomic collision integrals,²² evaluated at fixed orientation.

We have performed the MMA calculations for both the $\mathcal{G}(2000)$ and $\mathcal{G}'(1000)$ generalized cross sections, as described in Ref. 37, but with additional averaging for the spherical-top potential surface. Figure 11 illustrates the deviations from the CT values of the cross sections evaluated using the MMA. At low temperatures the cross sections evaluated by the MMA/IOSA decrease marginally more slowly with temperature than the corresponding CT values. This leads at low values of T^* to the underestimation of the CT cross sections by the MMA cross sections followed, at around $T^* = 0.5-0.6$, by an overestimation. Here, T^* is the usual reduced temperature, given by $T^* = k_B T / \epsilon$, where ϵ is the well depth of the spherical component of the interaction. At higher reduced temperatures the deviations, as expected, become progressively smaller. The maximum deviations observed for the $\mathcal{G}(2000)$ and $\mathcal{G}'(1000)$ cross sections are -4.2% and -7.0% , respectively.

Similar trends have been observed for the other molecules studied: N_2 ,⁷⁶ CO ,²⁸ and CO_2 .³⁷ The deviations, defined as $\Delta'(2000)$ (see Ref. 37), decrease with decreasing anisotropy of the intermolecular potential. Among the four

gases studied, methane has the smallest anisotropy, as measured by the value of the rotational relaxation number. Hence, in the high-temperature limit, methane exhibits the smallest deviations. For instance, at 1000 K the rotational relaxation numbers for CO₂, CO, N₂ and CH₄ are 2.6, 4.4, 5.3, and 13.1, respectively,^{37,77} while the $\Delta'(2000)$ values are -15.0%, -10.8%, -7.6%, and -3.9%, respectively. That methane possesses the smallest anisotropy is also consistent with the calculations of the contribution of the angular-momentum coupling to the second-order correction for the viscosity discussed in Sec. IV A.

In addition, the larger error in the MMA values for $\mathfrak{S}'(1000)$ cross sections than for $\mathfrak{S}(2000)$ cross sections has been observed previously^{28,37,76} in molecular gases and in atom-molecule mixtures, see, for example, Ref. 78.

Figure 10 shows the values of the ratio A^* [see Eq. (5)] evaluated by the MMA, and the values obtained by the CT calculations. The MMA values of A^* are, on average, 1.4%–3% lower, the deviations decreasing slightly with temperature.

The MMA calculation has also been used to approximate the second-order correction factor for viscosity $f_{\eta}^{(2')}$ (see Sec. II A). This small correction mimics the behavior of the corresponding CT value illustrated in Fig. 1, attaining a value of 1.006 at 1500 K. The differences in the value of the second-order correction factor between the two calculations are 0.1% at most.

In the MMA, the second-order viscosity correction factor reduces to the monatomic result.²⁸ Hence, one would expect the corresponding second-order self-diffusion correction factor $f_D^{(2')}$, not yet derived for molecular gases, also to reduce to the monatomic result. We have made use of this assumed limiting behavior to estimate the value of $f_D^{(2')}$ using the MMA. This correction shows very similar temperature dependence to its viscosity counterpart, attaining a value of 1.006 at 1500 K. Given that the experimental values of the self-diffusion coefficient have an accuracy of the order of $\pm 2\%$ at best, see Sec. IV C, the second-order correction for self-diffusion can be neglected, if our assumptions are indeed satisfied.

2. Spherical approximation

We have also calculated the viscosity and self-diffusion generalized cross sections using only the spherical average of the full intermolecular potential surface. The deviations of the values obtained using the spherically averaged potential from the CT values, shown in Fig. 11, follow the same trends as those shown for the MM approximation, also included in the figure. The deviations have maximum values for $\mathfrak{S}(2000)$ and $\mathfrak{S}'(1000)$ of -3.5% and -6.6%, respectively, and remain approximately constant in the high-temperature limit. The temperature dependences of the deviations for both cross sections are very similar to those obtained using the MMA (see Fig. 11). At low temperatures, both cross sections obtained using the spherically averaged potential are 1.0% below the equivalent MMA values, while at high temperatures they overestimate the MMA values by 2.0%. Using the spherical approximation to evaluate A^* , the deviations

from the CT values are almost indistinguishable from those obtained in the MM approximation (see Fig. 10).

V. SUMMARY AND CONCLUSIONS

We have performed the first calculations of the shear viscosity, viscomagnetic effects, and self-diffusion using a full anisotropic rigid-rotor methane-methane potential energy hypersurface. The classical-trajectory method has been employed to evaluate the generalized cross sections required in the best available kinetic theory.

For the shear viscosity, existing kinetic theory^{4,25,27} has been extended to include third-order contributions. The comparison with the most accurate experimental data by May *et al.*⁴⁷ shows relatively constant deviations of -0.5% to -0.7% in the temperature range of 210–390 K, indicating that the temperature dependence of the viscosity is very well described by the calculations. This allows accurate extrapolations of the viscosity to temperatures outside the range of the measurements by May *et al.*⁴⁷ We estimate that the uncertainty of the computed viscosity values is approximately $\pm 1\%$ at 80 and 1500 K.

The difference between the third-order and second-order correction factors to the shear viscosity was found to be very small, below 0.04%, suggesting that the second-order results are adequate for comparison with current experiments or applications. Velocity-coupling contributions²⁷ dominated the angular-momentum-coupling contributions²⁵ to second-order effects, which in total never exceeded 0.65%.

The viscomagnetic effects are due to angular-momentum transfer and hence probe directly the anisotropic part of the potential surface. For these effects, the contributions from the three most likely polarizations¹ ($\mathbf{j}\mathbf{j}$, $\mathbf{W}\mathbf{W}\mathbf{j}$, and $\mathbf{W}\mathbf{W}\mathbf{j}\mathbf{j}$) have been investigated, although previous analyses of the measurements^{30–35} have concentrated on the $\mathbf{j}\mathbf{j}$ polarization. While this polarization was indeed found to be dominant, the contribution of the $\mathbf{W}\mathbf{W}\mathbf{j}$ polarization was observed at high values of (B/P) , indicating that for the accurate analysis of the experimental data both polarizations need to be considered. Overall, the agreement with the measurements^{32–35} was generally reasonable, bearing in mind that no information on the experimental uncertainty was available and that experimental data from different laboratories were not entirely consistent. The general (B/P) dependence and the position of the maxima for the transverse coefficients were predicted well, but in a number of instances, the magnitude of the viscomagnetic effect was overestimated. It is difficult at this stage to attribute the observed overestimate to the uncertainty in the anisotropy of the potential rather than to uncertainties in the experimental data, or the first-order kinetic theory employed in the analysis, as additional anisotropy-sensitive properties are currently being evaluated.⁷⁷

The experimental data for self-diffusion are characterized by much larger differences from the calculated values than occurred for the shear viscosity. This behavior is due to the difficulties of the measurements, resulting in uncertainties estimated by the authors to be between $\pm 2\%$ and $\pm 8\%$. The comparison illustrates that some of these estimates may still be overoptimistic. Hence, the experimental data do not

provide a critical test of the potential energy surface. The calculated self-diffusion coefficients, even without higher-order corrections, should be distinctly more reliable than the experimental data.

The parameter A^* attains a value in the range of 1.14–1.15 above room temperature, displaying a weak temperature dependence in line with the other gases studied. The viscosity and self-diffusion cross sections were also evaluated by means of the MM/IOS approximation.^{15–17} The differences observed are smaller than those occurring for the linear molecules N_2 ,⁷⁶ CO ,²⁸ and CO_2 ,³⁷ consistent with the methane potential surface being less anisotropic. Use of only the spherical component of the full potential surface provides estimates of the viscosity and self-diffusion cross sections comparable with the MMA/IOSA values.

ACKNOWLEDGMENTS

This work was financially supported by the German Research Foundation (Deutsche Forschungsgemeinschaft), Grant No. VO 499/14–1.

- ¹F. R. W. McCourt, J. J. M. Beenakker, W. E. Köhler, and I. Kučer, *Nonequilibrium Phenomena in Polyatomic Gases* (Oxford Science, Oxford, 1990), Vol. 1.
- ²A. K. Dham, F. R. W. McCourt, and A. S. Dickinson, *J. Chem. Phys.* **127**, 054302 (2007).
- ³E. L. Heck and A. S. Dickinson, *Mol. Phys.* **81**, 1325 (1994).
- ⁴E. L. Heck and A. S. Dickinson, *Physica A* **217**, 107 (1995).
- ⁵E. L. Heck and A. S. Dickinson, *Physica A* **218**, 305 (1995).
- ⁶E. Bich, S. Bock, and E. Vogel, *Physica A* **311**, 59 (2002).
- ⁷S. Bock, E. Bich, E. Vogel, A. S. Dickinson, and V. Vesovic, *J. Chem. Phys.* **117**, 2151 (2002).
- ⁸S. Bock, E. Bich, E. Vogel, A. S. Dickinson, and V. Vesovic, *J. Chem. Phys.* **120**, 7987 (2004).
- ⁹S. Bock, E. Bich, E. Vogel, A. S. Dickinson, and V. Vesovic, *J. Chem. Phys.* **121**, 4117 (2004).
- ¹⁰F. R. W. McCourt, V. Vesovic, W. A. Wakeham, A. S. Dickinson, and M. Mustafa, *Mol. Phys.* **72**, 1347 (1991).
- ¹¹V. Vesovic, W. A. Wakeham, A. S. Dickinson, F. R. W. McCourt, and M. Thachuk, *Mol. Phys.* **84**, 553 (1995).
- ¹²C. F. Curtiss, *J. Chem. Phys.* **75**, 1341 (1981).
- ¹³A. S. Dickinson, R. Hellmann, E. Bich, and E. Vogel, *Phys. Chem. Chem. Phys.* **9**, 2836 (2007).
- ¹⁴R. Hellmann, E. Bich, and E. Vogel, *J. Chem. Phys.* **128**, 214303 (2008).
- ¹⁵L. Monchick and E. A. Mason, *J. Chem. Phys.* **35**, 1676 (1961).
- ¹⁶E. A. Mason and L. Monchick, *J. Chem. Phys.* **36**, 1622 (1962).
- ¹⁷G. A. Parker and R. T. Pack, *J. Chem. Phys.* **68**, 1585 (1978).
- ¹⁸J. Millat, V. Vesovic, and W. A. Wakeham, in *Transport Properties of Fluids: Their Correlation, Prediction and Estimation*, edited by J. Millat, J. H. Dymond, and C. A. Nieto de Castro (Cambridge University Press, Cambridge, UK, 1996), Chap. 4, pp. 29–65.
- ¹⁹E. L. Heck and A. S. Dickinson, *Comput. Phys. Commun.* **95**, 190 (1996).
- ²⁰R. Hellmann, E. Bich, and A. S. Dickinson (unpublished).
- ²¹W. E. Köhler and G. W. 't Hooft, *Z. Naturforsch.* **34a**, 1255 (1979).
- ²²G. C. Maitland, M. Rigby, E. B. Smith, and W. A. Wakeham, *Intermolecular Forces: Their Origin and Determination* (Clarendon, Oxford, 1987).
- ²³J. Kestin, K. Knierim, E. A. Mason, B. Najafi, S. T. Ro, and M. Waldman, *J. Phys. Chem. Ref. Data* **13**, 229 (1984).
- ²⁴J. H. Ferziger and H. G. Kaper, *The Mathematical Theory of Transport Processes in Gases* (North-Holland, Amsterdam, 1972).
- ²⁵Y. Kagan and A. M. Afanasev, *Sov. Phys. JETP* **14**, 1096 (1962).
- ²⁶L. A. Viehland, E. A. Mason, and S. I. Sandler, *J. Chem. Phys.* **68**, 5277 (1978).
- ²⁷G. C. Maitland, M. Mustafa, and W. A. Wakeham, *J. Chem. Soc., Faraday Trans. 2* **79**, 1425 (1983).
- ²⁸E. L. Heck, A. S. Dickinson, and V. Vesovic, *Chem. Phys. Lett.* **240**, 151 (1995).
- ²⁹L. J. F. Hermans, in *Status and Future Developments in the Study of Transport Properties*, NATO Advanced Studies Institute, Series C: Mathematical and Physical Sciences Vol. 361, edited by W. A. Wakeham, A. S. Dickinson, F. R. W. McCourt, and V. Vesovic (Kluwer, Dordrecht, 1992), pp. 155–174.
- ³⁰J. Korving, H. Hulsman, H. F. P. Knaap, and J. J. M. Beenakker, *Phys. Lett.* **17**, 33 (1965).
- ³¹J. Korving, H. Hulsman, G. Scoles, H. F. P. Knaap, and J. J. M. Beenakker, *Physica (Amsterdam)* **36**, 177 (1967).
- ³²H. Hulsman, E. J. van Waasdijk, A. L. J. Burgmans, H. F. P. Knaap, and J. J. M. Beenakker, *Physica (Amsterdam)* **50**, 53 (1970).
- ³³J. Korving, *Physica (Amsterdam)* **50**, 27 (1970).
- ³⁴H. Hulsman, F. G. van Kuik, K. W. Walstra, H. F. P. Knaap, and J. J. M. Beenakker, *Physica (Amsterdam)* **57**, 501 (1972).
- ³⁵A. L. J. Burgmans, P. G. van Ditzhuyzen, H. F. P. Knaap, and J. J. M. Beenakker, *Z. Naturforsch.* **28a**, 835 (1973).
- ³⁶E. L. Heck, A. S. Dickinson, and V. Vesovic, *Mol. Phys.* **83**, 907 (1994).
- ³⁷V. Vesovic, S. Bock, E. Bich, E. Vogel, and A. S. Dickinson, *Chem. Phys. Lett.* **377**, 106 (2003).
- ³⁸H. O'Hara and F. J. Smith, *J. Comput. Phys.* **5**, 328 (1970).
- ³⁹See EPAPS Document No. E-JCPSA6-129-607830 for electronic files that contain these tables. For more information on EPAPS, see <http://www.aip.org/pubservs/epaps.html>
- ⁴⁰R. A. Dawe, G. C. Maitland, M. Rigby, and E. B. Smith, *Trans. Faraday Soc.* **66**, 1955 (1970).
- ⁴¹E. Vogel, J. Wilhelm, C. Küchenmeister, and M. Jaeschke, *High Temp. - High Press.* **32**, 73 (2000).
- ⁴²J. C. Rainwater and D. G. Friend, *Phys. Rev. A* **36**, 4062 (1987).
- ⁴³E. Bich and E. Vogel, *Int. J. Thermophys.* **12**, 27 (1991).
- ⁴⁴E. Vogel, C. Küchenmeister, E. Bich, and A. Laesecke, *J. Phys. Chem. Ref. Data* **27**, 947 (1998).
- ⁴⁵P. Schley, M. Jaeschke, C. Küchenmeister, and E. Vogel, *Int. J. Thermophys.* **25**, 1623 (2004).
- ⁴⁶C. Evers, H. W. Lösch, and W. Wagner, *Int. J. Thermophys.* **23**, 1411 (2002).
- ⁴⁷E. F. May, R. F. Berg, and M. R. Moldover, *Int. J. Thermophys.* **28**, 1085 (2007).
- ⁴⁸J. J. Hurly and J. B. Mehl, *J. Res. Natl. Inst. Stand. Technol.* **112**, 75 (2007).
- ⁴⁹E. F. May, M. R. Moldover, R. F. Berg, and J. J. Hurly, *Metrologia* **43**, 247 (2006).
- ⁵⁰R. F. Berg, *Metrologia* **42**, 11 (2005).
- ⁵¹R. F. Berg, *Metrologia* **43**, 183 (2006).
- ⁵²E. Bich, R. Hellmann, and E. Vogel, *Mol. Phys.* **105**, 3035 (2007).
- ⁵³J. Kestin and J. Yata, *J. Chem. Phys.* **49**, 4780 (1968).
- ⁵⁴A. G. Clarke and E. B. Smith, *J. Chem. Phys.* **51**, 4156 (1969).
- ⁵⁵J. Kestin, S. T. Ro, and W. A. Wakeham, *Trans. Faraday Soc.* **67**, 2308 (1971).
- ⁵⁶J. M. Hellems, J. Kestin, and S. T. Ro, *Physica (Amsterdam)* **65**, 376 (1973).
- ⁵⁷G. C. Maitland and E. B. Smith, *Trans. Faraday Soc.* **70**, 1191 (1974).
- ⁵⁸V. P. Slyusar, N. S. Rudenko, and V. M. Tretyakov, *Fiz. Zhidk. Sostoyaniya* **2**, 100 (1974).
- ⁵⁹D. L. Timrot, M. A. Serednitskaya, and M. S. Bespalov, *Dokl. Akad. Nauk SSSR* **4**, 799 (1975).
- ⁶⁰D. W. Gough, G. P. Matthews, and E. B. Smith, *J. Chem. Soc., Faraday Trans. 1* **72**, 645 (1976).
- ⁶¹J. Kestin, H. E. Khalifa, and W. A. Wakeham, *J. Chem. Phys.* **67**, 4254 (1977).
- ⁶²Y. Abe, J. Kestin, H. E. Khalifa, and W. A. Wakeham, *Physica A* **93**, 155 (1978).
- ⁶³L. Zarkova, U. Hohm, and M. Damyanova, *J. Phys. Chem. Ref. Data* **35**, 1331 (2006).
- ⁶⁴J. Kestin and W. Leidenfrost, *Physica (Amsterdam)* **25**, 1033 (1959).
- ⁶⁵R. DiPippo, J. Kestin, and J. H. Whitelaw, *Physica (Amsterdam)* **32**, 2064 (1966).
- ⁶⁶E. Bich, R. Hellmann, and E. Vogel, *Mol. Phys.* **106**, 813 (2008).
- ⁶⁷E. B. Winn and E. P. Ney, *Phys. Rev.* **72**, 77 (1947).
- ⁶⁸E. B. Winn, *Phys. Rev.* **80**, 1024 (1950).
- ⁶⁹F. Hutchinson, *J. Chem. Phys.* **17**, 1081 (1949).

- ⁷⁰R. Dawson, F. Khoury, and R. Kobayashi, *AIChE J.* **16**, 725 (1970).
- ⁷¹P. H. Oosting and N. J. Trappeniers, *Physica (Amsterdam)* **51**, 418 (1971).
- ⁷²K. R. Harris, *Physica A* **94**, 448 (1978).
- ⁷³C. J. Gerritsma and N. J. Trappeniers, *Physica (Amsterdam)* **51**, 365 (1971).
- ⁷⁴A. S. Dickinson, *Comput. Phys. Commun.* **17**, 51 (1979).
- ⁷⁵D. J. Kouri, in *Atom-Molecule Collision Theory: A Guide for the Experimentalist*, edited by R. B. Bernstein (Plenum, New York, 1979), Chap. 9, pp. 301–358.
- ⁷⁶E. L. Heck, A. S. Dickinson, and V. Vesovic, *Chem. Phys. Lett.* **204**, 389 (1993).
- ⁷⁷R. Hellmann, E. Bich, E. Vogel, A. S. Dickinson, and V. Vesovic (unpublished).
- ⁷⁸F. A. Gianturco, M. Venanzi, and A. S. Dickinson, *J. Chem. Phys.* **93**, 5552 (1990).

4.5.2 II. Thermal conductivity, thermomagnetic effects, volume viscosity, and nuclear-spin relaxation

Robert Hellmann, Eckard Bich, Eckhard Vogel, Alan S. Dickinson, Velisa Vesovic
J. Chem. Phys. **130**, 124309(1-11) (2009).

Alle generalisierten Streuquerschnitte sowie die Wärmeleitfähigkeit und die Volumenviskosität wurden selbst berechnet. Der eigene Anteil beträgt etwa 40%.

Reprinted with permission from Robert Hellmann, Eckard Bich, Eckhard Vogel, Alan S. Dickinson, Velisa Vesovic, J. Chem. Phys. 130, 12, 124309, 2009. Copyright 2009, American Institute of Physics.

Calculation of the transport and relaxation properties of methane. II. Thermal conductivity, thermomagnetic effects, volume viscosity, and nuclear-spin relaxation

Robert Hellmann,¹ Eckard Bich,² Eckhard Vogel,¹ Alan S. Dickinson,^{2,a)} and Velisa Vesovic³

¹*Institut für Chemie, Universität Rostock, D-18059 Rostock, Germany*

²*School of Chemistry, Newcastle University, Newcastle upon Tyne NE1 7RU, United Kingdom*

³*Department of Earth Science and Engineering, Imperial College London, London SW7 2AZ, United Kingdom*

(Received 14 January 2009; accepted 20 February 2009; published online 25 March 2009)

Transport properties of pure methane have been calculated in the rigid-rotor approximation using the recently proposed intermolecular potential energy hypersurface [R. Hellmann *et al.*, *J. Chem. Phys.* **128**, 214303 (2008)] and the classical-trajectory method. Results are reported in the dilute-gas limit for the temperature range of 80–1500 K. The calculated thermal conductivity values are in very good agreement with the measured data and correlations. In the temperature range of 310–480 K the calculated values underestimate the best experimental data by 0.5%–1.0%. We suggest that the calculated values are more accurate, especially at low and high temperatures, than the currently available correlations based on the experimental data. Our results also agree well with measurements of thermal transpiration and of the thermomagnetic coefficients. We have shown that although the dominant contribution to the thermomagnetic coefficients comes from the \mathbf{W}_{jj} polarization in the spherical approximation, the contribution of a second polarization, \mathbf{W}_j , cannot be neglected nor can a full description of the \mathbf{W}_{jj} polarization. The majority of the volume viscosity measurements around room temperature are consistent with the calculated values but this is not the case at high and low temperatures. However, for nuclear-spin relaxation the calculated values consistently exceed the measurements, which are mutually consistent within a few percent. © 2009 American Institute of Physics. [DOI: 10.1063/1.3098317]

I. INTRODUCTION

The accurate calculation of the transport and relaxation properties of simple molecular gases directly from the intermolecular potential energy hypersurface has recently become possible.^{1–8} These calculations provide not only a stringent test of the accuracy of the potential surface but also an accurate data set at low and high temperatures, where experimental data are more difficult to measure and hence are of lower accuracy or nonexistent. For methane, which is relevant to a wide variety of topical issues including climate change and energy sustainability and may even have been observed⁹ on an exoplanet, the provision of accurate transport and relaxation properties is important since this reduces the uncertainty in modeling processes where methane properties play a major role.

In the first paper of this series,¹⁰ to be referred to as I, results of classical-trajectory calculations for the shear viscosity, viscomagnetic effects, and self-diffusion of pure methane have been reported. In the present paper we report on calculations for thermal conductivity, thermomagnetic coefficients, volume viscosity, and nuclear-spin relaxation. As methane has an isotropic polarizability, no depolarized Rayleigh light scattering measurements, available for other mol-

ecules studied,^{1,4,8} are possible. Thus this work completes the evaluation of transport and relaxation properties of methane. The calculations of these properties are based on formal kinetic theory, which provides a unified description of transport and relaxation phenomena in terms of generalized cross sections.¹¹ The relevant cross sections have been evaluated by means of classical-trajectory calculations directly from the recent *ab initio* potential.¹² This potential has been adjusted to and validated against accurate experimental second pressure virial coefficient data and subsequently its reliability confirmed using accurate viscosity data.¹⁰

The intermolecular potential employed was developed using the zero-point vibrationally averaged configuration, which limited the collision dynamics to treating methane molecules as rigid rotors. Although it was shown¹⁰ that results using the rigid-rotor assumption are consistent with experiment for the viscosity and self-diffusion coefficients of methane at temperatures up to 1050 K, for thermal conductivity the neglect of energy transport by vibrationally excited molecules becomes more questionable. In order to estimate the influence on the thermal conductivity of neglecting vibration we have employed the approximation described in our previous work.^{5–8} Hence we have corrected, where necessary, the generalized cross sections obtained from the classical-trajectory calculations based on the rigid-rotor assumption. For carbon dioxide the approximate procedure for

^{a)}Electronic mail: a.s.dickinson@newcastle.ac.uk. Author to whom correspondence should be addressed.

the inclusion of the effects of the vibrational degrees of freedom has been shown⁷ to lead to good agreement with the available experimental data on the thermal conductivity and the thermomagnetic effect.

The transport and relaxation properties are reported in the temperature range of 80–1500 K. It is not *a priori* clear that the classical-trajectory method will retain its accuracy at low temperatures. Comparison with the quantum calculations for the He–N₂ system^{13,14} indicates that the accuracy of the classical-trajectory calculations deteriorates rapidly with decreasing temperature. However, as there exist data for thermal conductivity and thermomagnetic effects somewhat below 100 K, these data can be used to estimate the accuracy of classical-trajectory calculations at such temperatures.

In Sec. II we summarize the basic theory employed and the results are discussed in Sec. III. A summary and conclusions are presented in Sec. IV.

II. THEORY

A. Thermal conductivity

The thermal conductivity λ of a polyatomic gas at zero density and in the absence of external fields can be expressed as¹¹

$$\lambda = \frac{5k_B^2 T}{2m\langle v \rangle_0} \frac{\mathfrak{S}(1001) - 2r\mathfrak{S}\left(\begin{smallmatrix} 1001 \\ 1010 \end{smallmatrix}\right) + r^2\mathfrak{S}(1010)}{\mathfrak{S}(1010)\mathfrak{S}(1001) - \mathfrak{S}\left(\begin{smallmatrix} 1001 \\ 1010 \end{smallmatrix}\right)^2} f_\lambda^{(n)}, \quad (1)$$

where $\langle v \rangle_0 = 4(k_B T / \pi m)^{1/2}$ is the average relative thermal speed, m is the molecular mass, T is the temperature, and k_B is Boltzmann's constant. The quantities $\mathfrak{S}(1010)$, $\mathfrak{S}(1001)$, and $\mathfrak{S}\left(\begin{smallmatrix} 1001 \\ 1010 \end{smallmatrix}\right)$ are generalized cross sections, and the notation and conventions employed are fully described elsewhere.^{10,11} The parameter r is given by

$$r = \left(\frac{2c_{\text{int}}}{5k_B} \right)^{1/2}, \quad c_{\text{int}} = c_{\text{rot}} + c_{\text{vib}}. \quad (2)$$

Here c_{int} is the contribution of both the rotational, c_{rot} , and the vibrational, c_{vib} , degrees of freedom to the isochoric heat capacity c_V .

The quantity $f_\lambda^{(n)}$ is the n th-order correction factor for the thermal conductivity and accounts for the effects of higher basis-function terms in the perturbation-series expansion of the solution of the Boltzmann equation.¹¹ Only the second-order correction factor has been derived for thermal conductivity, but it includes contributions from both velocity coupling^{11,15} and angular-momentum coupling.^{11,16,17} In second order the velocity coupling involves the inclusion of all the members of the usual basis set¹¹ Φ^{10st} with $s+t \leq 2$. The resulting expressions¹⁸ for thermal conductivity involve 15 generalized cross sections. The contribution due to angular momentum is dominated by the polarization $\mathbf{W}\mathbf{j}\mathbf{j}$ and requires the inclusion of the tensorial basis function $\Phi^{1200|1}$ in the expansion. The expressions for the thermal conductivity have been given by Viehland *et al.*¹⁷ and more recently, in an equivalent but simpler form by Bich *et al.*⁵ Our previous

calculations^{2,3,5,7} indicate that both contributions are small, of the order of $\pm(1-2)\%$, and numerous calculations based on spherical potentials¹⁹ confirm this for the velocity-coupling contribution. Hence the combined second-order contribution, $f_\lambda^{(2)}$, can be estimated by adding the two contributions. In total, a knowledge of 18 generalized cross sections is required to calculate the overall second-order contribution using the expressions given by Maitland *et al.*,¹⁸ Viehland *et al.*,¹⁷ or Bich *et al.*⁵

Traditionally the solution of Boltzmann's equation has been sought by using the basis functions that belong to the two-flux basis set and results in the expression given by Eq. (1).¹¹ For thermal conductivity this amounts to treating the transport of translational and internal energy separately. Thijsse *et al.*,²⁰ by using the same basis functions but choosing different scalars, constructed an equivalent total-energy basis set. In the first approximation in this basis the thermal conductivity, λ^{10E} , is governed by only one generalized cross section,

$$\lambda^{10E} = \frac{5k_B^2 T}{2m\langle v \rangle_0} \frac{1+r^2}{\mathfrak{S}(10E)}. \quad (3)$$

This new cross section, $\mathfrak{S}(10E)$, is a linear combination of the three cross sections used to describe the thermal conductivity in the two-flux approach,^{7,11,20}

$$\mathfrak{S}(10E) = \frac{1}{1+r^2} \left[\mathfrak{S}(1010) + 2r\mathfrak{S}\left(\begin{smallmatrix} 1010 \\ 1001 \end{smallmatrix}\right) + r^2\mathfrak{S}(1001) \right]. \quad (4)$$

For subsequent analysis of the experimental data on the closely related process of thermal transpiration we give here the expression for the dimensionless translational Eucken factor f_{tr} in terms of the relevant cross sections,

$$f_{\text{tr}} \equiv \frac{2m\lambda_{\text{tr}}}{3k_B\eta} \approx \frac{5}{3} \frac{\mathfrak{S}(2000) \left[\mathfrak{S}(1001) - r\mathfrak{S}\left(\begin{smallmatrix} 1001 \\ 1010 \end{smallmatrix}\right) \right] f_{\lambda,\text{tr}}^{(2)}}{\mathfrak{S}(1010)\mathfrak{S}(1001) - \mathfrak{S}\left(\begin{smallmatrix} 1001 \\ 1010 \end{smallmatrix}\right)^2} f_\eta^{(3)}. \quad (5)$$

Here λ_{tr} is the contribution of the translational degrees of freedom to the thermal conductivity and η denotes the shear viscosity coefficient. The first terms of Eq. (5) define f_{tr} and the final term relates this to generalized cross sections and higher-order correction factors.

B. Thermomagnetic effects

It is well documented¹¹ that in the presence of a magnetic (or electric) field the coupling between the velocity and angular momentum is partially destroyed and the thermal conductivity coefficient loses its isotropic character. Three independent thermal conductivity coefficients are necessary to describe fully the resulting behavior.

When the magnetic field is oriented perpendicular to the temperature gradient two thermomagnetic coefficients measure the change in thermal conductivity in the perpendicular,

$\Delta\lambda^\perp$, and transverse, λ^{tr} , directions. The remaining thermomagnetic coefficient $\Delta\lambda^\parallel$ measures the change in thermal conductivity when the field is oriented parallel to the temperature gradient.¹¹

For linear and spherical-top molecules there is overwhelming experimental evidence that the dominant polarization needed in the solution of Boltzmann's equation is $\mathbf{W}\hat{\mathbf{j}}\hat{\mathbf{j}}$.¹¹ However, this evidence is based on the analysis of the experimental data by means of a spherical approximation (SA), which simplifies the working equations.¹¹ It is unclear at present if small deviations of the experimental data from the theory are due to the use of the SA or to the neglect of other polarizations. The current work will allow us to investigate both possibilities and test the validity of the experimental analyses based solely on the $\mathbf{W}\hat{\mathbf{j}}\hat{\mathbf{j}}$ polarization.

The general expressions for the thermal conductivity in a magnetic field due to a single $\mathbf{W}\hat{\mathbf{j}}\hat{\mathbf{j}}$ polarization were first derived by Tip.²¹ For conciseness we give here an expression for the transverse thermomagnetic coefficient only using an alternative notation:²²

$$\frac{\lambda^{\text{tr}}}{\lambda} = -\frac{\Psi_{12}}{2} \{5K_1\xi_{12} + [10Y(2Z - K_1) - 2K_2K_3Z]\xi_{12}^3\} \times [1 + (9Z^2 - 4Y)\xi_{12}^2 + 4Y^2\xi_{12}^4]^{-1}. \quad (6)$$

Similar expressions for the other two coefficients and the definitions of the quantities K_L , Y , and Z are given in Ref. 7. The dimensionless field parameter ξ_{pq} is given by¹¹

$$\xi_{pq} = \frac{g_{\text{rot}}\mu_N k_B T}{\hbar \langle v \rangle_0} \frac{1}{\Theta(pq00)_0} \frac{B}{P}. \quad (7)$$

Here g_{rot} is the rotational g factor, μ_N is the nuclear magneton, B is the magnitude of the magnetic flux density, and P is the pressure.

The quantity Ψ_{pq} in Eq. (6), which governs the magnitude of the contribution for a given pq polarization, is given by¹¹

$$\Psi_{pq} = \frac{3}{5} \left\{ \overline{\Theta} \begin{pmatrix} 1010 \\ pq00 \end{pmatrix} \left[r \overline{\Theta} \begin{pmatrix} 1010 \\ 1001 \end{pmatrix} - \Theta(1001) \right] + \overline{\Theta} \begin{pmatrix} 1001 \\ pq00 \end{pmatrix} \left[\overline{\Theta} \begin{pmatrix} 1010 \\ 1001 \end{pmatrix} - r \Theta(1010) \right] \right\}^2 \times \left\{ \overline{\Theta}(pq00)^{(1)} \left[\Theta(1010)\Theta(1001) - \overline{\Theta} \begin{pmatrix} 1010 \\ 1001 \end{pmatrix}^2 \right] \right\} \times \left[\Theta(1001) - 2r \overline{\Theta} \begin{pmatrix} 1010 \\ 1001 \end{pmatrix} + r^2 \Theta(1010) \right]^{-1}. \quad (8)$$

In the SA, in which the collision operator acts separately on the directions of the velocities and of the angular momenta, it is assumed that $\overline{\Theta}(1200)^{(1)} = \overline{\Theta}(1200)^{(0)}$ and $K_1 = K_2 = K_3 = Y = Z = 1$. Equation (6) then reduces to the well-known, simple, expression¹¹

$$\frac{\lambda^{\text{tr}}}{\lambda} = -\frac{1}{2} \Psi_{12}^{\text{SA}} [g(\xi_{12}) + 2g(2\xi_{12})], \quad (9)$$

where $g(x) = x/(1+x^2)$.

As far as we are aware, no general expressions have been derived for thermomagnetic effects that include polarizations other than $\mathbf{W}\hat{\mathbf{j}}\hat{\mathbf{j}}$. Hence, the influence of other polarizations can only be examined within the spherical-approximation framework. Inclusion of the $\mathbf{W}\hat{\mathbf{j}}$ polarization leads to the following expression for the transverse thermomagnetic coefficient:

$$\frac{\lambda^{\text{tr}}}{\lambda} = -\frac{1}{2} \Psi_{12}^{\text{SA}} [g(\xi_{12}) + 2g(2\xi_{12})] + \Psi_{11}^{\text{SA}} g(\xi_{11}). \quad (10)$$

Similar expressions for the other two ratios are given in p. 346 of Ref. 11.

The present calculations provide us with all the cross sections necessary to calculate the quantities Ψ_{pq} , K_L , Y , Z , and the parameter ξ_{pq} , required for the evaluation of the three thermomagnetic coefficients. Hence we are in a position to ascertain what influence, if any, inclusion of the second polarization, Eq. (10), and/or the full treatment, Eq. (6), has on the thermomagnetic coefficients obtained by the traditional approach, Eq. (9).

C. Volume viscosity

The volume viscosity (also known as the bulk viscosity) can be inferred from measurements of the absorption and dispersion of ultrasonic waves in the gas.¹¹ As noted by Prangmsma *et al.*,²³ for the analysis of sound-absorption measurements the volume viscosity η_V is the fundamental quantity of interest. In this work we limit our investigation to the contribution to volume viscosity that arises from rotational relaxation only, as the nature of the intermolecular potential used in the calculation precludes investigation of the vibrational relaxation process.

The volume viscosity can be written as

$$[\eta_V]_n = \frac{k_B c_{\text{int}}}{c_V^2} \frac{k_B T}{\langle v \rangle_0 \Theta(0001)} f_{\eta_V}^{(n)}. \quad (11)$$

The quantity $f_{\eta_V}^{(n)}$ is the n th-order correction factor for the volume viscosity and accounts for the effects of higher basis-function terms in the perturbation-series expansion of the solution of the Boltzmann equation.¹¹ The explicit expression for the second-order kinetic theory expression, $[\eta_V]_2$, is given by Maitland *et al.*¹⁸ We have also investigated employing a third-order expression, $[\eta_V]_3$, obtained as for the second-order result¹⁸ but by using a basis set¹¹ Φ^{00st} with $s+t \leq 3$. (See also the discussion in I¹⁰ of the analogous higher-order expressions for the shear viscosity.)

A number of experimenters have presented their measurements of sound absorption and dispersion in terms of a relaxation time τ_{expt} . Because the volume viscosity, rather than the relaxation time, is the fundamental quantity measured, also because it is for the volume viscosity that higher-order kinetic theory is available, we have converted these relaxation time measurements to volume viscosity values using the first-order kinetic theory relation¹¹

$$[\eta_V]_1 = \frac{k_B c_{\text{int}} P \tau_{VT}}{c_V^2},$$

$$[\eta_V]_n \approx \frac{k_B c_{\text{int}} P \tau_{\text{exp}}}{c_V^2}, \quad (12)$$

where τ_{VT} is the isothermal relaxation time.^{23,24} Use of this equation to convert measured relaxation times to volume viscosity values is only approximately equivalent to analyzing the measurements in terms of the volume viscosity.

D. Nuclear-spin relaxation

Due to the alignment of the nuclear magnetic moments when a static magnetic field is present, a weak equilibrium magnetization occurs in a polyatomic gas. A nonequilibrium nuclear magnetization can then be caused by absorption of radio-frequency radiation and the nuclear-spin system will return to equilibrium. Johnson and Waugh²⁵ and Bloom *et al.*²⁶ concluded that spin rotation is the dominant relaxation mechanism in gaseous methane. Oosting and Trappeniers²⁷ showed that this mechanism is responsible for 90% or more of the relaxation. Jameson *et al.*²⁸ estimated that, for methane, mechanisms other than spin-rotation relaxation give relaxation rates orders of magnitude smaller than spin rotation. In principle two relaxation times are present for ¹²CH₄ molecules^{11,29} but, in practice, all measurements have been analyzed using just one. Furthermore, the measurements appear consistent, within experimental error, with a single relaxation time.^{26,28,29} In this case the cross section governing the relaxation¹¹ is $\mathfrak{S}'(0100)$, where the prime indicates that the contribution from just one of the collision partners is included. For a fuller discussion see Ref. 8.

III. RESULTS

The classical-trajectory calculations were performed using an extension of the TRAJECT software code for linear molecules,³⁰ modified³¹ to allow for the additional variables and averaging needed for asymmetric tops. The methane molecule was represented as a rigid spherical top and the interaction of two methane molecules is described by a six-dimensional *ab initio* intermolecular potential energy hypersurface.¹² All the details of the classical-trajectory calculations and the intermolecular potential are summarized in I.¹⁰

The calculated transport and relaxation cross sections¹¹ relevant to the present paper are characterized by the customary monotonic decrease with temperature, while some of the production cross sections¹¹ exhibit a maximum at low temperature. The values of the transport and relaxation cross sections are, on average, an order of magnitude larger than those of the production cross sections. Based on the convergence tests, the precision of most of the calculated transport and relaxation cross sections is estimated to be better than $\pm 0.1\%$, while the precision of most of the production cross sections is estimated to be better than $\pm 1.0\%$, at all except the very lowest temperatures.

Tables of all the relevant generalized cross sections resulting directly from the classical-trajectory computations and of the thermal conductivity coefficients calculated in this work have been deposited with the Electronic Physics Auxiliary Publication Service.³²

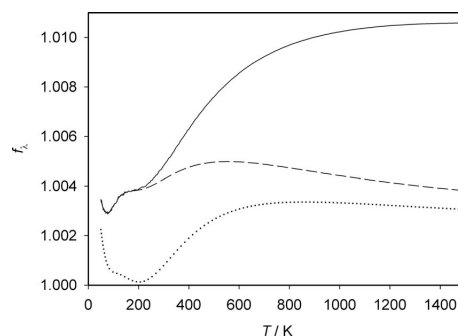


FIG. 1. Comparison of the values of the two second-order corrections $f_{\lambda}^{(2)}$ (---), $f_{\lambda}^{(2')}$ (.....), and of the rigid-rotor correction $f_{\lambda,rr00}^{(2)}$ (—) for the thermal conductivity coefficient.

A. Thermal conductivity

1. Vibrational degrees of freedom

To account for the vibrational degrees of freedom we have corrected, using the methodology and notation described in Ref. 7, all the cross sections $\mathfrak{S}_{p'q's't'}^{(pqst)_{\kappa}}$ with $t+t' > 0$ which enter the description of thermal conductivity both in the absence and presence of the field. In the first-order approximation for thermal conductivity, $n=1$ in Eq. (1), two such cross sections are present. The vibrational correction for $\mathfrak{S}(1001)_{rr00}$ is small and weakly dependent on temperature and the resulting $\mathfrak{S}(1001)_{\text{int}}$ is at most 6% lower than $\mathfrak{S}(1001)_{rr00}$ at 600 K. Here the subscripts “rr00” and “int” denote values calculated with and without the vibrational correction, respectively. The vibrational correction for the production cross section $\mathfrak{S}_{1001}^{(1010)_{\text{int}}}$ is larger and exhibits a strong temperature dependence, as already noted for CO₂. At 1500 K the ratio $\mathfrak{S}_{1001}^{(1010)_{\text{int}}}/\mathfrak{S}_{1001}^{(1010)_{rr00}}$ is 0.43. However, at high temperatures the production cross section is approximately 30 times smaller than the two transport cross sections; hence its contribution to the thermal conductivity is small. The overall effect on the thermal conductivity of correcting the cross sections for the vibrational degrees of freedom is almost negligible, of the order of 0.06% at 600 K, increasing in magnitude to 0.24% at 1500 K. For comparison the correction at 600 K for CO₂, with its low-lying vibrational level, amounted to 5%. Hence, we are confident that the present calculations, based on the rigid-rotor intermolecular potential, are accurate up to the quoted high-temperature limit of 1500 K.

2. Second-order contributions

The overall, second-order thermal conductivity correction factor $f_{\lambda}^{(2)}$ has been calculated as described in Ref. 7 using the expressions given by Maitland *et al.*¹⁸ and Bich *et al.*⁵ All the relevant cross sections of the type $\mathfrak{S}_{10s't'}^{(10st)}$ with $t+t' \neq 0$ that enter these expressions have been corrected for the influence of the vibrational degrees of freedom using the methodology described in Ref. 7.

Figure 1 illustrates the temperature dependence of the overall second-order thermal conductivity correction factor $f_{\lambda}^{(2)}$. The magnitude of the correction is small, reaching a

maximum value of 0.5% at approximately 550 K. As expected, the correction is smaller than that observed for carbon dioxide.

In order to ascertain the influence of the vibrational degrees of freedom we have also calculated the overall second-order correction factor using the rigid-rotor values for the cross sections and have labeled the resulting correction $f_{\lambda,rr00}^{(2)}$. As illustrated in Fig. 1, $f_{\lambda,rr00}^{(2)}$ increases with temperature, reaching the value of 1.01 at high temperature. Although the vibrational degrees of freedom exert an increasing influence with increasing temperature, their influence on the magnitude of the overall second-order correction factor is such that the thermal conductivity would change by less than 0.7%.

Figure 1 also illustrates the temperature dependence of the second-order thermal conductivity correction factor $f_{\lambda}^{(2)}$ due to the velocity polarization alone. Above temperatures of about 200 K the magnitude of this correction factor increases with temperature, reaching a maximum value of approximately 1.003. By comparing the values of $f_{\lambda}^{(2)}$ and $f_{\lambda}^{(2)}$ it can be seen that the angular-momentum coupling contribution is also small, exhibiting a maximum value of 1.0035 at 220 K but then rapidly decreasing with increasing temperature.

Similarly to viscosity, the angular-momentum coupling contribution is smaller for methane than for any of the other three gases studied, especially at temperatures above room temperature, consistent with the production cross sections, $|\mathcal{S}_{10sr}^{(200)}|$, being smaller for methane.

3. Use of the total-energy basis set

The values of thermal conductivity have been also calculated by means of the Thijssse approximation, Eq. (3). The agreement with the calculations based on the first-order, two-flux, approach [Eq. (1) with $f_{\lambda}^{(n)}=1$], is excellent, to better than $\pm 0.5\%$ over the whole temperature range. This confirms the finding that for all the molecules studied so far^{2,3,7} the Thijssse approximation gives very good estimates of the first-order thermal conductivity. It also provides further evidence that a single cross section, $\mathcal{S}(10E)$, is sufficient to describe closely the behavior of the thermal conductivity.

4. Translational Eucken factor

For a number of gases Millat *et al.*³³ performed a series of thermal transpiration experiments that allow the determination of the translational Eucken factor f_{tr} [see Eq. (5)] and consequently evaluation of the contribution of the translational degrees of freedom to the thermal conductivity. For methane, the thermal transpiration experiments were performed in the temperature range of 300–600 K. The primary pressure-temperature data obtained in the experiments were analyzed by means of the integrated-dusty-gas model to obtain the values of the translational Eucken factor. These values were subsequently fitted to a suitable temperature function and the authors estimated the uncertainty of their results as $\pm 1\%$.

Values of f_{tr} were calculated using Eq. (5). The agreement with the values inferred from the thermal transpiration

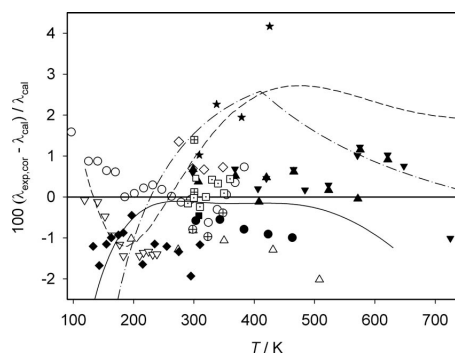


FIG. 2. Deviations of experimental and correlated zero-density thermal conductivity coefficients from values calculated for CH_4 . Experimental data: (○) Johnston and Grilly (Ref. 39); (△) Golubev (Ref. 40); (◇) Mistic and Thodos (Ref. 41); (▽) Sokolova and Golubev (Ref. 42); (▲) Le Neindre *et al.* (Ref. 43); (▼) Tufeu *et al.* (Ref. 44); (□) Clifford *et al.* (Ref. 45); (⊕) Tanaka *et al.* (Ref. 46); (⊞) Clifford *et al.* (Ref. 47); (■) Assael and Wakeham (Ref. 48); (◆) Roder (Ref. 49); (●) Hemminger (Ref. 50); (★) Millat *et al.* (Ref. 51); (◻) Pátek and Klomfar (Ref. 52). Correlations: (—) Friend *et al.* (Refs. 34 and 35); (---) Assael *et al.* (Ref. 36); (-·-·-) Uribe *et al.* (Refs. 37 and 38).

measurements³³ is excellent with deviations decreasing monotonically with increasing temperature from +1.2% at 300 K to -0.1% at 600 K.

5. Comparison with experiment

Around 1990 several correlations were performed for the thermal conductivity of methane in the limit of zero density.^{34–38} These correlations not only were based on a critical evaluation of thermal conductivity measurements but also employed theoretical considerations, especially when extrapolating to high temperatures.

In Fig. 2 the correlations and selected experimental data^{39–52} are compared with the calculations of the present paper. The hot-wire (HW) method,^{39,45} the concentric-cylinders (CC) method,^{40–44,46} the parallel-plates (PP) method,⁵⁰ and the transient hot-wire (THW) technique^{47–49,51,52} were used in the measurements of these data. In principle, the uncertainties associated with these experimental techniques decrease along this series of methods toward the THW method. However, most experimenters reported significantly lower error estimates than are accepted nowadays.

For the development of the zero-density contribution of their experimentally based correlation for methane Friend *et al.*³⁴ used as primary data the results of the THW measurements of Roder⁴⁹ and of the CC experiments of Le Neindre *et al.*⁴³ All the other available data were classified as secondary. Using a preliminary version of the residual contribution of their correlation, Friend *et al.* adjusted the lowest-density results of the isothermal measurements at atmospheric pressure of Le Neindre *et al.*⁴³ to zero density. For Roder's data⁴⁹ no such extrapolation was necessary as the tabulated values⁴⁹ were given in the limit of zero density. It should be noted that the effect of the initial density dependence of the thermal conductivity is in fact small and that the adjustment amounted to no more than 0.2%. Friend *et al.*³⁵ estimated the

uncertainty of their zero-density correlation to be $\pm 2.5\%$ between 130 and 625 K, the temperature range of the primary data selected.

Assael *et al.*³⁶ developed a theoretically based correlation for the zero-density thermal conductivity in the temperature range of 120–1000 K with uncertainties estimated to be $\pm 2\%$ between 300 and 500 K, $\pm 2.5\%$ at the lowest, and $\pm 4\%$ at the highest temperatures. These uncertainties originated from the analysis of thermal conductivity measurements, as well as from new theoretical results available at that time. Experimental THW values^{47–49,51} were chosen as primary data sets by Assael *et al.* They ascribed uncertainties of $\pm 0.5\%$ to these measurements, apart from those of Roder⁴⁹ ($\pm 2\%$). To avoid a limited temperature range, they also included less reliable values obtained with the HW technique^{39,45} [$\pm 3\%$ (Ref. 39) and $\pm 1\%$ (Ref. 45)] and the CC method⁴⁴ ($\pm 2.5\%$). They made use of the theoretical high-temperature limiting behavior of the ratio of the diffusion coefficient for internal energy, D_{int} , to the self-diffusion coefficient, D , in order to provide a reliable extrapolation of the experimental thermal conductivity data.

Uribe *et al.*^{37,38} used the THW data of Clifford *et al.*,⁴⁷ Assael and Wakeham,⁴⁸ and Millat *et al.*⁵¹ as primary data sets for their correlation for methane. Their correlation scheme combines kinetic theory with an extended principle of corresponding states to calculate the thermal conductivity of a series of polyatomic gases at zero density. This scheme offers somewhat more predictive power than the correlation of Assael *et al.*,³⁶ which fits each gas individually. Similarly to the procedure of Assael *et al.*,³⁶ kinetic theory has been used by Uribe *et al.*^{37,38} to underpin the extrapolation to high temperatures. The analysis resulted in a correlation depending on the high-temperature limiting value of the collision number for rotational relaxation $\zeta_{\text{rot}}^{\infty}$ and on a crossover temperature T_{cross} for switching between two relations for the temperature function of the diffusion coefficient for rotational energy D_{rot} . Both parameters have been treated as adjustable and have been fixed individually for each gas. Uribe *et al.*³⁸ estimated the uncertainty of their correlation for λ to be $\pm 1.5\%$ in the temperature range of 300–500 K, deteriorating to $\pm 3\%$ at lower and higher temperatures.

In addition to the experimental data considered by the authors of these three correlations, we included in our comparison further experimental values.^{40,50,52} In particular, the PP values of Hemminger⁵⁰ should be very useful, since he performed careful corrections for the contamination by air desorbed from the measuring instrument.

Figure 2 illustrates very good overall agreement between the calculated and measured values. In particular, the calculated values agree with the correlation of Friend *et al.*³⁴ within its estimated uncertainty over the whole of the temperature range. Similar agreement is observed with the correlations of Assael *et al.*³⁶ and of Uribe *et al.*,^{37,38} everywhere except in the temperature range of approximately 350–550 K, where the deviations are just outside the claimed uncertainty of the correlations. The direct comparison with the experimental data also illustrates very good agreement. In most cases,^{39–49,52} the agreement is within the experimental uncertainty ascribed to the data by correlation developers.

More importantly the calculated values are in excellent agreement (-0.5% to -1.0%) with the experimental point of Assael and Wakeham⁴⁸ at 308 K as well as the data of Hemminger.⁵⁰ Based partly on the agreement of Hemminger's measurements on nitrogen, which have already been discussed by Bich *et al.*⁵ (see Fig. 6 in that reference), both these data sets of Hemminger are considered to be of very high quality.

The only data set which is in disagreement with the calculated values is the transient HW data of Millat *et al.*,⁵¹ which up to now have been assumed to constitute excellent primary data. The experimental datum at 425 K is about 4% higher than both the correlation of Friend *et al.*³⁴ and the present calculated value. A detailed inspection of Fig. 2 also shows that the temperature dependence of the data of Millat *et al.*⁵¹ disagrees with that of most other data, as well as with that of our calculated values. It appears that the measurements of Millat *et al.*⁵¹ at higher temperatures are erroneous and that, at most, only the measurement at 309 K can be considered as a primary datum.

The experimental data of Millat *et al.*⁵¹ had a strong impact on the development of the correlations of Assael *et al.*³⁶ and Uribe *et al.*,^{37,38} as both correlations considered these as primary data. Hence both correlations mimic, up to about 400 K, the temperature dependence of these data. Not surprisingly, the inclusion of this data set in the analysis leads to a less accurate extrapolation to higher temperature for both correlations. Based on the good agreement of the calculated values with all the other high-temperature data and on the theoretical background of the calculated values of the present paper, we consider that the values of the thermal conductivity obtained in this work at high temperatures are more reliable than the values obtained from the correlations of Assael *et al.*³⁶ and of Uribe *et al.*^{37,38}

Concerning the low-temperature region, although there also exist differences between the three correlations and our calculated values, these differences fall within the uncertainty claimed for all the correlations. Because Friend *et al.*³⁴ and Assael *et al.*³⁶ selected different experimental values as primary data, their correlations differ quite significantly at low temperatures. Based on the agreement of our calculated values with the experimental data and on similar agreement observed for viscosity, we consider that the present calculations provide the best estimate of the thermal conductivity of methane at temperatures lower than 200 K. Taking account of the comparison with the available data, especially around room temperature, and the accuracy of the intermolecular potential used, we estimate the accuracy of the computed values to be of the order of $\pm(1-1.5)\%$ in the complete temperature range between 80 and 1500 K. Values of the calculated thermal conductivity are included in the information deposited with the Electronic Physics Auxiliary Publication Service.³²

B. Thermomagnetic effects

Seven independent measurements of thermomagnetic effects in methane^{53–59} have been reported. Following the analysis of the data by the authors and our own analysis, we

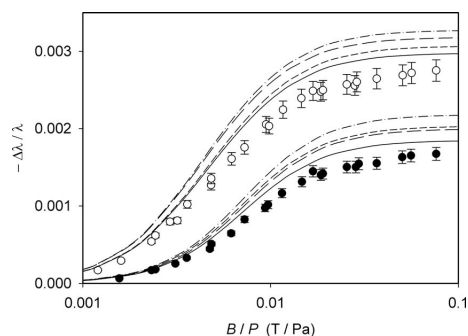


FIG. 3. Comparison of the measurements of Hermans *et al.* (Ref. 58) of the thermomagnetic effect at 300 K with the present calculations. Experimental values: (○) $-\Delta\lambda^\perp/\lambda$; (●) $-\Delta\lambda^\parallel/\lambda$. Calculations: (---) \mathbf{W}_{jj} polarization, SA only; (-.-.-) \mathbf{W}_{jj} polarization, full calculation; (—) $\mathbf{W}_{jj}+\mathbf{W}_j$ polarizations, both using the SA; (—) \mathbf{W}_{jj} polarization, full calculation, combined with \mathbf{W}_j polarization, SA. The error bars shown correspond to the estimated experimental uncertainty (Ref. 58) of $\pm 5\%$.

classified the four more recent measurements^{53,57–59} as primary. All the measurements were made either in single or double cylindrical cells placed between two parallel plates that could be heated. Hermans *et al.*⁵⁷ measured the transverse thermomagnetic coefficient at approximately 85 K for (B/P) values up to 0.076 T/Pa ($\equiv 100$ kOe/torr) with an accuracy of 15%.⁵⁹ Shortly afterwards Hermans *et al.*⁵⁸ carried out measurements of the two longitudinal coefficients, $\Delta\lambda^\perp/\lambda$ and $\Delta\lambda^\parallel/\lambda$, at 300 K at (B/P) values of up to 0.076 T/Pa ($\equiv 100$ kOe/torr), with an estimated accuracy of 3%–5%. As both longitudinal coefficients have been measured in the same apparatus, the authors assumed that cancellation of systematic errors will make the ratio of the two coefficients accurate to 2%. Both longitudinal coefficients were further measured by Heemskerk *et al.*⁵⁹ at about 85 K at (B/P) values of up to 0.16 T/Pa ($\equiv 220$ kOe/torr) with an estimated accuracy of 5%. Subsequently, Heemskerk *et al.*⁵³ measured the coefficients $\Delta\lambda^\perp/\lambda$ and $\Delta\lambda^\parallel/\lambda$ at 150 and 200 K at (B/P) values of up to 0.06 T/Pa ($\equiv 80$ kOe/torr), with uncertainties estimated at 2% for the ratio of these coefficients and 3% for their values at saturation, i.e., at high B/P values.

For the thermomagnetic coefficients $\Delta\lambda^\perp/\lambda$ and $\Delta\lambda^\parallel/\lambda$ Fig. 3 shows the comparison between the calculated values and the available experimental data (read from the published figures) at 300 K.⁵⁸ Although it is clear that the dominant contribution comes from \mathbf{W}_{jj} polarization, a single polarization cannot represent the experimental data within their uncertainties. Hence, to provide an improved description of the thermomagnetic effect, we tested the two approaches discussed in Sec. II B. As illustrated in Fig. 3, using the full \mathbf{W}_{jj} expression without making the SA will lower the values of the two coefficients and improve the agreement with the experiments. At saturation the full description lies about 7% below the SA values.

Taking a different approach and retaining the SA but invoking a second polarization, \mathbf{W}_j , results also shown on the figure, again leads to better agreement with experiment, yielding a lowering of the saturation values, $(\Delta\lambda^\perp/\lambda)_{\text{sat}}$ and

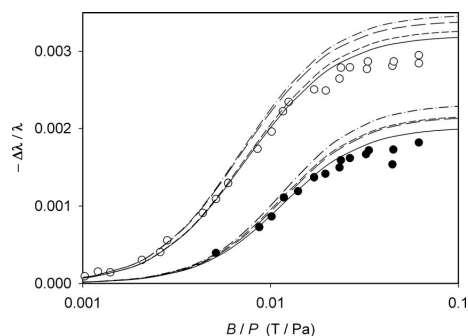


FIG. 4. Comparison of the measurements of Heemskerk *et al.* (Ref. 53) of the thermomagnetic effect at 200 K with the present calculations. Symbols and lines are the same as in Fig. 3.

$(\Delta\lambda^\parallel/\lambda)_{\text{sat}}$, by 3% and 9%, respectively, from the SA values with just the \mathbf{W}_{jj} polarization. There is currently no theory which provides a full treatment, without the SA, in terms of two polarizations. Considering that the effects of both improvements are small, less than 10%, we estimated their overall effect by adding the two effects. The overall longitudinal thermomagnetic coefficients estimated in this way are consistent with the experimental data, the slight overestimate of the experimental data being just outside the quoted uncertainties.

Figure 4 shows a similar comparison between the calculated and measured values of the longitudinal thermomagnetic coefficients at 200 K.⁵³ Based on the entries in Table III of this reference, we have taken the measured values from Fig. 7, as the caption appears to have been interchanged with that for Fig. 6. While the contributions due to the full treatment of \mathbf{W}_{jj} , or the addition of the \mathbf{W}_j polarization, decrease slightly with temperature, both these corrections are still necessary in order to get good agreement with experiment. The values of the $\Delta\lambda^\perp/\lambda$ and $\Delta\lambda^\parallel/\lambda$ coefficients calculated by combining the two effects are in very good agreement with the experimental data.

Finally, Fig. 5 shows the comparison of the calculated values of all three thermomagnetic coefficients, $\Delta\lambda^\perp/\lambda$,

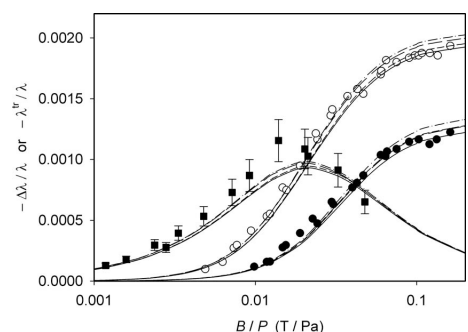


FIG. 5. Comparison of the measurements of Heemskerk *et al.* (Ref. 59) and of Hermans *et al.* (Ref. 57) of the thermomagnetic effect at about 85 K with the present calculations. Experimental values: (○) $-\Delta\lambda^\perp/\lambda$; (●) $-\Delta\lambda^\parallel/\lambda$; (■) $-\lambda^U/\lambda$. Lines are the same as in Fig. 3. The error bars shown for λ^U/λ correspond to the estimated experimental uncertainty of $\pm 15\%$.

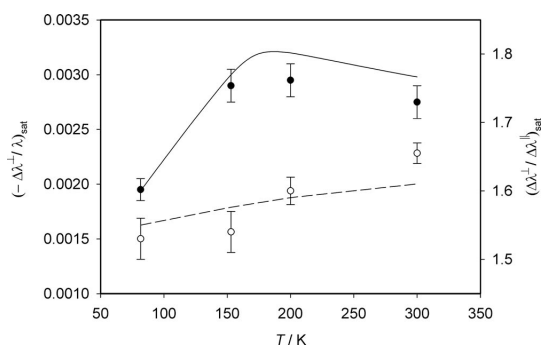


FIG. 6. Comparison between thermomagnetic coefficients at saturation obtained from the experimental analysis (Ref. 53) with the present full calculations as described in the text. Left ordinate: $(-\Delta\lambda^\perp/\lambda)_{\text{sat}}$; (●) experimental values; (—) calculations. Right ordinate: $(\Delta\lambda^\perp/\Delta\lambda^\parallel)_{\text{sat}}$; (○) experimental values; (---) calculations.

$\Delta\lambda^\parallel/\lambda$, and $\lambda^{\text{tr}}/\lambda$, with the available experimental data at about 85 K.^{57,59} Note that these data are available at a wider range of (B/P) values than those at the other temperatures. The agreement with the experimental data is excellent and not only are the two longitudinal coefficients reproduced within the experimental error, but so also is the transverse coefficient. The good agreement observed at such a low temperature is encouraging for the use of a classical-trajectory calculation.

Heemskerk *et al.*⁵³ analyzed the data^{53,58,59} on the thermomagnetic coefficients $\Delta\lambda^\perp/\lambda$ and $\Delta\lambda^\parallel/\lambda$ of methane to draw some conclusions about the variation with temperature of a number of parameters and cross sections. We will not carry out the comparison at the level of cross sections, as these were unduly influenced by the analysis of the experimental data based only on the dominant polarization $\mathbf{W}_{\mathbf{j}\mathbf{j}}$ in the SA. However it is useful to compare with quantities that could be extracted more directly from the experimental data.

One such quantity is the saturation value of the longitudinal thermomagnetic coefficients. Although Heemskerk *et al.*⁵³ obtained these quantities by extrapolating the experimental data using equations based on the dominant polarization, $\mathbf{W}_{\mathbf{j}\mathbf{j}}$, and the SA, the extent of the data is such that the extrapolation was carried out in the region where the sensitivity to these approximations is small.

Figure 6 shows the comparison between the best calculated values of the perpendicular thermomagnetic coefficient at saturation, $(\Delta\lambda^\perp/\lambda)_{\text{sat}}$, and the values obtained from the experimental analysis. The agreement between the calculated and the measured values⁵³ decreases somewhat with increasing temperature. At the lowest temperature of the measurements (at about 85 K) the calculated value of 1.94×10^{-3} is well within the experimental uncertainty of the quoted value, $(1.95 \pm 0.1) \times 10^{-3}$, while at the highest temperature, 300 K, the calculated value of 2.98×10^{-3} slightly overestimates the quoted value of $(2.75 \pm 0.1) \times 10^{-3}$. The position $(B/P)_{1/2}$, that is the (B/P) value for which the $(\Delta\lambda^\perp/\lambda)$ curve reaches half the saturation value, not shown in Fig. 6, is also in very good agreement at low temperature: 19.1 mT/Pa compared with the quoted value of 19.8 ± 1.0 mT/Pa. At 300 K the

calculated value of 4.67 mT/Pa underestimates the quoted value of 5.1 ± 0.2 mT/Pa. This is not surprising considering that at 300 K the SA description based on a single $\mathbf{W}_{\mathbf{j}\mathbf{j}}$ polarization is more in error and the value of $(B/P)_{1/2}$ is sensitive to the shape of the function used for its determination.

Heemskerk *et al.*⁵³ also quoted a value of $(\Delta\lambda^\perp/\Delta\lambda^\parallel)_{\text{sat}}$ as a function of temperature. If only the single polarization $\mathbf{W}_{\mathbf{j}\mathbf{j}}$ is included, this ratio, in the SA, is independent of temperature and equal to 1.5. Our results indicate that, using the full $\mathbf{W}_{\mathbf{j}\mathbf{j}}$ expression, the value of this ratio changes only slightly, from 1.50 to 1.51, the value being nearly independent of temperature. However, if one includes the second polarization, $\mathbf{W}_{\mathbf{j}}$, in a spherical-approximation description, our calculations indicate a stronger temperature variation: from 1.54 at 80 K to 1.59 at 300 K and 1.7 at 1500 K. Hence, as noted by Hermans *et al.*,⁵⁸ the ratio $(\Delta\lambda^\perp/\Delta\lambda^\parallel)_{\text{sat}}$ is rather useful as its deviation from 1.5 primarily shows the influence of additional polarizations. Figure 6 illustrates the comparison between the calculated values of this ratio and the values obtained from the experimental analysis.⁵³ The measured values are reproduced to within $\pm 3\%$, which is just outside their estimated uncertainty.

C. Volume viscosity

Before the comparison with experiment we consider the magnitude and the temperature dependence of the higher-order corrections to the volume viscosity. The second-order correction is below 2% at 80 K, increasing to about 10% at room temperature and rising to 18% at 1500 K. The third-order result differs from the second-order result by less than 0.2% at temperatures up to 1500 K. The second-order correction is larger than those found for carbon monoxide⁴ and carbon dioxide⁷ but smaller than that found for nitrogen.²

Sound-absorption and, in some cases, sound dispersion, measurements in methane have been performed by Kelly⁶⁰ at 314 K, Holmes *et al.*⁶¹ at 303 K, Hill and Winter⁶² at 298, 573, 773, and 1073 K, Kistemaker *et al.*⁶³ at 308.3 K, and Prangma *et al.*²³ at 77.1, 180, 260, and 293 K. Of these, all except Prangma *et al.*²³ analyzed their results in terms of a relaxation time. We have converted these relaxation time values to volume viscosity values using Eq. (12). Figure 7 shows the comparison between our theoretical results and the measurements. The inset enlarges the region around room temperature. If an experimental uncertainty has been quoted we have shown it in the figure. For the measurement of Kelly⁶⁰ we have taken the uncertainty as the difference (18%) between values he obtained using the sound-absorption and the sound dispersion methods of analyzing his data.

The lowest temperature measurements, those at 77 and 180 K, uncertainty of $\pm 10\%$, exceed the calculated values by about 55% and 25%, respectively. For the measurements^{23,60-62} around room temperature, 293–314 K, our result is consistent with that of Prangma *et al.*²³ at 293 K but about 20% below the other measurements (derived from relaxation times), although the uncertainties of two of these are comparable with the difference.

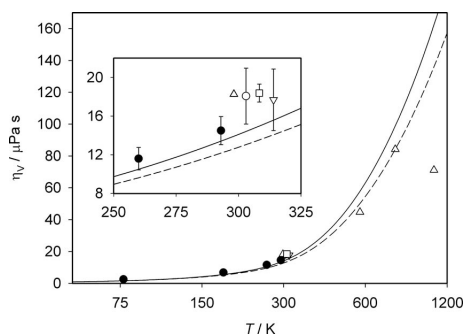


FIG. 7. Comparison of experimentally based values for the volume viscosity with the present calculations. Values inferred from rotational relaxation times: (∇) Kelly (Ref. 60); (\circ) Holmes *et al.* (Ref. 61); (Δ) Hill and Winter (Ref. 62); (\square) Kistemaker *et al.* (Ref. 63). Experimental volume viscosity data: (\bullet) Prangma *et al.* (Ref. 23). Calculations: (---) first-order theory; (—) third-order theory.

While the high-temperature, 773 K, result of Hill and Winter⁶² is within 20% of the calculated value, at 1073 K the calculated value is more than twice that inferred from the measured relaxation time. We note that the vibrational relaxation time inferred by Hill and Winter⁶² at 298 K, 1.86 μ s, is almost double that measured more recently by Trusler and Zarari,⁶⁴ 0.997 ± 0.006 μ s at 300 K.

Theory is generally consistent with the measurements, particularly when it is recalled²³ that a small error in the primary quantity measured, the sound-absorption coefficient, causes a relatively large error in derived quantities such as η_v . Examining the temperature dependence of the data of Hill and Winter⁶² in the whole of the measured range (298–1073 K) one comes to the conclusion that the accuracy of the highest temperature value may be relatively low. In this case the separation of the rotational and vibrational contributions to the measurements may need further refinement.

More recently, measurements of relaxation in free jets have been used by Abad *et al.*⁶⁵ to infer a value of the rotational relaxation cross section, $\mathfrak{S}(0001)$. Because of the nature of these experiments the authors were able to conclude only that the expression $\mathfrak{S}(0001)(T) = 5.0 \text{ \AA}^2 (298 \text{ K}/T)^{0.9}$ was consistent with their measurements over the temperature range of 15–100 K. From their Fig. 9, indicating the range of cross section values compatible with their measurements, we have inferred an uncertainty of between 25% and 35%. We note that this result is consistent with that of Prangma *et al.*²³ at 77.1 K, discussed above. At this temperature the third-order result for the volume viscosity differs from the first-order result by about 3%. At a temperature of 100 K the calculated value of $\mathfrak{S}(0001)$ is about 50% larger than the value of Abad *et al.*,⁶⁵ so outside their estimated uncertainty of about 35%.

Strekalov⁶⁶ analyzed Q -branch Raman line-shape data at 295 K to infer a value for $\mathfrak{S}(0001)$ of 5.4 \AA^2 , compared to the calculated value of 7.2 \AA^2 . As Strekalov⁶⁶ did not provide any estimate of the uncertainty in his value, necessarily obtained via an elaborate analysis, it is difficult to assess the significance of the apparent discrepancy with theory.

In He–N₂ collisions¹⁴ quantal effects for $\mathfrak{S}(0001)$ are

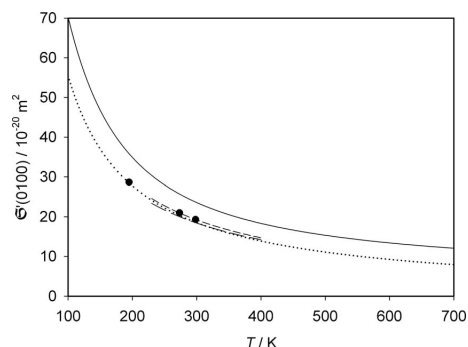


FIG. 8. Comparison of values of the cross section $\mathfrak{S}'(0100)$ inferred from nuclear-spin relaxation measurements with the present calculations. Experimental values: (·····) Bloom *et al.* (Ref. 26) and Lalita and Bloom (Ref. 67), using ¹H; (\bullet) Gerritsma *et al.* (Ref. 70), using ¹H; (---) Jameson *et al.* (Ref. 28), using ¹H; (·····) Jameson *et al.* (Ref. 28), using ¹³C. This work: (—).

less than 4% for temperatures above 77 K. However, while the rotor constant for nitrogen is 2.01 cm^{-1} , that for methane is 5.4 cm^{-1} and, because of the nuclear-spin symmetry, methane has more complex selection rules for transitions between rotational energy levels. Hence quantal effects may be significant at low temperatures.

D. Nuclear-spin relaxation

Bloom *et al.*²⁶ measured the relaxation of the proton spins in methane for temperatures between 100 and 300 K. These measurements were complemented by Lalita and Bloom,⁶⁷ who covered the temperature range from room temperature to 700 K. They noted that their expression for the cross section as a function of temperature was consistent with earlier measurements at or below room temperature.^{25,26,68,69} Other measurements at temperatures of 194.75, 273.15, and 298.15 K were reported at about the same time by Gerritsma *et al.*⁷⁰ For these we have employed the values at the lowest number density for which results are reported. Jameson *et al.*²⁸ repeated the measurements of proton spin relaxation and extended these measurements to the relaxation of the ¹³C nuclear spin in ¹³CH₄ for temperatures between 230 and 400 K. The analogous spin-rotation relaxation mechanism applies. The relative error in the relaxation time was estimated²⁸ to be typically less than 1% and the uncertainty in the inferred cross section values was about 2%. The proton spin relaxation measurements appear consistent, within experimental error, with a single relaxation time.^{26,28,29}

Calculated values of $\mathfrak{S}'(0100)$ are compared in Fig. 8 with the values inferred from the measurements.^{26,28,67,70} Agreement among the measured values is good. The theoretical results are consistently higher than the experimental values based on proton relaxation by about 25% at 100 K, 27% at room temperature, and 50% at 700 K. For the temperatures of 230–400 K for which ¹³C results are also available, the difference from the calculated values is about 4% smaller. It should be realized that the analysis of the ¹³C nuclear-spin relaxation does not require such an elaborate

discussion²⁹ as that for the four proton spins in $^{12}\text{CH}_4$. This quite independent measurement using ^{13}C nuclear-spin relaxation gives strong confirmation of the accuracy of the series of measurements of $\mathcal{S}'(0100)$ using $^{12}\text{CH}_4$.

For carbon dioxide the calculated value⁸ of the $\mathcal{S}'(0100)$ cross section using three different potential surfaces generally underestimated the value obtained by Jameson *et al.*⁷¹ from NMR relaxation measurements. In carbon monoxide the calculated value⁴ overestimated the corresponding measured value. In nitrogen the calculated values⁷² were broadly consistent with the measurements for both the $\mathcal{S}'(0100)$ and $\mathcal{S}'(0\hat{2}00)$ cross sections. Clearly NMR observations are among the most difficult to reproduce accurately.

IV. SUMMARY AND CONCLUSIONS

We have calculated the values of the thermal conductivity, thermomagnetic effects, thermal transpiration, volume viscosity, and nuclear-spin relaxation by means of the classical-trajectory method using a full anisotropic rigid-rotor methane-methane potential energy hypersurface.

For thermal conductivity very good agreement is obtained between the calculated and measured values. In most cases the agreement with the primary experimental data is within the uncertainty ascribed to the data by the correlation developers. The comparison with the most accurate experimental data by Assael and Wakeham⁴⁸ and Hemminger⁵⁰ shows relatively constant deviations of -0.5% to -1.0% in the temperature range of 310–480 K indicating that, analogous to viscosity, a correction at room temperature to the calculated values of the thermal conductivity of the order of -0.5% could be appropriate.

The influence of the vibrational degrees of freedom and the second-order contribution were established to be small, less than 0.2% and 0.5%, respectively, in thermal conductivity. The Thijssse approximation, Eq. (3), gave very good estimates, in line with the findings for other molecules studied. Overall, the theoretical background of the calculated thermal conductivity values is well founded, and their uncertainty is estimated to be of the order of $\pm(1-1.5)\%$. These calculations are expected to be more reliable than the correlations currently available in the open literature, as well as most of the measurements in the complete temperature range between 80 and 1500 K. While the temperature dependence of the calculated values at high temperatures should be very reliable, quantal effects cannot be excluded at low temperatures. Good agreement is also obtained with the values inferred from thermal transpiration experiments for the translational Eucken factor f_{tr} .

We have made use of our calculation of the thermomagnetic effect to establish the influence of a second polarization and of the full treatment on the thermomagnetic coefficients. Although the dominant contribution comes from the $\mathbf{W}_{\mathbf{j}\mathbf{j}}$ polarization in the SA, the influence of the second polarization $\mathbf{W}_{\mathbf{j}}$ and of the full $\mathbf{W}_{\mathbf{j}\mathbf{j}}$ description should not be ignored. At saturation the combined effect of the latter two contributions is of the order of 10%–15% at room temperature.

Measurements of the thermomagnetic effect are in very good agreement with the calculated values over the whole temperature range (85–300 K) examined. It is especially encouraging that all three thermomagnetic coefficients at 85 K are reproduced within their experimental accuracy as this gives further support for the use of classical-trajectory calculations at such low temperatures. Further good agreement was observed with the measured values of the longitudinal thermomagnetic coefficients at saturation and also with the position of the half-saturation value. The agreement at room temperature was just outside the claimed uncertainty.

The experimental data for volume viscosity are characterized by much larger uncertainty than for other properties studied. The claimed uncertainty of the individual data sets, more often than not, is much less than the differences obtained between what should be comparable data sets from independent observations. Furthermore, most of the available values have been inferred from the measurements of the relaxation times by means of an approximate relationship. Nevertheless, the majority of the measurements around room temperature yielding the volume viscosity are consistent with the calculated values. At high and low temperatures our calculated values underestimate and overestimate, respectively, the measured data by approximately 20%–100%. It is possible that at low-temperatures quantal effects might influence the volume viscosity more than they do thermal conductivity and thermomagnetic effects. However, at high temperatures we believe that the claimed accuracy of the experimental values may be rather optimistic and that further refinement of the separation of the rotational and vibrational contributions should be undertaken.

A number of available nuclear-spin relaxation data sets from different laboratories are mutually consistent within a few percent. However, the calculated values of nuclear-spin relaxation, sensitive primarily to the anisotropy, consistently exceed the measurements by between approximately 25% and 50% in the temperature range of 100–700 K. For other molecules studied the nuclear-spin relaxation data were also difficult to reconcile with the calculated values. The reason for this disagreement is unclear at this stage. However, the theory is not as well tested as that for the thermal conductivity and the thermomagnetic properties.

Measurements are also available for the volume viscosity^{23,61,73} and the nuclear-spin relaxation⁷⁴ of tetradecuteromethane. These will be discussed in a separate publication.

ACKNOWLEDGMENTS

This work was financially supported by the German Research Foundation (Deutsche Forschungsgemeinschaft), Grant No. VO 499/14-1.

¹E. L. Heck and A. S. Dickinson, *Mol. Phys.* **81**, 1325 (1994).

²E. L. Heck, A. S. Dickinson, and V. Vesovic, *Mol. Phys.* **83**, 907 (1994).

³E. L. Heck and A. S. Dickinson, *Physica A* **217**, 107 (1995).

⁴E. L. Heck and A. S. Dickinson, *Physica A* **218**, 305 (1995).

⁵E. Bich, S. Bock, and E. Vogel, *Physica A* **311**, 59 (2002).

⁶S. Bock, E. Bich, E. Vogel, A. S. Dickinson, and V. Vesovic, *J. Chem. Phys.* **117**, 2151 (2002).

⁷S. Bock, E. Bich, E. Vogel, A. S. Dickinson, and V. Vesovic, *J. Chem.*

- Phys.* **120**, 7987 (2004).
- ⁸S. Bock, E. Bich, E. Vogel, A. S. Dickinson, and V. Vesovic, *J. Chem. Phys.* **121**, 4117 (2004).
- ⁹M. R. Swain, G. Vasisht, and G. Tinetti, *Nature (London)* **452**, 329 (2008).
- ¹⁰R. Hellmann, E. Bich, E. Vogel, A. S. Dickinson, and V. Vesovic, *J. Chem. Phys.* **129**, 064302 (2008).
- ¹¹F. R. W. McCourt, J. J. M. Beenakker, W. E. Köhler, and I. Kučšer, *Nonequilibrium Phenomena in Polyatomic Gases* (Oxford Science, Oxford, 1990), Vol. 1.
- ¹²R. Hellmann, E. Bich, and E. Vogel, *J. Chem. Phys.* **128**, 214303 (2008).
- ¹³F. R. W. McCourt, V. Vesovic, W. A. Wakeham, A. S. Dickinson, and M. Mustafa, *Mol. Phys.* **72**, 1347 (1991).
- ¹⁴V. Vesovic, W. A. Wakeham, A. S. Dickinson, F. R. W. McCourt, and M. Thachuk, *Mol. Phys.* **84**, 553 (1995).
- ¹⁵J. H. Ferziger and H. G. Kaper, *The Mathematical Theory of Transport Processes in Gases* (North Holland, Amsterdam, 1972).
- ¹⁶Y. Kagan and A. M. Afanasev, *Sov. Phys. JETP* **14**, 1096 (1962).
- ¹⁷L. A. Viehland, E. A. Mason, and S. I. Sandler, *J. Chem. Phys.* **68**, 5277 (1978).
- ¹⁸G. C. Maitland, M. Mustafa, and W. A. Wakeham, *J. Chem. Soc., Faraday Trans. 2* **79**, 1425 (1983).
- ¹⁹G. C. Maitland, M. Rigby, E. B. Smith, and W. A. Wakeham, *Intermolecular Forces: Their Origin and Determination* (Clarendon, Oxford, 1987).
- ²⁰B. J. Thijsse, W. A. P. Denissen, L. J. F. Hermans, H. F. P. Knaap, and J. J. M. Beenakker, *Physica A* **97**, 467 (1979).
- ²¹A. Tip, *Physica (Amsterdam)* **37**, 82 (1967).
- ²²G. W. 't Hooft, E. Mazur, J. M. Bienfait, L. J. F. Hermans, H. F. P. Knaap, and J. J. M. Beenakker, *Physica A* **98**, 41 (1979).
- ²³G. J. Prangma, A. H. Alberga, and J. J. M. Beenakker, *Physica (Amsterdam)* **64**, 278 (1973).
- ²⁴J. D. Lambert, *Vibrational and Rotational Relaxation in Gases* (Clarendon, Oxford, 1977).
- ²⁵C. S. Johnson, Jr. and J. S. Waugh, *J. Chem. Phys.* **35**, 2020 (1961).
- ²⁶M. Bloom, F. Bridges, and W. N. Hardy, *Can. J. Phys.* **45**, 3533 (1967).
- ²⁷P. H. Oosting and N. J. Trappeniers, *Physica* **51**, 418 (1971).
- ²⁸C. J. Jameson, A. K. Jameson, N. C. Smith, J. K. Hwang, and T. Zia, *J. Phys. Chem.* **95**, 1092 (1991).
- ²⁹P. A. Beckmann, M. Bloom, and I. Ozier, *Can. J. Phys.* **54**, 1712 (1976).
- ³⁰E. L. Heck and A. S. Dickinson, *Comput. Phys. Commun.* **95**, 190 (1996).
- ³¹R. Hellmann, E. Bich, and A. S. Dickinson, *Comput. Phys. Commun.* (in preparation).
- ³²See EPAPS Document No. E-JCPSA6-130-049912 for electronic files that contain these tables. For more information on EPAPS, see <http://www.aip.org/pubservs/epaps.html>.
- ³³J. Millat, A. Plantikow, D. Mathes, and H. Nimz, *Z. Phys. Chem. (Leipzig)* **269**, 865 (1988).
- ³⁴D. G. Friend, J. F. Ely, and H. Ingham, *J. Phys. Chem. Ref. Data* **18**, 583 (1989).
- ³⁵D. G. Friend, J. F. Ely, and H. Ingham, National Institute of Standards and Technology Technical Note No. 1325, 1989.
- ³⁶M. J. Assael, J. Millat, V. Vesovic, and W. A. Wakeham, *J. Phys. Chem. Ref. Data* **19**, 1137 (1990).
- ³⁷F. J. Uribe, E. A. Mason, and J. Kestin, *Physica A* **156**, 467 (1989).
- ³⁸F. J. Uribe, E. A. Mason, and J. Kestin, *J. Phys. Chem. Ref. Data* **19**, 1123 (1990).
- ³⁹H. L. Johnston and E. R. Grilly, *J. Chem. Phys.* **14**, 233 (1946).
- ⁴⁰I. F. Golubev, *Teplotnergetika* **10**, 78 (1963).
- ⁴¹D. Mistic and G. Thodos, *Physica (Amsterdam)* **32**, 885 (1966).
- ⁴²V. P. Sokolova and I. F. Golubev, *Teplotnergetika* **14**, 91 (1967).
- ⁴³B. Le Neindre, R. Tufeu, P. Bury, P. Johannin, and B. Vodar, *Proceedings of the Eighth Conference on Thermal Conductivity*, 1968, edited by C. Y. Ho and R. E. Taylor (Plenum, New York, 1969), p. 229.
- ⁴⁴R. Tufeu, B. Le Neindre, and P. Bury, *Physica (Amsterdam)* **44**, 81 (1969).
- ⁴⁵A. A. Clifford, E. Dickinson, and P. Gray, *J. Chem. Soc., Faraday Trans. 1* **72**, 1997 (1976).
- ⁴⁶Y. Tanaka, M. Noguchi, H. Kubota, and T. Makita, *J. Chem. Eng. Jpn.* **12**, 171 (1979).
- ⁴⁷A. A. Clifford, J. Kestin, and W. A. Wakeham, *Physica A* **97**, 287 (1979).
- ⁴⁸M. J. Assael and W. A. Wakeham, *J. Chem. Soc., Faraday Trans. 1* **77**, 697 (1981).
- ⁴⁹H. M. Roder, *Int. J. Thermophys.* **6**, 119 (1985).
- ⁵⁰W. Hemminger, *Int. J. Thermophys.* **8**, 317 (1987).
- ⁵¹J. Millat, M. Ross, W. A. Wakeham, and M. Zalaf, *Physica A* **148**, 124 (1988).
- ⁵²J. Pátek and J. Klomfar, *Fluid Phase Equilib.* **198**, 147 (2002).
- ⁵³J. P. J. Heemskerk, F. G. Van Kuik, H. F. P. Knaap, and J. J. M. Beenakker, *Physica (Amsterdam)* **71**, 484 (1974).
- ⁵⁴L. J. F. Hermans, P. H. Fortuin, H. F. P. Knaap, and J. J. M. Beenakker, *Phys. Lett.* **25A**, 81 (1967).
- ⁵⁵J. Korving, W. I. Honeywell, T. K. Bose, and J. J. M. Beenakker, *Physica (Amsterdam)* **36**, 198 (1967).
- ⁵⁶L. J. F. Hermans, J. M. Koks, H. F. P. Knaap, and J. J. M. Beenakker, *Phys. Lett.* **30A**, 139 (1969).
- ⁵⁷L. J. F. Hermans, A. Schutte, H. F. P. Knaap, and J. J. M. Beenakker, *Physica (Amsterdam)* **46**, 491 (1970).
- ⁵⁸L. J. F. Hermans, J. M. Koks, A. F. Hengeveld, and H. F. P. Knaap, *Physica (Amsterdam)* **50**, 410 (1970).
- ⁵⁹J. P. J. Heemskerk, L. J. F. Hermans, G. F. Bulting, and H. F. P. Knaap, *Physica (Amsterdam)* **57**, 381 (1972).
- ⁶⁰B. T. Kelly, *J. Acoust. Soc. Am.* **29**, 1005 (1957).
- ⁶¹R. Holmes, G. R. Jones, and N. Pustat, *Trans. Faraday Soc.* **60**, 1220 (1964).
- ⁶²G. L. Hill and T. G. Winter, *J. Chem. Phys.* **49**, 440 (1968).
- ⁶³P. G. Kistemaker, M. M. Hanna, A. Tom, and A. E. de Vries, *Physica (Amsterdam)* **60**, 459 (1972).
- ⁶⁴J. P. M. Trusler and M. Zarari, *J. Chem. Thermodyn.* **24**, 973 (1992).
- ⁶⁵L. Abad, D. Bermejo, V. J. Herrero, J. Santos, and I. Tanarro, *J. Phys. Chem. A* **101**, 9276 (1997).
- ⁶⁶M. L. Strekalov, *Mol. Phys.* **100**, 1049 (2002).
- ⁶⁷K. Lalita and M. Bloom, *Chem. Phys. Lett.* **8**, 285 (1971).
- ⁶⁸M. Bloom, M. Lipsicas, and B. H. Muller, *Can. J. Phys.* **39**, 1093 (1961).
- ⁶⁹N. J. Trappeniers, C. J. Gerritsma, and P. H. Oosting, *Physica (Amsterdam)* **31**, 202 (1965).
- ⁷⁰C. J. Gerritsma, P. H. Oosting, and N. J. Trappeniers, *Physica (Amsterdam)* **51**, 381 (1971).
- ⁷¹C. J. Jameson, A. K. Jameson, N. C. Smith, and K. Jackowski, *J. Chem. Phys.* **86**, 2717 (1987).
- ⁷²D. Cappelletti, F. Pirani, F. Vecchiocattivi, E. L. Heck, and A. S. Dickinson, *Mol. Phys.* **93**, 485 (1998).
- ⁷³P. G. Kistemaker, M. M. Hanna, and A. E. de Vries, *Physica (Amsterdam)* **78**, 457 (1974).
- ⁷⁴M. A. ter Horst, C. J. Jameson, and A. K. Jameson, *Magn. Reson. Chem.* **44**, 241 (2006).

4.6 Calculation of the transport and relaxation properties of dilute water vapor

Robert Hellmann, Eckard Bich, Eckhard Vogel, Alan S. Dickinson, Velisa Vesovic
J. Chem. Phys. **131**, 014303(1-11) (2009).

Alle generalisierten Streuquerschnitte und die Transport- und Relaxationseigenschaften wurden selbst berechnet. Die vier Wechselwirkungspotentiale des Schrifttums wurden eigenständig programmiert und in die erweiterte Version des Programmcodes TRAJECT implementiert. Der eigene Anteil beträgt etwa 60%.

Reprinted with permission from Robert Hellmann, Eckard Bich, Eckhard Vogel, Alan S. Dickinson, Velisa Vesovic, J. Chem. Phys. 131, 1, 014303, 2009. Copyright 2009, American Institute of Physics.

Calculation of the transport and relaxation properties of dilute water vaporRobert Hellmann,¹ Eckard Bich,¹ Eckhard Vogel,¹ Alan S. Dickinson,^{2,a)} and Velisa Vesovic³¹*Institut für Chemie, Universität Rostock, D-18059 Rostock, Germany*²*School of Chemistry, Newcastle University, Newcastle upon Tyne NE1 7RU, United Kingdom*³*Department of Earth Science and Engineering, Imperial College, London SW7 2AZ, United Kingdom*

(Received 21 April 2009; accepted 4 June 2009; published online 6 July 2009)

Transport properties of dilute water vapor have been calculated in the rigid-rotor approximation using four different potential energy hypersurfaces and the classical-trajectory method. Results are reported for shear viscosity, self-diffusion, thermal conductivity, and volume viscosity in the dilute-gas limit for the temperature range of 250–2500 K. Of these four surfaces the CC-pol surface of Bukowski *et al.* [J. Chem. Phys. **128**, 094314 (2008)] is in best accord with the available measurements. Very good agreement is found with the most accurate results for viscosity in the whole temperature range of the experiments. For thermal conductivity the deviations of the calculated values from the experimental data increase systematically with increasing temperature to around 5% at 1100 K. For both self-diffusion and volume viscosity, the much more limited number of available measurements are generally consistent with the calculated values, apart from the lower temperature isotopically labeled diffusion measurements. © 2009 American Institute of Physics. [DOI: 10.1063/1.3158830]

I. INTRODUCTION

The formal kinetic theory for dilute gaseous systems¹ describes their transport and relaxation properties in terms of generalized cross sections. These cross sections are determined by the dynamics of binary collisions, which are governed by the intermolecular potential energy hypersurface, characteristic of the specific molecular interaction.

Transport and relaxation properties of dilute simple molecular gases can be calculated directly nowadays from their intermolecular potential with an accuracy comparable to that of the best available experimental data, see, for example, Refs. 2–11. The comparison between the calculated and the best experimental values provides a unique and stringent test of the accuracy of the potential surface. At low and high temperatures, where experimental data are of lower accuracy or nonexistent, calculations provide an accurate and reliable way of estimating transport and relaxation properties.

Ideally a quantum-mechanical description should be employed for the calculation of the generalized cross sections. However, for molecule-molecule systems this is at present not computationally feasible, apart possibly for pure hydrogen. For the temperatures relevant to the present work (250–2500 K), the method of choice is a classical-trajectory calculation, which is computationally relatively efficient and at the same time accurate. This was tested and confirmed by detailed comparison with quantum calculations for the He–N₂ system.^{12,13} In addition, the accuracy of the classical-trajectory method has recently been supported by computations of the viscosity of carbon dioxide⁷ and methane,¹⁰ for which close agreement with highly accurate viscosity measurements near room temperature has been obtained.

The work presented in this paper is a continuation of our previous studies^{7–11} and aims to improve our knowledge of transport and relaxation properties. So far we have confined our calculations to dilute gases consisting of linear or spherical top and nonpolar or weakly polar molecules. Water is the first asymmetric top, strongly polar, molecule for which classical-trajectory calculations have ever been performed with a full-dimensional rigid-molecule potential surface. As such the present work represents a significant step forward in our ability to calculate accurately transport and relaxation properties.

Water vapor is relevant in a particularly wide variety of both engineering and scientific contexts. For instance, it is used as working fluid in steam turbines, it is used for energy storage, it is a significant greenhouse gas whose effects must be included in climate modeling, and water masers have been observed in the interstellar medium. The accuracy of available shear viscosity and thermal conductivity data for water vapor, see Sec. IV below, is generally very good at lower temperatures. At higher temperatures, relevant for steam turbines, only very few data sets exist and these have relatively large uncertainties.

In the present paper we report on calculations of the shear viscosity, the thermal conductivity, the self-diffusion coefficient, and the volume viscosity of dilute water vapor. The relevant generalized cross sections have been evaluated by means of classical-trajectory calculations directly from accurate intermolecular potential energy hypersurfaces. For linear molecules the working expressions for the generalized cross sections in terms of properties of individual trajectories were derived by Curtiss.¹⁴ The extension to rigid asymmetric tops (such as water) has been provided.¹⁵

We have used four different intermolecular potentials for the H₂O–H₂O interaction: SAPT-5s¹⁶ and SAPT-5st,¹⁷ based

^{a)}Electronic mail: a.s.dickinson@ncl.ac.uk.

on symmetry-adapted perturbation theory (SAPT),¹⁸ SDFT-5s,¹⁹ based on SAPT(DFT),²⁰ which used density-functional theory (DFT) for the description of the monomers, and CC-pol,^{21–23} based on supermolecular MP2 (second-order Møller–Plesset perturbation theory) and CCSD(T) (coupled-cluster theory with iterative single and double excitations and noniterative perturbation treatment of triple excitations)²⁴ calculations. Of these four potentials, CC-pol is the most recent and most accurate and was tested for a number of properties (such as second pressure virial coefficients and rovibrational spectra of dimers), but not yet for transport and relaxation properties.

As we were completing our calculations a new potential, CC-pol-8s,²⁵ has become available. Although its accuracy is deemed slightly better than that of CC-pol, attested by a better description of the rovibrational spectra, the improvement in accuracy has not been judged sufficient to justify performing a new set of classical trajectories, which would be computationally expensive due to the much more complex expressions for the potential. The CC-pol-8s potential was therefore not considered in the present study.

All interaction potentials considered were developed using rigid monomers in the zero-point vibrationally averaged structure. The deepest well in the CC-pol potential surface has a depth of 1783 cm⁻¹, and this system has much stronger long-range (dipole-dipole) interactions than any considered previously.

It was shown^{7,10} that results using the rigid-rotor assumption are consistent with experiment for the viscosity and self-diffusion coefficients of carbon dioxide and methane up to very high temperatures. However, for thermal conductivity the neglect of energy transport by vibrationally excited molecules becomes more questionable. In order to estimate the influence on the thermal conductivity of neglecting vibration, we have employed the approximation described in our previous work.^{6–9,11} Hence we have corrected, where necessary, the generalized cross sections obtained from the classical-trajectory calculations based on the rigid-rotor assumption. For carbon dioxide and methane, which are more vibrationally active than water, the approximate procedure for the inclusion of the effects of the vibrational degrees of freedom has been shown to produce good agreement with the available experimental data on the thermal conductivity and the thermomagnetic effect.^{9,11}

II. THEORY

A. Transport properties

The shear viscosity η , the self-diffusion coefficient D , and the thermal conductivity λ of a polyatomic gas in the limit of zero density and in the absence of external fields can be expressed as^{1,26}

$$[\eta]_n = \frac{k_B T}{\langle v \rangle_0} \frac{f_\eta^{(n)}}{\mathfrak{S}(2000)}, \quad (1)$$

$$[D]_n = \frac{k_B T}{nm \langle v \rangle_0} \frac{f_D^{(n)}}{\mathfrak{S}'(1000)}, \quad (2)$$

$$[\lambda]_n = \frac{5k_B^2 T}{2m \langle v \rangle_0} \frac{\mathfrak{S}(1001) - 2r \mathfrak{S} \left(\begin{smallmatrix} 1001 \\ 1010 \end{smallmatrix} \right) + r^2 \mathfrak{S}(1010)}{\mathfrak{S}(1010) \mathfrak{S}(1001) - \mathfrak{S} \left(\begin{smallmatrix} 1001 \\ 1010 \end{smallmatrix} \right)^2} f_\lambda^{(n)}, \quad (3)$$

where $\langle v \rangle_0 = 4(k_B T / \pi m)^{1/2}$ is the average relative thermal speed, n is the number density, m is the molecular mass, T is the temperature, and k_B is Boltzmann's constant. The quantities $\mathfrak{S}(2000)$, $\mathfrak{S}'(1000)$, $\mathfrak{S}(1010)$, $\mathfrak{S}(1001)$, and $\mathfrak{S} \left(\begin{smallmatrix} 1001 \\ 1010 \end{smallmatrix} \right)$ are generalized cross sections, and the notation and conventions employed are fully described elsewhere.^{1,10} The parameter r is given by

$$r = \left(\frac{2 c_{\text{int}}}{5 k_B} \right)^{1/2}, \quad c_{\text{int}} = c_{\text{rot}} + c_{\text{vib}}. \quad (4)$$

Here c_{int} is the contribution of both the rotational, c_{rot} , and the vibrational, c_{vib} , degrees of freedom to the isochoric heat capacity, c_V .

The quantities $f_\eta^{(n)}$, $f_D^{(n)}$, and $f_\lambda^{(n)}$ are n th-order correction factors and account for the effects of higher basis-function terms in the perturbation-series expansion of the solution of the Boltzmann equation.¹ In this work we consider the second-order approximations for viscosity and thermal conductivity, but only the first-order approximation for self-diffusion ($f_D^{(n)} = 1$), as no higher-order expressions are available. Contributions from both velocity coupling^{1,27} and angular-momentum coupling^{1,28,29} are included in the second-order approximations.

B. Volume viscosity

The volume viscosity (also known as the bulk viscosity) can be inferred from measurements of the absorption and dispersion of ultrasonic waves in the gas.¹ As noted in Ref. 30, for the analysis of sound-absorption measurements the volume viscosity η_V is the fundamental quantity of interest. In this work we limit our investigation to the contribution to volume viscosity that arises from rotational relaxation only, as the nature of the intermolecular potential used in the calculation precludes investigation of the vibrational relaxation process.

The volume viscosity can be written as

$$[\eta_V]_n = \frac{k_B c_{\text{int}}}{c_V^2} \frac{k_B T}{\langle v \rangle_0 \mathfrak{S}(0001)} f_{\eta_V}^{(n)}. \quad (5)$$

The quantity $f_{\eta_V}^{(n)}$ is the n th-order correction factor for the volume viscosity and accounts for the effects of higher basis-function terms in the perturbation-series expansion of the solution of the Boltzmann equation.¹ The explicit expression for the second-order kinetic theory expression, $[\eta_V]_2$, is given by Ref. 31.

A number of experimenters have presented their measurements of sound absorption and dispersion in terms of a rotational relaxation time τ_{exp} or the corresponding rotational relaxation rate or as a rotational collision number.

We have converted from the relaxation time or rate measurements to volume viscosity values using the first-order kinetic theory relation,¹

$$\begin{aligned} [\eta_V]_1 &= \frac{k_B c_{\text{int}} P \tau_{VT}}{c_V^2}, \\ [\eta_V]_n &\approx \frac{k_B c_{\text{int}} P \tau_{\text{exp}}}{c_V^2}, \end{aligned} \quad (6)$$

where τ_{VT} is the isothermal relaxation time.^{30,32} Use of this equation to convert measured relaxation times or rates to volume viscosity values is only approximately equivalent to analyzing the measurements in terms of the volume viscosity. For collision-number results we have first used the standard relation^{1,9} with the rotational relaxation time.

III. CLASSICAL-TRAJECTORY CALCULATIONS

The classical-trajectory calculations were performed using an extension of the TRAJECT software code for linear molecules,³³ previously employed for pure nitrogen, carbon monoxide, and carbon dioxide (Refs. 7–9 and references therein). This code has been modified³⁴ to allow for the additional variables and averaging needed for rigid asymmetric tops and has recently been successfully used for pure methane.^{10,11}

The water molecule was represented in the trajectory calculations as a rigid asymmetric top. The geometry of the monomers corresponds to the zero-point vibrationally averaged structure used for the determination of the four interaction potentials considered in this work. For a given total energy, translational plus rotational, classical trajectories describing the collision of two molecules were obtained by integrating Hamilton's equations from pre- to postcollisional values (initial and final separation of 500 Å). We have used all four potentials as published for distances up to 500 Å. The fits employed included the long-range behavior correctly.

The total-energy-dependent generalized cross sections can be represented as 13-dimensional integrals, which were evaluated by means of a Monte Carlo procedure. The initial values of the momenta for the relative motion and for the rotation of the two molecules, as well as the angles defining their relative orientation, were chosen using a pseudorandom number generator.

At very small intermolecular distances the fits to the four potential surfaces yield highly negative potential energies. This unphysical behavior would cause numerical problems in the trajectory calculations for very high collision energies, those above about 20 000 K. (For convenience in the context of temperature-dependent observables we quote energies of interest as the equivalent temperatures.) To avoid this problem all potentials were augmented by an extremely short-ranged, highly repulsive, additional term of the form $V_{\text{rep}}(R) = (2.15 \text{ Å}/R)^{100}$ K. The value of 2.15 Å was found to be large enough to ensure that the potential energy always increases as the intermolecular separation decreases but

small enough to ensure that, to the accuracy of our calculations, this term does not influence the values of the thermally averaged cross sections up to 2500 K.

The classical trajectories were determined at 25 values of the total energy, divided into three ranges. In each range the energy values were chosen as the pivot points for Chebyshev interpolation in order to facilitate calculations of the cross sections at a number of temperatures.^{34,35} The highest energy used was 50 000 K, which is more than sufficient for the temperature range considered in this work. At each energy up to 100 000 classical trajectories (80 000 for CC-pol) were evaluated. The number of trajectories had to be reduced towards lower energies, those comparable or less than the well depth, because the low-energy trajectories require much longer computing times. For example, at 120 K, the lowest energy considered for SAPT-5s, SAPT-5st, and SDFT-5s, only 12 000 trajectories were calculated. For CC-pol the lowest energy was 200 K with 6000 trajectories. The smaller number of trajectories and the higher minimum energy for CC-pol was necessary because this potential function, in contrast to the other potentials used, is polarizable and thus requires more computing time for the evaluation of the potential and its derivatives. Contributions to the cross sections from trajectories with collision energies below 200 K were found to be totally negligible for all temperatures considered because they have only a very small weight in the thermal averaging process. Also the much smaller number of trajectories at low energies has negligible influence on the uncertainty of the calculated cross sections.

The precision of the calculations was assessed by estimating the convergence of the final temperature-dependent generalized cross sections as a function of the number of trajectories used. Furthermore, the symmetry of production cross sections under time reversal,¹ $\mathfrak{S}_{p'q's't'}^{pqst} = (-1)^{q+q'} \mathfrak{S}_{pqst}^{p'q's't'}$, allows the comparison between two cross sections calculated using independent expressions. This symmetry was used as a further indicator of precision.

IV. RESULTS

The calculations of the generalized cross sections were performed on a modern Linux workstation and took about 3 months of CPU time for the CC-pol surface and about 1 month for each of the other three surfaces. The evaluation of the classical trajectories was the most time-consuming part in the computations.

All the calculated transport and relaxation¹ cross sections are characterized by the customary monotonic decrease with temperature, while some of the production cross sections exhibit a maximum at low temperature. The values of the transport and relaxation cross sections are, on average, an order of magnitude larger than that of the production cross sections. The precision of most of the calculated transport and relaxation cross sections is estimated to be better than $\pm 0.3\%$, while the precision of most of the production cross sections is estimated to be better than $\pm 3.0\%$.

Tables of the cross sections employed in this work and

of the calculated transport properties, all evaluated using the CC-pol potential, have been deposited with the Electronic Physics Auxiliary Publication Service.³⁶

A. Shear viscosity

1. Second-order contributions

Using Eq. (1) the viscosity values were calculated from the generalized cross section $\mathfrak{S}(2000)$ combined with the second-order correction factor $f_{\eta}^{(2)}$, evaluated employing expressions given in our previous work.⁷ The calculations indicate that the values of $f_{\eta}^{(2)}$ are close to unity for all temperatures and all potentials considered. The differences between the values of the correction factor calculated using the four potentials studied are small and hence results for only the CC-pol potential are discussed. For this potential $f_{\eta}^{(2)}$ has a value of 1.0055 at 250 K and its magnitude decreases with increasing temperature. At about 1000 K $f_{\eta}^{(2)}$ reaches a minimum of 1.0025 and then increases again with temperature to reach a value of 1.0048 at 2500 K. Overall, the effect of the second-order correction on the viscosity of water is similar to that observed for the other molecules studied so far. The contribution from angular-momentum coupling is very small, at most 0.01%, for all temperatures considered in this work. This contribution is at least an order of magnitude smaller than those observed for the other molecules studied, indicating that the influence of a magnetic field on the viscosity of water vapor is negligible. Hence, our assumption of including only the leading polarization in the description (see the discussion in Ref. 7) is justified.

2. Comparison with experiment

A critical evaluation of viscosity measurements on water, based on data available in 2007, was performed in a joint project between the IAPWS (International Association for the Properties of Water and Steam) and the IATP (International Association for Transport Properties, formerly the Subcommittee on Transport Properties of the International Union of Pure and Applied Chemistry) and resulted in a "Release on the IAPWS Formulation 2008 for the Viscosity of Ordinary Water Substance"^{37,38} to be referred to as "the IAPWS 2008 correlation." This formulation enables the calculation of the viscosity of water for wide ranges of fluid conditions up to 1173 K and 1000 MPa, including the zero-density limit. In 2005 Teske *et al.*³⁹ derived another zero-density viscosity correlation using reliable data sets from the literature and new experimental data at low density, obtained in our laboratory using an all-quartz oscillating-disk viscometer.

As will be shown later in this section, of the four intermolecular potential energy surfaces considered here, the CC-pol surface^{21–23} gives the best agreement with experiment. Accordingly most comparisons for shear viscosity between theory and experiment will be performed using this surface. Figure 1 illustrates the comparison between the values calculated for the CC-pol surface and the two correlations and also with different experimental data. For this comparison we employed the same zero-density viscosity values as Teske *et al.*³⁹ The reader is referred to Refs. 38 and 39 for a com-

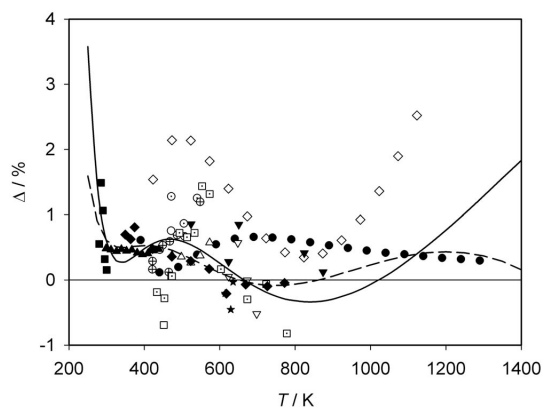


FIG. 1. Deviations of experimental and experimentally based zero-density viscosity coefficients from the values $\eta_{\text{calc-CCpol}}$ calculated for the CC-pol potential of Bukowski *et al.* (Refs. 21–23) for H₂O. Deviations are defined as: $\Delta = (\eta_{\text{exp}} - \eta_{\text{calc-CCpol}}) / \eta_{\text{calc-CCpol}}$. Experimental data: (\diamond) Shifrin (Ref. 40); (\circ) Kestin and Wang (Ref. 41); (\odot) Moszynski (Ref. 42); (\oplus) Kestin and Richardson (Ref. 43); (\bullet) Latto (Ref. 44); (\triangle) Rivkin and Levin (Ref. 45); (∇) Rivkin *et al.* (Ref. 46); (\square) Sato *et al.* (Ref. 47); (\square) Sato *et al.* (Ref. 48); (\blacksquare) Yasumoto (Ref. 49); (\blacklozenge) Timrot *et al.* (Ref. 50); (\blacktriangledown) Nagashima *et al.* (Ref. 51); (\star) Oltermann (Ref. 52); (\blacktriangle) Teske *et al.* (Ref. 39). Experimentally based values: (---) Teske *et al.* (Ref. 39); (—) IAPWS 2008 (Ref. 37).

prehensive account of how the zero-density extrapolation was performed for data of different authors, together with a discussion of the ascribed experimental uncertainties.

Figure 1 shows that in the temperature range from 300 to 1200 K the zero-density viscosity correlations of Teske *et al.*³⁹ and of Huber *et al.*³⁸ (the IAPWS 2008 correlation) are in close agreement with the values calculated for the CC-pol surface.^{21–23} Being based on the same experimental material, the two correlations are generally mutually consistent. However, at high temperatures they extrapolate differently due to the weights chosen for the data of Shifrin⁴⁰ and of Latto⁴⁴ in the fitting procedures used to generate the correlations.

The figure demonstrates that the experimental data of Teske *et al.* in the temperature range of 298–438 K deviate from the calculated values by about +0.5%. In principle, this difference should be decreased by 0.1%–0.2% because Teske *et al.* used an old reference value for the viscosity of argon of Kestin and Leidenfrost⁵³ to calibrate their oscillating-disk viscometer at room temperature. It should be noted that in this temperature range the temperature dependence of these experimental viscosity data is essentially reproduced perfectly by the values calculated using the CC-pol intermolecular potential. The figure reveals further that nearly all experimental data deviate from the calculated values by between –0.5% and +1.5%, apart from the data of Shifrin,⁴⁰ which are characterized by deviations in excess of +2%, not only at very high but also at moderate temperatures around 500 K. In contrast, the experimental data of Latto⁴⁴ are within 1% of the calculated values up to 1350 K.

An essential aspect of the new values calculated with the CC-pol intermolecular potential energy surface^{21–23} is their behavior at low and high temperatures, where experiments are most difficult. As illustrated in Figs. 1 and 2, the devia-

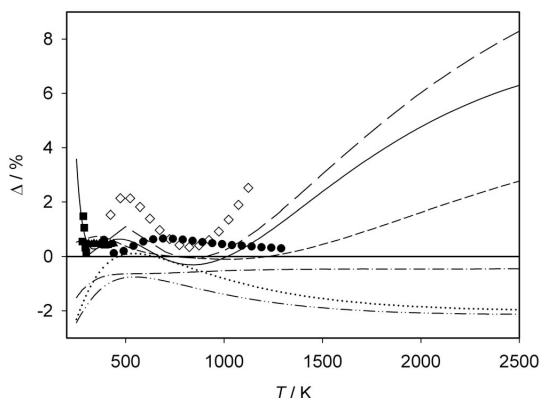


FIG. 2. For H_2O comparison of the extrapolation behavior at low and high temperatures of the values $\eta_{\text{calc-CCpol}}$ calculated for the CC-pol potential of Bukowski *et al.* (Refs. 21–23), with experimental data, experimentally based values considering some input from kinetic theory and simple potential models, calculated values for the other intermolecular potential energy surfaces. Deviations are defined as $\Delta = (\eta_{\text{exp,calc}} - \eta_{\text{calc-CCpol}}) / \eta_{\text{calc-CCpol}}$. Experimental data: (\diamond) Shifrin (Ref. 40); (\bullet) Latto (Ref. 44); (\blacksquare) Yasumoto (Ref. 49); (\blacktriangle) Teske *et al.* (Ref. 39). Experimentally based values: (---), Aleksandrov *et al.* (Ref. 54); (— · —), Fokin and Kalashnikov (Ref. 55); (—), IAPWS 2008 (Ref. 37). Theoretically calculated values: (- · · · · -), SAPT-5s potential of Mas *et al.* (Ref. 16); (· · · · ·), SAPT-5st potential of Groenboom *et al.* (Ref. 17); (- - - - -), SDFT-5s potential of Bukowski *et al.* (Ref. 19).

tions increase rapidly in the low temperature limit. Both correlations in this temperature range rely entirely on the experimental data by Yasumoto.⁴⁹ These data are characterized by relatively large scatter due to the experimental difficulties at the very low water vapor densities. Although in developing the two correlations, Yasumoto's estimated uncertainty of $\pm 0.5\%$ was ascribed to these data, a more realistic estimate appears to be $\pm 1\%$.

Figure 2 illustrates the behavior of the IAPWS 2008 correlation for temperatures up to 2500 K, the temperature considered to be the limit of a physically reasonable extrapolation by the IAPWS.³⁷ The deviations from the calculated values increase with increasing temperature, reaching a maximum of 6% at 2500 K. This is entirely due to the weighting given to the data of Shifrin⁴⁰ in the fitting procedure for the IAPWS correlation.

In addition, it is of interest to compare the calculated values with both a correlation proposed by Aleksandrov *et al.*⁵⁴ and recommended values by Fokin and Kalashnikov.^{55,56} Aleksandrov *et al.* took into account the general behavior as $T \rightarrow 0$ and $T \rightarrow \infty$ of the collision integrals used in kinetic theory for monatomics and determined the parameters in their equation using reliable low-density viscosity data from the literature at temperatures up to 1400 K. Fokin and Kalashnikov⁵⁵ fitted a generalized four-parameter Stockmayer potential to selected experimental viscosity and self-diffusion data of rarefied steam ranging for temperatures between 280 and 1773 K and used the Mason–Monchick^{57,58} approximation to infer values up to 2500 K. In their more recent paper⁵⁶ they used the new experimental data of Ref. 39 at low temperatures to improve their fit slightly but reported viscosity values up to a tem-

perature of 2000 K only. With respect to the high-temperature behavior, we restrict the comparison to the earlier values,⁵⁵ in particular, since the newer values are less than half a percent higher. There exists good agreement between the IAPWS 2008 correlation and the recommended values of Fokin and Kalashnikov,⁵⁵ within their mutual uncertainties. This is not surprising since Fokin and Kalashnikov used a similar data set at high temperatures as the IAPWS 2008 correlation. However, the extrapolation to 2500 K differs significantly from our calculated values. The theoretical basis of the extrapolations of Fokin and Kalashnikov,^{55,56} as well as that of Aleksandrov *et al.*,⁵⁴ is much less well founded than the methods employed here. In particular, the Fokin and Kalashnikov^{55,56} extrapolation relies on the unrealistic model potential where the softness of the repulsive wall is determined by a single empirical parameter that is sensitive to the high temperature data used in its determination.

Figure 2 also compares the values calculated for the CC-pol intermolecular potential energy hypersurface^{21–23} with those computed using the other potential surfaces being considered here.^{16,17,19} Taking into account the agreement with the experimental data, CC-pol proves to be the best of these surfaces. With differences of no more than 2% at most between the results using all four surfaces, this level of agreement is very encouraging. In particular, the SDFT-5s potential,¹⁹ based on a very different theoretical approach to that used for CC-pol, yields viscosities which are only slightly smaller than those obtained with the CC-pol surface for temperatures above 500 K. The older SAPT-5s (Ref. 16) and SAPT-5st (Ref. 17) potentials show somewhat larger deviations, especially at higher temperatures, indicating that they are, on average, too repulsive.

We consider that the present calculations provide the best estimate of the viscosity of water at temperatures down to 250 K. Noting the excellent agreement with our computed values of the temperature dependence of the experimental data by Teske *et al.*³⁹ between 298 and 438 K, and also of the consistency with the experimental data by Latto⁴⁴ up to 1350 K, we expect that our calculations provide the most reliable results in the temperature range up to 2500 K, previously covered by extrapolations. We estimate the accuracy of the computed values to be of the order of $\pm 1\%$ at 250 and 2500 K and even better at intermediate temperatures.

B. Self-diffusion

In contrast to the situation for the shear viscosity and thermal conductivity, (see Sec. IV C 3), there are very few measurements of self-diffusion in low-density water vapor. We are aware of only two: a relatively old measurement by Swinton⁵⁹ in 1971 of the diffusion of tritiated water, HTO, in H_2O and a more recent measurement in 2006 using the NMR spin-echo method by Yoshida *et al.*^{60,61}

Swinton⁵⁹ measured self-diffusion at five temperatures between 363 and 517 K with pressures of 0.01–0.3 bar. The precision of his results ranged from $\pm 1.5\%$ at 363 K to $\pm 4\%$ at 517 K. There was no discussion of any pressure dependence of the diffusion coefficients. We have assumed that the

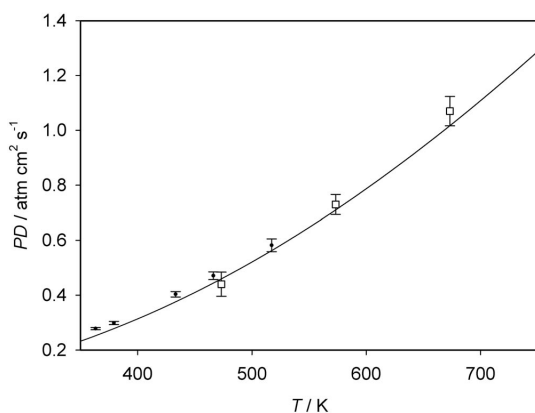


FIG. 3. Comparison of measured and calculated values of the diffusion coefficient at one atmosphere (PD) for H_2O . Experimental data: (●) Swinton (Ref. 59); (□) Yoshida *et al.* (Refs. 60 and 61). The error bars shown correspond to the estimated experimental uncertainties (see text). The uncertainties for the three intermediate temperatures of Swinton (Ref. 59) have been loosely interpolated between the values at 363 and 517 K. Calculated values: (—) CC-pol potential surface of Bukowski *et al.* (Refs. 21–23).

tabulated values are reduced to a pressure of 1 atm. When comparing with calculated values we have scaled these measured values by the usual factor to allow for the different reduced masses of $HTO-H_2O$ and H_2O-H_2O collisions. This factor would be exact for systems described classically by a spherically symmetric potential common to both isotopomers.

The spin-echo measurements^{60,61} were taken at 473, 573, and 673 K and the results at the two higher temperatures were extrapolated to the zero-density limit. However, measurements at just two pressures were available at 473 K and the value at the lower density (0.0041 g cm^{-3}) was taken as the zero-density limit.^{60,61} The uncertainty of the measurements is listed as $\pm 5\%$. When Fokin and Kalashnikov⁵⁶ employed these results, they assigned an uncertainty of $\pm 10\%$ to the 473 K diffusion coefficient and $\pm 5\%$ to the values at the other two temperatures, and we have adopted these uncertainties.

Both these sets of results are compared in Fig. 3 with the calculated values using the CC-pol potential surface. Neglecting the temperature difference between the Swinton⁵⁹ result at 466.2 K and the Yoshida *et al.*⁶¹ result at 473.2 K, these two measurements by quite different techniques are seen to be mutually consistent. Our calculated values are smaller than the measured values of Swinton⁵⁹ with the difference falling from 10% at 363 K to 3% at 517 K. These differences are significantly larger than the estimated experimental uncertainty, except at the highest temperature. Given the possible effect on the measured values of the reduction to zero density, it is difficult to assess the significance of these differences at the lower temperatures. The three spin-echo measurements^{60,61} are all consistent with theory within the estimated experimental uncertainty.

The differences between the values calculated using the four surfaces considered here are less than 1.5% at all tem-

peratures considered, with the CC-pol results almost always the largest. As the differences are very similar to those in Fig. 2 for shear viscosity they are not shown.

Matsunaga and Nagashima⁶² have estimated the self-diffusion coefficient of water vapor in the dilute-gas limit for temperatures between 273 and 2000 K, based on values calculated for a spherical potential whose parameters were chosen to yield agreement with the shear viscosity measurements. They estimated the accuracy of their results as $\pm(6-8)\%$. Comparison with values calculated using the CC-pol potential shows agreement within $\pm 2\%$ for temperatures in the range of 500–2000 K. The largest difference, +13%, occurred at 273 K but the difference fell rapidly with increasing temperature to about 5% at 350 K and 2% at 500 K.

Fokin and Kalashnikov⁵⁶ have also estimated values of the self-diffusion coefficient based on a nonspherical potential and the Mason–Monchick^{57,58} approximation, as discussed previously (see Sec. IV A 2). The values of Fokin and Kalashnikov⁵⁶ lie between 3% above and 5% below our calculated values, consistent with their estimate of the uncertainty of their results as 6%–8%. While the largest deviations of the results of Ref. 56 for shear viscosity and self-diffusion from our calculated values are comparable, their temperature dependence is rather different.

C. Thermal conductivity

1. Vibrational degrees of freedom

All the cross sections in this work have been calculated assuming that the water molecules can be represented as rigid rotors (rr) in their ground vibrational state (00). However, calculation of the thermal conductivity requires knowledge of cross sections that take into account both rotational and vibrational degrees of freedom, as energy stored in the vibrational degrees of freedom will influence the transport of energy through the gas. To account for the presence of the vibrational degrees of freedom in a water molecule, we have corrected, using the methodology and notation described in Ref. 8, all the cross sections $\mathfrak{S}_{p'q's't'}^{pqs't'}$ with $t+t' > 0$ which enter the description of thermal conductivity. In line with our previous work, we use the subscript “int” to show that the particular generalized cross section has been corrected. The correction is based on the assumption that the vibrational energy is “frozen” during the collision and that the vibrational states of the molecules will have negligible influence on the differential cross section for the scattering of two rotationally active molecules.

In the first-order approximation for thermal conductivity, $n=1$ in Eq. (3), two cross sections, $\mathfrak{S}_{1001}^{(1010)}$ and $\mathfrak{S}(1001)$, require correction. The correction for the production cross section $\mathfrak{S}_{1001}^{(1010)}$ is the larger of the two and exhibits a strong temperature dependence, as already noted for carbon dioxide and methane. The ratio $\mathfrak{S}_{1001}^{(1010)}_{\text{int}}/\mathfrak{S}_{1001}^{(1010)}$ is near unity at 300 K, but decreases to 0.78 at 1000 K and 0.64 at 2000 K. However, similarly to methane at high temperatures, this production cross section is approximately 20 times smaller than the two transport cross sections, and hence its contribution to the thermal conductivity is small.

For $\mathfrak{S}(1001)_{\text{int}}$ it can be shown⁸ that the correction is of the form

$$\mathfrak{S}(1001)_{\text{int}} = \left(\frac{c_{\text{rot}}}{c_{\text{int}}}\right)\mathfrak{S}(1001)_{\text{rr}00} + \left(\frac{c_{\text{vib}}}{c_{\text{int}}}\right)\mathfrak{S}'(1000)_{\text{rr}00}. \quad (7)$$

Rotational relaxation of water molecules is relatively slow (our calculations yield a rotational collision number $\zeta_{\text{rot}}=5-12$ for temperatures between 300 and 2000 K), so one would expect that, on average, rotational energy is primarily transported by the translational motion of the molecules. Hence, one would expect the value of $\mathfrak{S}(1001)_{\text{rr}00}$ to be approximately equal to that of $\mathfrak{S}'(1000)_{\text{rr}00}$. This behavior was certainly observed for methane where the rotational relaxation number is comparable with that of water. However, our calculations indicate that the ratio $\mathfrak{S}'(1000)_{\text{rr}00}/\mathfrak{S}(1001)_{\text{rr}00}$ lies between 0.38 and 0.54 over the temperature range considered. This clearly indicates that in strongly polar molecules, such as water, rotationally resonant collisions play an important part, as has been anticipated by Ref. 58. Such collisions nearly double the value of $\mathfrak{S}(1001)_{\text{rr}00}$ cross sections. As a result of these rotationally resonant collisions, the correction for $\mathfrak{S}(1001)_{\text{int}}$ is much larger than in previous studies and the ratio $\mathfrak{S}(1001)_{\text{int}}/\mathfrak{S}(1001)_{\text{rr}00}$ falls off from near unity at 300 K to 0.7 at 2000 K. The behavior of the magnitude of this ratio resembles more that of a very much more rotationally active molecule, such as carbon dioxide, than it does the behavior of the rotationally similar methane molecule.

The overall effect on the thermal conductivity of correcting the cross sections for the vibrational degrees of freedom is strongly dependent on temperature. Although the effect is small at 300 K, of the order of 0.3%, at 1000 K it increases to 8.6%, and at 2000 K it reaches 16.6%. For comparison, the correction at 1000 K for carbon dioxide amounted to approximately 5%. The smallness of the effect for carbon dioxide is due to the much larger contribution of the production cross section $\mathfrak{S}_{1001}^{(1010)}_{\text{int}}$, which largely canceled the effect of correcting $\mathfrak{S}(1001)_{\text{rr}00}$.

In the full second-order approximation (see below), the effect of this vibrational correction on the thermal conductivity coefficient is very similar: at 1000 K the overall effect on the thermal conductivity is 8.4%, while at 2000 K it is 15.8%.

2. Second-order contributions

The values of thermal conductivity were calculated in the second-order approximation from the generalized cross sections using Eq. (3), where the second-order correction factor $f_{\lambda}^{(2)}$ has been calculated by means of expressions given in our previous work.⁸ Similarly to the viscosity, the value of the correction factor is close to unity for all the temperatures and all the potentials considered. Furthermore, the value of $f_{\lambda}^{(2)}$ exhibits a similar temperature dependence to that observed for $f_{\eta}^{(2)}$ and is also very weakly dependent on the intermolecular potential. At the lowest temperature (250 K) considered in this work, the magnitude of $f_{\lambda}^{(2)}$ for CC-pol is 1.009. The correction factor initially decreases with increas-

ing temperature, reaching a minimum of 1.0076 at about 400 K, followed by an increase to 1.027 at 2500 K. The contribution from angular-momentum coupling is again very small for all temperatures considered, increasing from about 0.01% at 250 K to 0.26% at 2500 K.

3. Comparison with experiment

The ‘‘Revised Release on the IAPS Formulation 1985 for the Thermal Conductivity of Ordinary Water Substance,’’ issued in 1998 and to be referred to as ‘‘the Revised IAPS 1998 correlation,’’⁶³ is the latest and most accurate correlation proposed for the thermal conductivity of water, based on the critical assessment of experimental measurements. The low-density thermal conductivity values of this correlation are characterized by uncertainties of $\pm 2\%$ at temperatures below about 850 K and of $\pm 3\%$ at higher ones. For the comparison with our calculated values at zero density, we have selected the experimental values of Refs. 64–81, proposed by a Special Committee of IAPS as primary data sets.⁸² Additional suitable experimental data of Refs. 83–91, of comparable accuracy, taken from the open literature or from the data bank by Assael *et al.*⁹² were also selected. In order to obtain the experimental value of thermal conductivity at zero density either isothermal values as a function of density were extrapolated to this limit or individual values at low density were corrected to it using the density dependence of the Revised IAPS 1998 correlation.⁶³

The hot-wire (HW) method,^{64–69,71,73,80,83,84,89,91} the concentric-cylinder (CC) method,^{68,70,72,74–79,81,85,87,90,93} the parallel-plate method,^{86,88} and the transient HW (THW) technique⁹⁴ were employed in performing the measurements on water vapor and steam. In principle, the uncertainties achieved with these experimental techniques decrease along this series of methods towards the THW method. However, in the case of water vapor and steam, the situation is complicated, since the temperatures required were often very high so that numerous difficulties limited the accuracy of the experiments. In particular, convection, radiative heat transfer, parasitic heat transfer via the ends of the measuring device, temperature jumps at the solid-fluid boundaries, especially at low fluid density, contamination of the solid surfaces during the experiment, and irregularities in the idealized temperature profile required for the application of the working equations were cited as possible causes of lower accuracy.

Figures 4 and 5 illustrate the deviations of experimental data for the thermal conductivity in the limit of zero density from our calculations based on the CC-pol potential of Bukowski *et al.*^{21–23} For clarity, because of the quantity of available data, the earlier data are presented in Fig. 4 and the later in Fig. 5. The best data of the selected measurements still show a scatter of the order of $\pm 2\%$ at most temperatures. But there exist larger differences between the measurements of different workers. Notwithstanding this observation, it is also clear that there is a systematic trend of the calculated values progressively underestimating the experimental data as the temperature increases.

This trend is confirmed in both figures where the calculations are compared with the thermal conductivity in the limit of zero density based on the Revised IAPS 1998

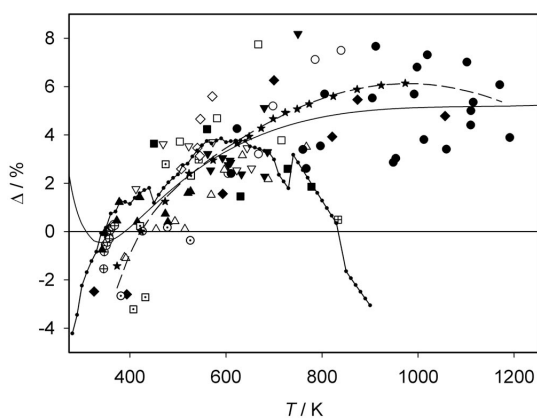


FIG. 4. Deviations of experimental and experimentally based zero-density thermal conductivity coefficients from the calculated values $\lambda_{\text{calc-CCpol}}$ for the CC-pol potential of Bukowski *et al.* (Refs. 21–23) for H_2O . Deviations are defined as $\Delta = (\lambda_{\text{exp}} - \lambda_{\text{calc-CCpol}}) / \lambda_{\text{calc-CCpol}}$. Experimental data: (\oplus) Milverton (Ref. 64); (\blacktriangle) Timrot and Vargaftik (Ref. 65); (\blacktriangledown) Vargaftik (Ref. 66); (\blacklozenge) Vargaftik and Oleshchuk (Ref. 67); (\square) Vargaftik and Smirnova (CC method) (Ref. 68); (\blacksquare) Vargaftik and Smirnova (HW method) (Ref. 68); (\circ) Vargaftik and Tarzimanov (Ref. 69); (\boxplus) Vines (Ref. 70); (\diamond) Tarzimanov (Ref. 71); (\triangle) Vargaftik and Zaitseva (at 0.5 bar) (Ref. 83); (∇) Keyes and Vines (Ref. 72); (\bullet) Vargaftik and Zimina (Ref. 73); (\odot) Baker and Brokaw (Ref. 84); (\square) Venart (Ref. 74). Experimentally based values: (— — —), Vargaftik and Zimina (Ref. 73); (\star) IAPS Skeleton Tables 1964 (Refs. 95 and 96); (—•—•—), Standard Reference Values of Powell *et al.* (Ref. 97); (—), Revised IAPS 1998 correlation (Ref. 63).

correlation.⁶³ It is obvious that from 400 to 1100 K the difference between the values using this correlation and the values for the CC-pol potential increases continuously up to more than +5%. Further the extrapolation behavior at low temperatures down to 273 K differs markedly. Although the differences at higher temperatures are just outside the mutual uncertainties of the experimentally based correlation ($\pm 3\%$) and of the theoretical calculation ($\pm 1\%$), it is the temperature dependence of the Revised IAPS 1998 correlation that is not reproduced by the calculations.

The pre-1965 experiments mostly measured near to atmospheric pressure: the experimentally based correlation of Vargaftik and Zimina,⁷³ the IAPS Skeleton Tables from 1964,^{95,96} and standard reference values of Powell *et al.*,⁹⁷ all reported for atmospheric pressure, are compared, after correction to zero density, in Fig. 4. It should be mentioned that Vargaftik and Zimina developed their correlation including the experimental data of Refs. 66–68, 70, 72, and 73, with a correction to the data point at 833 K of Vines⁷⁰ for a possible temperature-jump effect. This correction is the reason for the large difference between the correlation by Vargaftik and Zimina and the standard reference values of Powell *et al.*⁹⁷ at high temperatures. The figure makes evident that the correlated values by Vargaftik and Zimina establish the basis for the IAPS Skeleton Tables from 1964 and for the later Revised IAPS 1998 correlation.

The experiments performed between 1967 and 1989 are compared with our calculations in Fig. 5. These experiments were mostly directed to the determination of the density dependence of the thermal conductivity and to its critical en-

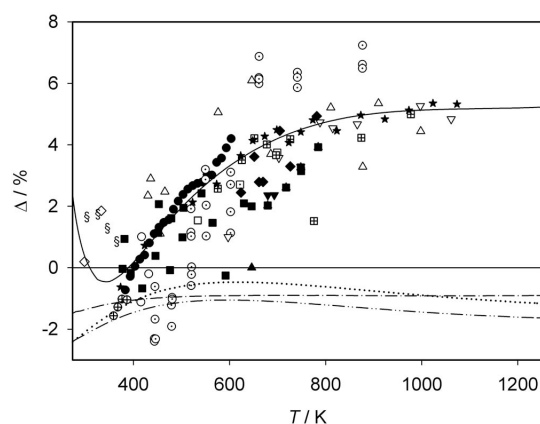


FIG. 5. Deviations of experimental data, of experimentally based values, and of calculated values for different intermolecular potential energy surfaces from the zero-density thermal conductivity coefficients $\lambda_{\text{calc-CCpol}}$ calculated for the CC-pol potential of Bukowski *et al.* (Refs. 21–23) for H_2O . Deviations are defined as $\Delta = (\lambda_{\text{exp,calc}} - \lambda_{\text{calc-CCpol}}) / \lambda_{\text{calc-CCpol}}$. Experimental data: (\circ) Brain (Ref. 75); (\bullet) Bury *et al.* (Ref. 76); (\odot) Brain (Ref. 77); (\diamond) Dijkema *et al.* (Ref. 85); (\blacktriangle) Le Neindre *et al.* (Ref. 78); (\square) Tarzimanov and Zainullin (Ref. 79); (\triangle) Vargaftik *et al.* (Ref. 80); (\blacksquare) Bury *et al.* (Ref. 81); (\square) Sirota *et al.* (Refs. 86 and 88); (∇) Popov and Dulnev (Ref. 87); (\boxplus) Curtiss *et al.* (Ref. 89); (\blacktriangledown) Tufeu and Le Neindre (Ref. 90); (\S) Miroshnichenko and Makhrov (Ref. 91); (\blacklozenge) Tufeu and Le Neindre (Ref. 93); (\boxplus) Tarzimanov and Gabitov (Ref. 94). Experimentally based values: (\star) IAPS Skeleton Tables 1977 (Refs. 82, 98, and 99); (—), Revised IAPS 1998 correlation (Ref. 63). Calculated values: (—•—•—), SAPT-5s potential of Mas *et al.* (Ref. 16); (\cdots), SAPT-5st potential of Groenenboom *et al.* (Ref. 17); (—•—•—), SDFT-5s potential of Bukowski *et al.* (Ref. 19).

hancement. In terms of zero-density thermal conductivity extracted from these measurements, the somewhat more recent experiments by a French group^{78,81,90,93} tend to support lower values, whereas the newer Russian papers confirm consistently the older ones, which formed the basis of the original correlation by Vargaftik and Zimina.⁷³

Not all of these measurements are independent, however. Those of Bury *et al.*⁷⁶ were adjusted to the IAPS Skeleton Tables from 1964 at atmospheric pressure, as reported by Grigull.¹⁰⁰ For the evaluation of the measurements with their parallel-plate apparatus, Sirota *et al.*^{86,88} changed the value of the emissivity coefficient of the stainless-steel plates from 0.48 given in their earlier paper¹⁰¹ to 0.32, resulting in a thermal conductivity value at atmospheric pressure close to the correlation by Vargaftik and Zimina.⁷³ Nonetheless, there is overwhelming experimental support for the temperature dependence of the Revised IAPS 1998 correlation.

At this stage it is not clear why the current calculations cannot reproduce this temperature dependence, especially as the CC-pol potential reproduces very accurate viscosity data (see Sec. IV A 2). Nevertheless, the results using the CC-pol potential are, at temperatures below 500 K, within 2% of the Revised IAPS 1998 correlation.

We suggest that further discussion of the differences between the experimental data and the calculated values needs to focus primarily on the HW method with which most of the early experiments included in the correlation of Vargaftik and Zimina⁷³ were performed. The urgency for new and ac-

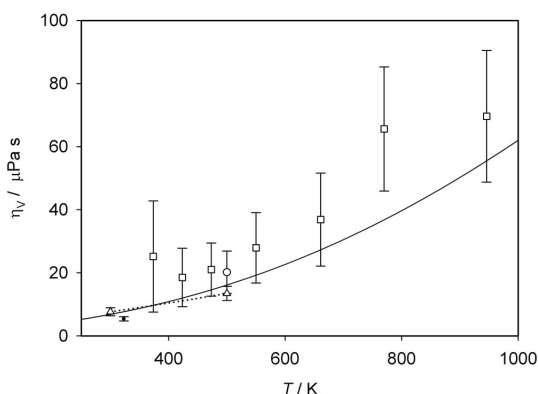


FIG. 6. Comparison of measured and calculated values of the volume viscosity η_v for H_2O . Experimental data: (●) Roesler and Sahn (Ref. 102); (□) Bass *et al.* (Ref. 103); (○) Keaton and Bass (Ref. 104); (Δ····Δ) Synofzik *et al.* (Ref. 105). The error bars shown correspond to the estimated experimental uncertainties (see text). Second-order calculations: (—) CC-pol potential surface of Bukowski *et al.* (Refs. 21–23).

curate measurements above 1000 K, already stressed by Fokin and Kalashnikov,⁵⁶ is also strongly supported.

The comparison between the different values calculated for the CC-pol intermolecular potential energy surface^{21–23} and for the other potential surfaces^{16,17,19} is also shown in Fig. 5. The agreement among the potentials is similar to that observed for viscosity. The other potentials considered here give results differing even more from the Revised IAPS 1998 correlation at high temperatures.

D. Volume viscosity

Results for the volume viscosity were calculated for the four potential energy surfaces of interest. For the CC-pol surface the difference between the first-order and second-order results increased slowly with increasing temperature but never exceeded 3% for temperatures between 250 and 2500 K. The results in second order using the four surfaces involved never differed from the CC-pol values by more than 1.5%.

Four sets of measurements in water vapor of rotational collision numbers or relaxation times or rates are available: one at 323.15 K by Roesler and Sahn,¹⁰² with a quoted uncertainty of $\pm 25\%$, one by Bass *et al.*¹⁰³ covering the temperature range from 373 to 946 K with uncertainties falling from $\pm 70\%$ at 373 K to $\pm 30\%$ at 946 K, a measurement at 500 K with an uncertainty of $\pm 33\%$ by Keaton and Bass,¹⁰⁴ and measurements between 300 and 500 K with uncertainties of about $\pm 20\%$ by Synofzik *et al.*¹⁰⁵ All four papers mentioned the difficulty of these measurements. The results have been converted to volume-viscosity values using Eq. (6). Comparison is made in Fig. 6 with results obtained in second order using the CC-pol surface. It can be seen that almost all the measurements are consistent with the calculated values, and for those for which the calculated value lies outside the error bars, the difference is less than twice the listed experimental uncertainty.

While the accuracy of these measurements does not allow a stringent test of the potential surface employed, for the properties considered here, the volume viscosity is the one most sensitive to the anisotropy of the surface.

V. SUMMARY AND CONCLUSIONS

We have calculated the shear viscosity, thermal conductivity, self-diffusion, and volume viscosity of low-density water vapor over the temperature range of 250–2500 K. The generalized cross sections required in the best available kinetic theory were computed by means of the classical-trajectory method employing four different rigid-rotor water-water intermolecular potential energy hypersurfaces.

For the viscosity, very good agreement with the best experimental data is obtained when using the CC-pol potential of Bukowski *et al.*^{21–23} The data of Teske *et al.*,³⁹ which are the most accurate at low temperatures, differ from the values calculated using the CC-pol surface by only about +0.5%. The high-temperature data of Latto,⁴⁴ which extend up to 1350 K, show also similar small deviations. The IAPWS 2008 correlation³⁷ shows relatively large deviations from the calculated values at very high, and particularly very low, temperatures. The calculated values are expected to be more accurate than the IAPWS 2008 correlation at such temperatures. We estimate the uncertainties of the computed values to be about $\pm 1\%$ at 250 K and 2500 K, and even better at intermediate temperatures.

Differences between theory and experiment for self-diffusion were found to be consistent with the experimental uncertainties for the more recent NMR spin-echo measurements.^{60,61} However, at all but the highest temperature available (517 K), the differences with the HTO– H_2O diffusion measurements⁵⁹ were significantly larger than the estimated experimental precision. No reduction to the zero-density limit was performed for these observations.

For the thermal conductivity the deviations between most of the experimental data and the values calculated with the four potential energy surfaces are comparably small at low temperatures, but increase with higher temperatures to about +5% compared with calculated values using the CC-pol surface. Considering the very good agreement between theory and experiment in the case of viscosity, it seems unlikely, but not impossible, that the calculated values for the thermal conductivity are characterized by such large uncertainties. These differences need further investigation of both possible deficiencies of the theory, especially for strongly polar molecules, and also of all the corrections used for the evaluation of the thermal conductivity measurements, particularly with the HW method. Further measurements above 1000 K are highly desirable.

In the case of the volume viscosity, where experiments are especially difficult, theory and experiment^{102–105} were generally consistent within the rather large uncertainty of most of the measurements.

While differences between the results using the four potential energy surfaces considered^{16–23} were small, the CC-pol surface^{21–23} gave the best overall agreement with the measurements.

ACKNOWLEDGMENTS

This work was financially supported by the German Research Foundation (Deutsche Forschungsgemeinschaft) Grant No. VO 499/14-1.

- ¹F. R. W. McCourt, J. J. M. Beenakker, W. E. Köhler, and I. Kučer, *Nonequilibrium Phenomena in Polyatomic Gases* (Oxford Science Publications, Oxford, 1990), Vol. 1.
- ²E. L. Heck and A. S. Dickinson, *Mol. Phys.* **81**, 1325 (1994).
- ³E. L. Heck, A. S. Dickinson, and V. Vesovic, *Mol. Phys.* **83**, 907 (1994).
- ⁴E. L. Heck and A. S. Dickinson, *Physica A* **217**, 107 (1995).
- ⁵E. L. Heck and A. S. Dickinson, *Physica A* **218**, 305 (1995).
- ⁶E. Bich, S. Bock, and E. Vogel, *Physica A* **311**, 59 (2002).
- ⁷S. Bock, E. Bich, E. Vogel, A. S. Dickinson, and V. Vesovic, *J. Chem. Phys.* **117**, 2151 (2002).
- ⁸S. Bock, E. Bich, E. Vogel, A. S. Dickinson, and V. Vesovic, *J. Chem. Phys.* **120**, 7987 (2004).
- ⁹S. Bock, E. Bich, E. Vogel, A. S. Dickinson, and V. Vesovic, *J. Chem. Phys.* **121**, 4117 (2004).
- ¹⁰R. Hellmann, E. Bich, E. Vogel, A. S. Dickinson, and V. Vesovic, *J. Chem. Phys.* **129**, 064302 (2008).
- ¹¹R. Hellmann, E. Bich, E. Vogel, A. S. Dickinson, and V. Vesovic, *J. Chem. Phys.* **130**, 124309 (2009).
- ¹²F. R. W. McCourt, V. Vesovic, W. A. Wakeham, A. S. Dickinson, and M. Mustafa, *Mol. Phys.* **72**, 1347 (1991).
- ¹³V. Vesovic, W. A. Wakeham, A. S. Dickinson, F. R. W. McCourt, and M. Thachuk, *Mol. Phys.* **84**, 553 (1995).
- ¹⁴C. F. Curtiss, *J. Chem. Phys.* **75**, 1341 (1981).
- ¹⁵A. S. Dickinson, R. Hellmann, E. Bich, and E. Vogel, *Phys. Chem. Chem. Phys.* **9**, 2836 (2007).
- ¹⁶E. M. Mas, R. Bukowski, K. Szalewicz, G. Groenenboom, P. E. S. Wormer, and A. van der Avoird, *J. Chem. Phys.* **113**, 6687 (2000).
- ¹⁷G. C. Groenenboom, P. E. S. Wormer, A. van der Avoird, E. M. Mas, R. Bukowski, and K. Szalewicz, *J. Chem. Phys.* **113**, 6702 (2000).
- ¹⁸B. Jeziorski, R. Moszynski, and K. Szalewicz, *Chem. Rev. (Washington, D.C.)* **94**, 1887 (1994).
- ¹⁹R. Bukowski, K. Szalewicz, G. Groenenboom, and A. van der Avoird, *J. Chem. Phys.* **125**, 044301 (2006).
- ²⁰A. J. Misquitta, R. Podaszwa, B. Jeziorski, and K. Szalewicz, *J. Chem. Phys.* **123**, 214103 (2005).
- ²¹R. Bukowski, K. Szalewicz, G. C. Groenenboom, and A. van der Avoird, *Science* **315**, 1249 (2007).
- ²²R. Bukowski, K. Szalewicz, G. C. Groenenboom, and A. van der Avoird, *J. Chem. Phys.* **128**, 094313 (2008).
- ²³R. Bukowski, K. Szalewicz, G. C. Groenenboom, and A. van der Avoird, *J. Chem. Phys.* **128**, 094314 (2008).
- ²⁴K. Raghavachari, G. W. Trucks, J. A. Pople, and M. Head-Gordon, *Chem. Phys. Lett.* **157**, 479 (1989).
- ²⁵W. Cencek, K. Szalewicz, C. Leforestier, R. van Harrevelt, and A. van der Avoird, *Phys. Chem. Chem. Phys.* **10**, 4716 (2008).
- ²⁶J. Millat, V. Vesovic, and W. A. Wakeham, in *Transport Properties of Fluids: Their Correlation, Prediction and Estimation*, edited by J. Millat, J. H. Dymond, and C. A. Nieto de Castro (Cambridge University Press, Cambridge, 1996), Chap. 4, pp. 29–65.
- ²⁷J. H. Ferziger and H. G. Kaper, *The Mathematical Theory of Transport Processes in Gases* (North Holland, Amsterdam, 1972).
- ²⁸Y. Kagan and A. M. Afanasev, *Sov. Phys. JETP* **14**, 1096 (1962).
- ²⁹L. A. Viehland, E. A. Mason, and S. I. Sandler, *J. Chem. Phys.* **68**, 5277 (1978).
- ³⁰G. J. Prangma, A. H. Alberga, and J. J. M. Beenakker, *Physica (Amsterdam)* **64**, 278 (1973).
- ³¹G. C. Maitland, M. Mustafa, and W. A. Wakeham, *J. Chem. Soc., Faraday Trans. II* **79**, 1425 (1983).
- ³²J. D. Lambert, *Vibrational and Rotational Relaxation in Gases* (Clarendon, Oxford, 1977).
- ³³E. L. Heck and A. S. Dickinson, *Comput. Phys. Commun.* **95**, 190 (1996).
- ³⁴R. Hellmann, E. Bich, and A. S. Dickinson (unpublished).
- ³⁵H. O'Hara and F. J. Smith, *J. Comput. Phys.* **5**, 328 (1970).
- ³⁶See EPAPS supplementary material at <http://dx.doi.org/10.1063/1.3158830> for electronic files that contain these tables.
- ³⁷IAPWS, *Release on the IAPWS Formulation 2008 for the Viscosity of Ordinary Water Substance* (International Association for the Properties of Water and Steam, 2008), www.iapws.org.
- ³⁸M. L. Huber, R. A. Perkins, A. Laesecke, D. G. Friend, J. V. Sengers, M. J. Assael, I. N. Metaxa, E. Vogel, R. Mareš, and K. Miyagawa, *J. Phys. Chem. Ref. Data* **38**, 101 (2009).
- ³⁹V. Teske, E. Vogel, and E. Bich, *J. Chem. Eng. Data* **50**, 2082 (2005).
- ⁴⁰A. S. Shifrin, *Teplotnergetika (Moscow, Russ. Fed.)* **6**(9), 22 (1959).
- ⁴¹J. Kestin and H. E. Wang, *Physica (Amsterdam)* **26**, 575 (1960).
- ⁴²J. R. Moszynski, *ASME J. Heat Transfer* **83**, 111 (1961).
- ⁴³J. Kestin and P. D. Richardson, *ASME J. Heat Transfer* **85**, 295 (1963).
- ⁴⁴B. Latto, *Int. J. Heat Mass Transfer* **8**, 689 (1965).
- ⁴⁵S. L. Rivkin and A. Y. Levin, *Teplotnergetika (Moscow, Russ. Fed.)* **13**(4), 79 (1966).
- ⁴⁶S. L. Rivkin, A. Y. Levin, and L. B. Izrailevskii, *Teplotnergetika (Moscow, Russ. Fed.)* **15**(12), 74 (1968).
- ⁴⁷K. Sato, T. Minamiyama, J. Yata, and T. Oka, in *Proceedings Seventh International Conference on the Properties of Steam, Tokyo 1968*, edited by R. W. Haywood (ASME, New York, 1970), Paper No. B-5.
- ⁴⁸K. Sato, T. Minamiyama, J. Yata, T. Oka, and M. Suzuki, *Proceedings 45th Annual Meeting, Kansai [Trans. Jpn. Soc. Mech. Eng.]* **704**, 7 (1970)].
- ⁴⁹I. Yasumoto, *Bull. Chem. Soc. Jpn.* **43**, 3917 (1970).
- ⁵⁰D. L. Timrot, M. A. Serednitskaya, and M. S. Bespalov, *Teplotnergetika (Moscow, Russ. Fed.)* **20**(8), 11 (1973).
- ⁵¹A. Nagashima, I. Tanashita, and Y. Murai, *J. Chem. Eng. Data* **19**, 212 (1974).
- ⁵²G. Oltmann, "Measurement of the viscosity of steam near the critical point," Ph.D. thesis, Technische Universität Hannover, 1977.
- ⁵³J. Kestin and W. Leidenfrost, *Physica (Amsterdam)* **25**, 1033 (1959).
- ⁵⁴A. A. Aleksandrov, A. B. Matveev, and I. V. Tsarev, *Proceedings Symposium on Chemistry of Water and Steam in Power Plants (IAPWS, Tokyo, 1991)*, pp. 13–57.
- ⁵⁵L. R. Fokin and A. N. Kalashnikov, *High Temp.* **38**, 224 (2000).
- ⁵⁶L. R. Fokin and A. N. Kalashnikov, *High Temp.* **46**, 614 (2008).
- ⁵⁷L. Monchick and E. A. Mason, *J. Chem. Phys.* **35**, 1676 (1961).
- ⁵⁸E. A. Mason and L. Monchick, *J. Chem. Phys.* **36**, 1622 (1962).
- ⁵⁹F. L. Swinton, in *Diffusion Processes. Proceedings of the Thomas Graham Memorial Symposium*, edited by J. N. Sherwood, A. V. Chadwick, W. M. Muir, and F. L. Swinton (Gordon and Breach, London, 1971), Vol. 1, pp. 53–63.
- ⁶⁰K. Yoshida, N. Matubayasi, and M. Nakahara, *J. Chem. Phys.* **125**, 074307 (2006).
- ⁶¹K. Yoshida, N. Matubayasi, and M. Nakahara, *J. Chem. Phys.* **126**, 089901 (2007).
- ⁶²N. Matsunaga and A. Nagashima, *J. Phys. Chem.* **87**, 5268 (1983).
- ⁶³IAPWS, *Revised Release on the IAPS Formulation 1985 for the Thermal Conductivity of Ordinary Water Substance* (International Association for the Properties of Water and Steam, 1998), www.iapws.org.
- ⁶⁴S. W. Milverton, *Proc. R. Soc. London, Ser. A* **150**, 287 (1935).
- ⁶⁵D. L. Timrot and N. B. Vargaftik, *Izvestiya Vses. Teplotekh. Inst.* **(9)**, 1 (1935).
- ⁶⁶N. B. Vargaftik, *Izvestiya Vses. Teplotekh. Inst.* **(12)**, 20 (1935).
- ⁶⁷N. B. Vargaftik and O. N. Oleshchuk, *Izvestiya Vses. Teplotekh. Inst.* **(6)**, 7 (1946).
- ⁶⁸N. B. Vargaftik and E. V. Smirnova, *Zh. Tekh. Fiz.* **26**, 1251 (1956).
- ⁶⁹N. B. Vargaftik and A. A. Tarzimanov, *Teplotnergetika (Moscow, Russ. Fed.)* **7**(7), 12 (1960).
- ⁷⁰R. G. Vines, *Trans. ASME, Ser. C: J. Heat Transfer* **82**, 48 (1960).
- ⁷¹A. A. Tarzimanov, *Teplotnergetika (Moscow, Russ. Fed.)* **9**(7), 73 (1962).
- ⁷²F. G. Keyes and R. G. Vines, *Int. J. Heat Mass Transfer* **7**, 33 (1964).
- ⁷³N. B. Vargaftik and N. Kh. Zimina, *Teplotnergetika (Moscow, Russ. Fed.)* **11**(12), 84 (1964).
- ⁷⁴J. E. S. Venart, "The thermal conductivity of water/steam," Ph.D. thesis, University of Glasgow, 1964; *Proceedings Third Symposium on Thermophysical Properties*, edited by S. Gratch (ASME, New York, 1965), pp. 237–245.
- ⁷⁵T. J. S. Brain, *Int. J. Heat Mass Transfer* **10**, 737 (1967).
- ⁷⁶P. Bury, B. Le Neindre, R. Tufeu, P. Johannin, and B. Vodar, in *Proceedings 7th International Conference on the Properties of Steam, Tokyo, 1968*, edited by R. W. Haywood (ASME, New York, 1970), Paper No. C-2, p. 231.
- ⁷⁷T. J. S. Brain, *J. Mech. Eng. Sci.* **11**, 392 (1969).
- ⁷⁸B. Le Neindre, R. Tufeu, P. Bury, and J. V. Sengers, *Ber. Bunsenges. Phys. Chem.* **77**, 262 (1973).

- ⁷⁹A. A. Tarzimanov and M. M. Zainullin, *Teplotoenergetika* (Moscow, Russ. Fed.) **20**(8), 2 (1973).
- ⁸⁰N. B. Vargaftik, N. A. Vanicheva, and L. V. Yakush, *Inzh.-Fiz. Zh.* **25**, 336 (1973).
- ⁸¹P. Bury, P. Johannin, B. Le Neindre, R. Tufeu, and B. Vodar, in *Proceedings 8th International Conference on the Properties of Steam, Giens, France, 1974*, edited by P. Bury, H. Perdon, and B. Vodar (Editions Européennes Thermiques et Industries, Paris, 1975), Vol. 1, pp. 227–242.
- ⁸²J. V. Sengers, J. T. R. Watson, R. S. Basu, B. Kamgar-Parsi, and R. C. Hendricks, *J. Phys. Chem. Ref. Data* **13**, 893 (1984).
- ⁸³N. B. Vargaftik and L. S. Zaitseva, *Inzh.-Fiz. Zh.* **6**(5), 3 (1963).
- ⁸⁴C. E. Baker and R. S. Brokaw, *J. Chem. Phys.* **40**, 1523 (1964).
- ⁸⁵K. M. Dijkema, J. C. Stouthart, and D. A. de Vries, *Waerme- Stoffuebertrag.* **5**, 47 (1972).
- ⁸⁶A. M. Sirota, V. I. Latunin, and G. M. Belyaeva, *Teplotoenergetika* (Moscow, Russ. Fed.) **23**(5), 70 (1976).
- ⁸⁷V. N. Popov and S. G. Dulnev, *Trudy Moskovskogo Energeticheskogo Instituta* **336**, 57 (1977).
- ⁸⁸A. M. Sirota, V. I. Latunin, G. M. Belyaeva, and I. I. Goldshtein, *Teplotoenergetika* (Moscow, Russ. Fed.) **25**(2), 21 (1978).
- ⁸⁹L. A. Curtiss, D. J. Frurip, and M. Blander, *J. Chem. Phys.* **71**, 2703 (1979).
- ⁹⁰R. Tufeu and B. Le Neindre, *Inzh.-Fiz. Zh.* **36**, 472 (1979).
- ⁹¹V. I. Miroshnichenko and V. V. Makhrov, *Teplotoenergetika* (Moscow, Russ. Fed.) **31**(1), 64 (1984).
- ⁹²M. J. Assael, E. Bekou, D. Giakoumakis, D. G. Friend, M. A. Killeen, J. Millat, and A. Nagashima, *J. Phys. Chem. Ref. Data* **29**, 141 (2000).
- ⁹³R. Tufeu and B. Le Neindre, *Int. J. Thermophys.* **8**, 283 (1987).
- ⁹⁴A. A. Tarzimanov and F. R. Gabitov, *Teplotoenergetika* (Moscow, Russ. Fed.) **36**(7), 5 (1989).
- ⁹⁵F. Mayinger and U. Grigull, *Brennst.-Waerme-Kraft* **17**, 53 (1965).
- ⁹⁶J. Kestin and J. H. Whitelaw, *ASME J. Eng. Power* **88**, 82 (1966).
- ⁹⁷R. W. Powell, C. Y. Ho, and P. E. Liley, *NSRDS-NBS 8 (Cat. 5): Thermal Conductivity of Selected Materials* (United States Department of Commerce, National Bureau of Standards, Washington, D.C., 1966), pp. 165–168.
- ⁹⁸K. Scheffler, N. Rosner, J. Straub, and U. Grigull, *Brennst.-Waerme-Kraft* **31**, 326 (1979).
- ⁹⁹A. A. Aleksandrov, *Teplotoenergetika* (Moscow, Russ. Fed.) **27**(4), 70 (1980).
- ¹⁰⁰U. Grigull, in *Proceedings Seventh International Conference on the Properties of Steam, Tokyo, 1968*, edited by R. W. Haywood (ASME, New York, 1970), pp. 38–61.
- ¹⁰¹A. M. Sirota, V. I. Latunin, and G. M. Belyaeva, *Teplotoenergetika* (Moscow, Russ. Fed.) **21**(10), 52 (1974).
- ¹⁰²H. Roesler and K.-F. Sahn, *J. Acoust. Soc. Am.* **37**, 386 (1965).
- ¹⁰³H. E. Bass, J. R. Olson, and R. C. Amme, *J. Acoust. Soc. Am.* **56**, 1455 (1974).
- ¹⁰⁴R. G. Keeton and H. E. Bass, *J. Acoust. Soc. Am.* **60**, 78 (1976).
- ¹⁰⁵R. Synofzik, W. Garen, G. Wortberg, and A. Frohn, in *Proceedings 11th International Symposium on Shock Tube and Shock Wave Research, 1977*, edited by B. Ahlborn, A. Hertzberg, and D. Russell (University of Washington Press, Seattle, 1978), pp. 127–131.

5 Zusammenfassung

Das Ziel dieser Arbeit bestand in der hochgenauen Berechnung thermophysikalischer Eigenschaften der reinen Gase Helium, Neon, Methan und Wasserdampf bei niedrigen Dichten über weite Temperaturbereiche. Dazu wurden die statistische Thermodynamik für die Bestimmung von zweiten und dritten Druckvirialkoeffizienten und die kinetische Gastheorie für die Ermittlung von Transport- und Relaxationseigenschaften genutzt. Die für alle Berechnungen benötigten zwischenatomaren- bzw. zwischenmolekularen Wechselwirkungspotentiale wurden für Helium, Neon und Methan mit quantenchemischen *ab initio*-Methoden nach dem Supermolekülansatz ermittelt und für Wasser aus dem Schrifttum entnommen.

Für die Bestimmung des Helium-Helium-Potentials wurden *ab initio*-Methoden bis *full-CI* und sehr große neu entwickelte Basissätze verwendet. Zudem wurden Korrekturen für relativistische Effekte und Korrekturen zur Born-Oppenheimer-Näherung ermittelt. Eine analytische Potentialfunktion wurde an die berechneten *ab initio*-Wechselwirkungsenergien angepasst und für die quantenmechanische Berechnung der zweiten und dritten Druckvirialkoeffizienten, der Scherviskosität und der Wärmeleitfähigkeit von ^3He und ^4He verwendet. Die Unsicherheit der verfügbaren experimentellen Daten ist deutlich höher als die der berechneten Werte, so dass letztere für metrologische Anwendungen und zur Kalibrierung von Messapparaturen besser geeignet sind.

Das Neon-Neon-Potential wurde mit den größten im Schrifttum verfügbaren Basissätzen und *ab initio*-Methoden bis *CCSDT(Q)* ermittelt. Korrekturen für relativistische Effekte wurden ebenfalls bestimmt. An die berechneten Wechselwirkungsenergien wurde eine analytische Potentialfunktion angepasst, mit der die Rotations-Schwingungsspektren sowie die zweiten und dritten Druckvirialkoeffizienten, die Viskosität und die Wärmeleitfähigkeit quantenmechanisch berechnet wurden. Die erreichte Unsicherheit der berechneten Werte für die unterschiedlichen Eigenschaften ist mit der der besten experimentellen Daten bei Raumtemperatur vergleichbar. Weit entfernt von Raumtemperatur sind die berechneten Werte hingegen deutlich zuverlässiger als die verfügbaren experimentellen Daten.

Für die Bestimmung des Methan-Methan-Wechselwirkungspotentials, das sowohl vom Abstand der beiden Moleküle als auch von deren gegenseitiger Orientierung abhängt, wur-

den CCSD(T)-Rechnungen mit den Basissätzen aug-cc-pVTZ und aug-cc-pVQZ für 17 verschiedene gegenseitige Orientierungen mit jeweils 16 Schwerpunktsabständen, also insgesamt für 272 Punkte auf der Potentialenergiefläche, durchgeführt. Die berechneten Wechselwirkungsenergien wurden auf vollständigen Basissatz extrapoliert und das Potential durch eine *site-site*-Funktion in analytischer Form dargestellt. Die mit diesem Potential berechneten zweiten Druckvirialkoeffizienten beschreiben die zuverlässigsten experimentellen Daten innerhalb ihrer angegebenen Fehlerbreite, nachdem ein einzelner Potentialparameter so adjustiert wurde, dass der berechnete zweite Druckvirialkoeffizient bei Raumtemperatur den besten verfügbaren experimentellen Wert exakt wiedergibt.

Die Transport- und Relaxationseigenschaften von Methan wurden in der Gasphase mittels der kinetischen Theorie über große Temperaturbereiche berechnet. Die dazu benötigten generalisierten Streuquerschnitte wurden mittels klassischer Trajektorien zur Beschreibung der Dynamik der Stoßprozesse ermittelt. Da die Methode der klassischen Trajektorien nur für Stöße zwischen linearen Molekülen entwickelt und im Softwarecode TRAJECT implementiert worden war, mussten umfangreiche Erweiterungen sowohl der zugrunde liegenden kinetischen Gastheorie als auch des TRAJECT-Codes durchgeführt werden, um für nicht-lineare Moleküle wie Methan die generalisierten Streuquerschnitte bestimmen zu können. Die berechneten Viskositätskoeffizienten zeigen Abweichungen von deutlich unter einem Prozent zu den besten experimentellen Daten, und auch im Falle der Wärmeleitfähigkeit ist die Übereinstimmung sehr gut. Alle weiteren Eigenschaften, wie visko- und thermomagnetische Effekte, Selbstdiffusion, Volumenviskosität und Kernspinrelaxation sind experimentell zum Teil nur mit großen Unsicherheiten bestimmbar, so dass die hier gefundenen größeren Abweichungen bezüglich der Qualität der durchgeführten Berechnungen nur geringe Aussagekraft haben.

Analog zu Methan wurden die Transport- und Relaxationseigenschaften von Wasserdampf berechnet, wobei vier verschiedene Potentialfunktionen aus dem Schrifttum getestet wurden. Mit dem genauesten Potential ergaben sich Abweichungen von nur etwa einem halben Prozent zu den besten experimentellen Viskositätsdaten. Im Falle der Wärmeleitfähigkeit wurden bei hohen Temperaturen sehr große Abweichungen von bis zu 5% erhalten, was wahrscheinlich an den großen experimentellen Unsicherheiten liegt.

In der Perspektive sind Erweiterungen der kinetischen Theorie und des TRAJECT-Codes für die Beschreibung von Gasmischungen vorzunehmen, um neue Anwendungsbereiche wie beispielsweise feuchte Luft, Erdgase und Verbrennungsgase zu erschließen.

Literaturverzeichnis

- [1] D. M. Bishop und J. Pipin, *Inter. J. Quantum Chem.* **45**, 349 (1993).
- [2] T. Korona, H. L. Williams, R. Bukowski, B. Jeziorski und K. Szalewicz, *J. Chem. Phys.* **106**, 5109 (1997).
- [3] B. Jeziorski, R. Moszynski und K. Szalewicz, *Chem. Rev.* **94**, 1887 (1994).
- [4] J. van de Bovenkamp und F. B. van Duijneveldt, *J. Chem. Phys.* **110**, 11141 (1999).
- [5] T. van Mourik und T. H. Dunning Jr., *J. Chem. Phys.* **111**, 9248 (1999).
- [6] J. Komasa, *J. Chem. Phys.* **110**, 7909 (1999).
- [7] A. J. Thakkar, *J. Chem. Phys.* **89**, 2092 (1988).
- [8] J. J. Hurly und M. R. Moldover, *J. Res. Natl. Inst. Stand. Technol.* **105**, 667 (2000).
- [9] R. J. Gdanitz, *Mol. Phys.* **99**, 923 (2001).
- [10] J. B. Anderson, *J. Chem. Phys.* **115**, 4546 (2001).
- [11] J. B. Anderson, *J. Chem. Phys.* **120**, 9886 (2004).
- [12] W. Cencek, M. Jeziorska, R. Bukowski, M. Jaszuński, B. Jeziorski und K. Szalewicz, *J. Phys. Chem. A* **108**, 3211 (2004).
- [13] W. Cencek, J. Komasa, K. Pachucki und K. Szalewicz, *Phys. Rev. Lett.* **95**, 233004 (2005).
- [14] J. Komasa, W. Cencek und J. Rychlewski, *Chem. Phys. Lett.* **304**, 293 (1999).
- [15] H. B. G. Casimir und D. Polder, *Phys. Rev.* **73**, 360 (1948).
- [16] W. J. Meath und J. O. Hirschfelder, *J. Chem. Phys.* **44**, 3210 (1966).
- [17] M.-K. Chen und K. T. Chung, *Phys. Rev. A* **53**, 1439 (1996).
- [18] R. D. Cowan und D. C. Griffin, *J. Opt. Soc. Am.* **66**, 1010 (1976).
- [19] R. A. Aziz und M. J. Slaman, *Chem. Phys.* **130**, 187 (1989).
- [20] T. van Mourik, A. K. Wilson und T. H. Dunning Jr., *Mol. Phys.* **96**, 529 (1999).
- [21] J. van de Bovenkamp und F. B. van Duijneveldt, *Chem. Phys. Lett.* **309**, 287 (1999).

- [22] S. M. Cybulski und R. R. Toczyłowski, *J. Chem. Phys.* **111**, 10520 (1999).
- [23] R. J. Gdanitz, *Chem. Phys. Lett.* **348**, 67 (2001).
- [24] M. Venkatraj, M. G. Müller, H. Huber und R. J. Gdanitz, *Collect. Czech. Chem. Commun.* **68**, 627 (2003).
- [25] A. Wüest und F. Merkt, *J. Chem. Phys.* **118**, 8807 (2003).
- [26] A. E. Nasrabad, R. Laghaei und U. K. Deiters, *J. Chem. Phys.* **121**, 6423 (2004).
- [27] J. S. Lee, *Theor. Chem. Acc.* **113**, 87 (2005).
- [28] S. Tsuzuki, T. Uchimaru und K. Tanabe, *Chem. Phys. Lett.* **287**, 202 (1998).
- [29] S. F. Boys und F. Bernardi, *Mol. Phys.* **19**, 553 (1970).
- [30] R. L. Rowley und T. Pakkanen, *J. Chem. Phys.* **110**, 3368 (1999).
- [31] E. M. Mas, R. Bukowski, K. Szalewicz, G.C. Groenenboom, P. E. S. Wormer und A. van der Avoird, *J. Chem. Phys.* **113**, 6687 (2000).
- [32] G. C. Groenenboom, P. E. S. Wormer, A. van der Avoird, E. M. Mas, R. Bukowski und K. Szalewicz, *J. Chem. Phys.* **113**, 6702 (2000).
- [33] E. A. Mason und T. H. Spurling, *The Virial Equation of State*, Pergamon, Oxford (1969).
- [34] M. E. Boyd, S. Y. Larsen und J. E. Kilpatrick, *J. Chem. Phys.* **50**, 4034 (1969).
- [35] B. M. Axilrod und E. Teller, *J. Chem. Phys.* **11**, 299 (1943).
- [36] B. M. Axilrod, *J. Chem. Phys.* **19**, 719 (1951).
- [37] K. Lucas, *Angewandte Statistische Thermodynamik*, Springer, Berlin (1986).
- [38] R. T. Pack, *J. Chem. Phys.* **78**, 7217 (1983).
- [39] P. E. S. Wormer, *J. Chem. Phys.* **122**, 184301 (2005).
- [40] M. Takahashi und M. Imada, *J. Phys. Soc. Jpn.* **53**, 3765 (1984).
- [41] R. P. Feynman und A. R. Hibbs, *Quantum Mechanics and Path Integrals*, McGraw-Hill, New York (1965).
- [42] H. Kleinert, *Path Integrals in Quantum Mechanics Statistics and Polymer Physics*, World Scientific, New Jersey (1995).
- [43] G. K. Schenter, *J. Chem. Phys.* **117**, 6573 (2002).
- [44] E. A. Uehling und G. E. Uhlenbeck, *Phys. Rev.* **43**, 552 (1933).
- [45] C. F. Curtiss, *J. Chem. Phys.* **75**, 376 (1981).

- [46] C. F. Curtiss, *J. Chem. Phys.* **97**, 1416 (1992).
- [47] Y. M. Kagan und L. M. Maksimov, *Zh. Eksp. Teor. Fiz.* **51**, 1893 (1966) [*Sov. Phys. — JETP* **24**, 1272 (1967)].
- [48] Y. M. Kagan und L. M. Maksimov, *Zh. Eksp. Teor. Fiz.* **60**, 1339 (1971) [*Sov. Phys. — JETP* **33**, 725 (1971)].
- [49] L. Waldmann, *Z. Naturforsch.* **12a**, 661 (1957); *ibid* **13a**, 609 (1958); *Handbuch der Physik*, Band **XII**, ed. S. Flügge, Springer-Verlag, Berlin (1958), p. 295.
- [50] R. F. Snider, *J. Chem. Phys.* **32**, 1051 (1960).
- [51] S. Chapman, *Phil. Trans. Roy. Soc.* **A216**, 279 (1916).
- [52] D. Enskog, *Kinetische Theorie der Vorgänge in mäßig verdünnten Gasen*, Dissertation, Uppsala, Almqvist und Wiksell (1917).
- [53] F. R. W. McCourt, J. J. M. Beenakker, W. E. Köhler und I. Kuščer, *Nonequilibrium Phenomena in Polyatomic Gases*, Vol. **1**, Oxford Univ. Press, Oxford (1990).
- [54] S. Chapman und T. G. Cowling, *Mathematical Theory of Nonuniform Gases*, 3rd ed., Cambridge Univ. Press, Cambridge (1970).
- [55] J. O. Hirschfelder, C. F. Curtiss und R. B. Bird, *Molecular Theory of Gases and Liquids*, Wiley, New York (1954).
- [56] J. H. Ferziger und H. G. Kaper, *Mathematical Theory of Transport Processes in Gases*, North-Holland Publ. Co., Amsterdam (1972).
- [57] F. R. Meeks, T. J. Cleland, K. E. Hutchinson und W. L. Taylor, *J. Chem. Phys.* **100**, 3813 (1994).
- [58] C. F. Curtiss, *J. Chem. Phys.* **75**, 1341 (1981).
- [59] E. L. Heck und A. S. Dickinson, *Comput. Phys. Commun.* **95**, 190 (1996).
- [60] S. Bock, E. Bich, E. Vogel, A. S. Dickinson und V. Vesovic, *J. Chem. Phys.* **117**, 2151 (2002).
- [61] S. Bock, E. Bich, E. Vogel, A. S. Dickinson und V. Vesovic, *J. Chem. Phys.* **120**, 7987 (2004).
- [62] S. Bock, E. Bich, E. Vogel, A. S. Dickinson und V. Vesovic, *J. Chem. Phys.* **121**, 4117 (2004).
- [63] F. R. W. McCourt, V. Vesovic, W. A. Wakeham, A. S. Dickinson und M. Mustafa, *Mol. Phys.* **72**, 1347 (1991).

- [64] V. Vesovic, W. A. Wakeham, A. S. Dickinson, F. R. W. McCourt und M. Thachuck, *Mol. Phys.* **84**, 553 (1995).
- [65] R. Gdanitz, *J. Chem. Phys.* **113**, 5145 (2000).
- [66] T. H. Dunning Jr., *J. Chem. Phys.* **90**, 1007 (1989).
- [67] D. E. Woon und T. H. Dunning Jr., *J. Chem. Phys.* **100**, 2975 (1994).
- [68] J. J. Hurly und J. B. Mehl, *J. Res. Natl. Inst. Stand. Technol.* **112**, 75 (2007).
- [69] K. Patkowski, W. Cencek, M. Jeziorska, B. Jeziorski und K. Szalewicz, *J. Phys. Chem. A* **111**, 7611 (2007).
- [70] M. Jeziorska, W. Cencek, K. Patkowski, B. Jeziorski und K. Szalewicz, *J. Chem. Phys.* **127**, 124303 (2007).
- [71] W. Cencek und K. Szalewicz, *Int. J. Quant. Chem.* **108**, 2191 (2008).
- [72] C. Gaiser, B. Fellmuth und N. Haft, *Int. J. Thermophys.* **29**, 18 (2008).
- [73] F. Luo, G. C. McBane, G. Kim, C. F. Giese und W. R. Gentry, *J. Chem. Phys.* **98**, 3564 (1993).
- [74] R. E. Grisenti, W. Schöllkopf, J. P. Toennies, G. C. Hegerfeldt, T. Köhler und M. Stoll, *Phys. Rev. Lett.* **85**, 2284 (2000).
- [75] R. J. LeRoy, *LEVEL 7.7. A Computer Program for Solving the Radial Schrödinger Equation for Bound and Quasibound Levels*, University of Waterloo, Chemical Physics Research Report CP-661, Waterloo, Ontario, Canada.
- [76] M. Nakata und K. Kuchitsu, *J. Chem. Soc. Jpn.*, 1446 (1986).
- [77] J. F. Stanton, *Mol. Phys.* **97**, 841 (1999).
- [78] T. J. Lee, J. M. L. Martin und P. R. Taylor, *J. Chem. Phys.* **102**, 254 (1995).
- [79] A. J. Russell und M. A. Spackman, *Mol. Phys.* **84**, 1239 (1995).
- [80] D. M. Bishop, F. L. Gu und S. M. Cybulski, *J. Chem. Phys.* **109**, 8407 (1998).
- [81] G. F. Thomas und W. J. Meath, *Mol. Phys.* **34**, 113 (1977).
- [82] R. Kleinrahm, W. Duschek, W. Wagner und M. Jaeschke, *J. Chem. Thermodyn.* **20**, 621 (1988).
- [83] E. F. May, R. F. Berg und M. R. Moldover, *Int. J. Thermophys.* **28**, 1085 (2007).
- [84] L. Monchick und E. A. Mason, *J. Chem. Phys.* **35**, 1676 (1961).
- [85] E. A. Mason und L. Monchick, *J. Chem. Phys.* **36**, 1622 (1962).

- [86] M. J. Assael und W. A. Wakeham, *J. Chem. Soc., Faraday Trans 1* **77**, 697 (1981).
- [87] R. Bukowski, K. Szalewicz, G. C. Groenenboom und A. van der Avoird, *J. Chem. Phys.* **125**, 044301 (2006).
- [88] A. J. Misquitta, R. Podeszwa, B. Jeziorski und K. Szalewicz, *J. Chem. Phys.* **123**, 214103 (2005).
- [89] R. Bukowski, K. Szalewicz, G. C. Groenenboom und A. van der Avoird, *Science* **315**, 1249 (2007).
- [90] R. Bukowski, K. Szalewicz, G. C. Groenenboom und A. van der Avoird, *J. Chem. Phys.* **128**, 094313 (2008).
- [91] R. Bukowski, K. Szalewicz, G. C. Groenenboom und A. van der Avoird, *J. Chem. Phys.* **128**, 094314 (2008).
- [92] V. Teske, E. Vogel und E. Bich, *J. Chem. Eng. Data* **50**, 2082 (2005).

Erklärung

Ich versichere hiermit an Eides statt, dass ich die vorliegende Arbeit selbstständig angefertigt und ohne fremde Hilfe verfasst habe, keine außer den von mir angegebenen Hilfsmitteln und Quellen dazu verwendet habe und die den benutzten Werken inhaltlich und wörtlich entnommenen Stellen als solche kenntlich gemacht habe.

Rostock, 25. April 2009

Robert Hellmann

Lebenslauf

Persönliche Daten

Name: Hellmann
Vorname: Robert
Geburtsdatum: 12. November 1981
Geburtsort: Rostock
Familienstand: ledig
Staatsangehörigkeit: Bundesrepublik Deutschland

Schulbildung

09/1988–07/1992: Grundschule Lütten-Klein, Rostock
08/1992–10/1995: Ahorn-Gymnasium, Rostock
11/1995–07/2000: Christophorus-Gymnasium, Rostock
07/2000: Abitur

Studium

10/2000–08/2005: Studium der Fachrichtung Chemie an der Universität Rostock
Abschluss: Diplom-Chemiker
10/2005–04/2009: Anfertigung der Dissertation im Arbeitskreis von
Prof. Dr. Eckhard Vogel an der Universität Rostock

Berufstätigkeit

10/2000–03/2004: Studentische Hilfskraft am Institut für Chemie der Universität
Rostock, Abteilung Physikalische Chemie
seit 10/2005: Wissenschaftlicher Mitarbeiter am Institut für Chemie der
Universität Rostock, Abteilung Physikalische Chemie